11-25-2014

The Adaptor Protein 1 (AP-1) Complex at the Heart of Post-Golgi Trafficking in a Corticotrope Tumor Cell Line

Mathilde L. Bonnemaison
bonnemaison@uchc.edu

The Adaptor Protein 1 Complex (AP-1) at the Heart of Post-Golgi Trafficking in a Corticotrope Tumor Cell Line

Mathilde L. Bonnemaison, PhD

University of Connecticut, 2014

Peptides act as chemical messengers to regulate physiological functions. First synthesized as inactive precursors, peptides undergo a set of post-translational modifications to gain bioactivity en route through the secretory pathway. Peptides exit the Golgi apparatus in secretory granules (SGs) that are stored until a stimulus triggers their exocytosis. The adaptor protein 1A (AP-1A) is required for SG maturation in neuroendocrine cells and for the formation of specialized SGs such as the glue granules in *Drosophila*, Weibel-Palade bodies in endothelial cells and rhoptries in *Toxoplasma gondii*. AP-1A is a heterotetrameric complex ($\gamma/\beta1/\mu1A/\sigma1$) that interacts with cargo proteins and clathrin to transport proteins between the *trans*-Golgi network (TGN) and endosomes. Lack of any AP-1A subunit is sufficient to impair AP-1A function.

A decrease in expression of the $\mu1A$ subunit in AtT-20 cells, a corticotrope tumor cell line (sh-$\mu1A$), resulted in vacuolization of the TGN, formation of non-condensing SGs and impaired responsiveness to secretagogue. Impaired AP-1A function in AtT-20 cells also dramatically altered the endocytic pathway. Early and recycling endosomes accumulated

above the Golgi complex instead of peripherally and endosome maturation was altered in sh-μ1A cells.

Clinically, patients with MEDNIK syndrome, a rare genetic disorder caused by lack of expression of σ1A, exhibit clinical and biochemical signs of impaired copper homeostasis. Peptidylglycine α-amidating monooxygenase 1 (PAM-1), a SG membrane protein that catalyzes peptide amidation, requires copper for activity. Atp7a brings copper from the cytosol to the lumen of the secretory pathway for delivery to cuproproteins such as PAM. The endosomal trafficking of both Atp7a and PAM was altered when AP-1 function was diminished, resulting in increased sensitivity of peptide amidation to copper chelation. Although ATP7A moves from the Golgi to the cell periphery under high copper conditions in HeLa cells, treatment of mouse neuroendocrine cells with high copper levels increased Atp7a protein level.

PAM expression profile in the developing cortex and hippocampus indicated that PAM-1, the major isoform, was distributed in perikaryon, dendrites and axons in cultured hippocampal neurons. Future directions to investigate AP-1 and PAM-1 trafficking in hippocampal neurons and neuroendocrine cells are discussed last.

The Adaptor Protein 1 Complex (AP-1) at the Heart of Post-Golgi Trafficking in a Corticotrope Tumor Cell Line

Mathilde L. Bonnemaison

B.Sc., Université de Bordeaux, France, 2008

A Dissertation

Submitted in Partial Fulfillment of the

Requirements for the Degree of Doctor of Philosophy

at the

University of Connecticut

2014

APPROVAL PAGE

Doctor of Philosophy Dissertation

The Adaptor Protein 1 Complex (AP-1) at the Heart of Post-Golgi Trafficking in a Corticotrope Tumor Cell Line

Presented by

Mathilde L. Bonnemaison B.Sc

Major Advisor

Elizabeth A. Eipper

Associate Advisor

Richard E. Mains

Associate Advisor

Stephen M. King

Associate Advisor

Ann E. Cowan

University of Connecticut

2014

Acknowledgements

That is why scientists persist in their investigations, why we struggle so desperately for every bit of knowledge, stay up nights seeking the answer to a problem, climb steepest obstacles to the next fragment of understanding, to finally reach that joyous moment of the kick in the discovery, which is part of the pleasure of finding things out.

- Richard Feynman

Go to school and learn as much as you can because what you've learned is the last thing people can take from you.

- My grandmother, Marie Marcelle Bonnemaison

It all started in 1976

My adventure in Connecticut started with a friendship between my mother, Catherine, and Sara Frey, an American citizen from West Harftord, Connecticut. Sara went to France to learn more French and ended up living in the same building as my mother. In 2007, I contacted Sara's sister, Amy Frey, to help me find an internship or job in the US. Thanks to her, I was able to spend a summer under the supervision of Dr. George Kuchel, Dr. Carol Pilbeam, Dr. Lawrence G. Raisz, Olga Voznesensky and Dr. John Taylor at the University of Connecticut Health Center. These people formed a fantastic scientific group and made me fall in love with research. I applied for the PhD program thanks to them.

The door

My mentor, Dr. Betty A. Eipper and my co-mentor, Dr. Richard E. Mains put education as one of their priorities. I have grown and learned so much in their presence and I hope

this thesis reflects well the knowledge and methodology I have acquired in their laboratory. Most of what I know today has a lot to do with their office door. Their door was kept open which meant that they were available to answer questions, to teach new aspects of science, to help in preparing and designing experiments, to help in writing papers and preparing for oral presentations. I would like to thank Dr. Eipper and Dr. Mains for leaving their door open and giving me the tools for a successful career.

I would like to thank the other members of my thesis committee, Dr. Ann Cowan and Dr. Stephen King. These Professors never lost an opportunity to make me think and look at my work differently, to help me improve my oral skills and grow as a scientist.

145

The work presented in this thesis would not have been possible without the constant support and constructive criticism of the rest of the laboratory. Most of it happened during our weekly lab meeting during which Dr. Eipper and Dr. Mains kindly provided bagels for all the members of the laboratory. After intensive calculations, I had about 145 delicious bagels +/- 3 bagels over the past five years. I again would like to thank Dr. Eipper and Dr. Mains, not only for the bagels, but for making those meetings in a way that helped everyone in the room become a better scientist and a better person.

Every lab has a Mother who makes sure everything runs properly. Ours is Darlene D'Amato. Observing how she works and behaves in a lab was an excellent example of professionalism and common sense. The meticulousness of Yanping Wang was also a good source of learning. Molecular biology has no secret to Yanping Wang and working with her was always a success. Thanks to Darlene and Ping for showing and teaching me your work.

I would like to thank my colleague and friend, Dr. Vishwanatha Kurutihalli who was always open to scientific discussions or family stories. I was lucky to have Vishwa as an office neighbor. His presence made my passage here, at the University of Connecticut Health Center, much more enjoyable.

I met Taylor LaRese soon after I joined the lab. I would like to thank her for being a good friend and an excellent co-worker with great optimism. It was always refreshing to talk to her and I am really grateful to have met this wonderful woman during my graduate studies. I wish her good luck in her professional career.

I would like to thank Dr. Yan Yan, Jennifer Kirkland and Kristina Carlson, for the lunches spent together and our friendship. Our conversations helped me think about the job market, scientific problems and the world in general.

Megan Miller and Dhivya Kumar, the two current graduate students in the lab, are dedicated and hard-working women. It was reassuring to have them around because we understood each other when we had to study for Journal Club, Work In Progress, General Examination or prepare our posters. Thanks to Megan and Dhivya.

The MBB and Neuroscience departments

I would like to thank Dr. Sandra Weller for her dynamism and for making me feel welcome in the department of Molecular Biology and Biophysics (previously known as the Molecular, Microbial and Structural Biology department). I also would like to thank Dr. Chitra Rajagopal and Dr. Pantelis Rompolas who were two graduate students in the MBB department. They changed the way I was looking and thinking about science and Academia.

Going to Journal Club and Work In Progress talks in this department helped me grow as

a scientist and observe problems from a different angle. When my turn to present my work or a paper was approaching, it was always a challenge as I wanted to do better every year. I have to thank Dr. Christopher Heinen and my thesis committee for providing feedback after my presentations. I greatly appreciated their honesty and guidance.

Although I was not a student from the Neuroscience department, I was treated as one. This is why I would like to thank the Neuroscience department. The weekly Neuroscience seminars and our lab meetings allowed me to learn more about Neuroscience than I originally expected. I also would like to thank the neuroscience administration for their continuous help in processing paperwork, organizing events and seminars.

Friends and family

This thesis would not have been possible without knowing that Sara, Alan, Amy, Mickey, Isaac, Gabriel, Schuyler and Tessa were around and ready to help me whenever. I always felt welcomed with them and I cannot thank them enough.

I would like to thank the Romagnoli family (Pablo, Marina, Emilia and Nico), Nevena Radonjic, Alberto Ortega, Erika and Neil, the Vyas family (Jay, Evelyn, Addison and the newly born Jay), Ina Oikonomu, Sonali and Krishna, Victor Francone, Heloise, the Benechet family (Alex, Juliette, Elizabeth and Madeline) and Esther Kott, for their friendship and support over the years.

My husband, Matthew Fenwick gave me to courage to continue and do better. At night, he was here to listen to me whatever my day was. He understood when I had to work late or come in on weekends to finish experiments. I want to thank him. I am also very grateful to have met his family who welcomed me immediately. Over the years, I have learned to know

them. This friendship is still growing and I hope it will continue on the same pace. Special thanks to the Fenwick family.

I would like to thank my uncles, aunts and cousins for staying together and helping each other no matter where, no matter when. This gave me strength to continue my studies while being far away. I would like to thank my grandmothers, Marie Marcelle Bonnemaison and Marie Madeleine Cochet, for their constant support, guidance and for sharing their point of view about life. Lastly, I would like to thank my brothers, Jean-Baptiste and Antoine, and my parents, Catherine and Jean-Marc, for letting me realize my dreams, for always pushing me to learn and explore more even if this meant that I had to go to the other side of the world. I dedicate this thesis to my family.

Contents

List of Tables

List of Figures

Chapter 1

Role of Adaptor Proteins in Secretory Granule Biogenesis and Maturation

Mathilde L. Bonnemaison, Betty A. Eipper and Richard E. Mains.

This chapter is a duplicate version of a published manuscript in Front. Endocrinol. (Lausanne), 2013, vol.4: 101.

Drafting of the manuscript

Mathilde L. Bonnemaison, Richard E. Mains and Betty A. Eipper.

Critical revision of the manuscript

Vishwanatha Kurutihalli and Yan Yan.

1.1 Abstract

In the regulated secretory pathway, secretory granules (SGs) store peptide hormones that are released on demand. SGs are formed at the *trans*-Golgi network (TGN) and must undergo a maturation process to become responsive to secretagogues. The production of mature SGs requires concentrating newly synthesized soluble content proteins in granules whose membranes contain the appropriate integral membrane proteins. The mechanisms underlying the sorting of soluble and integral membrane proteins destined for SGs from other proteins are not yet well understood. For soluble proteins, luminal pH and divalent metals can affect aggregation and interaction with surrounding membranes. The trafficking of granule membrane proteins can be controlled by both luminal and cytosolic factors. Cytosolic adaptor proteins, which recognize the cytosolic domains of proteins that span the SG membrane, have been shown to play essential roles in the assembly of functional SGs. Adaptor protein 1A (AP-1A) is known to interact with specific motifs in its cargo proteins and with the clathrin heavy chain, contributing to the formation of a clathrin coat. AP-1A is present in patches on immature SG membranes, where it removes cargo and facilitates SG maturation. AP-1A recruitment to membranes can be modulated by PACS-1 (Phosphofurin Acidic Cluster Sorting protein 1), a cytosolic protein which interacts with both AP-1A and cargo that has been phosphorylated by casein kinase II. A cargo/PACS-1/AP-1A complex is necessary to drive the appropriate transport of several cargo proteins within the regulated secretory pathway. The GGA (Golgi-localized, γ-ear containing, ADP-ribosylation factor binding) family of adaptor proteins serve a similar role. We review the functions of AP-1A, PACS-1 and GGAs in facilitating the retrieval of proteins from immature SGs and review examples of cargo proteins whose trafficking within the regulated secretory pathway is governed by

adaptor proteins.

1.2 The regulated secretory pathway

Neuroendocrine cells synthesize, process and store peptide hormones so that they are available for secretion upon demand [1]. These professional secretory cells devote as much as half of their total protein synthesis to the production of a single hormone [2]. The regulated secretory pathway allows intracellular storage of peptide hormones until an external stimulus triggers exocytosis of the secretory granules that contain the peptides. Neuroendocrine tumors and metabolic disease are linked to defects in hormone secretion, observed via an increase in circulating hormone levels due to impaired intracellular storage or cellular response. The alterations which result in loss of storage and secretagogue responsiveness are poorly understood.

Peptide hormones are first synthesized as inactive precursors. The signal peptide found at the N-terminus of the preprohormone is recognized by signal recognition particle, which stops translation and directs entry of the nascent preprohormone into the lumen of the endoplasmic reticulum [3]; removal of the signal peptide by signal peptidase yields the prohormone. Most proteins which are going to be secreted undergo this step. The endoplasmic reticulum is also the site at which disulfide-bond formation and N-linked glycosylation occur (Figure 1.1) [3, 4, 5]. Professional secretory cells have developed specialized sensing mechanisms to avoid triggering the endoplasmic reticulum stress pathway, which can lead to cell death; for example, increased expression of SERP1 (Stress-associated Endoplasmic Reticulum Protein 1) prevents endoplasmic reticulum stress in the anterior pituitary and pancreas [6]. After exiting the endoplasmic reticulum, prohormones are transported to the Golgi apparatus,

where additional post-translational modifications such as oligosaccharide maturation and phosphorylation can occur (Figure 1.1) [7, 5]. When they reach the *trans*-Golgi network (TGN), prohormones and their processing enzymes are concentrated into granules budding from the TGN; these structures presumably represent newly forming secretory granules (SGs) [1]. These new SGs are immature and must undergo a maturation process before they are capable of secreting peptide hormone in response to secretagogue. Maturation involves remodeling of the immature SG membrane by removal of non-regulated secretory proteins and excess membrane; this process involves clathrin-coated vesicles mediated by adaptor proteins (Figure 1.1) [8, 9], acidification of the lumen, aggregation of content proteins and, at least in some cell systems, fusion of immature SGs [10, 11]. The final post-translational modifications needed to generate bioactive peptide hormones occur in immature and mature SGs [12, 13]. Mature SGs, which appear dense in the electron microscope and during sucrose density gradient centrifugation, can contain more than 300 mg/ml protein, largely peptide hormones [14]. Unlike constitutively secreted proteins, which are found in the extracellular compartment within minutes after exit from the TGN, it takes about 90 minutes for peptide hormones to go from the TGN to mature SGs (Figure 1.1) [15, 16]. In addition, mature SG content can be stored for many days before being secreted into the extracellular compartment in response to a stimulus (Figure 1.1) [17, 18]; proteins and peptides stored in the regulated secretory pathway are released at a low rate (basal secretion) even in the absence of secretagogue [19, 20]. The study of immature SGs remains a challenge due to their transient role as intermediates between the TGN and mature SGs. Morphologists describe immature SGs as vacuoles found in close proximity to the TGN which contain dense material surrounded by a loose membrane with a partial clathrin coat, while biochemists

distinguish immature SGs from mature SGs by their inability to respond to secretagogue or by their release of incompletely processed newly synthesized products [14, 1]. Early studies using $^{35}SO_4$ to label sugars and Tyr residues demonstrated high K^+/Ca^{2+}-stimulated release of $^{35}SO_4$-labeled SG components as soon as 15 min after synthesis [16]; it is not clear how to relate $^{35}SO_4$ labeling to biosynthetic or endocytic trafficking . In the end, what controls and triggers the formation and maturation of immature SGs remains unclear. Both soluble and membrane proteins destined for the regulated secretory pathway must enter immature SGs when they exit the TGN, but how the trafficking of soluble and membrane proteins is coordinated is still under debate.

1.3 Formation of immature SGs

Proteins destined for the regulated secretory pathway are sorted in the TGN and in immature SGs. Although the sorting mechanisms are not completely understood, the diverse biophysical and biochemical properties of soluble and membrane proteins suggest that they are targeted to the regulated secretory pathway through different mechanisms. The TGN is a cellular crossroad; departing proteins can enter vesicles targeted to endosomes, lysosomes, endoplasmic reticulum or the plasma membrane [21, 1]. One of the first studies demonstrating sorting of regulated secretory proteins at the TGN was performed using a cell free system from PC12 cells, a neuroendocrine tumor cell line: vesicles budding from the TGN contained either heparin sulfate proteoglycan, a soluble protein of the constitutive secretory pathway, or secretogranin II, a soluble protein of the regulated secretory pathway [22].

1.3.1 View from the luminal side

The mildly acidic pH (pH 6.4) and high calcium (1-10 mM) environment of the TGN can induce aggregation of selected proteins (e.g., secretogranin II, chromogranin B and prolactin) destined for the regulated secretory pathway, resulting in their segregation from the constitutive secretory pathway (Figure 1.2A) [23, 24, 25]. Other regulated secretory granule proteins bind specific lipids in the TGN, resulting in their sorting and entry into immature SGs; prohormone convertase 1/3 and prohormone convertase 2 interact with lipid rafts and secretogranin III binds to cholesterol (Figure 1.2A) [26, 27, 28]. Indeed, chromogranin A, which enhances prohormone aggregation, interacts at the TGN with secretogranin III and thus with cholesterol-rich membranes (Figure 1.2A) [28, 29]. If the interaction of chromogranin A with secretogranin III is blocked, chromogranin A is not sorted correctly [30]. Finally, a role for receptor-mediated sorting of regulated secretory proteins exiting the TGN has been considered. Carboxypeptidase E was proposed as a prohormone sorting receptor because it interacts with the N-terminal region of proopiomelanocortin (POMC), which was previously reported to serve as a sorting domain [15, 31]. This conclusion is controversial because the sorting of proinsulin, luteinizing hormone and follicle stimulating hormone does not depend on carboxypeptidase E [32, 33]. Although the sorting of cargo upon binding to a receptor is an attractive concept, SG protein sorting appears to involve multiple processes. Carboxypeptidase E was recently shown to interact with phogrin, a SG membrane protein of the IA-2 (Insulinoma Associated protein 2) family; this interaction involves the pro-region of the luminal domain of phogrin and mature carboxypeptidase E (Figure 1.2B). When one binding partner is missing, the other does not accumulate in SGs, instead localizes to the perinuclear region; the sorting of carboxypeptidase E and phogrin at the TGN is

inter-dependent [34].

1.3.2 View from the cytosolic side

Sorting signals contributed by SG membrane protein trafficking.

Membrane proteins cannot aggregate as extensively as soluble proteins. The identification of trafficking signals in the cytosolic domains of endocytic cargo led to the postulate that the cytosolic domains of SG membrane proteins would carry signals to ensure their entry into immature SGs (Figure 1.2B). Indeed, deletion or mutation of the cytosolic domain of phogrin results in a decrease in its entry into SGs [35, 36]. Similar observations were made for peptidylglycine α-amidating monooxygenase 1 (PAM-1) (Figure 1.2B). PAM-1 is a bifunctional enzyme catalyzing the amidation of glycine-extended peptides, rendering them bioactive. Exogenous expression of a truncated PAM-1 protein lacking its cytosolic domain resulted in its inefficient storage in SGs. Metabolic labeling revealed that 20 to 40% of the newly synthesized truncated PAM protein entered the regulated secretory pathway, but endocytic trafficking and SG re-entry of the truncated PAM-1 protein were eliminated [37]. The cytosolic domain of PAM-1, which is highly phosphorylated, interacts with several cytosolic proteins [38]. Two sites in the cytosolic domain of PAM-1 are phosphorylated by casein kinase II (CKII) (Table 1.1); both sites were mutated to Asp (PAM-1/TS/DD) to try to mimic phosphorylation or to Ala (PAM-1/TS/AA) to prevent phosphorylation. When expressed in AtT-20 corticotrope tumor cells, exogenous PAM-1/TS/DD entered immature SGs more efficiently than PAM-1, while PAM-1/TS/AA did not enter immature SGs efficiently and was degraded [39]. This study suggests that phosphorylation of the cytosolic tail of PAM-1 enhances its entry into immature SGs.

Similar conclusions were reached in studies of two different neurotransmitter transporters, VMAT2 (Vesicular Monoamine Transporter 2) and VAChT (Vesicular Acetylcholine Transporter). Using the pH gradient established by the vacuolar proton pump, VMAT2 and VAChT translocate monoamines and acetylcholine, respectively, from the cytosol into the lumen. VMAT2 and VAChT enter two different types of vesicles in PC12 cells: VMAT2 is preferentially targeted to SGs while VAChT is found in synaptic-like microvesicles (Figure 1.2B) [40]. The cytoplasmic domain of the VAChT contains a dileucine motif with adjacent conserved Glu and Ser residues. Phosphorylation of this Ser by protein kinase C or mutation to a phosphomimetic residue results in a preference for VAChT entry into SGs, rather than into synaptic-like microvesicles [40]. Additionally, VMAT2 contains two conserved Glu residues upstream of its dileucine-like motif (Table 1.1, in blue); mutation of these Glu residues into Ala results in accumulation of VMAT2 in synaptic-like microvesicles [40].

These studies suggest that the sorting of membrane proteins into the regulated secretory pathway requires cytosolic signals and/or luminal/transmembrane signals. The negatively charged region within the cytosolic domain of membrane proteins is probably required for efficient sorting and entry into SGs. Since the cytosolic domain is involved in their sorting, cytosolic proteins must come into play in the formation of immature SGs and protein sorting in the regulated secretory pathway.

ADP ribosylation factor 1 (Arf1) is required for SG biogenesis.

In the 1990's, the cytosolic protein Arf1, a member of the ADP ribosylation family (Arf), was shown to promote the formation of immature SGs using cell-free systems from PC12 and GH3 cells, two neuroendocrine cell lines [41, 42]. Arf proteins, which belong to the

Ras superfamily of small GTPases, were originally identified as necessary for the ADP ribosylation reaction catalyzed by cholera toxin [43]. Despite their names, the cellular function of Arfs does not involve ADP ribosylation, but rather membrane trafficking [44]. Arf proteins are divided into three classes: class I (Arf1, Arf2 and Arf3), class II (Arf4 and Arf5) and class III (Arf6). Class I and class II Arfs are present at the Golgi and their main function is to regulate Golgi trafficking, while Arf6 functions at the plasma membrane and in the endocytic pathway. Arfs exist in two states: GDP-bound Arf is cytosolic and inactive while GTP-bound Arf is membrane-associated and active (Figure 1.3) [44, 45]. All Arfs contain an N-terminal myristoylated amphipathic helix, which allows their association with membranes. This region is buried in a hydrophobic pocket when GDP is bound, but becomes accessible to membranes when GTP replaces GDP, triggering conformational changes in the switch 1 and switch 2 regions which surround the nucleotide binding site [44, 46, 45]. A resident TGN protein, cargo or lipid may interact with GDP-bound Arf1, bringing it near the TGN (Figure 1.3). In the context of COPI vesicles, which are involved in retrograde transport from the Golgi to the endoplasmic reticulum, p23, a transmembrane resident Golgi protein, is thought to recruit GDP-bound Arf [47].

The removal of GDP and binding of GTP is catalyzed by a guanine nucleotide exchange factor (GEF) (Figure 1.3) [44, 45]. The two Arf GEFs identified at the TGN are BIG1 and BIG2 (brefeldin A inhibited GEFs). Interestingly, GBF1, a GEF known to be involved in the GDP/GTP exchange of Arf4 and Arf5 in the *cis*-Golgi compartment, has recently been identified on the TGN membrane [48]. BIG1 and BIG2 are recruited to the TGN membrane upon binding to GTP-bound Arf4 and Arf5, whose nucleotide exchange was mediated by GBF1 [48]. Both BIGs contain a Sec7 domain, which is the active site for the nucleotide

switch and the target of brefeldin A, a fungal product. Treatment of neuroendocrine and exocrine cells with brefeldin A blocks the formation and maturation of immature SGs but does not alter mature SG exocytosis [49, 50].

Once nucleotide exchange has occurred, GTP-bound Arf recruits adaptor proteins, enzyme modifying lipids and effectors to the membrane before reacting with a GTPase activating protein (GAP) that promotes hydrolysis of GTP to GDP and release of Arf from the membrane (Figure 1.3). The Arf-GAP family is composed of 24 members, each with a GAP domain essential for its activity on Arf [44]. GAP activity is modulated by the presence of coat proteins previously recruited by the GTP-bound Arf. When COPI is bound to Arf1, GAP activity is increased [46]. GGA3 (Golgi-localized, γ-adaptin ear-containing, Arf-binding 3) is a coat protein involved in TGN-to-endosome transport. In contrast, when Arf1 recruits GGA3, it blocks the hydrolysis of GTP-bound to Arf1 [51].

Using the cell free PC12 system, Arf1 was shown to enhance the formation of SGs and constitutive vesicles [41]. Moreover, when Arf1 is bound to membranes isolated from PC12 cells, it recruits a set of different proteins, including the adaptor protein 1A (AP-1A) [52, 53, 54]. In non-endocrine secretory systems, such as rhoptries in *Toxoplasma gondii* [55], glue granules in *Drosophila* [56] and Weibel-Palade bodies in endothelial cells [57], AP-1A is required for the formation of SGs. Although it is not clear if AP-1A is required for SG formation in neuroendocrine cells, there is evidence that AP-1A is required for SG maturation (Figure 1.4A).

Membranes and SG formation: phosphatidylinositol-4-phosphate (PI4P) and cholesterol.

The appropriate lipid composition is essential for normal TGN function and SG biogenesis. The TGN membrane is enriched in PI4P. In mammalian cells, three enzymes that synthesize PI4P from phosphatidylinositol (PI) have been found at the Golgi, PI4KIIα, PI4KIIIα and PI4KIIIβ; PI4KIIα [58] and PI4KIIIβ [59] have been implicated in export of material from the Golgi to the plasma membrane. PI4KIIα resides primarily in the TGN, endosomes and SGs [60, 61, 62, 63]. Indeed, PI4KIIα was found on adrenal chromaffin granule membranes [64, 65, 66], cellugyrin-positive Glucose Transporter 4 vesicles [67], *Drosophila* salivary gland glue granules [68], synaptic vesicles [69] and immature SG membranes from PC12 cells [70]. PI4KIIα is recruited to membranes upon palmitoylation of a central CCPCC motif [61]. Deletion of the CCPCC motif or prevention of its palmitoylation resulted in loss of PI4KIIα perinuclear localization and loss of PI4KIIα activity [61]. PI4KIIα palmitoylation is required for kinase activity and for localization to lipid rafts at the TGN but its targeting motif to Golgi membranes remains to be determined [71, 62]. Lipid rafts are enriched in cholesterol and reduction of endogenous cholesterol levels resulted in loss of PI4P synthesis by PI4KIIα [62, 72]. The membranes of neuroendocrine SGs contain high levels of cholesterol [73, 74]. A decrease in the cholesterol level in AtT-20 cells inhibited the formation of constitutive secretory vesicles and SGs [75]. Since PI4KIIα requires cholesterol for activity and membrane localization [62] and cholesterol is required for SG formation, this suggests that PI4KIIα is required for SG biogenesis.

1.3.3 Maturation of SGs

Once immature SGs are formed, they are not responsive to secretagogues and must undergo a maturation process to gain this ability. SG maturation involves a decrease in lumenal pH, SG fusion and membrane remodeling.

pH decrease

The lumen of the TGN and the lumen of immature SGs are comparable in pH (pH 6.3), while mature SGs are more acidic (luminal pH 5.5). Secretogranin II processing in PC12 cells exogenously expressing prohormone convertase 2 occurs in immature SGs but not in the TGN [76]. Although similar in lumenal pH, the TGN and immature SGs are two distinctly different compartments; the proteolytic processing of some prohormones and granins starts in immature SGs, not in the TGN. The decrease in pH during SG maturation is necessary for full processing of prohormones and granins because some hormone processing enzymes, such as PAM-1, exhibit maximal catalytic activity at pH 4.5-5 [77].

SG fusions

Maturation of SGs can be characterized by a decrease or an increase in size. Analysis of immature and mature SGs in PC12 cells and mammotrophs revealed an increase in SG size during maturation [78, 16]. An elegant biochemical assay revealed that the increase of SG size in PC12 cells was due to homotypic fusion of immature SGs [11]. SG fusion involves syntaxin 6, a target (t)-SNARE (SNAP [Soluble NSF (N-ethylmaleimide-Sensitive Factor) Associated Protein] Receptor) protein and synaptotagmin IV [79, 80]. The SNARE complex is involved in membrane fusion and is composed of two t-SNAREs, located on the

target membrane, and one vesicle (v)-SNARE on the vesicle membrane. Members of the synaptotagmin family are associated with the vesicular membrane and regulate membrane fusion with the SNARE complex. Syntaxin 6 localizes to the TGN, endosomes and immature SGs [81, 82], while synaptotagmin IV is largely present at the Golgi and in immature SGs [83, 84]. Blocking the fusion event decreases prohormone convertase 2 processing and activity, resulting in impaired SG maturation [79]. Although this concept is attractive, there is no evidence of SG fusion in other types of neuroendocrine cells. SG fusion of a different type is clearly observed during compound exocytosis; mature SGs fuse together to promote rapid release of SG content [85].

Membrane remodeling

The reduction of SG size during maturation may be explained by membrane remodeling. The presence of a clathrin coat on patches of immature SG membrane revealed egress of material in clathrin-coated vesicles, mediated by the adaptor protein, AP-1A [53, 8, 9]. As a result, proteins like VAMP4 [86, 87], furin [88] and both mannose 6-phosphate receptors [89, 82, 90, 91], each of which is known to have a canonical AP-1A binding site in its cytosolic domain, are found in immature SGs but not in mature SGs. Although the fate of the material retrieved from immature SGs is not entirely clear, there are lines of evidence suggesting that it can be recycled to the TGN or secreted in a process called constitutive-like secretion (Figure 1.1). The study of constitutive-like secretion is difficult to monitor since it refers only to the non-stimulated secretion of regulated SG proteins as they traverse immature SGs; without a means of assessing the time since synthesis, it is impossible to distinguish basal from constitutive-like secretion. Nevertheless, constitutive-like secretion has held

many scientists' attention due to its potential link to cancer and metabolic disease. Much of our knowledge of constitutive-like secretion comes from studying retrieval of material from immature SGs. The cytosolic machinery involved in this process contains the adaptor proteins, AP-1A and GGAs, and their partner PACS-1. The discovery of an interaction between the cytosolic tail of membrane SG proteins retrieved during SG maturation with these cytosolic proteins has expanded our understanding of membrane remodeling during SG maturation. Each cytosolic component essential for maturation is presented below, followed by the description of SG membrane proteins trafficking involving AP-1A, GGAs or PACS-1.

1.4 Cytosolic Machinery

1.4.1 Adaptor protein 1A (AP-1A)

The adaptor protein (AP) family.

The AP family includes five cytosolic heterotetrameric complexes: AP-1 (γ/β1/μ1/σ1), AP-2 (α/β2/μ2/σ2), AP-3 (δ/β3/μ3/σ3), AP-4 (ϵ/β4/μ4/σ4) and AP-5 (ζ/β5/μ5/σ5) [92, 93, 94, 95]. In mammals, several isoforms have been reported for subunits of AP-1, AP-2 and AP-3: AP-1 has two γ subunits (γ1 and γ2), two μ subunits (μ1A and μ1B) and three σ subunits (σ1A, σ1B and σ1C); AP-2 has two α subunits (α1 and α2); AP-3 has two β subunits (β3A and β3B), two μ subunits (μ3A and μ3B) and two σ subunits (σ3A and σ3B) [92, 96, 97, 98, 99, 100]. Every subunit is ubiquitously expressed except for μ1B, which is found exclusively in polarized epithelial cells, and β3B and μ3B, which are only found in neurons and neuroendocrine cells [97, 101, 99]. Each AP carries transmembrane proteins on a defined intracellular route: AP-1 brings cargo between the TGN and endosomes and removes

material from immature SGs; AP-2 is an important player in clathrin-mediated endocytosis; AP-3 carries cargo to lysosomes and lysosome-related organelles; AP-4 transports cargo from the TGN to the plasma membrane or endosomes; AP-5 is found on late endosomal membranes.

The cytosolic domains of cargo proteins present motifs which are recognized by AP complexes. For example, the Tyr sorting motif (YXXϕ, where X is any residue and ϕ is a hydrophobic residue) is recognized by the μ subunit of all AP complexes, with the possible exception of AP-5, which has not yet been studied (Figure 1.4A) [102, 103, 104, 98]. The dileucine sorting motif [(D/E)XXXL(L/I)] interacts at the interface of two subunits: γ/σ1 in AP-1, α/σ2 in AP-2 and ϵ/σ3 in AP-3 (Figure 1.4A) [105, 106]; AP-4 and AP-5 have not been shown to interact with the dileucine motif. The γ/α/δ/ϵ/ζ and β1-5 subunits contain a large N-terminal trunk domain that associates with the other three subunits of the complex, followed by a hinge region and a C-terminal ear domain, which can interact with cytosolic proteins (Figure 1.4A) [107, 108, 109, 110]. The hinge region of the β subunits of AP-1, AP-2 and AP-3 is capable of binding the terminal domain of the clathrin heavy chain *in vitro*, while the β subunits of AP-4 and AP-5 lack such a motif (Figure 1.4A) [111, 112, 113]. Although the β3 subunit of AP-3 can bind clathrin, purified clathrin-coated vesicles lack AP-3, suggesting that AP-3 works independently of clathrin [114]. In addition, there is also evidence that the γ and α hinge domains of AP-1 and AP-2 interact with clathrin (Figure 1.4A) [115, 116].

AP-1A recruitment to membranes depends on Arf1 and PI4P.

AP-1A (γ/β1/μ1A/σ1) accumulates at the TGN, which is enriched in PI4P. *In vitro* binding assays revealed that purified AP-1A interacts preferentially with PI4P (Figure 1.4A) [58]. Indeed, structural studies on the AP-1A core confirmed the presence of a PI4P binding site within the γ subunit [117]. Reduction of PI4KIIα levels in a monkey kidney cell line decreased the TGN content of PI4P and disrupted the TGN localization of AP-1A [58]. However, a recent study on development of the *Drosophila* salivary gland revealed no change in the localization of AP-1 in PI4KIIα null flies, suggesting that PI4P synthesis in flies can be carried out by another PI4K [68]. Although the presence of PI4KIIα on the membranes of immature SGs suggests that PI4P can be formed there, there is no evidence that AP-1A recruitment to immature SGs requires PI4P in neuroendocrine cells.

Brefeldin A treatment of intact cells produces a diffuse cytoplasmic localization of AP-1A instead of the normal perinuclear, membrane-associated localization. However, pretreatment with GTPγS, a non-hydrolyzable analog of GTP, prevented the membrane dissociation of AP-1A upon addition of brefeldin A in permeabilized normal rat kidney cells [118]. Indeed, AP-1A is recruited to membranes upon the binding of GTP-bound Arf1 to the trunk region of its β1 and γ subunits (Figure 1.4A) [52, 119, 120, 121]. Studies on PC12 cells also show that AP-1A recruitment to immature SG membranes requires Arf1 [52, 53]. Interestingly, AP-1A cannot be recruited to mature SG membranes in PC12 cells, in agreement with morphological studies indicating that AP-1A/clathrin coats are not found on mature SGs [52]. A recent structural study of AP-1A in complex with GTP-bound Arf1 revealed that Arf1 can change the conformation of μ1A without the presence of PI4P or cargo; the addition of cargo promotes this conformational change [119]. This shift in μ1A conformation is thought to promote the

association of μ1A with cargo.

In addition to Arf1 and PI4P, AP-1A phosphorylation affects its localization; cytosolic AP-1A is phosphorylated on its β1 subunit, while membrane associated AP-1A is phosphorylated on its μ1A subunit [122]. Phosphorylation of the β1 subunit prevents clathrin binding, while phosphorylation of μ1A may promote conformational changes in the subunit that enable it to interact with cargo [123, 117]. The phosphorylation status of AP-1A is thus essential for protein trafficking.

1.4.2 Phosphofurin Acidic Cluster Sorting Protein 1 (PACS-1) – an enhancer of AP-1A function.

AP-1A is not the only adaptor protein involved in the retrieval of material from immature SGs. Furin, a type I transmembrane endoprotease, cleaves peptides after the last Arg of an R-X-[K/R]-R motif; its discovery was a key advance contributing to the identification of the prohormone convertases that are essential to SG function. Furin is concentrated in the TGN and travels between the TGN, endosomes and plasma membrane [124]. In cells containing a regulated secretory pathway, furin was identified in immature SGs but not in mature SGs [88]. The removal of furin from immature SGs involves AP-1A and clathrin-coated vesicles [88]. Its cytoplasmic domain contains a Tyr-based sorting motif and an acidic cluster, which includes two Ser residues, both of which are substrates for CKII (Table 1.1) [125, 126]. The Tyr motif found in the cytosolic domain of furin mediates TGN exit and plasma membrane internalization; the acidic cluster is important for retrieval of furin from endosomes and immature SGs [88, 127, 126]. Mutation of the two CKII phosphorylation sites in furin to Ala (to prevent phosphorylation) resulted in the accumulation in mature SGs in a corticotrope

tumor cell line [128, 88]. Since AP-1A does not bind to acidic clusters, another interactor was sought. A search for proteins with high affinity for the phosphorylated acidic cluster through yeast two-hybrid screens led to the discovery of Phosphofurin Acidic Cluster Sorting protein 1 (PACS-1) [126].

PACS-1 is a ubiquitously expressed cytosolic protein comprised of four domains: at its N-terminus is an ARR (atrophin-1-related region), with limited homology to atrophin-1; this region is followed by a furin binding region (FBR), the middle region (MR) and the C-terminal region (CTR) (Figure 1.4B) [126]. The functions of the ARR and the CTR are unknown. The FBR of PACS-1 interacts with acidic clusters in cargo proteins, with adaptor proteins (AP-1A, AP-3 and GGA) and with CKII (Figure 1.4B) [128, 129, 126]. The MR contains an autoinhibition domain, which is composed of an acidic cluster with a CKII phosphorylation site (Figure 1.4C); when this region is not phosphorylated, the MR binds the FBR, resulting in inhibition of PACS-1 binding to its cargo [130]. When the MR is phosphorylated by CKII, it reduces MR affinity for FBR, allowing the FBR to bind to acidic clusters in cargo proteins [129, 130]. Furin has been identified in a heterotrimeric complex with AP-1A and PACS-1 [128]. Expression of a PACS-1 mutant capable of binding the furin acidic cluster, but not AP-1A, does not alter the distribution of AP-1A, instead resulting in the accumulation of furin in mature SGs [128]. This demonstrates that removal of furin from immature SGs is a cooperative process involving both AP-1A and PACS-1 (Figure 1.5).

1.4.3 GGAs – another family of adaptor proteins essential for SG maturation.

Golgi-localizing, γ-adaptin ear homology domain, ARF-binding proteins (GGAs) were discovered by several groups interested in different aspects of the proteins. Boman et al.

screened for Arf3 binding partners using a yeast two-hybrid system, while Hirst et al. used a bioinformatic approach to look for proteins with homology to the ear region of the γ subunit of AP-1 [131, 108]. These studies, combined with the fact that the proteins discovered concentrated in the TGN area, explain the origin of the name GGA [132, 108]. The GGA family contains three members in humans (GGA1, GGA2 and GGA3), two in Saccharomyces cerevisiae (Gga1p and Gga2p), and one in *Drosophila* melanogaster and *Caenorhabditis elegans* [131, 133, 108]. Each member is ubiquitously expressed and acts as a monomeric clathrin adaptor [131, 134]. From their N-terminus to their C-terminus, they are composed of a VHS (Vps27, Hrs, Stam) domain, a GAT (GGA and TOM) domain, a hinge and a GAE (γ-adaptin ear) domain (Figure 1.4D) [133].

The VHS domain was identified based on its role in the trafficking of yeast Vps27p (Vacuolar Protein Sorting 27) and for its homology to two other monomeric endosome-localized clathrin adaptor proteins, Hrs (Hepatocyte-growth factor-receptor substrate) and Stam (Signal-Transducing Adaptor Molecule) [131, 108, 135]. A yeast two-hybrid screen revealed that the cytosolic domains of proteins containing either a tyrosine sorting motif (YXXϕ) or a dileucine sorting motif [(D/E)XXXL(L/I)] were not recognized by any GGA proteins, but were specific to AP complexes [125, 136]. The VHS domain of GGAs recognize a motif called acidic cluster-dileucine motif (DXXLL), which is different from the AP dileucine sorting motif [(D/E]XXXL(L/I)] (Figure 1.4D) [133, 136].

TOM1 (Target of Myb1), a protein involved in the trafficking of ubiquitinated proteins, contains a GAT domain similar to the GAT domain in GGAs. Indeed, both yeast Gga1p and mammalian GGAs bind monoubiquitin via their GAT domain [137, 133, 138, 139, 140]. This interaction is required for the sorting of some ubiquitinated cargo proteins in S. cerevisiae,

such as Gap1 and Arn1 [137, 133, 141, 142]. The GAT domain interacts with GTP-bound Arf1 and Arf3 and the C-terminus of GAT binds PI4P; as for AP-1A, both binding sites are required for proper membrane localization of GGA in cells (Figure 1.4D) [131, 132, 140]. Indeed, brefeldin A treatment results in the dissociation of GGAs from TGN membranes and in their accumulation in the cytosol, as seen for AP-1A [131, 132, 108, 134]. Interestingly, association of the GAT domain of GGA3 to Arf1 blocks GAP proteins from acting on GTP-bound Arf1, thus stabilizing it on TGN membranes [51].

The hinge region between the GAT and the GAE domains is predicted to lack secondary structure [133] and contains a clathrin binding motif which is necessary for the recruitment of clathrin *in vitro* and in cells (Figure 1.4D) [108, 51]). While the GAE domain of GGA1 also interacts with clathrin heavy chain *in vitro*, the GAE domains of GGA2 and GGA3 are unable to do so [51]. GGAs are important for the recruitment of clathrin to membranes; overexpression of GGAs increases the TGN localization of clathrin while overexpression of truncated GGA1 lacking the hinge and GAE domains reduces the TGN level of clathrin [51]. Moreover, *in vitro* studies revealed that the GGA1-hinge region and the γ subunit of AP-1 interact (Figures 1.4, A and D) [143, 107]. In addition, the hinge region of both GGA1 and GGA3 contains a DXXL[L/M] motif, which can bind the VHS domain when the surrounding Ser residue has been phosphorylated by CKII (Figures 1.4, D and E) [144, 107]; this internal binding results in autoinhibition of the adaptor protein by loss of cargo binding [144, 107, 122]. The autoinhibition is removed when the Ser residue is dephosphorylated by a protein phosphatase 2A-like enzyme [145]. *In vitro* phosphorylation by CKII was not observed for GGA2, suggesting that GGA2 is controlled differently [125, 144]. Although the autoinhibition concept is attractive, a recent structural report refutes the existence of such a

motif within GGA1 and possibly within GGA3 as well [146]. These conflicting results are currently unclear, but emphasize the fact that our knowledge of GGAs is incomplete.

The GAE domain has homology to the ear domain of γ-adaptin of AP-1 [131, 132, 108, 134, 147]. It interacts with several cytosolic proteins including rabaptin-5, a Rab4/Rab5 effector involved in membrane fusion at the endosomes [108, 148, 149] and γ-synergin [147].

In neuroendocrine cells, reducing the levels of GGA3 or overexpressing a dominant negative form of GGA1 resulted in impaired egress of syntaxin 6, cation-independent mannose 6-phosphate receptor and VAMP4 from immature SGs and in decreased proteolytic processing of prohormone convertase 2 and secretogranin II [150]. Thus GGAs, AP-1A and PACS-1 are all key components in the maturation of SGs in neuroendocrine cells.

1.4.4 Do GGAs and AP-1A work together?

Despite differences in their cargo recognition motifs, GGAs and AP-1A are both recruited to TGN membranes in an Arf1 and PI4P dependent manner, interact with clathrin and share common cargoes, such as cation independent mannose 6-phosphate receptor (Table 1.1). Using transmission electron microscopy, vesicles budding from the TGN were seen to contain one adaptor protein or both GGA2 and AP-1A [144] . A novel technique developed in mammalian cells to rapidly inactivate AP-1A or GGA2 revealed that AP-1A is the main adaptor protein required for trafficking between the TGN and endosomes; when AP-1A is inactivated, GGA2 is no longer present in clathrin-coated vesicles [151]. In addition, GGA2 is thought to be required for proper localization of rabaptin-5, a group of lysosomal hydrolases, both types of mannose 6-phosphate receptors and sortilin in clathrin-coated vesicles. Other substrates, such as Arf1, carboxypeptidase D, furin, the copper transporters (ATP7A and

ATP7B) or the SNARE proteins require AP-1A for localization in clathrin-coated vesicles [151]. In agreement with these data, mutation of the GGA binding site in the cytosolic tail of the cation independent mannose 6-phosphate receptor decreases its amount in clathrin coats at the TGN, suggesting that GGAs help recruit specific cargo with adaptor proteins and clathrin [144]. However, a recent study in yeast using fluorescently tagged proteins suggested that the Gga proteins come into play first, and then recruit other proteins along with AP-1A after being released from the membrane [152]. The yeast study also suggested that AP-1 and Gga proteins work mainly in separate vesicles. This divergence between yeast and mammals is unclear and may be linked to changes during evolution. Nevertheless, these studies do not provide information on the mechanism which governs the egress of material at the immature SG. In addition, yeast do not have a regulated secretory pathway, limiting their use in understanding SG maturation.

1.5 Real life examples

Most of the integral membrane proteins found in post-TGN membranes contain multiple signaling motifs in their cytosolic tails. The study of protein retrieval from immature SGs was facilitated by our growing knowledge of adaptor proteins and the motifs they recognize. While our understanding of the rules governing retention vs. retrieval of membrane proteins from immature SGs is not yet complete, detailed studies of the interactions of several immature SG cargo protein cytosolic tails with multiple adaptor proteins reveals many of the key features (Figure 1.5 and Table 1.1).

1.5.1 SNARE proteins

Similar observations to furin were made with the v-SNARE component, VAMP4 (Vesicle Associated Membrane Protein 4), which contains an AP-1A binding motif (di-leucine sorting motif) and an acidic cluster surrounding a CKII phosphorylation site (Table 1.1) [86]. VAMP4 accumulates at the TGN, on endosomes and on immature SGs of PC12 and AtT-20 cell lines [86, 153]. As for furin, overexpression of a PACS-1 mutant unable to interact with AP-1A but capable of interacting with VAMP4 resulted in accumulation of VAMP4 in mature SG [86]. Interestingly, VAMP4 accumulates in mature SGs only if both the AP-1A and the PACS-1 binding motifs are mutated; if either binding motif is remaining, VAMP4 is efficiently removed from immature SGs [86]. This is different from furin which accumulated in mature SGs when the CKII sites were mutated. The AP-1A/PACS-1/clathrin sorting system seems to work differently with VAMP4 and furin.

In addition, VAMP4 interacts with syntaxin 6, which binds synaptotagmin IV [79, 153]. All three proteins are retrieved from immature SGs [83, 82, 153]. Although *in vitro* studies failed to show binding between syntaxin 6 and AP-1A [86], observation of immature SGs using electron microscopy showed that syntaxin 6 is retrieved in AP-1A and clathrin containing vesicles [82]. It remains unclear whether synaptotagmin IV interacts with AP-1A, but since the removal of VAMP4 and syntaxin 6 has been linked with AP-1A, it seems likely that synaptotagmin IV removal is also dependent on the AP-1A/PACS-1/clathrin sorting system due to its indirect binding with VAMP4. Interestingly synaptotagmin IV is known to inhibit calcium triggered exocytosis [83], suggesting that its removal is necessary to make mature SG responsive to secretagogues. Since synaptotagmin IV plays a critical role in SG fusion, which is an essential step in SG maturation, these studies would suggest that SG fusion occurs

before membrane remodeling.

1.5.2 The mannose 6-phosphate receptors

Mannose 6-phosphate receptors (MPRs) transport soluble lysosomal hydrolases from the TGN to endosomes [154, 136]. MPRs are found in immature SGs and are removed during maturation in clathrin-coated vesicles that contain AP-1A [82]. Two MPRs have been described: MPR300, the cation-independent MPR (CI-MPR), and MPR46, the cation-dependent MPR (CD-MPR). Much has been learned by studying the multiple trafficking signals in both MPRs. Both MPRs contain Tyr sorting motifs (YXXϕ) and an acidic cluster-dileucine motif (DXXLL) next to a CKII phosphorylation site (Table 1.1). Early studies revealed that the Tyr motif of CI-MPR is recognized by AP-2 but not by AP-1A [155]. CD-MPR contains two tyrosine motifs: the first tyrosine motif is located next to the transmembrane domain, and may not be a signaling motif because of the hindrance caused by the membrane (Table 1.1, Y^{211}QRL). The second tyrosine motif is found away from the membrane (Table 1.1, Y^{256}RGV) and is implicated in the protein internalization [156].

The DXXLL motif is recognized by the VHS domain of GGAs [136, 149]. Interestingly, the DXXLL motif found on the cytosolic tail of the CI-MPR binds the VHS domain of all GGAs while the DXXLL motif of the CD-MPR interacts with the VHS domain of GGA1, interacts weakly with GGA3 and does not interact with GGA2 [136, 149]. Mutational analyses revealed that the residues surrounding the motif are important for establishing GGA specificity [136]. Down-regulation of GGA3 or inhibition of GGA1 results in the accumulation of CI-MPR in mature SGs, suggesting that retrieval of CI-MPR from immature SGs requires GGAs [150].

Independent *in vitro* studies focusing on either CD-MPR or CI-MPR showed that removal of the dileucine motif from either receptor had little effect on its ability to recruit AP-1A. In CI-MPR, elimination of the CKII phosphorylation site abolished recruitment of AP-1A [89, 126]. Indeed, binding of AP-1A to CI-MPR requires prior phosphorylation of its cytosolic domain by CKII [90, 157]. These features suggested that PACS-1 might be involved in the trafficking of CI-MPR. In non-neuroendocrine cells, reducing the cellular level of PACS-1 or overexpressing a PACS-1 mutant unable to interact with acidic clusters resulted in accumulation of CI-MPR in endocytic compartments, suggesting that PACS-1 recruitment is necessary for MPR retrieval from the endosomes to the TGN [128, 126]. AP-1A binding to CD-MPR requires the acidic cluster; experiments aimed at understanding the role of phosphorylation at the Ser CKII site in CD-MPR in its binding of AP-1A have yielded conflicting results (Table 1.1, Ser268) [90, 158]. It is not yet known whether MPRs are retrieved from immature SGs in a PACS-1 dependent manner.

GGA and PACS-1 interact with the CI-MPR at sites that are overlapping, but not identical (Table 1.1) [129]. The FBR region of PACS-1 binds CKII, enhancing its kinase activity [129]. This results in phosphorylation of the MR of PACS-1, releasing the FBR for cargo interaction (Figure 1.4C). In addition, CKII phosphorylates GGA3, decreasing its affinity for cargo and thus making space for PACS-1 to bind (Figures 1.4E and 1.5B) [129]. Although this study did not focus on immature SGs, it provides a mechanism of how GGA and AP-1A/PACS-1 are necessary for SG maturation.

1.5.3 Carboxypeptidase D (CPD) binds AP-1A

The exopeptidase CPD, a type I transmembrane protein, accumulates in the TGN and cycles between the TGN and plasma membrane via endosomes [159]. In AtT-20 cells, CPD is found in immature, but not in mature SGs suggesting that it is removed during SG maturation [160]. The isolated luminal domain of CPD primarily enters the constitutive secretory pathway, suggesting that signals in its cytosolic tail play an essential role in CPD entry into immature SGs and in the TGN retention of CPD [160]. The CPD cytosolic tail contains an acidic cluster with two CKII phosphorylation sites (TDT), but lacks classical AP and GGA binding motifs (Table 1.1). *In vitro* binding assays revealed that the CPD cytosolic tail binds to AP-1A and AP-2 only when its two CKII phosphorylation sites are phosphorylated or have been mutated to phosphomimetic residues (EDE) (Table 1.2) [161]. Deletion of the C-terminus of the CPD tail, which contains the CKII phosphorylation sites does not abolish AP-1A or AP-2 binding (Table 1.2) [161], suggesting a role for additional CPD/AP-1A/2 interaction motifs. A tyrosine-like motif (Table 1.2, F^{1332}HRL) located upstream of the acidic cluster is thought to be important for TGN export and endocytosis and is necessary for AP-1A and AP-2 binding [161]. In addition, the C-terminus of CPD may bind another cytosolic protein which would prevent adaptor proteins interactions. This unidentified protein probably loses its affinity for the C-terminus of CPD when the CKII sites are phosphorylated or removed, allowing adaptor proteins to interact. Phosphorylation of CPD by CKII promotes AP-1A binding, suggesting that PACS-1 plays a role in its trafficking. The trafficking of CPD at immature SGs probably results from the coordinated work of multiple cytosolic proteins including AP-1A and PACS-1.

1.5.4 VMAT2 suggests the existence of additional adaptor proteins

The monoamine transporter, VMAT2, accumulates in mature SGs in neuroendocrine cells. Its cytosolic domain contains an acidic cluster with two CKII sites at the C-terminus; upon CKII phosphorylation, this site interacts with PACS-1 [162]. As for furin, expression of VMAT2 in which the CKII sites have been replaced with phosphomimetic mutations promotes its retrieval from immature SGs. Mutation of these same two residues into Ala to prevent phosphorylation promotes VMAT2 accumulation in mature SGs [162]; interestingly, expression of VMAT2 lacking the acidic cluster/CKII domain resulted in its egress from immature SGs [162]. Unlike furin, which accumulates in the TGN at steady state, VMAT2 concentrates in mature SG raising the question of VMAT2 retention mechanism. These findings suggest that additional cytosolic proteins are involved in the sorting of SG proteins at the immature SG and may explain the retention of other membrane proteins in SGs during maturation. Indeed the amidating enzyme, PAM, remains in SGs during maturation and presents an acidic cluster with two CKII phosphorylation sites [38]. Although direct binding between PAM cytosolic domain and PACS-1 has not been shown, it is possible that PAM interacts with the same cytosolic proteins which bind VMAT2 for its retention in SG.

1.5.5 Phogrin

Phogrin is a transmembrane protein that spans the membrane of immature and mature SGs. The cytosolic domain of phogrin contains a protein-tyrosine phosphatase-like (PTP) domain preceded by a 105 residue-long domain and followed by 10 residues at its C-terminus (Figure 1.2B and Table 1.1). The PTP domain of phogrin is an active phosphatidylinositol (PI) phosphatase; its enzymatic activity is thought to play an essential role in its ability to regulate

peptide hormone secretion [163]. Both domains surrounding the PTP domain are involved in the correct sorting of phogrin in the regulated secretory pathway [35, 36]. The 105 residue stretch close to the transmembrane domain contains a tyrosine-extended motif (Table 1.1, Y^{655}QEL) and the 10 residues at the C-terminus present a dileucine-like motif (Table 1.1, E^{993}EVNAIL). Both motifs are required for entry of phogrin into SGs and internalization at the plasma membrane [35, 36]. Interestingly, both motifs are involved in the binding of phogrin to AP-1A and AP-2. Mutation of one of these motifs decreases the binding strength of adaptor proteins for phogrin but does not abolish the interaction [35, 36]. Although phogrin binds AP-1A via unconventional motifs, it still remains to be determined what prevents this transmembrane protein from being removed during SG maturation.

1.5.6 Sortilin and pro-BDNF

Sortilin, a type I transmembrane protein, binds the pro-region of brain-derived neurotrophic factor (pro-BDNF) and transports it to SGs for processing [164]. As for CPD, expression of the luminal domain of sortilin results in its entry into the constitutive secretory pathway, suggesting that entry into SGs is mediated by the cytosolic tail [165]. A recent study revealed that interaction of sortilin with Huntingtin associated protein 1 (HAP-1) and pro-BDNF must occur for pro-BDNF entry into SGs and subsequent proteolytic processing [166]. In the absence of HAP-1, sortilin and pro-BDNF are targeted to lysosomes. Interestingly, the cytosolic tail of sortilin contains both a tyrosine motif and an acidic cluster-dileucine motif, classical AP and GGA binding sites, respectively (Table 1.1). Both motifs are implicated in sortilin internalization [167]. As expected, the VHS domain of GGA2 interacts with the acidic cluster-dileucine motif of sortilin [167]. However, the tyrosine motif is recognized by

the retromer complex, not by AP-1A [168]. The AP-1A binding motif on sortilin remains to be elucidated. Both GGA2 and AP-1A were shown to be important for the TGN-to-endosome transport of sortilin. It is possible that HAP-1 interacts with sortilin to prevent GGA and AP-1A binding and mediates the entry of sortilin and pro-BDNF into SGs. Although sortilin contains adaptor protein binding motifs, it is not clear if sortilin is retrieved from immature SGs. One could assume that once in immature SGs, sortilin can release pro-BDNF and be retrieved during SG maturation.

1.6 Conclusions and future directions

Little is known about the cytosolic machinery involved in sorting membrane proteins at the TGN for their entry into immature SGs. A recent study in *Drosophila* suggested that AP-3, the adaptor protein transporting proteins to lysosomes, was involved in sorting proteins into the regulated secretory pathway at the TGN level [169]. Unfortunately, it is not known whether this is also true in the mammalian neuroendocrine system. In addition, studies on the trafficking of individual proteins raises many questions regarding the cytosolic machinery necessary for their retrieval or retention during SG maturation. It remains to be explained how a membrane protein which contains an adaptor protein (AP-1A, PACS-1 or GGAs) binding motif can remain in SGs during maturation. One possibility is that other cytosolic proteins bind the tails of membrane proteins, preventing their interaction with adaptor proteins. Recent proteomic studies on purified SGs are an excellent source of information and may help identify additional proteins involved in the egress of membrane proteins [170, 171]. Another possibility is a binding site within the cytosolic tail of membrane proteins which could prevent adaptor protein interaction; a post-translational modification, such as phosphorylation, can

abolish this internal interaction while promoting the interaction with adaptor proteins. Lastly, the membrane of the immature SG may play an important role in concentrating membrane proteins to be removed during maturation. Katsumata et al. addressed this question using the rat parotid gland as a source of SGs. The immature SG membrane revealed spatial segregation of membrane proteins: VAMP2 and Rab3D were in GM1a rich microdomains, while syntaxin 6 and VAMP4 were not. Since VAMP2 and Rab3D remain in mature SGs while syntaxin 6 and VAMP4 are removed from immature SGs, membrane rearrangement could explain how the right proteins are sorted for retrieval of material at the immature SG [172]. The trafficking of individual proteins found in immature SGs can differ based on the cell type or animal model. It is evident that professional secretory cells share a common mechanism, and that the differences they present are probably required for their physiological function.

1.7 Acknowledgements

This work was supported by National Institutes of Health Grants DK32948 and DK32949. We thank Dr. Vishwnatha Kuruthihalli and Dr. Yan Yan for thoughtful comments on the manuscript.

1.8 Tables

Protein	Host	ID	Amino acid sequence of the cytosolic tail
Furin	Rat	P23377.1	*TMD* H^{736}RCSGFSFRGVKVYTMDRGLISYKGLPPEAWQEECP**S**D**S**EEDEGRGERTAFIKDQSAL^{793} *COOH*
PAM	Rat	P14925.1	*TMD* R^{891}WKKSRAFGD^{900} […]Y^{936}SRKGFDRVS**T**EG**S**DQEKDEDDGTESEEEYSAPLPKPAPSS^{976} *COOH*
Phogrin	Rat	NP_113788.1	*TMD* A^{625}YCLRHN^{631} […] A^{645}DPSADATEAYQELCRQRMAVRPQ^{668} […] E^{993}EVNAILKALPQ^{1004} *COOH*
CPD	Rat	NP_036968.1	*TMD* C^{1319}ICSIKSNRHKDGFHRL^{1335} […] S^{1356}LLSHEFQDE**T**D**T**EEETLYSSKH^{1378} *COOH*
Sortilin	Rat	O54861.3	*TMD* V^{776}KKYVCGGRFLVHRYSVLQQHAEADGVEALDTASHAKSGYHDD**S**DEDLLE^{825} *COOH*
VAMP4	Mouse	O70480	*NH_2* M^{1}PPKFKRHLNDDDVTGSVKSERRNLLEDD**S**DEEEDFFLRGPSGPRF^{46} […] R^{112}GCKIKAI^{119} *TMD*
VMAT2	Rat	Q01827.2	*TMD* F^{464}APLCFFLRSPPAKEEKMAILMDHNCPIKRKMYTQNNVQSYPIGDDEE**S**E**S**D^{515} *COOH*
CI-MPR	Mouse	Q07113.1	*TMD* H^{2317} […] C^{2333}RRSSGVSYKYSKVSKEEETDENETE^{2358} […] V^{2478}SFHDD**S**DEDLLHI^{2493} *COOH*
CD-MPR	Mouse	Q6AY20	*TMD* L^{210}YQRLVVGAKG^{220} […] R^{250}SVPAAYRGVGDDQLGEE**S**EERDDHLLPM^{278} *COOH*

Table 1.1: Summary of known motifs for membrane proteins in SGs. Protein, host and ID are shown. Acidic clusters are in red. CKII sites are in bold. AP-1 and AP-1-like sites are in blue and GGA sites are underlined in green. TMD, transmembrane domain; COOH, C-terminus of the protein; NH2, N-terminus of the protein.

Protein	Sequence	AP-1 binding?
CPD-tail full, not phosphorylated	*TMD* C^{1319}ICSIKSNRHKDGFHRL^{1335} […] S^{1356}LLSHEFQDE**T**D**T**EEETLYSSKH^{1378} *COOH*	-
CPD-tail full, phosphomimetic	*TMD* C^{1319}ICSIKSNRHKDGFHRL^{1335} […] S^{1356}LLSHEFQDE**E**D**E**EEETLYSSKH^{1378} *COOH*	++
CPD-tail missing the last 18 residues	*TMD* C^{1319}ICSIKSNRHKDGFHRL^{1335} […] S^{1356}LLSH^{1360} *COOH*	+

Table 1.2: Summary of mutational analysis of CPD-tail. Results adapted from [161]. TMD, transmembrane domain; COOH, C-terminus of the protein.

1.9 Figures

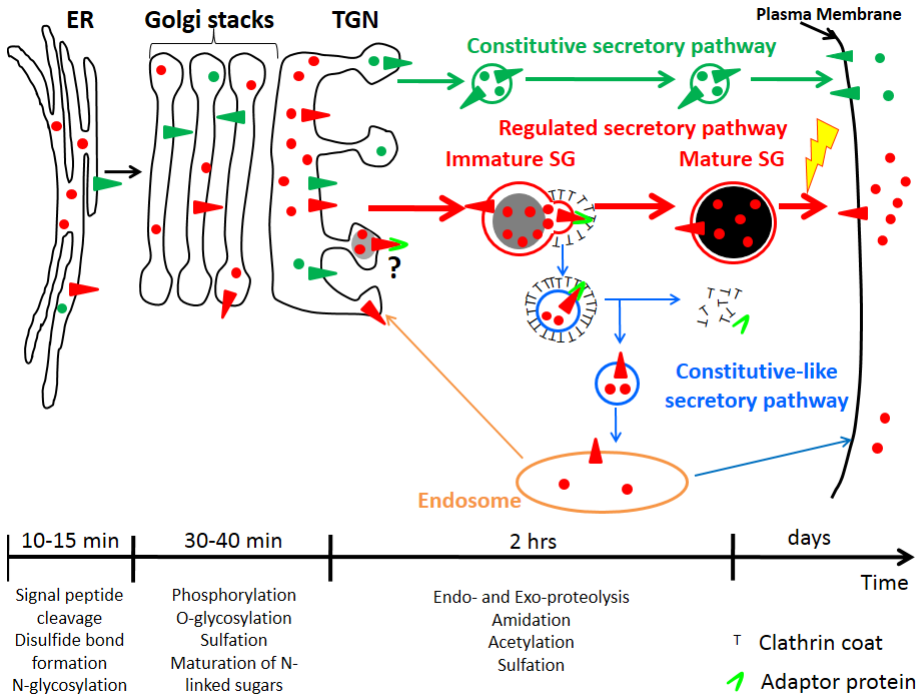

Figure 1.1: Constitutive and regulated secretory pathways. Soluble and membrane proteins are represented with circles and triangles, respectively. Constitutive secretory pathway proteins are green; regulated secretory pathway proteins are red. Examples of post-translational modifications that occur in each organelle are shown. The time-scale is representative of the time spent by hormones and hormone processing enzymes in each organelle of the regulated secretory pathway. Until newly synthesized proteins reach the *trans*-Golgi network (TGN), proteins from both secretory pathways share the same compartments. Secretory proteins are sorted into constitutive secretory vesicles or immature secretory granule (SGs) in the TGN. Immature SGs undergo a maturation process to become mature SGs. The yellow lightning bolt represents the external stimulus triggering secretion of mature SG content. The maturation process involves remodeling of immature SG membranes, generating the constitutive-like secretory pathway (blue); the fate of the vesicles leaving immature SGs is not clear; return to an endosomal compartment from which proteins can be secreted in a constitutive-like fashion or recycled to the TGN is shown. ER, Endoplasmic Reticulum.

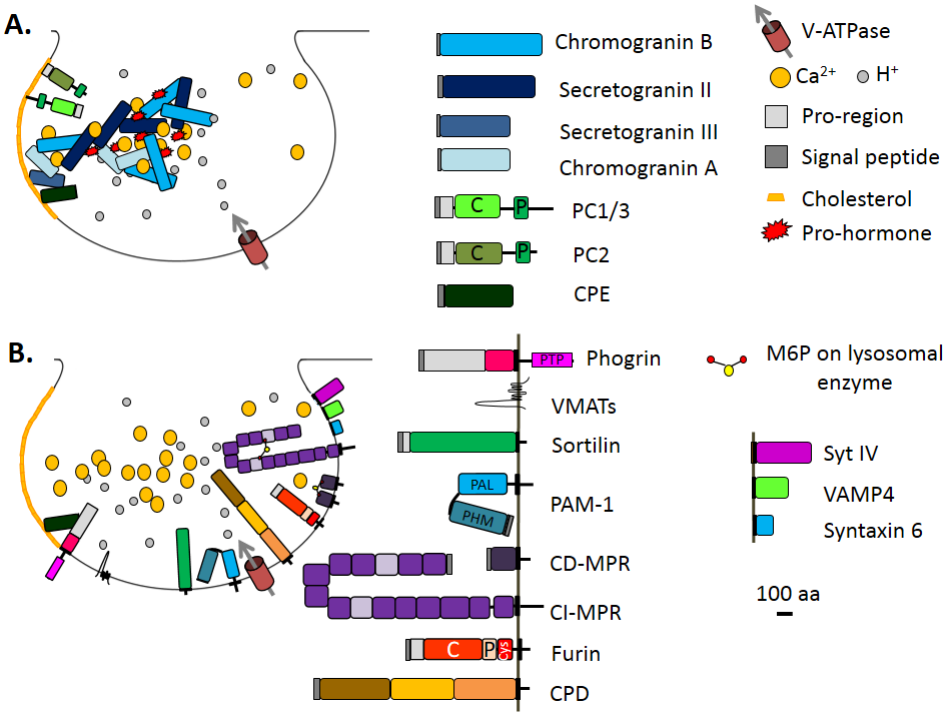

Figure 1.2: Immature SG formation at the TGN. (A) Granins and prohormones aggregate in response to the high calcium, mildly acidic conditions in the TGN. Several soluble proteins interact with cholesterol or cholesterol-rich membranes; their sorting into immature SGs depends on this interaction. (B) Membrane proteins identified in immature SGs and discussed in the main text are shown; their cytosolic tails can interact with adaptor proteins. The SNARE and synaptotagmin proteins that enter immature SGs (synaptotagmin IV, VAMP4, syntaxin 6) are replaced during the maturation process. Proteins known to enter immature SGs are drawn approximately to scale (except for the vacuolar proton pump, V-ATPase and VMATs). PC, prohormone convertase; C, catalytic domain; P, P domain; PTP, protein tyrosine-like phosphatase; PHM, peptidylglycine α-hydroxylating monooxygenase; PAL, peptidylglycine α-amidating lyase; CI-MPR contains 15 domains; CPD contains 3 similar domains; Cys, Cysteine-rich domain.

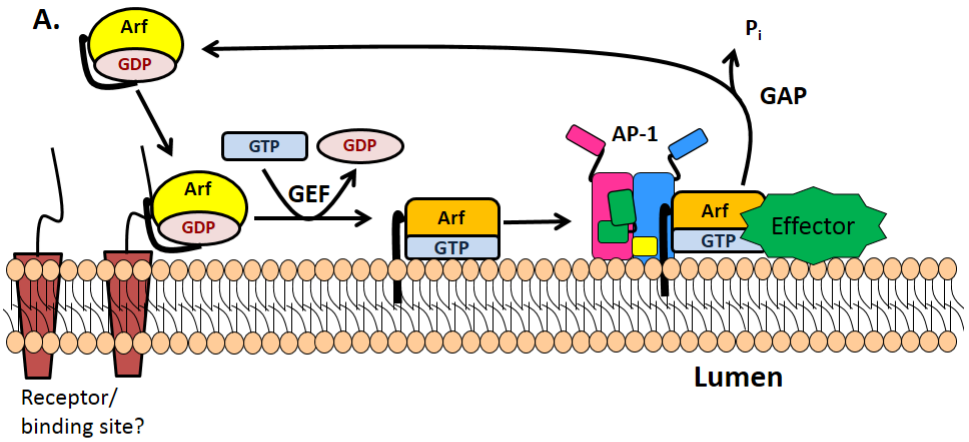

B.

Effector types	Examples
Adaptor proteins	AP-1, AP-3, AP-4, GGA1-3, COPI
Lipid modifying enzymes	PI4KIIIβ, phospholipase D, PI(4)P(5) kinase α
Other	ArfGAP, Arfaptin, FAPP1-2

Figure 1.3: The Arf/GEF/GAP cycle. (A) GDP-Arf is cytosolic and is thought to be recruited to its target membrane by interaction with a receptor. The exchange of Arf-bound GDP for GTP is catalyzed by an Arf-GEF, which induces a conformational change in Arf and release of GDP. GTP-bound Arf binds to the membrane through its N-terminal myristoylated amphipathic helix and recruits cytosolic proteins which function in membrane trafficking (effectors). One of these effectors is an Arf-GAP, which promotes the GTPase activity of Arf, resulting in its detachment from the membrane. (B) Table identifying type of effectors.

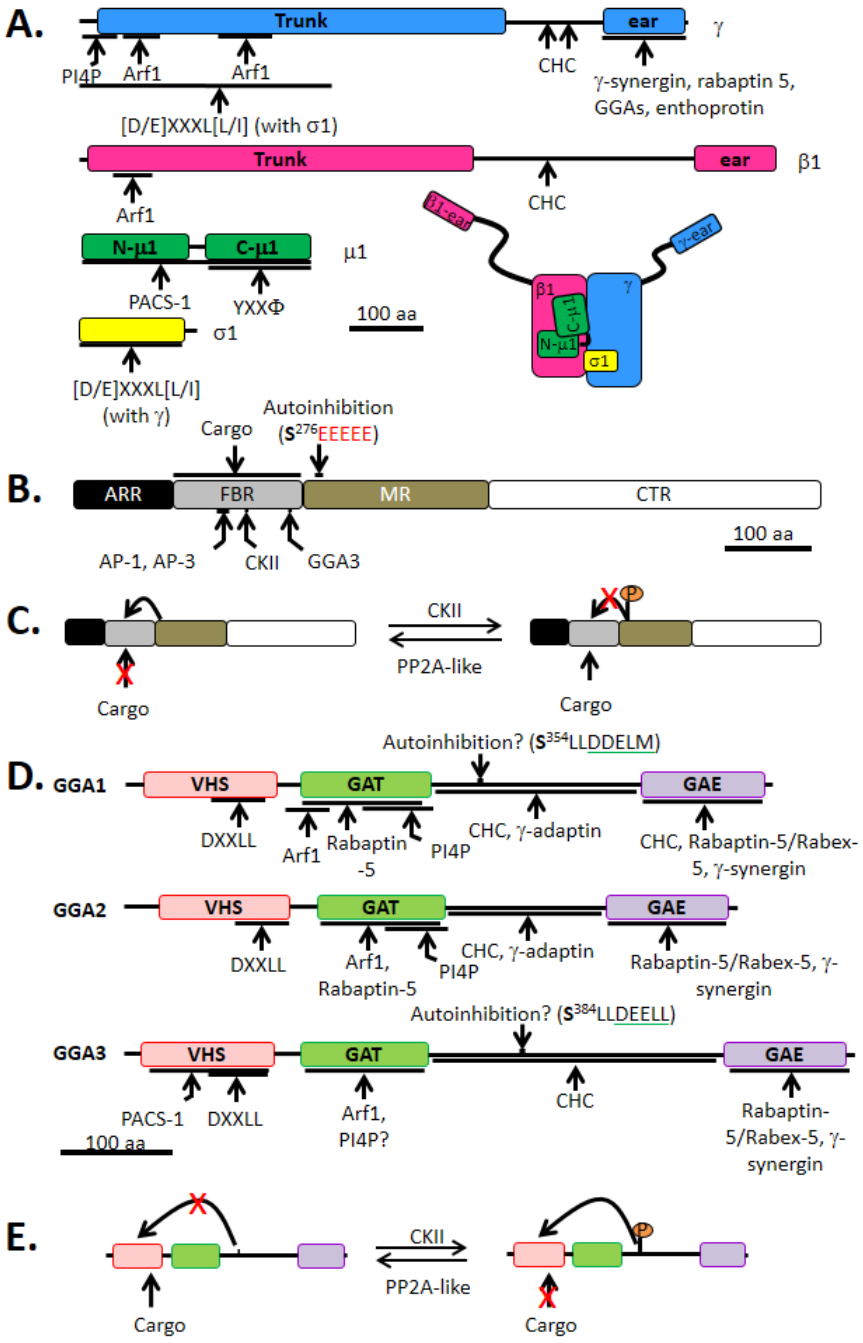

Figure 1.4: Schematic of the AP-1 complex, PACS-1 and mammalian GGAs.

Figure 1.4: (A) AP-1 is made of four different subunits: γ (blue), $\beta 1$ (pink), $\mu 1$ (green) and $\sigma 1$ (yellow). For each subunit, binding partners or binding motifs that are recognized are indicated; ϕ indicates a hydrophobic residue; X can be any amino acid. The overall organization of the complex is shown at the bottom right. (B) PACS-1 is composed of four domains: ARR (black), FBR (grey), MR (tan) and CTR (white). The autoinhibition sequence in the MR is shown (CKII phosphorylation site is in bold and the acidic cluster in red), along with the CKII binding site in the FBR. AP-1 and AP-3 interact with the same site in the FBR while GGA3 interacts with a different site. The FBR is also responsible for interactions with cargo. (C) Autoinhibition mechanism: the autoinhibition domain binds FBR, preventing PACS-1 interaction with cargo. When CKII phosphorylates Ser^{276} of the autoinhibition domain, it inhibits the internal binding and promotes cargo interaction with PACS-1. ARR, atrophin-1-related region; FBR, furin binding region; MR, middle region; CTR, C-terminus region; PP2A, protein phosphatase 2A. (D) Each GGA is composed of four domains: VHS (pink), GAT (green), hinge (bar) and GAE (purple). Regulatory domain and site of proteins-protein interaction are shown. Autoinhibition sequence is shown (CKII phosphorylation site is in bold and the DXXLL motif in green). VHS, Vps27p, Hrs, Stam; GAT, GGA and TOM; GAE, γ-adaptin ear. (E) Autoinhibition mechanism: when phosphorylated by CKII, the autoinhibition domain binds VHS preventing cargo interaction. When the autoinihibition is dephosphorylated, no internal binding occurs allowing cargo interaction with GGA. The single letter code for amino acids was used; CHC, clathrin heavy chain; CKII, casein kinase II.

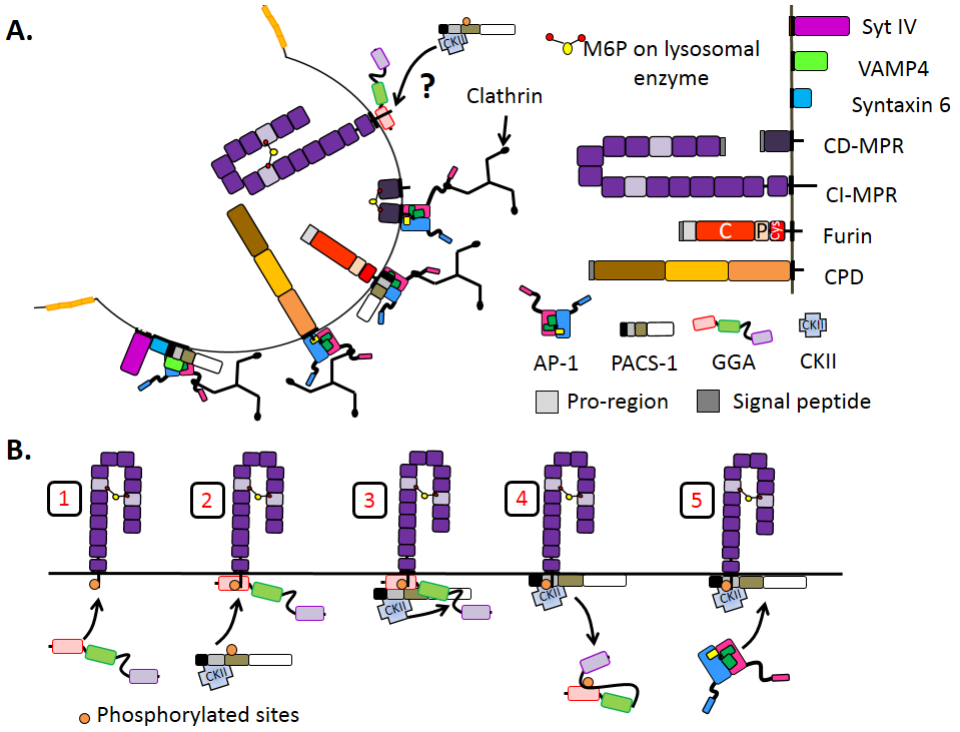

Figure 1.5: Segregation of proteins at the immature SG during membrane remodeling. Schematic of proteins introduced in Figure 2 are reused. (A) Proteins removed during SG maturation involving the recruitment of clathrin and clathrin adaptor protein. Proteins shown to interact with AP-1 and/or PACS-1 or GGAs are shown. In the case of CI-MPR, it is not clear whether GGAs help the recruitment of PACS-1 and AP-1 thus promoting its retrieval. (B) Model of adaptor protein recruitment for CI-MPR transport: GGA3 binds CI-MPR cytosolic tail (step 1). Then, PACS-1, presumably already interacting with CKII, is recruited to the GGA3/cargo complex (step 2). CKII phosphorylates the GGA3 hinge autoinhibitory region (step 3) resulting in GGA3 dissociation from membranes (step 4). PACS-1 then recruits AP-1 for the CI-MPR transport (step 5). Model adapted from [173].

Summary of the thesis

The Golgi complex is a sorting organelle which receives newly synthesized proteins along with proteins from the endocytic pathway and release cargo to go to the plasma membrane or the endocytic pathway. In professional secretory cells, peptides and their processing enzymes leave the Golgi complex in secretory granules, which is a storage organelle for bioactive peptides until a stimulus triggers their exocytosis. The adaptor protein 1 complex (AP-1) is a cytosolic complex involved in the trafficking of cargo between the Golgi apparatus and endosomes and mediates the biogenesis and maturation of secretory granules in professional secretory cells. This thesis explores the function of the adaptor protein 1 complex (AP-1) in post-Golgi trafficking into the following six chapters:

- The second chapter provides evidence about the necessity of AP-1 in generating secretagogue responsive secretory granules in a classical neuroendocrine cell line.
- Since AP-1 was reported to traffic cargo between the Golgi apparatus and endosomes, AP-1 function in the endocytic pathway of the same cell line was explored in the third chapter.
- MEDNIK, a rare disorder caused by lack of a subunit of AP-1, is characterized by altered copper homeostasis. The consequences of reducing AP-1 function on the trafficking of Atp7a, a copper pump bring copper from the cytosol to the lumen of the secretory pathway, and the function of PAM, a peptide processing enzyme requiring copper for activity, were investigated in chapter 4.
- Many studies have focused on copper in the liver and the brain; chapter 5 introduces what the copper concentration and distribution is in the pituitary gland.

- PAM is an essential enzyme for development in mice and flies and is highly expressed in the brain. PAM expression profile during the development of cortex and hippocampus and the distribution of PAM in hippocampal neurons were studied in chapter 6.

- Unravelling the dynamics of PAM trafficking in neuroendocrine cells and neurons and the information this can provide to the scientific community are discussed last.

Chapter 2

AP-1A controls secretory granule biogenesis and trafficking of membrane secretory granule proteins

Mathilde Bonnemaison, Nils Bäck, Yimo Lin, Juan S. Bonifacino, Richard Mains, Betty Eipper.

This chapter is a duplicate version of a published manuscript in Traffic, 2014, vol.15(10): 1099-1121.

Drafting of the manuscript

Mathilde L. Bonnemaison, Richard E. Mains, Betty A. Eipper and Nils Bäck.

Acquisition of data

Nils Bäck did the electron microscopy study; Yimo Lin and Juan S. Bonifacino did the yeast two-hybrid screen; Yanping Wang, Richard E. Mains and Mathilde L. Bonnemaison did the directed mutagenesis; Mathilde L. Bonnemaison did the remaining experiments under the guidance and supervision of Richard E. Mains and Betty A. Eipper.

Critical revision of the manuscript

Vishwanatha Kurutihalli and Megan Miller.

2.1 Abstract

The adaptor protein 1A complex (AP-1A) transports cargo between the *trans*-Golgi network (TGN) and endosomes. In professional secretory cells, AP-1A also retrieves material from immature secretory granules (SGs). The role of AP-1A in SG biogenesis was explored using AtT-20 corticotrope tumor cells expressing reduced levels of the AP-1A μ1A subunit. A two-fold reduction in μ1A resulted in a decrease in TGN cisternae and immature SGs and the appearance of regulated secretory pathway components in non-condensing SGs. Although basal secretion of endogenous SG proteins was unaffected, secretagogue-stimulated release was halved. The reduced μ1A levels interfered with the normal trafficking of carboxypeptidase D (CPD) and peptidylglycine α-amidating monooxygenase-1 (PAM-1), integral membrane enzymes that enter immature SGs. The non-condensing SGs contained POMC products and PAM-1, but not CPD. Based on metabolic labeling and secretion experiments, the cleavage of newly synthesized PAM-1 into PHM was unaltered, but PHM basal secretion was increased in sh-μ1A PAM-1 cells. Despite lacking a canonical AP-1A binding

motif, yeast two-hybrid studies demonstrated an interaction between the PAM-1 cytosolic domain and AP-1A. Co-immunoprecipitation experiments with PAM-1 mutants revealed an influence of the luminal domains of PAM-1 on this interaction. Thus, AP-1A is crucial for normal SG biogenesis, function and composition.

2.2 Introduction

Pituitary endocrine cells, islet β-cells and peptidergic neurons store bioactive peptides in mature secretory granules (SGs) and release them upon stimulation. SG biogenesis starts in the *trans*-most cisterna of the Golgi and requires acquisition of the appropriate peptide precursors, processing enzymes, granule membrane proteins and cytosolic machinery for trafficking to the plasma membrane and regulated exocytosis. The mildly acidic pH and high calcium concentration in the lumen of the *trans*-Golgi network (TGN), along with the properties of the soluble content proteins, contribute to their aggregation and association with lipid rafts and cholesterol-rich membranes [26, 24, 25, 174]. Integral membrane proteins cannot aggregate as extensively and SG entry by the vesicular monoamine transporter, phogrin, carboxypeptidase D (CPD) and peptidylglycine α-amidating monooxygenase (PAM) involves both luminal and cytosolic domain signals [175, 161, 40, 176, 35].

The process of SG formation is poorly understood, but early observations in pituitary lactotropes, pancreatic β-cells and AtT-20 corticotrope tumor cells revealed clathrin coats on the *trans*-most cisterna of the Golgi and on immature SGs, the vesicular compartments formed from these cisternae [177]. Members of the adaptor protein (AP) complex family interact with the heavy chain of clathrin and membrane proteins to form clathrin coats. These complexes bind specific membrane cargo proteins and localize to different regions of the cell

[92, 93, 94, 95]. Each member of the AP family (AP-1 through AP-5) is composed of two large subunits (γ/α/δ/ϵ/ζ, and β1-5), a medium subunit (μ1-5) and a small subunit (σ1-5). AP-1A (γ/β1/μ1A/σ1) is concentrated in the TGN area and on endosomes, where it binds the cytosolic tails of transmembrane protein cargo, facilitating their entry into budding vesicles [115, 178, 179]. AP-1 interacts directly with clathrin [115, 179], and mediates the transport of cargo between the TGN and endosomes [178]. Cargo recognition by AP-1A is mediated by the μ1A subunit, which binds a tyrosine-based sorting signal (YXXϕ, where X is any residue and ϕ is a hydrophobic residue), and by the γ/σ1 interface, which interacts with a dileucine-based sorting signal ([D/E]XXXL[L/I]) [105, 106, 98]. The interaction of cargo proteins with AP-1 affects its oligomerization and coordination of the sorting process [178].

Immature SGs are not responsive to secretagogues [180]. It is clear that AP-1A plays an essential role in the maturation process that leads to secretagogue responsiveness. The removal of VAMP4, furin and mannose-6-phosphate receptors from immature SGs involves AP-1A binding motifs in their cytosolic domains [125]. During the maturation process, soluble content proteins are also removed from immature SGs; these soluble proteins undergo basal or constitutive-like secretion [14, 181, 174]. For prohormones like pro-opiomelanocortin (POMC) and pro-brain derived neurotrophic factor, the more highly processed products released from mature SGs have biological effects distinct from their basally secreted precursors [164, 182], making the balance between basal and stimulated secretion an important variable.

Although SGs play an essential role in many endocrine systems, the endocrine consequences of limited AP-1A function have not been explored. Yeast lacking AP-1 and AP-2 are viable [92], but mice lacking γ-adaptin die before implantation and mice lacking μ1A develop only until E13.5 [178, 183]. Growth is stunted in mice heterozygous for γ-adaptin

[183] and patients with mutations in PREPL, which binds to μ1A and regulates AP-1A recycling, exhibit growth retardation and anorexia [184]. In hippocampal neurons, AP-1A plays a key role in excluding somatodendritic proteins from the SGs that enter axons [185]. Genetic studies demonstrate a role for AP-1A in the biogenesis of glue granules in the larval salivary gland of *Drosophila* [56], secretory lysosomal granules (rhoptries) in *Toxoplasma gondii* [55] and Weibel-Palade bodies in endothelial cells [57]. AP-1 plays an essential role in melanosome biogenesis and in delivering cargo from endosomes to maturing melanosomes, a lysosome-related organelle that stores pigment in melanocytes [186].

AtT-20 corticotrope tumor cells have served as a model system in which to explore SG biogenesis and maturation [83, 187, 9, 75]. The behavior of soluble granule content proteins can be assessed by monitoring POMC and prohormone convertase 1 (PC1) processing and secretion. The behavior of SG membrane proteins can be assessed by monitoring CPD, which enters immature SGs but is removed during SG maturation [161]. AtT-20 lines stably expressing PAM-1 provide another means of monitoring the behavior of a SG membrane protein that catalyzes one of the final modifications in peptide processing. A SG-specific cleavage in its luminal domain makes it possible to monitor PAM-1 entry into immature SGs [188]. Although the cytosolic domain of PAM (PAM-CD) affects its trafficking, it is important to note that its two luminal domains each enter immature SGs efficiently on their own [188, 189].

To investigate the role of AP-1A in SG biogenesis, expression of its medium subunit, μ1A, was reduced in AtT-20 corticotrope tumor cells and in AtT-20 cells expressing exogenous PAM-1 (PAM-1 cells). PAM-CD lacks a consensus site for interacting with AP-1A, but metabolic labeling studies suggest that PAM-1 is retrieved from immature SGs [190], a

process that generally involves AP-1A.

2.3 Results

Down-regulation of the medium subunit of AP-1A in PAM-1 cells alters TGN morphology

We first compared the localization of AP-1A and adrenocorticotropic hormone (ACTH), an accepted marker for the regulated secretory pathway, in PAM-1 cells (Figure 2.1A) [191, 189, 192]. AP-1A was visualized using an antibody for γ-adaptin. Use of an ACTH antibody that recognizes its precursors (referred to as POMC/ACTH staining) allowed visualization of the entire regulated secretory pathway. In PAM-1 cells, POMC products accumulate in the perinuclear TGN area, while tip staining corresponds to mature SGs (open arrowhead in Figure 2.1A) [193, 194, 189]. As expected, γ-adaptin staining was concentrated in the same perinuclear region, with little γ-adaptin staining at the tips of processes (Figure 2.1A). For our immunofluorescence studies, we distinguished three regions: the perinuclear region containing the Golgi (which can be demarcated using antisera to TGN38, PAM or GM130) (Figures 2.11A and B), the tips of processes and the intervening region (referred to as intermediate). Signal intensity in each region was quantified (see Materials and Methods), confirming the enrichment of POMC/ACTH, but not of γ-adaptin, at the tips of processes (Figures 2.11A and C). Vesicular staining for POMC/ACTH and γ-adaptin was observed throughout the region between the Golgi and the tips; although the POMC/ACTH and γ-adaptin staining patterns in this intermediate region clearly differed, the intensity ratios for POMC/ACTH and γ-adaptin staining in the intermediate region vs. the Golgi region were

similar (Figure 2.11C).

SG biogenesis begins at the TGN, where both γ-adaptin and POMC/ACTH are located. To test the hypothesis that AP-1A is necessary for SG formation and maturation, we generated PAM-1 cells with reduced levels of μ1A; μ1A was selected as our target because its cargo recognition motifs are known [105, 106, 98]. Lentiviruses encoding shRNAs targeted to five regions of μ1A mRNA were used to generate multiple stable cell lines (see Materials and Methods). Infected PAM-1 cells were selected using puromycin and μ1A levels were determined by Western blot analysis. In PAM-1 cells infected with lentivirus #549 (sh-μ1A PAM-1 cells), μ1A levels were reduced to 50% of their normal value, the greatest effect observed. Removal of one subunit of the AP-1A core complex alters the stability of the remaining complex [117]; consistent with this, levels of other AP-1A subunits are reduced in fibroblasts lacking μ1A [178, 183]. To see whether a similar effect was observed in PAM-1 cells, γ-adaptin levels were quantified; levels of γ-adaptin in sh-μ1A PAM-1 cells were 80% +/- 4% of control values (data not shown). Cells infected with a lentivirus encoding a non-target shRNA were used as a control (scramble PAM-1 cells) (Figure 2.1B). The morphology of sh-μ1A and scramble PAM-1 cells was not consistently different.

To resolve the complex cisternal and vacuolar structures in the TGN region and the small, punctate structures observed with AP-1A and POMC/ACTH immunofluorescent staining, we turned to transmission electron microscopy and compared the morphology of the TGN in scramble and sh-μ1A PAM-1 cells (Figure 2.1C). The TGN was defined as the tubulovesicular cellular domain at the *trans*-side of the Golgi stack, bordered by endoplasmic reticulum and mitochondria. This domain corresponds to the distribution of the TGN marker syntaxin 6 and the steady state distribution of PAM in these cells; the distribution of the TGN marker

TGN38 is more restricted within this domain [195, 189]. Stereological analyses of the Golgi stacks revealed no difference in stack membrane area (Figure 2.1Ca) and the percentage of the whole Golgi volume fraction attributed to the TGN was not different in the two cell lines (Figure 2.1Cb). However, the surface area of TGN cisternal membranes decreased in sh-μ1A PAM-1 cells compared to scramble PAM-1 cells; pronounced vacuolization of the TGN was observed in sh-μ1A PAM-1 cells (Figure 2.1Cc).

When newly synthesized SG content proteins reach the TGN, the decreased luminal pH and increased calcium concentration facilitate the formation of aggregates, which must acquire membrane of the appropriate composition before budding from the TGN to form immature SGs [1, 174]. To investigate this process, immature and mature SGs were examined in scramble and sh-μ1A PAM-1 cells.

2.3.1 The formation of immature SGs is impaired in sh-μ1A PAM-1 cells

SGs in scramble and sh-μ1A PAM-1 cells were first analyzed using the POMC/ACTH antibody; the Golgi region was visualized using antibody to GM130, a *cis*-Golgi marker, (Figure 2.2A); as expected from the TGN and endosomal localization and function of AP-1A, the steady state distribution of GM130 was unaltered in scramble and sh-μ1A PAM-1 cells. POMC/ACTH positive puncta accumulated at the tips of processes in both cell types; the ratio of tip to Golgi area POMC/ACTH signal intensities did not differ between scramble and sh-μ1A PAM-1 cells (Figure 2.2A and Figure 2.12A). However, the POMC/ACTH-positive puncta located between the Golgi/TGN region and the tips differed in sh-μ1A PAM-1 cells. Instead of the evenly distributed, small POMC/ACTH-positive puncta observed in scramble PAM-1 cells, a smaller number of what appeared to be larger and more scattered

POMC/ACTH positive puncta were observed in sh-μ1A PAM-1 cells (red arrows in Figure 2.2A). The ratio of intermediate to Golgi POMC/ACTH signal intensities decreased by 40% in sh-μ1A PAM-1 cells compared to scramble PAM-1 cells (Figure 2.12A).

To understand why POMC/ACTH staining differed in scramble vs sh-μ1A PAM-1 cells, we turned to transmission electron microscopy. Mature SGs of similar appearance were observed at the tips of cellular processes in both cell lines (Figure 2.2B, left). Immature SGs can be distinguished from mature SGs in these cells by their localization in the TGN area and their electron dense core surrounded by an electron lucent halo. The number of immature SGs in the TGN area decreased by 50% in sh-μ1A PAM-1 cells (Figure 2.2B).

In sh-μ1A PAM-1 cells, vacuolar structures were common in the region between the Golgi complex and the surrounding plasma membrane (Figures 2.1C and 2.2C). In contrast to the high density consistently observed in mature SGs, the electron density of these vacuolar structures varied from lucent to moderately dense. Vacuoles located in a 500 nm peripheral zone of cytoplasm overlying the Golgi complex were counted in scramble and sh-μ1A PAM-1 cells; their number increased almost three-fold in sh-μ1A PAM-1 cells (Figure 2.2C).

Since a decrease in the number of immature SGs and the appearance of these vacuolar structures were the most dramatic morphological changes observed in response to reducing levels of μ1A, we hypothesized that these vacuolar structures derived from the regulated secretory pathway. We thus searched for additional markers that could be used to characterize them.

2.3.2 Diminished levels of μ1A result in altered localization of PAM and CPD

Immature SGs contain proteins targeted to mature SGs along with proteins that function in the regulated secretory pathway but are removed during the maturation process. Since PAM-1 and CPD fall into this category [190, 160], we used immunofluorescence to determine whether reducing μ1A expression altered their localization. We visualized PAM-1 and GM130 in scramble and sh-μ1A PAM-1 cells (Figure 2.3A). As expected, using an antiserum to its C-terminus, PAM-1 was found in the perinuclear Golgi region identified by GM130 and in vesicular structures distributed throughout the cell [189]. Quantification of PAM-staining intensities in the tips vs. the Golgi region did not differ (Figure 2.12B). As observed for POMC/ACTH staining (Figure 2.2A and Figure 2.12A), bright PAM-positive puncta located between the Golgi/TGN region and the tips of processes were prevalent in sh-μ1A cells (red arrows in Figure 2.3A). The ratio of intermediate to Golgi PAM signal intensities decreased by 30% in sh-μ1A PAM-1 cells compared to scramble PAM-1 cells (Figure 2.12B).

CPD, which removes Arg or Lys residues from the C-terminus of proteins and peptides, enters immature SGs but is absent from mature SGs [160]. Despite lacking an AP binding motif, *in vitro* studies demonstrated that its cytosolic domain (CPD-CD) interacts with AP-1A and AP-2 [161]. In scramble PAM-1 cells, endogenous CPD localized to the Golgi (GM130) area, with some staining of nearby vesicles (Figure 2.3B). A clear change in CPD localization occurred in sh-μ1A PAM-1 cells; CPD was more prevalent in vesicles distributed throughout the cytoplasm. The ratio of intermediate to Golgi CPD signal intensities increased almost 3-fold in sh-μ1A PAM-1 cells (Figure 2.12C). Decreasing the levels of μ1A in HeLa cells resulted in a similar shift in the localization of a CD8/CPD chimera [196].

We took advantage of the dramatic difference in CPD localization observed in sh-μ1A

cells to verify that the phenotype could be reversed by expressing mCherry-μ1A*, in which the coding sequence was mutated to make the fluorescently-tagged protein resistant to the shRNA #549. CPD was visualized in sh-μ1A PAM-1 cells transiently expressing mCherry-μ1A* (Figure 2.3C). Transfected sh-μ1A PAM-1 cells expressed varying levels of mCherry-μ1A*. Only sh-μ1A PAM-1 cells expressing mCherry-μ1A* whose distribution resembled that of γ-adaptin (Figure 2.1A) were used for the analysis; in these cells, the endogenous CPD was concentrated in the perinuclear region, as seen in scramble PAM-1 cells. Average intensity of intermediate over Golgi ratios from transfected and non-transfected cells showed an almost 50% decrease in cells transfected with the rescue plasmid. sh-μ1A PAM-1 cells expressing high levels of the construct showed a diffuse mCherry-μ1A* distribution and were excluded from the analysis (not shown). These data confirmed that the phenotype observed in sh-μ1A PAM-1 cells was due to the diminished levels of μ1A.

Reducing the levels of μ1A in PAM-1 cells altered the localization of three regulated secretory pathway markers, POMC/ACTH, PAM and CPD. To find out whether the vacuolar structures that appeared in the sh-μ1A PAM-1 cells derived from the regulated secretory pathway, we turned to immunoelectron microscopy using these three marker proteins.

2.3.3 ACTH and PAM accumulate in the vacuolar structures that appear in sh-μ1A PAM-1 cells

POMC endoproteolytic cleavage generates multiple products (Figure 2.4A). The initial cleavage occurs at the C-terminus of ACTH; although detectable in the TGN, this cleavage occurs primarily in immature SGs. An antiserum specific for the C-terminus of ACTH and unable to cross-react with POMC allowed identification of cleaved product [192]. Using

immunoelectron microscopy, we previously identified PAM-1 in the TGN cisternae, mature SGs and multivesicular bodies of PAM-1 cells [195]. Cisternal structures in the TGN area of scramble and sh-μ1A PAM-1 cells did not differ from the same structures in PAM-1 cells; an accumulation of PAM protein was apparent (Figure 2.4B, left). The morphology of the PAM-1 positive SGs at the tips of scramble and sh-μ1A PAM-1 cells did not differ; in both cell lines, staining for ACTH was concentrated in these structures (Figure 2.4B, right).

To determine whether the vacuoles observed in sh-μ1A PAM-1 cells (Figure 2.2C) derived from the regulated secretory pathway, ACTH and PAM-1 were visualized simultaneously (Figure 2.4C). The vacuolar structures were enriched in both ACTH and PAM; as expected, the multivesicular bodies (MVBs) in the sh-μ1A cells contained PAM, but did not contain ACTH. The vacuoles did not accumulate at the tips of processes, where mature SGs accumulated (Figure 2.4C, left). The presence of ACTH in these vacuolar structures identified them as a derivative of the regulated pathway. The vacuoles lack the high electron density consistently observed in immature and mature SGs, suggesting a lack of content condensation and are tentatively referred to as non-condensing SGs.

To determine whether these vacuolar structures were part of the endosomal system, we assessed the ability of wheat germ agglutinin (WGA) tagged with horseradish peroxidase (HRP) to enter them. The sh-μ1A PAM-1 cells were incubated with tagged WGA for 10 minutes at 37°C; cells were then fixed and stained for HRP (Figure 2.4D). WGA-HRP was readily detected on the plasma membrane and in early endosomes; it was not, however, apparent in the vacuolar structures. The vacuolar structures that appear near the plasma membrane in the region of the cell that contains the Golgi complex in cells with reduced μ1A levels are therefore referred to as non-condensing SGs.

Like PAM-1, CPD was located in cisternal and vacuolar structures in the TGN area of scramble PAM-1 cells (Figure 2.4Ea). Double staining for CPD and ACTH confirmed their co-localization in immature SGs in the TGN area of scramble PAM-1 cells (Figure 2.4Eb). Very few mature SGs in scramble or sh-μ1A PAM-1 cells contained CPD (Figures 2.4Ec and Ef). In the TGN area of sh-μ1A PAM-1 cells, CPD was identified in cisternal structures rather than vacuolar structures (Figure 2.4Ed) and was absent from immature SGs containing PAM (Figure 2.4Ee). Very few of the PAM containing non-condensing SGs found in sh-μ1A PAM-1 cells contained CPD (Figure 2.4Eg); instead, CPD was localized in small vesicular or tubular structures generally devoid of PAM (Figure 2.4Eh). Immunofluorescent and immuno-EM staining indicated that the trafficking of PAM-1 and CPD responded very differently to reduced μ1A levels. To evaluate the functional consequences of these morphological changes, the cleavage of SG proteins and their basal and stimulated secretion were assessed.

2.3.4 Regulated secretion of soluble SG proteins is impaired in sh-μ1A cells

The non-condensing SGs that appeared in sh-μ1A PAM-1 cells contain ACTH and PAM and would be expected to contain prohormone convertase 1 (PC1), a soluble SG component [197, 198, 199]. Based on previous studies, analysis of PC1 and POMC products provides a means of distinguishing secretion from immature vs. mature SGs [12]. PC1 is synthesized as an 87 kDa precursor (proPC1); autoproteolytic cleavage in the endoplasmic reticulum generates an 81 kDa intermediate (Figure 2.5A). When exiting the TGN, 81 kDa PC1 is cleaved to generate a more active 63 kDa form. While 81 kDa PC1 is secreted basally, secretion of 63 kDa PC1 is secretagogue responsive. Using an antibody which recognizes all three forms of PC1, no significant differences were observed in the steady state levels of

these PC1 cleavage products in the three cell lines (Figure 2.5B).

In order to determine whether the content of these non-condensing SGs was stored or released rapidly into the medium, we assessed secretion using a simple stimulation paradigm. Duplicate wells of cells were exposed to control medium or to medium containing 2 mM $BaCl_2$, a mimic of calcium that causes sustained secretion of mature SGs [20]. As expected, proPC1 (87 kDa) was not detected in the medium. The 81 kDa form of PC1, which is not stored in mature SGs, was secreted at a similar rate by all three cell lines. The 63 kDa form of PC1 is stored in mature SGs; stimulation with $BaCl_2$ produced a significant increase in its secretion in all three cell lines. Basal secretion of 63 kDa PC1 was not altered in sh-μ1A PAM-1 cells but $BaCl_2$ stimulated secretion of 63 kDa PC1 was significantly diminished (Figure 2.5C). These data indicate that the decrease in μ1A levels observed in sh-μ1A PAM-1 cells was sufficient to impair SG maturation.

Since AtT-20 cells are specialized in producing and storing ACTH, we next asked whether POMC processing and secretion was altered when μ1A levels were reduced. In order to generalize our observations beyond the PAM-1 cell line and since exogenous expression of PAM-1 alters cytoskeletal organization and limits POMC processing and secretion [193], we addressed this question using wild-type (wt) AtT-20 cells; wt AtT-20 cells were infected with the non-target virus (scramble wt) or the #549 virus (sh-μ1A wt) and multiple stable cell lines were selected. Levels of μ1A were reduced by about 40% in the sh-μ1A wt lines (Figure 2.6A).

In addition to ACTH, POMC cleavage generates 16 kDa fragment (Figure 2.4A). Antibodies to 16 kDa fragment also recognize intact POMC and its cleavage product, ACTH biosynthetic intermediate (ABI). The amount of 16 kDa fragment stored in the three cell lines

at steady state was indistinguishable (Figure 2.6B). Basal secretion of 16 kDa fragment was unaltered in sh-μ1A wt AtT-20 cells, but $BaCl_2$ stimulated secretion of 16 kDa fragment was reduced by almost a factor of two (Figure 2.6C).

Analysis of two soluble SG content proteins (POMC and proPC1) supports the conclusion that μ1A plays an essential role in SG maturation in both wt and PAM-1 AtT-20 cells. The fact that basal secretion of processed products of POMC and PC1 was not increased in sh-μ1A cells supports the hypothesis that the vacuolar structures characteristic of sh-μ1A cells are non-condensing SGs. We next turned to PAM-1, a SG membrane protein whose localization is altered when expression of μ1A is reduced, to examine the role of μ1A in granule membrane protein processing.

2.3.5 PAM processing is altered in sh-μ1A PAM-1 cells

When PAM-1 enters immature SGs, it can be cleaved by prohormone convertases; the major cleavage takes place between the two catalytic core domains, forming soluble PHM and PAL membrane (PALm). Cleavage between PAL and the transmembrane domain occurs less frequently, generating soluble PAL (Figure 2.7A). Unlike soluble SG proteins, PAM-1 and PALm can be retrieved from the regulated secretory pathway; in addition, PAM-1 and PALm that reach the plasma membrane undergo endocytosis and can be returned to the regulated pathway or degraded [190, 176]. PAM-1 cleavage in non-infected, scramble and sh-μ1A cells was assessed using Western blots and antisera specific for PHM or PAL (Figures 2.7B and C). The percentage of the total PHM or PAL signal represented by cleaved product (soluble PHM or PALm) was significantly lower in sh-μ1A PAM-1 cells than in non-infected or scramble PAM-1 cells (Figures 2.7B and C). Although metabolic labeling studies indicated that PAM-1

was synthesized at similar rates in sh-μ1A and scramble PAM-1 cells, total levels of PAM protein were consistently lower in sh-μ1A PAM-1 cells; increased secretion and increased degradation could each contribute to this difference.

The steady state level of PAM protein reflects newly synthesized PAM-1 trafficking through the biosynthetic pathway along with a substantial amount of PAM that has traversed the endocytic pathway [195]. Metabolic labeling was used to assess the trafficking of newly synthesized PAM-1, which must enter the regulated secretory pathway before it can be cleaved to form soluble PHM. Cells incubated in medium containing [^{35}S]Met/Cys for 20 minutes were either collected after 10 min (pulse) or incubated in medium containing unlabeled Met/Cys for 0.5, 1 or 2 hours (chase). PHM-containing proteins were isolated from cell extracts and spent media by immunoprecipitation; following SDS-PAGE, newly synthesized PAM proteins were visualized by fluorography (Figure 2.7D). The time course over which newly synthesized 120 kDa PAM-1 was converted into PHM was indistinguishable in scramble and sh-μ1A PAM-1 cells (Figure 2.7E). Data from several metabolic labeling experiments were quantified, supporting the conclusion that access of PAM-1 to the protease that produces PHM was unaltered in sh-μ1A PAM-1 cells (Figure 2.7F). AP-1A was shown to play a role in the regulated, but not in the basal, release of 63 kDa PC1 and the 16 kDa fragment of POMC. We next evaluated the role of AP-1A in the basal and stimulated secretion of PHM.

2.3.6 Regulated secretion of PHM is impaired in sh-μ1A PAM-1 cells

We used non-infected, scramble and sh-μ1A PAM-1 cells for these studies. As above, we used 2 mM $BaCl_2$ [20] to stimulate secretion from mature SGs (Figure 2.8A). The sh-μ1A

PAM-1 cells secreted about twice as much PHM under basal conditions as non-infected or scramble PAM-1 cells (Figure 2.8A, boxed graph). Metabolic labeling experiments also indicated that more of the newly synthesized PHM appeared in the medium during the 0-1 h and 0-2 h chase periods in sh-μ1A PAM-1 cells than in scramble PAM-1 cells (Figure 2.7D). Contributions from newly synthesized PAM-1 in the biosynthetic pathway and from recycled PAM-1 in the endocytic pathway could explain the increase in PHM basal secretion. This result is consistent with the decreased steady state content of PHM observed by Western blot (Figure 2.7B). The ability of $BaCl_2$ to stimulate the secretion of PHM from mature SGs was reduced by 40% in sh-μ1A PAM-1 cells (Figure 2.8A).

To determine whether the reduced regulated secretion seen in sh-μ1A PAM-1 cells was due to an impairment in SG maturation, we again turned to metabolic labeling. Based on studies of rat intermediate pituitary and parotid cells, it takes about 2 hours for newly synthesized POMC products and amylase to get to mature SGs [17, 200]. A metabolic labeling experiment was designed to compare the time at which secretion of newly synthesized PHM produced in scramble vs. sh-μ1A PAM-1 cells became responsive to secretagogue. After the pulse, media were collected every hour for the next 4 hours of chase. After 2 hours of chase, one well received medium containing 2 mM $BaCl_2$ (stim.) while the other well received control medium (basal). After 3 hours of chase, both wells were incubated in basal medium for 1 hour (Figure 2.8B). PAM proteins were isolated from cells and spent media by immunoprecipitation and newly synthesized PAM proteins were visualized by fluorography. Secretion of newly synthesized PHM was barely detected during the first collection period. Addition of 2 mM $BaCl_2$ to the 2-3 h chase medium increased PHM secretion by 50% in scramble PAM-1 cells but failed to stimulate secretion of newly synthesized PHM from

sh-μ1A PAM-1 cells (Figures 2.8C and D). Taken together, our data suggest that the entry of newly synthesized PHM into secretagogue-responsive granules requires a longer time in sh-μ1A PAM-1 cells than in scramble PAM-1 cells.

2.3.7 The cytosolic domain of PAM interacts with the μ subunit of AP-1A

Since our analysis revealed a role for AP-1A in PAM trafficking, we hypothesized that the cytosolic domain of PAM-1 interacts with AP-1A; the trafficking determinants in this 86 amino acid unstructured region of PAM-1 have been localized to residues 933-950 (Figure 2.9A) [176]. We turned to the yeast two-hybrid system to screen for an interaction between the cytosolic domain of PAM (PAM-CD) and μ1A, μ2, μ3A, μ3B and μ4 (Figure 2.9B): in this system, PAM-CD interacted only with μ1A. We used several PAM-CD mutants to identify the region responsible for this interaction and to assess its biological relevance (Figure 2.9C). PAM-1 truncated at residue 961 is trafficked normally and PAM-CD 961s interacted with μ1A. PAM-1 in which the only Tyr residue in the cytosolic domain had been mutated to Ala (Y936A) is endocytosed less rapidly, a process expected to be dependent of AP2 [176]; PAM-CD bearing this mutation continued to interact with μ1A. The major trafficking determinants in the cytosolic domain of PAM are located between residues 933 and 950; PAM-CD lacking these residues (Δ933-950) did not interact with μ1A in the yeast two-hybrid screen.

In order to determine whether PAM and AP-1A interact *in vivo*, we turned to pituitary, a tissue in which PAM-1 is highly expressed [201]. A solubilized particulate fraction prepared from adult mouse pituitary was immunoprecipitated using antibodies to γ-adaptin (Figure 2.9D) or to the linker region between PHM and PAL (Figure 2.9E). The availability of an

excellent antibody to γ-adaptin and the fact that γ-adaptin (100 kDa), but not μ1A (50 kDa), could be readily resolved from the IgG heavy chain governed the choice of antibody. In both cases, co-immunoprecipitation of PAM-1 and the AP-1A complex was observed. Based on quantification of multiple experiments, 3% of the PAM-1 in pituitary lysates co-immunoprecipitated with γ-adaptin while only 0.6% of the AP-1A co-immunoprecipitated with PAM-1 (graphs in Figures 2.9D and E).

To allow manipulation of the interaction, similar co-immunoprecipitation experiments were conducted using lysates prepared from PAM-1 cells (Figures 2.9F and G). When the γ-adaptin antibody was used to capture the endogenous AP-1A complex, PAM-1 was again co-immunoprecipitated. Although the cytosolic domain of PALm has the same amino acid sequence as the cytosolic domain of PAM-1, PALm was not co-immunoprecipitated by the γ-adaptin antibody. Quantification revealed a significant interaction (graph in Figure 2.9F). The different behavior of PALm and PAM-1 could reflect their phosphorylation state [38] or a contribution from their luminal domains. Using affinity-purified PAM-1 antibody, γ-adaptin was again co-immunoprecipitated (Figure 9G; quantification shown in graph in Figure 2.9G). As for the pituitary, about 2% of the total PAM-1 co-immunoprecipitated with γ-adaptin (Figure 2.9E). Almost 2% of the γ-adaptin co-immunoprecipitated with PAM-1, a higher percentage than observed in pituitary tissue (Figure 2.9G).

When expressed independently as soluble secretory pathway proteins, both catalytic domains of PAM are efficiently stored in regulated secretory granules [190, 188]. To determine whether luminal interactions contributed to the co-immunoprecipitation of PAM-1 and AP-1A, we prepared lysates from AtT-20 cells stably expressing PAM-1 899s, which includes the transmembrane domain but only nine of the 86 residues in PAM-CD (Figure

2.9A, blue arrow). Co-immunoprecipitation of PAM-1 899s with γ-adaptin was observed using antibodies to PAM-1 or γ-adaptin (Figures 2.10A and B). While the PAM-CD/μ1A interaction revealed using the yeast two-hybrid assay presumably contributes to the interactions that occur in cells, it is clear that mutations that eliminate the ability of PAM-CD to interact with μ1A in the yeast two-hybrid screen are not readily detected by co-immunoprecipitation from cells with a regulated secretory pathway.

We turned to transient transfection of pEAK Rapid cells, a cell line that lacks a regulated secretory pathway, to see if these cells could be used to explore the interactions of μ1A with the cytosolic domain of PAM. Co-immunoprecipitation of endogenous AP-1A with transiently expressed PAM-1 or PAM-1 899s was detected using antibody to PAM (Figure 2.10C); an exploration of the interaction between the cytosolic domain of PAM and AP-1 will require the use of PAM proteins that lack their luminal domains.

2.4 Discussion

2.4.1 The role of AP-1A in SG formation and function

It is striking that a 50% reduction in μ1A levels had such a profound effect on the architecture of the TGN and on SG maturation in AtT-20 corticotrope tumor cells. This could reflect both the role of AP-1A in the trafficking of newly synthesized proteins as they exit the TGN and the role of AP-1A in endocytic trafficking. Formation of clathrin coats on TGN membranes is dependent on close cooperation between AP-1A and GGA proteins [152, 151]. Lack of this membrane sorting mechanism and membrane proteins normally retrieved after endocytosis may contribute to the breakup of cisternal elements seen in the TGN of sh-μ1A PAM-1 cells.

The structure of the Golgi stacks was unperturbed when μ1A levels were reduced.

Ultrastructural analysis indicated that sh-μ1A PAM-1 cells had fewer immature SGs and more vacuolar structures than scramble cells. The fact that cleavage of proPC1, POMC and PAM-1 proceeded normally in sh-μ1A PAM-1 and sh-μ1A wt AtT-20 cells supports the conclusion that these vacuoles are cleavage competent. Based on their appearance, staining for PAM-1 and ACTH and lack of accessibility to an endocytic marker, these vacuolar structures were referred to as non-condensing SGs. They cluster in the mid-region of the cell instead of accumulating at the tips of processes, where mature SGs accumulate [194]. In AtT-20 cells, as in pancreatic β-cells and exocrine pancreatic cells, immature SGs have a clathrin-coat which is lost during maturation [177, 202, 9] and the simplest hypothesis is that non-condensing SGs accumulate when the formation and maturation of SGs is inhibited. The molecular mechanisms involved in condensation are not yet clear, but isolation and examination of these non-condensing SGs may provide insight into the process.

Efficient sorting and packaging of proteins in SGs involves the pH and calcium dependent formation of aggregates and their interaction with TGN membranes of the appropriate composition. With its ability to interact with transmembrane cargo proteins, AP-1A is thought to assist in the sorting of granule membrane proteins into forming vesicles. The accumulation of non-condensing SGs in sh-μ1A PAM-1 cells may be a consequence of the absence of multiple AP-1A cargo proteins. A failure to acidify the lumen or an inability to accumulate calcium could also contribute. Early work on mammotrophs demonstrated interactions between the regulated secretory pathway and the degradative pathway [203]. Steady state levels of the products of proPC1 and POMC processing were unaltered in sh-μ1A cells, suggesting that the degradative pathway is not altering the state of the regulated

secretory pathway.

Basal secretion of proPC1 and POMC cleavage products was unaltered in sh-μ1A PAM-1 and sh-μ1A wt AtT-20 cells, suggesting that non-condensing SGs are not rapidly released. As SGs mature, their ability to respond to secretagogues increases [83]. Our metabolic labeling experiments indicated that it takes longer for the SGs in sh-μ1A PAM-1 cells to become secretagogue responsive than it does for immature SGs in scramble PAM-1 cells. The formation of secretagogue-responsive SGs is known to require the AP-1 mediated removal of VAMP4 and synaptotagmin IV, leaving VAMP2 and synaptotagmin I in mature SGs [83]. Consistent with this, $BaCl_2$-stimulated secretion of PHM, ACTH and 63 kDa PC1 was reduced to half in sh-μ1A cells. Mature SGs of normal appearance were located at the tips of cellular processes in sh-μ1A PAM-1 cells. Non-condensing SGs may contain proteins that block their maturation and transport to the tips or processes. Decreased responsiveness to secretagogue, as observed in sh-μ1A PAM-1 cells, is a hallmark of metabolic diseases like diabetes [204, 205] and of peptide secreting neuroendocrine tumors [206, 207].

2.4.2 The role of AP-1A in PAM-1 and CPD trafficking

Reducing μ1A levels had vastly different effects on PAM-1 and CPD, proteins selected for study because both were known to enter into and be retrieved from immature SGs [175, 161, 12]. PAM accumulated in non-condensing SGs and in mature SGs in sh-μ1A PAM-1 cells. Cleavage of newly synthesized PAM-1 by PC1, which produces PHM and PALm, does not start until PAM-1 enters immature SGs [12]; the timing of this event was unaltered in sh-μ1A PAM-1 cells. The ability of its PHM and PAL domains to enter SGs [188] may minimize the need for signal-mediated entry of PAM into immature and non-condensing

SGs.

Reducing μ1A levels had a very different effect on endogenous CPD trafficking; instead of its normal localization in TGN cisternae and immature SGs, CPD appeared in small vesicles dispersed throughout sh-μ1A PAM-1 cells. Most notably, CPD and PAM rarely co-localized in sh-μ1A PAM-1 cells. CPD is a major transmembrane glycoprotein in clathrin-coated vesicles in human placenta and rat liver [196]. Its cytosolic domain is well conserved and essential for its trafficking [175, 161]. The cytosolic domain of CPD lacks a canonical AP binding motif, but *in vitro* binding assays revealed that it interacts with AP-1A when phosphorylated by CKII [161].

The different effects of μ1A knockdown on PAM-1 and CPD trafficking may in part reflect the properties of their luminal domains. Membrane and soluble forms of duck CPD have been expressed in AtT-20 cells [160]. About 80% of the membrane form was located at the TGN, with 14% in immature SGs; the soluble form was found in small vesicles (45%) and immature SGs (40%). Metabolic labeling studies indicated that soluble duck CPD was primarily targeted to the constitutive secretory pathway. The entry of membrane CPD into immature SGs seems to require AP-1A. Consistent with our data, down-regulation of μ1A in HeLa cells expressing a CD8/CPD chimera (luminal and transmembrane domains of CD8 linked to the cytosolic domain of CPD) caused its redistribution from the TGN to small vesicles throughout the cell [196].

Although PAM-1 was synthesized at the same rate in sh-μ1A and scramble PAM-1 cells, steady state levels of PAM were reduced in sh-μ1A PAM-1 cells; a detailed evaluation of the endocytic trafficking of PAM-1 in sh-μ1A cells will be required to interpret these observations. The secretion of cleavage products unique to the regulated secretory pathway in the absence

of secretagogue, often referred to as constitutive-like secretion [14, 208], is a major pathway in AtT-20 cells [49, 12]. The increased constitutive-like secretion of PHM observed in sh-μ1A PAM-1 cells could be due to a change in PAM trafficking in both the regulated secretory and endocytic pathway. AP-1A/clathrin coated vesicle budding from immature SGs has a well-established role in the retrieval of lysosomal and constitutive membrane proteins from the regulated secretory pathway [82, 208]. Increased aggregation of POMC and PC1 products would be expected to decrease their entry into budding vesicles [187], accounting for the unaltered constitutive-like secretion of 16K fragment and 63 kDa PC1. The kinetics of constitutive-like secretion suggest the occurrence of an additional sorting step in an endosomal intermediate [209, 210, 211], presumably allowing additional sorting for secretion or recycling toward the TGN.

2.4.3 PAM-1 and AP-1A: a novel interaction

The PAM-1/AP-1A interaction described here is not driven by a canonical AP interaction motif. Non-canonical interactions of cargo with AP-2 and AP-4 have been described. The Kir2.3 potassium channel is internalized in clathrin-coated vesicles containing AP-2; mutational analysis revealed a tandem di-hydrophobic motif at its C-terminus that recognizes an α/σ2 interface in AP-2 [212]. The cytosolic domain of amyloid precursor protein contains a tyrosine-based signal (YKFFE) that binds to μ4 at a site that is different from that of canonical YXXϕ signals [213]. Our findings suggest that AP-1A can also bind non-canonical signals.

Immunoprecipitation of the AP-1A complex pulled down PAM-1 but not PALm. The cytosolic domains of PAM-1 and PALm are identical in amino acid sequence, but differ in phosphorylation status [38, 214]. While our yeast two-hybrid screen pointed to a role for PAM

(933-950), co-immunoprecipitation of the AP-1A complex and a truncated PAM-1 protein lacking its cytosolic domain (PAM-1 899s) revealed an important role for the luminal domains. The proteins that contribute to this interaction have not been identified, but studies using luminal fragments of ATP7A, the P-type ATPase responsible for transporting copper into the lumen of the secretory pathway, demonstrated an interaction with PAM-1 [215]. ATP7A localizes to the TGN when copper levels are low, receiving copper from a cytosolic chaperone and delivering it to luminal cuproenzymes like PHM [216]. Mutations in the genes encoding the σ1A [217] or σ1B [218] subunits of human AP-1 result in two developmental disorders, MEDNIK (mental retardation, enteropathy, deafness, peripheral neuropathy, ichthyosis and keratodermia) and Fried syndrome, respectively. Deficiency in σ1A correlates with a defect in copper metabolism recently characterized by abnormal localization of ATP7A [219]. The C-terminus of ATP7A contains a di-leucine motif that could be recognized by AP-1A and ATP7A recycling from the plasma membrane to the TGN in HeLa cells is AP-1A dependent [220].

Our studies suggest that diminished responsiveness of peptide secreting neurons and endocrine cells may occur in response to minor alterations in AP-1A function. Lack of AP-1A recycling due to reduced levels of PREPL alters growth hormone secretion [184]. Furthermore, γ-adaptin$^{+/-}$ mice are smaller than wild-type, which could also reflect impaired endocrine function [183]. In our study, a modest reduction in μ1A levels in corticotrope tumor cells resulted in vacuolization of the TGN and accumulation of cleavage competent, non-condensing SGs. Although processing of POMC and proPC1 in the regulated secretory pathway proceeded normally, the ability of the cells to secrete stored product in response to secretagogue was substantially diminished. The interaction of AP-1A complexes with

membrane proteins known to enter and exit immature SGs is affected by their luminal domains and may not rely only on canonical interaction sites.

2.5 Materials and Methods

2.5.1 Antibodies

The antibodies used in this study are summarized in Table 2.1.

2.5.2 Cell Culture

A mouse corticotrope tumor cell line, AtT-20, was grown at 37°C with 5% CO_2 in Dulbecco's modified Eagle's medium/F-12 (DMEM/F-12) containing 25 mM HEPES, 10% NuSerum, 10% fetal bovine serum, 100 units/ml penicillin, 100 μg/ml streptomycin, and passaged weekly using trypsin. Stably transfected AtT-20 cells expressing wild-type PAM-1 or PAM-1 899s were grown in the same medium and selected using 0.5 mg/ml G418 [176].

2.5.3 Lentiviruses

Wild type AtT-20 cells and stably transfected AtT-20 cells expressing PAM-1 were grown until about 80% confluency and then infected with a lentivirus expressing an shRNA directed against μ1A (Sigma) (Table 2.2). In parallel, cells were infected with a lentivirus expressing a non-target shRNA (Sigma # SHC002V). At 24 hours post-infection, the medium was removed and cells were selected using growth medium containing 0.4 μg/ml puromycin. In order to obtain lines expressing a constant level of μ1A, cells were subcloned; for each type of cell line, nine to ten clones were used to measure the level of μ1A (Figures 2.1B and 2.6A). Three sh-μ1A clones were selected based on their low level of μ1A and three scramble clones were

selected based on their unaltered μ1A levels.

2.5.4 Immunofluorescent staining, confocal imaging and image quantification

Cells were plated onto 0.16 to 0.19 mm thick, 12-mm round coverslips (Fisher Scientific) which were coated with 0.1 mg/ml poly-L-lysine for 5 minutes followed by a rinse in NuSerum and two rinses in growth medium. Cells were fixed in 4% formaldehyde in PBS (50 mM NaH_2PO_4, 150 mM NaCl, pH 7.4) for 20 minutes at room temperature. After rinsing in PBS, cells were permeabilized in 0.075% Triton X-100, 2 mg/ml BSA in PBS for 20 minutes at room temperature and then incubated in block buffer (2 mg/ml BSA in PBS) for 20 minutes at room temperature. Primary antibodies diluted in block buffer were incubated with the cells overnight at 4°C. After three rinses in PBS, cells were incubated for one hour in block buffer containing either fluorescein isothiocyanate (FITC, 1:500 dilution) or Cy3 (1:2000 dilution) conjugated donkey antibody to mouse or rabbit immunoglobulin (Jackson ImmunoResearch). After three rinses, coverslips were mounted on slides using ProLong® Gold (Invitrogen). Cells were visualized on a Zeiss LSM 510-Meta using an oil immersion 63X Plan Apochromat objective (NA 1.4). Linescans were done using Metamorph; for both markers, the value with the highest fluorescence intensity value was set to 1. Quantification of fluorescence images was done using Metamorph. Three regions were identified in each cell analyzed: Golgi (based on staining for GM130, TGN38 or PAM), Tip (based on morphology) and Intermediate (non-nuclear, located between the Golgi and a tip, but clearly distinct from each). Figure 2.11 identifies the three regions in line scans. For each picture, red and green colors were first separated. Background values were determined by measuring the average intensity in parts of the picture without cells for both green and red images. Background

was then subtracted for both green and red images using the average intensity measured as a constant value for the entire image. One to nine 2.5 x 2.5 μm boxes were systematically placed over each region and the average fluorescence signal intensity in each region was measured for 10 to 37 cells. Tip/Golgi and Intermediate/Golgi ratios are shown. Statistical analyses were made using paired t-tests on the ratios calculated.

2.5.5 Electron microscopy

For electron microscopy, cells were fixed with 2.5% glutaraladehyde in 0.1 M cacodylate buffer, scraped and pelleted in gelatin, postfixed with 1% osmium tetroxide and 1.5% potassium ferrocyanide, dehydrated and embedded in an Epon resin. Ultrathin sections were post-stained with uranyl acetate and lead citrate and 30 Golgi complexes in each specimen were systematically sampled and photographed at 6000X with a Jeol JEM-1400 electron microscope equipped with a Gatan Orius SC 1000B bottom mounted CCD-camera. The pictures were viewed at a final magnification of 160,000X. A point grid [221] was overlaid and the volume fractions of the Golgi stack and the TGN were determined by point counting. A line grid was used for measuring the surface to volume ratios of Golgi stack membrane and cisternal membrane in the TGN according to the formula S/V = 4c/lh, where c is the number of times the lines intersected the surface of interest, h is the number of times the end points of the lines fell on the structure and l is the length of a test line. Immature granules in the TGN were identified on the basis of their electron dense interior surrounded by an electron lucent halo. Vacuoles/granules in the middle of the cells were counted in the 500 nm peripheral zone of the cytoplasm surrounding the Golgi complex (extending 2.5 μm in both directions from the point overlying the center of the Golgi complex). All graphs represent the results

from 3 experiments. Statistical analyses were made with Student's t-test for the mean values of each experiment (n = 3).

For immunoelectron microcopy, cells were fixed with 4% paraformaldehyde (for PAM staining) or 4% paraformaldehyde + 0.5 % glutaraldehyde (for CPD staining) in 0.1 M phosphate buffer for 2 h, scraped, pelleted and embedded in gelatin. Polyvinylpyrrolidone/sucrose infiltrated specimens were sectioned at -120oC; sections were collected with methyl cellulose/sucrose, blocked with 1% fish skin gelatin (Sigma) and 1% BSA (Sigma) and incubated with antibody (JH629 diluted 1:200 for PAM; AE142, diluted 1:50 for CPD) for 1 h followed by Protein A conjugated to 10 nm gold particles (University of Utrecht, Utrecht, Netherlands) for 1 h and embedded in uranyl acetate-methyl cellulose. For double staining with ACTH or CPD antibody, PAM was first detected with Protein A/10 nm gold conjugate; the sections were then fixed for 5 min with 1% (for ACTH) or 0.5% (for CPD) glutaraldehyde to block interfering binding, then incubated with antibody to ACTH (antiserum Kathy diluted 1:1000) (Schnabel et al., 1989) or CPD (antiserum AE142 diluted 1:50) followed by protein A conjugated to 15 nm gold particles.

For the detection of endosomal uptake cells were incubated with 30 μg/ml peroxidase conjugated wheat germ agglutinin (Sigma) on ice for 30 min, rinsed, chased for 10 min at 37°C and fixed with 1.5% glutaraldehyde in 0.1M phosphate buffer, then incubated with 0.25 mg/ml diaminobenzidine and 0.6 mg/ml hydrogen peroxide for 10 min on ice, rinsed and pelleted as above.

2.5.6 Rescue experiment

Briefly, sh-μ1A PAM-1 cells were transfected with a plasmid encoding μ1A mRNA resistant to shRNA provided by virus #549. The rescue was tested by immunofluorescent staining looking at the distribution of carboxypeptidase D. pReceiver-M55-mCherry-Ap1m1A was purchased from GeneCopoeia (catalog number: EX-Mm01216-M55; Rockville, MD). In order to create shRNA-resistant mCherry-μ1A (μ1A*), mutations that did not alter the amino acid sequence were introduced using site-directed mutagenesis with the following primer: 5' CTGTCACCTATCTTGGCCCATGGTGGGGTGAGATTCATGTGGATTAAGCACAA-CAACCTGTAC 3' (Tm = 70.2°C). Scramble and sh-μ1A PAM-1 cells were plated onto 12-mm diameter coverslips (0.16 to 0.19 mm thick, Fisher Scientific) in 24-well dishes; the coverslips were coated with 0.1 mg/ml poly-L-lysine for 5 minutes followed by a rinse in NuSerum and two rinses in growth medium. Two days later, cells were incubated in serum free medium for 30 minutes before being transfected (0.125 μg DNA/well); the Lipofectamine 2000 ® and DNA were mixed in Optimem (Optimem:DNA:Lipofectamine 2000 ® = 200 μl:1 μg: 2.5 μl) and allowed to sit for 25 minutes. After application of the mixture, cells were incubated at 37°C for 6 hours. Transfection medium was then replaced with growth medium and the cells were allowed to recover overnight. Cells were fixed the following day in 4% formaldehyde in PBS and immunostained as described above.

2.5.7 Stimulation of secretion

Cells were plated into 12-well dishes. Secretion experiments were carried out in DMEM/F-12 air medium containing ITS, 25 mM HEPES, pH 7.4, 50 μg/ml bovine serum albumin (BSA). Cells were equilibrated in air medium during two consecutive 30 minute incubations at 37°C.

Each experiment consisted of a 30 minute incubation in air medium (basal secretion) followed by a 30 minute incubation in either air medium (basal secretion) or in air medium containing 2 mM $BaCl_2$ (stimulated secretion). After each incubation, the medium was centrifuged to remove any non-adherent cells and protease inhibitors were added to the supernatant. After the final incubation, cells were extracted into SDS lysis buffer [0.5% (w/v) SDS, 50 mM Tris, pH 8.0, 1 mM DTT, 2 mM EDTA, 50 mM NaF] containing protease inhibitors.

2.5.8 Biosynthetic labeling

Cells plated into a 4-well dish were equilibrated in DMEM/F-12 air medium as described above for secretion experiments. Cells were incubated in DMEM/F-12 air medium lacking methionine (Met^- medium) for 10 minutes at 37°C before incubation in Met^- medium containing [^{35}S]Methionine/Cysteine protein labeling mix (final activity 1 mCi/ml; PerkinElmer) for 20 minutes. Radioactive medium was removed and replaced with DMEM/F-12 air medium. Cells were either harvested 10 minutes after removal of the radioactive medium (Pulse) or after a 30-240 min incubation in non-radioactive medium (Chase). Cells were lysed in 200 μl of TMT, pH 7.4 containing protease inhibitors. After centrifugation at 8,000 x g for 15 minutes, supernatants were used for immunoprecipitation. Medium samples were centrifuged at 2,000 x g for 5 minutes and protease inhibitors were added before analysis. To assess labeling efficiency, incorporation of [^{35}S]Methionine/Cysteine into protein was assessed using aliquots (2 μl) of cell extracts and media. Proteins were precipitated by adding 25% tricholoracetic acid (TCA) to 1% of the total cell extract, resuspended in 2% SDS, 0.2M $NaHCO_3$ and added to liquid scintillation fluid for measurement in a scintillation counter. Typically, 1-2 % of the label was incorporated into protein during the 20 min labeling/10

minute pulse.

For immunoprecipitation, affinity-purified PHM antibody (0.8-1 μg) was added to cell extracts, which were incubated at 4°C overnight; after centrifugation for 15 minutes, supernatants were incubated with protein A agarose beads (10 μl packed beads) for 30 minutes at room temperature. Beads were pelleted and washed twice in TMT, pH 7.4 containing protease inhibitors, and once in TM, pH 7.4 containing protease inhibitors. Bound proteins were eluted by incubation for 5 minutes at 95°C in Laemmli sample buffer. Immunoprecipitates were fractionated by SDS-PAGE on 4-15% gradient gels (Bio-Rad). After electrophoresis, gels were incubated in 10% acetic acid, 30% isopropanol for 20 minutes at room temperature, followed by 20 minutes in Enhance (Perkin Elmer) at room temperature. After two rinses in water, the gel was dried and analyzed by fluorography.

2.5.9 Yeast two-hybrid screen

A cDNA fragment encoding the cytosolic domain of rat PAM (PAM-CD; R891WK to PSS976) was inserted into pGBKT7 (Gal4 DNA-binding domain, TRP1). A cDNA encoding medium subunit μ1A, 2, 3A, 3B or 4 was inserted into pACTII (Gal4 Activation Domain, LEU2) as described [102, 222]. The AH109 yeast reporter strain was grown on Yeast Peptone Dextrose agar plates. Yeast were co-transfected with a PAM-CD plasmid and a medium subunit plasmid; to test the PAM-CD/μ interaction, yeast were grown for 5 days at 30°C on medium lacking leucine, tryptophan and histidine. The growth medium contained 3-amino-1,2,4-triazole (3-AT), a competitive inhibitor of HIS3, where indicated. Construction of the following mutants was previously described: PAM-CD truncated at residue 961 (961s), PAM-CD with Ala replacing Tyr936 (Y936A), PAM-CD lacking residues 933-950 (Δ933-950)

[176].

2.5.10 Co-immunoprecipitation

A confluent well of a 6-well dish of AtT-20 cells expressing PAM-1 or a PAM-1 mutant were lysed in 500 μl of 20 mM Na-N-Tris[hydroxymethyl]methyl-2-aminoethanesulfonic acid (TES), 10 mM mannitol (TM), 1% Triton X-100 (TMT), pH 6.4, 1 mM EDTA and a cocktail of protease inhibitors (final concentrations 0.34 mg/ml phenylmethylsulfonyl fluoride, 50 μg/ml lima bean trypsin inhibitor, 2 μg/ml leupeptin, 16 μg/ml benzamidine, and 2 μg/ml pepstatin) were added. Cell extracts were centrifuged at 22,000 x g for 15 minutes at 4°C. Anterior pituitaries were collected from adult mice and homogenized in TM, pH 6.4 containing 1 mM EDTA and protease inhibitors. Homogenates were centrifuged at 1,000 x g for 5 minutes at 4°C to remove cell debris. Particulate material was collected by centrifugation at 435,000 x g for 15 minutes at 4°C. Membrane associated proteins were solubilized by suspending this pellet in 250 μl TMT, pH 6.4 containing 1 mM EDTA and protease inhibitors. After incubation at 4°C for 30 min, pituitary lysates were clarified by centrifugation at 22,000 x g for 15 minutes at 4°C. Supernatants (250 μl - PAM-1 cells and pituitary cells) were pre-cleared by incubation with 10 μl packed protein A (Repligen BioProcessing) or protein A/G (Thermo Scientific) beads for 30 minutes at 4°C. After centrifugation at 1,000 x g for 5 minutes, 10 μl of supernatant was collected as the input for the Western blot and the rest of supernatant was transferred into a new tube containing 1 μg of antibody (affinity-purified rabbit antibody to PAM exon 16 or mouse monoclonal antibody to γ-adaptin); as a control, lysates were incubated with mouse or rabbit immunoglobulin. Samples were tumbled overnight at 4°C and then centrifuged at 22,000 x g for 15 minutes at 4°C to remove insoluble

material. The supernatants were added to protein A (rabbit antibodies) or protein A/G (mouse antibodies) beads (10 μl packed resin) and tumbled for 1 hour at 4°C. Beads were washed twice in pH 6.4 TMT containing 1 mM EDTA and protease inhibitors, and once in pH 6.4 TM containing 1 mM EDTA and protease inhibitors. The bound fraction was eluted by incubation for 5 minutes at 95°C in Laemmli sample buffer, fractionated by SDS-PAGE on 4-15% gradient gels (Bio-Rad) and subjected to Western blot analysis.

2.5.11 Transfection of pEAK Rapid cells

pEAK Rapid cells (Edge Biosystems, Gaithersburg, MD) a derivative of HEK293 cells, were plated on a 6-well dish which had been coated with 0.1 mg/ml poly-L-lysine for 5 minutes followed by a rinse in NuSerum and two rinses in growth medium. When about 70% confluent, cells were transfected with 1 μg DNA/well using Lipofectamine 2000 ® as described above. After 6 hours, transfection medium was replaced with growth medium; cell extracts were collected the following day for co-immunoprecipitation experiments.

2.6 Acknowledgments

We thank Darlene D'Amato and Yanping Wang for their constant technical support. We thank Dr. Kurutihalli Vishwanatha and Megan Miller for their helpful comments on the manuscript. We thank Dr. Lloyd Fricker for his generous gift of carboxypeptidase D antibodies and Dr. Ann Cowan for guidance with our fluorescence imaging experiments. We thank the Electron Microscopy Unit of the Institute of Biotechnology, University of Helsinki for providing laboratory facilities. This work was supported by the National Institutes of Health (DK32949), Scoville Endowment, Janice and Rodney Reynolds Endowment, Liv och Halsa

Foundation, the Magnus Ehrnrooth Foundation, the Perklén Foundation and the Intramural Program of NICHD, NIH. The authors declare they have no conflicts of interest.

2.7 Tables

Antigen	Working dilution	Identity, source
rat PAM-1:		
C-STOP, PAM-1(965-976)	1:1000	C-stop [223]
Exon 16, PAM-1(409-497)	1:1000	JH629 [224]
PHM, PAL-1(37-382)	1:1000	JH1761 [225]
PAL, PAM-1(498-604)	1:1000	JH877 [77]
SG proteins:		
PC1(359-373)	1:1000	JH888 [199]
POMC(γ_3MSH)	1:1000	JH189 [226]
Carboxypeptidase D	1:1000 and see EM	CPD AE 142, gift from Dr. Lloyd Fricker [227]
ACTH (Rabbit)	See EM	C-terminus of ACTH [192]
POMC/ACTH (Rabbit)	1:1000	JH93 (N-terminus of ACTH) [228]
AP-1 components:		
μ1A	1:500	ProteinTech Group
γ-adaptin	1:1000	BD Biosciences
Golgi:		
GM130	1:1000	BD Biosciences
TGN38 (155-249)	1:1000	[189]

Table 2.1: List of antibodies with working dilutions for Western Blot and fluorescent immunostaining along with the source used in this study.

Clone ID	Name in the study	Target region
TRCN0000111545	545	3'-UTR
TRCN0000111546	546	CDS
TRCN0000111547	547	CDS
TRCN0000111548	548	CDS
TRCN0000111549	549	CDS

Table 2.2: List of viruses clone IDs used in this study. 3'-UTR: 3' untranslated region. CDS: coding sequence.

2.8 Figures

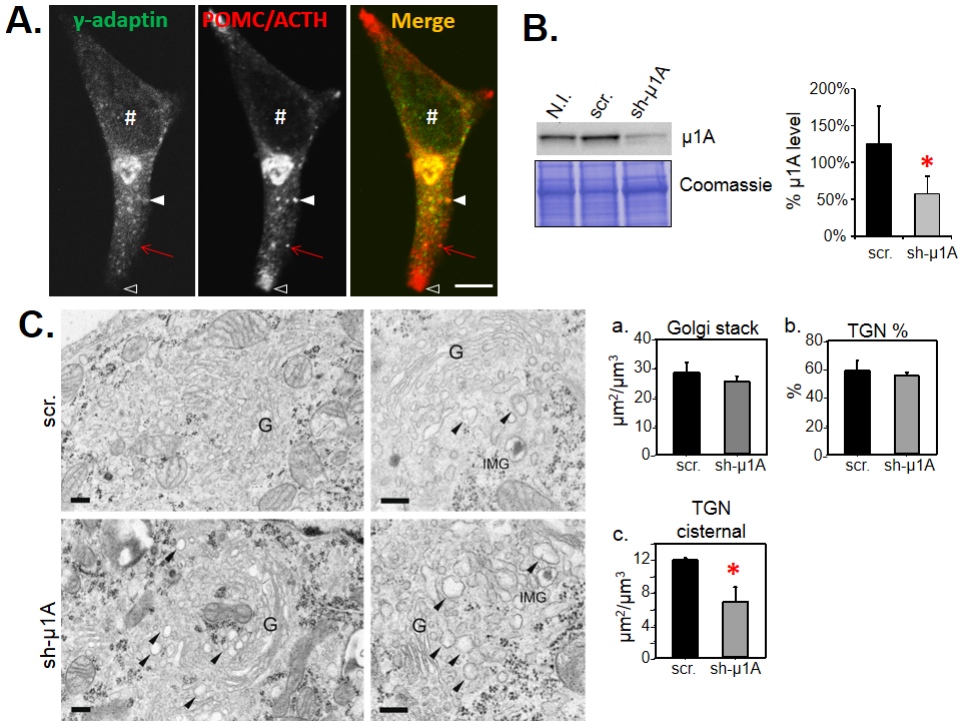

Figure 2.1: PAM-1 cells expressing reduced levels of μ1A have a more vacuolated TGN structure. (A) Indirect immunofluorescent staining of γ-adaptin (FITC anti-mouse) and POMC/ACTH (Cy3 anti-rabbit) in AtT-20 cells stably expressing PAM-1 (PAM-1 cells); #, nucleus; filled arrowhead, vesicle positive for γ-adaptin and POMC/ACTH; red arrow, vesicle positive for POMC/ACTH but negative for γ-adaptin; open arrowhead, tip of the cell where SGs accumulate; scale bar, 10 μm. Quantification is shown in Figure 2.11C. (B) Left, Western blot comparing μ1A expression in non-infected (N.I.) PAM-1 cells, PAM-1 cells infected with a non-target shRNA expressing lentivirus (scramble, scr.) or PAM-1 cells infected with the #549 lentivirus (sh-μ1A); Coomassie staining showed similar amounts of protein in the three cell lines. Right, quantification of μ1A level in nine clones for the scramble PAM-1 cells and ten clones for the sh-μ1A PAM-1 cells. (C) Left, Architecture of the Golgi stack and TGN in scramble and sh-μ1A PAM-1 cells. Vacuoles of varying electron density were more frequent in the TGN of sh-μ1A PAM-1 cells (black arrowheads): G, Golgi stack; IMG, immature SG; scale bar, 200 nm. Right, graphs show the surface to volume ratio of Golgi stack membrane (a), the volume fraction of the TGN in relation to the total volume of the Golgi complex (b) and the surface to volume ratio of cisternal elements in the TGN (c) (* $p<0.05$).

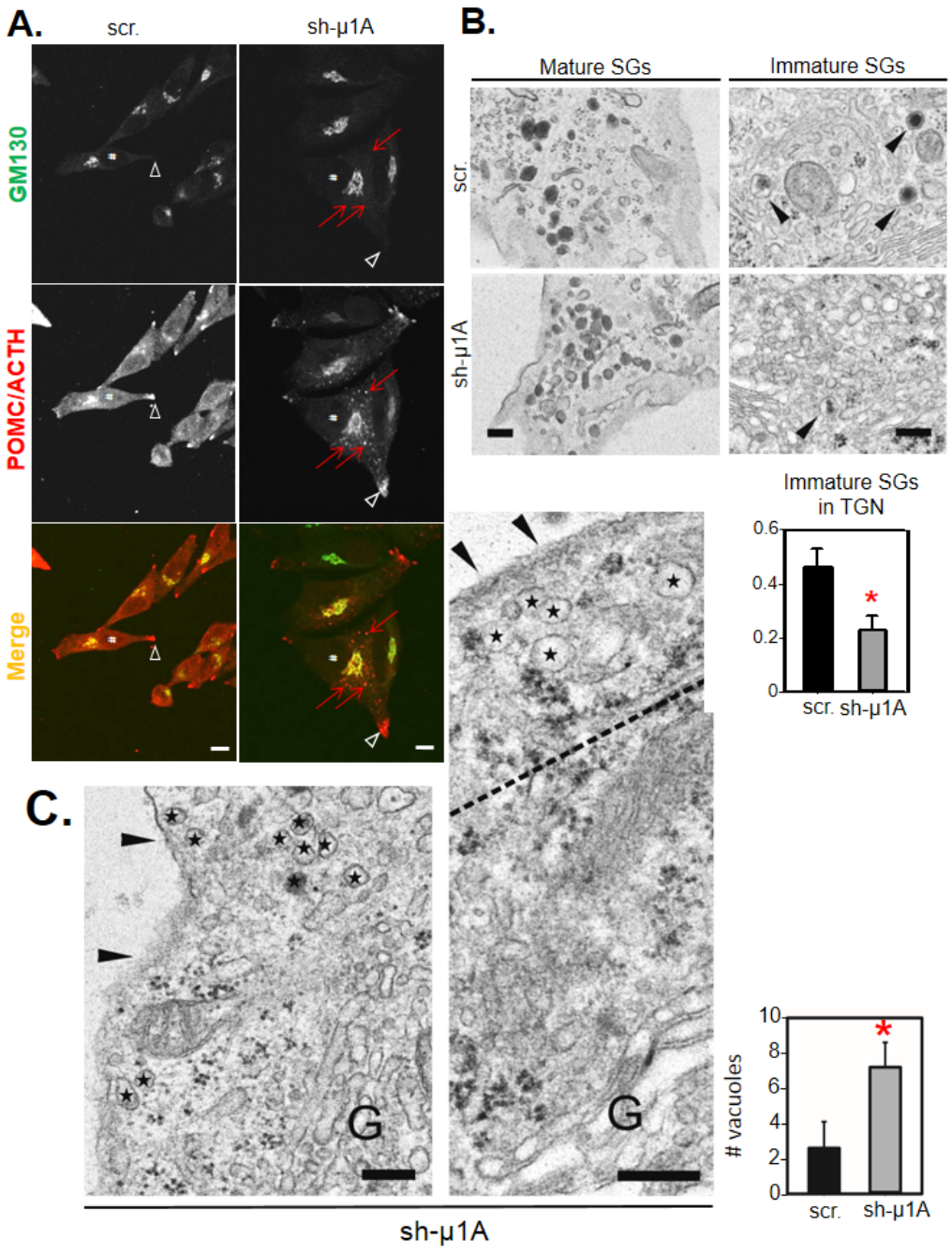

Figure 2.2: The formation of immature SGs is impaired in sh-μ1A PAM-1 cells.

Figure 2.2: (A) Indirect immunofluorescent staining of GM130 (FITC anti-mouse), a *cis*-Golgi marker, and POMC/ACTH (Cy3 anti-rabbit) in scramble and sh-μ1A PAM-1 cell lines; #, nucleus; red arrows, bright puncta positive for POMC/ACTH seen only in sh-μ1A PAM-1 cells; open arrowhead, tip of the cell, where SGs accumulate; scale bar, 10 μm. Quantification of Golgi, intermediate and tip staining is shown in Figures 2.12A (PAM) and 2.12B (CPD). (B) Transmission electron micrographs showing mature SGs at the tips of cell processes (left) and immature SGs in the TGN area (black arrowheads, right) in scramble (scr.) and sh-μ1A PAM-1 cells. The graph shows the number of immature SGs in the TGN area (* $p<0.01$). (C) Transmission electron micrographs of sh-μ1A PAM-1 cells; black stars mark vacuolar structures located between the Golgi complex and the plasma membrane. Inset: graph shows the number of vacuoles in the 500 nm peripheral zone (between the dashed line and the cell membrane, * $p<0.05$).

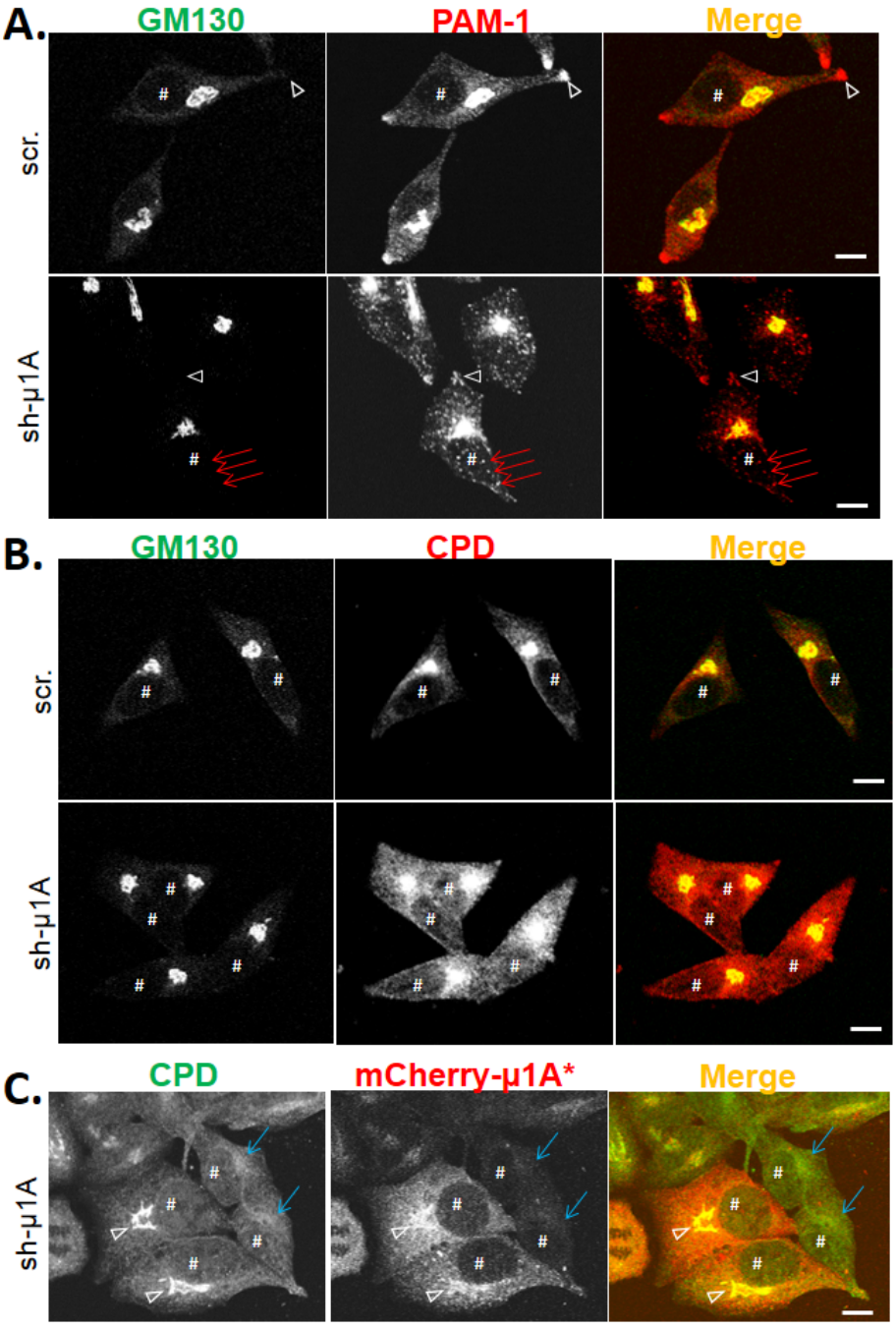

Figure 2.3: CPD and PAM-1 localization are sensitive to μ1A knockdown.

Figure 2.3: (A) Indirect immunofluorescent staining of PAM-1 (C-terminus, Cy3-anti-rabbit) and GM130 (FITC-anti-mouse), a *cis*-Golgi marker, in scramble (scr.) and sh-μ1A PAM-1 cell lines. Red arrows point to bright PAM-1 puncta seen only in sh-μ1A PAM-1 cells. (B) Immunofluorescent staining of endogenous CPD and GM130 in scramble and sh-μ1A PAM-1 cells; CPD was visualized using an antibody to its luminal domain (Cy3-anti-rabbit). #, nucleus; open arrowhead, tip of the cell; scale bar, 10 μm. Quantification of Golgi, intermediate and tip staining is shown in Figures 2.12B (PAM) and C (CPD). (C) sh-μ1A PAM-1 cells were transiently transfected with plasmid encoding mCherry-μ1A*. Cells were fixed the day following transfection and stained for CPD (FITC-anti-rabbit). Blue arrows point to non-transfected cells where CPD distribution was diffuse throughout the cell. Open arrowheads point to the Golgi apparatus of transfected cells; CPD was concentrated in the Golgi region, as in scramble PAM-1 cells. Quantification is shown in Figure 2.12D.

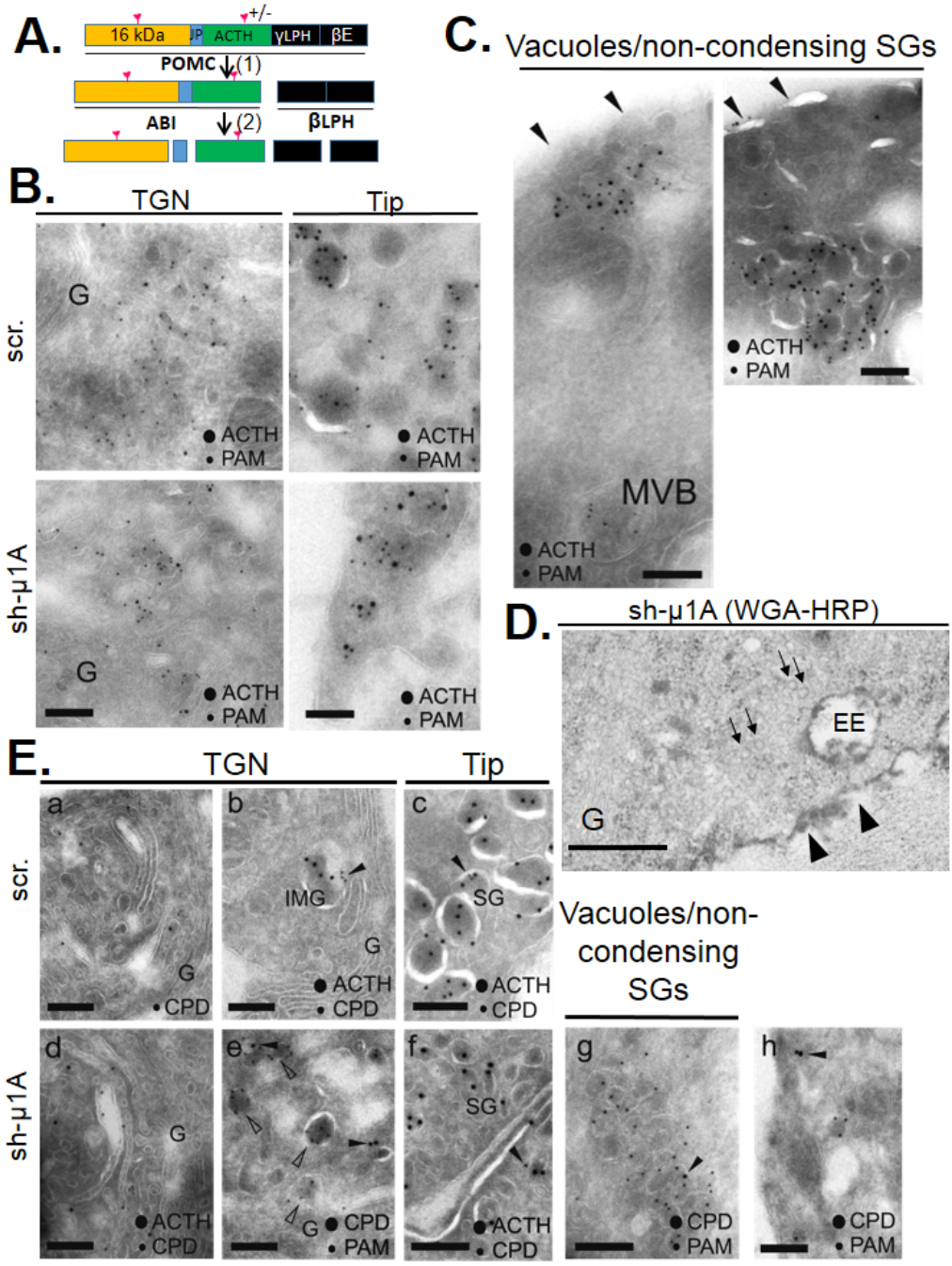

Figure 2.4: Formation of PAM and ACTH containing vacuoles in sh-μ1A PAM-1 cells.

Figure 2.4: (A) Diagram of POMC processing: the cleavage generating ACTH biosynthetic intermediate (ABI) and β-lipotropin (βLPH) starts in the TGN [indicated as (1)] while cleavages producing 16 kDa fragment, joining peptide (JP), ACTH, γ-lipotropin (γLPH) and β-endorphin (βE) occur in SGs [(indicated as (2)] [12]. (B) ACTH (15 nm gold) and PAM (10 nm gold) co-localized in the TGN and in mature SGs at the tips of scramble and sh-μ1A PAM-1 cells. G, Golgi. (C) Cryosections (two panels) of sh-μ1A PAM-1 cells show immunoreactivity for ACTH and PAM in vacuolar/non-condensing SG structures; the PAM-positive multivesicular body (MVB) defines the middle of the cell. Black arrowheads indicate the cell membrane. (D) HRP was detected at the plasma membrane (black arrowheads) and in early endosomes (EE) after sh-μ1A PAM-1 cells were incubated in HRP-WGA for 10 min. Black arrows point to non-condensing SGs which lack HRP staining. Scale bar, 500 nm. (E) CPD, ACTH and PAM were localized using 15 nm and 10 nm gold as indicated. CPD was present in cisternal and vacuolar elements of the TGN in scramble and sh-μ1A PAM-1 cells (a, d). Although CPD was found in immature SGs in scramble PAM-1 cells (immature SGs, IMG, identified by ACTH; black arrowhead) (b), CPD was largely absent from PAM positive immature SGs or non-condensing SGs in sh-μ1A PAM-1 cells (e, open arrowheads); only one of these structures contained CPD (e, upper black arrowhead). CPD was readily identified in TGN membranes (e, lower black arrowhead). Very few mature SGs contained CPD (c,f, black arrowhead). The non-condensing SGs found in sh-μ1A PAM-1 cells contained PAM, but rarely contained CPD (g, black arrowhead). Peripheral vesicular or tubular structures usually stained distinctly for CPD or PAM (h, black arrowhead). Except for panel D, scale bar, 200 nm.

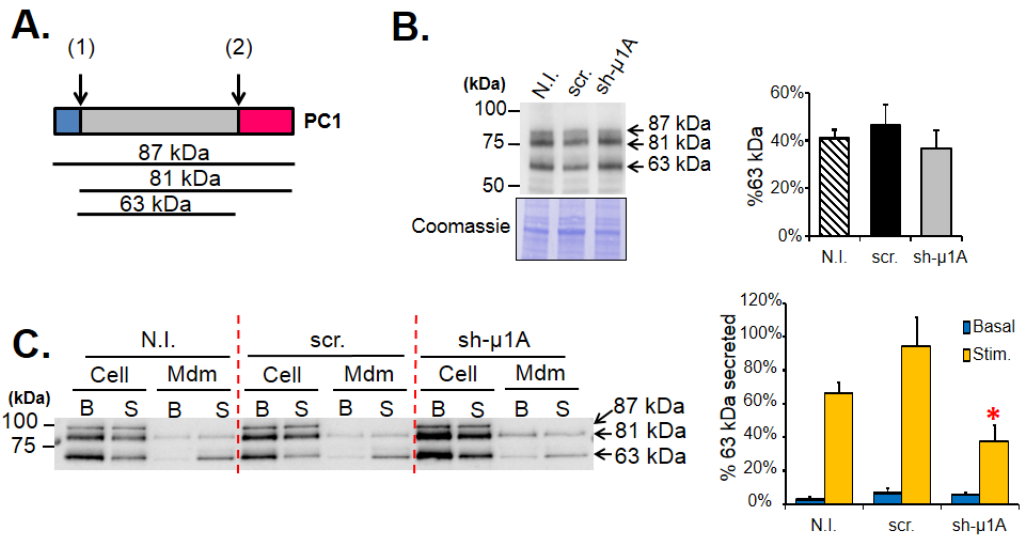

Figure 2.5: Regulated secretion of soluble content proteins is impaired in sh-μ1A PAM-1 cells. (A) Diagram showing the processing of PC1: arrow (1) indicates a cleavage occurring in the endoplasmic reticulum; arrow (2) points to a cleavage happening in mature SGs. (B) Left, Western blot of non-infected (N.I.), scramble (scr.) and sh-μ1A PAM-1 cell extracts using a PC1 antibody showed no change in the amounts of PC1 processed products. Coomassie staining showed similar amounts of protein among the three cell lines. Right, quantification of the 63 kDa form of PC1 (63 kDa/(63 kDa + 81 kDa + 87 kDa)) using densitometry (n = 3-8; no statistical differences were seen using a t-test). (C) Left, Western blot showing the level of the different forms of PC1 secreted under basal and stimulated conditions in N.I., scr. and sh-μ1A PAM-1 cells. Right, graph showing the secretion rate of the 63 kDa form of PC1 ($63\ kDa_{mdm}/(63\ kDa_{mdm} + 63\ kDa_{cell})$) after densitometry. Four sets of data from two independent experiments are represented in the graphs. (* $p<0.05$)

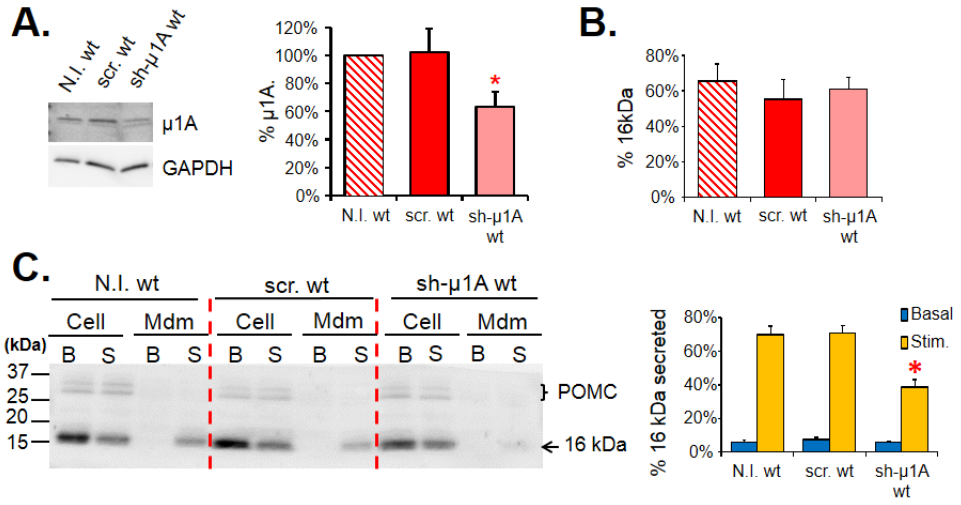

Figure 2.6: Regulated secretion of soluble content proteins is impaired in wt cells. (A) Left, Western blot showing the level of μ1A after infection of wild type (wt) AtT-20 cells with the non-target virus (scr. wt) or with the #549 virus (sh-μ1A wt). Right, quantification of μ1A level of nine sh-μ1A wt clones and ten scramble wt clones relative to μ1A level in non-infected cells (N.I. wt). (B) Graph representing the percentage of 16 kDa fragment in all three cell lines (16 kDa/(16 kDa + POMC)). These data were collected by densitometry (n = 5-7; no statistical differences were seen using a t-test). (C) Left, Western blot after stimulation of secretion experiment looking at 16 kDa fragment secretion. Right, graph showing 16 kDa fragment secretion rate ($16\ kDa_{mdm}/(16\ kDa_{mdm} + 16\ kDa_{cell})$) after densitometry. Four sets of data from two independent experiments are represented on the graphs (* $p<0.05$ when comparing secretion rate in sh-μ1A wt with N.I.wt and scr. wt cells using a t-test; mdm, medium; B, basal; S, stimulated).

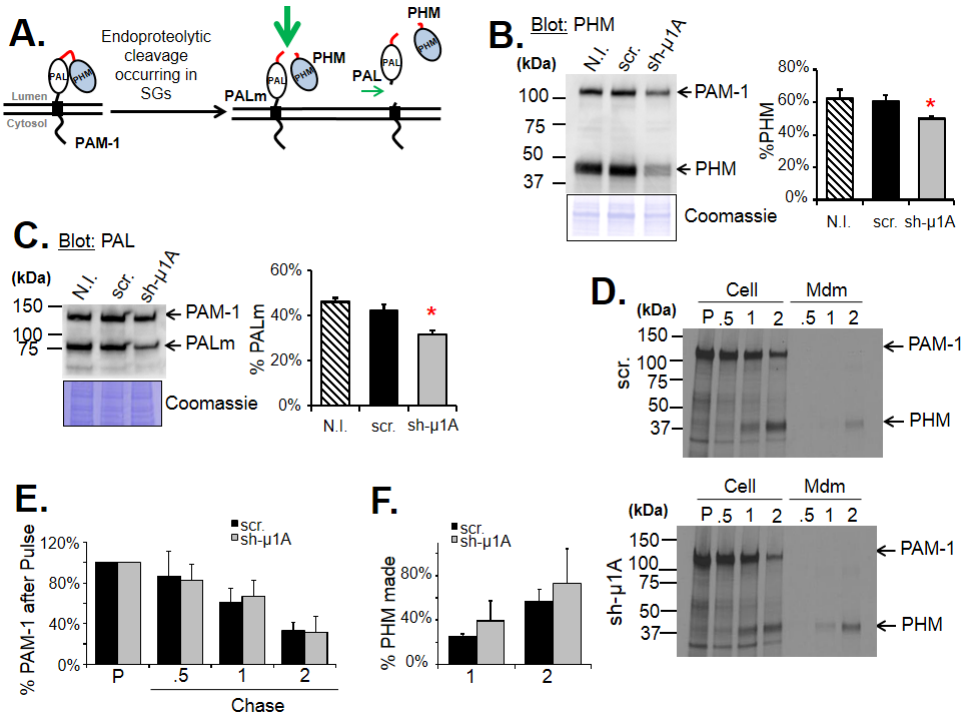

Figure 2.7: PAM-1 trafficking is altered in sh-μ1A PAM-1 cells. (A) Diagram showing the sites at which PAM-1 is cleaved in SGs (green arrow) and the cleavage products created; endoproteolytic cleavage between PHM and PAL occurs more frequently than cleavage between PAL and the transmembrane domain. (B, C) Left, Western blots of non-infected (N.I.), scramble (scr.) and sh-μ1A PAM-1 cell extracts using a PHM antibody (B) or a PAL antibody (C). Coomassie staining showed similar amounts of protein among the three cell lines for each blot. Right, quantification of the level of PHM (PHM/(PHM + PAM-1)) (B) and PAL (PALm/(PALm + PAM-1)) (C) using densitometry (n = 3 for the data shown; * $p<0.05$ from a t-test comparing sh-μ1A values with N.I. and Scr.; no statistical difference was observed between N.I. and scr.). (D - F) PAM-1 cells (scramble and sh-μ1A) were incubated in medium containing [^{35}S]Met/Cys for 20 min. PAM-1 cells were either collected 10 minutes later (P) or chased for 0.5, 1 or 2 hours; medium was collected for each chase time. Samples were immunoprecipitated with a PHM antibody and analyzed after fractionation by SDS-PAGE and fluorography. (D) Films from two independent experiments were densitized. (E) The stability of the newly synthesized PAM-1 was quantified with reference to the amount present after the pulse ([^{35}S]PAM-1$_{chase}$/[^{35}S]PAM-1$_{pulse}$). (F) Total PHM synthesis (cells plus medium) from newly synthesized PAM-1 was similar in scramble and sh-μ1A PAM-1 cells (([^{35}S]PHM$_{cell}$ + [^{35}S]PHM$_{mdm}$)/[^{35}S]PAM-1$_{pulse}$).

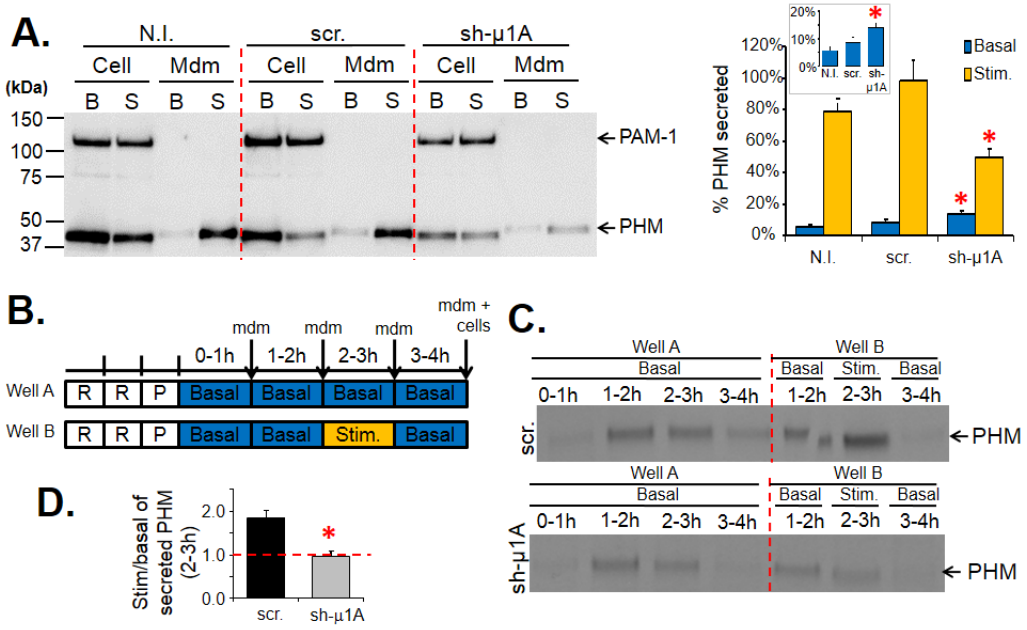

Figure 2.8: Regulated secretion of PHM is impaired in sh-μ1A PAM-1 cells. (A) Left, Western blot showing the level of PHM secreted under basal and stimulated conditions in non-infected (N.I.), scramble (scr.) and sh-μ1A PAM-1 cells. Right, graph showing the secretion rate of PHM ($PHM_{mdm}/(PHM_{mdm} + PHM_{cell})$) after densitometry. Four sets of data from two independent experiments are represented on the graph. Boxed graph shows PHM secretion rate under basal conditions. (B) Experimental paradigm for both scramble and sh-μ1A PAM-1 cells: identical wells of cells were rinsed (R) and incubated with [^{35}S]Met/Cys medium for 20 min (P). Spent medium was collected and replaced by basal medium every hour for 4 hours, except during the 2-3 h chase period, when well A received basal medium and well B received secretagogue (stim., basal medium with 2 mM $BaCl_2$). (C) Fluorograms showing secretion of newly synthesized PHM purified by immunoprecipitation. (D) Graph showing the ratio of newly synthesized PHM secreted under stimulated vs. basal conditions during the 2-3h chase period (mdm, medium; B, basal; S, stimulated; * $p<0.05$).

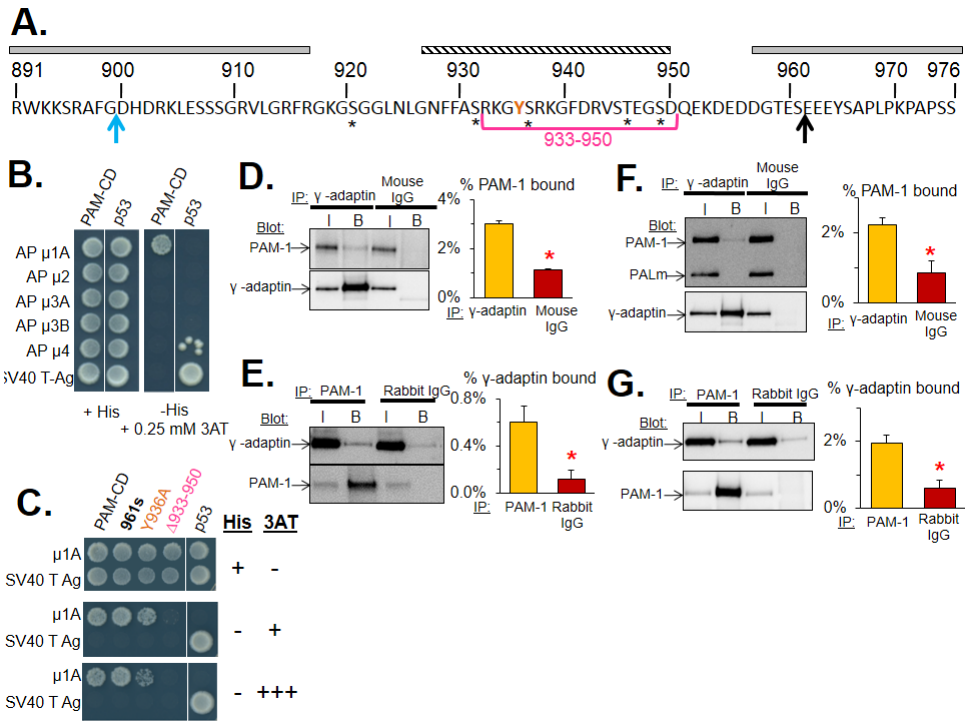

Figure 2.9: The cytosolic domain of PAM (PAM-CD) interacts with the μ1A subunit of AP-1A.

Figure 2.9: (A) Amino acid sequence of the cytosolic domain of PAM. Phosphorylation sites are shown with asterisks. Gray rectangles show regions of PAM-CD which do not alter PAM-1 trafficking upon deletion; striped rectangle shows region involved in trafficking. The blue and black arrows mark residues 899 and 961, respectively. (B) Yeast two-hybrid screen for interaction between PAM-CD and the medium subunits of the AP family. Left set, yeast grown in absence of tryptophan and leucine. Right set, yeast grown in absence of tryptophan, leucine and histidine. 3AT, 3-amino-1,2,4-triazole, an inhibitor of histidine synthesis, was used to prevent false positive results. The p53 and SV40 T Ag interaction served as a positive control. (C) Yeast two-hybrid screen for interaction of wild-type and mutant PAM-CD with μ1A. Top set, growth of yeast in absence of tryptophan and leucine. Middle and bottom sets, yeast grown in absence of leucine, tryptophan and histidine in presence of increasing amounts of 3AT (+: 0.25 mM 3AT; +++: 1 mM 3AT). Co-immunoprecipitation was used to demonstrate an interaction of PAM-1 and the AP-1A complex in mouse pituitary (D, E) and in PAM-1 AtT-20 cells (F, G). Tissue and cell lysates were prepared in TMT, pH 6.4 to preserve the clathrin coat [229]. Mouse γ-adaptin antibody was used to capture the AP-1A complex (D, F) and affinity-purified rabbit antibody directed against the linker region between the PHM and PAL domains of PAM-1 was used to immunoprecipitate PAM-1 (E, G); mouse and rabbit IgG were used as controls for background. The amount of input analyzed represents 1/20th of the amount of immunoprecipitate analyzed. Quantification of each blot revealed a significant interaction between PAM-1 and AP-1A. I, input; B, bound; n = 4-6; *P<0.05.

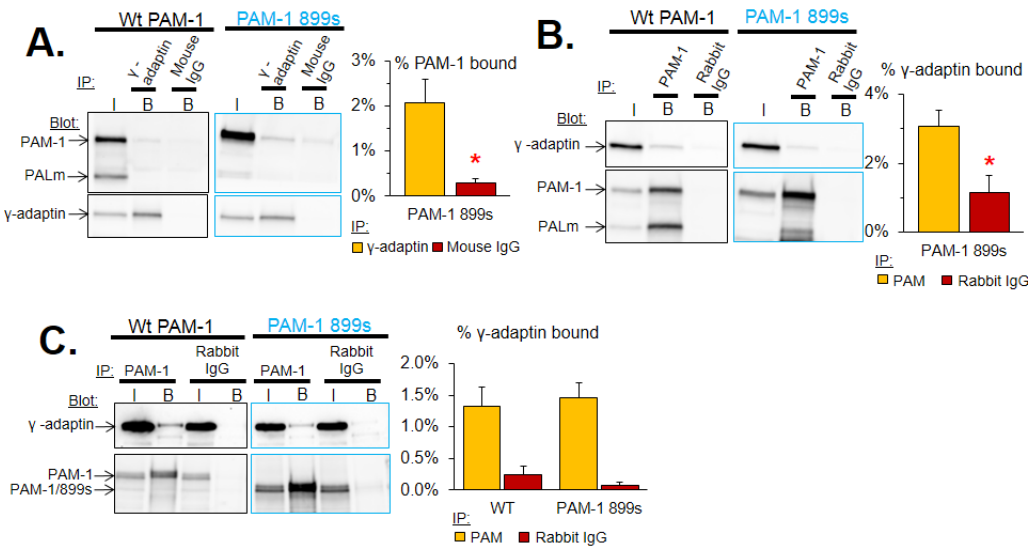

Figure 2.10: PAM luminal domain contribution to the PAM/AP-1 interaction. (A, B) Co-immunoprecipitation of PAM and AP-1A was examined in AtT-20 cells expressing PAM-1 or PAM-1 899s (PAM-1 lacking its cytosolic domain) as described in Figure 2.9. Although it includes only 9 amino acids of the cytosolic domain, PAM-1 899s co-immunoprecipitated with the γ-adaptin antibody (n=4) and γ-adaptin co-immunoprecipitated with the PAM antibody. (C) pEAK Rapid cells transiently expressing PAM-1 or PAM-1 899s were analyzed as described for AtT-20 cells. Co-immunoprecipitation was observed using antibody to PAM (n=4).

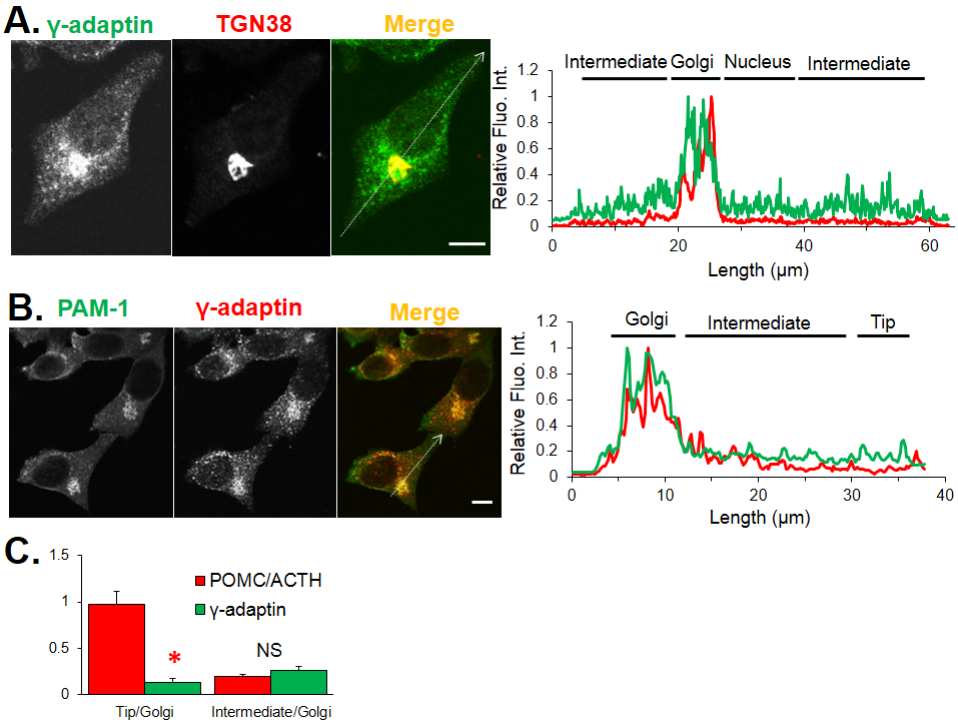

Figure 2.11: γ-adaptin and PAM-1 both concentrate in the TGN area in AtT-20 cells. (A) Single color and merged images for γ-adaptin (FITC-anti-mouse) and TGN38 (Cy3-anti-rabbit) in PAM-1 AtT-20 cells. Scale bar, 10 μm. Linescan (white arrow on merged image) showing relative fluorescence intensity; γ-adaptin and TGN38 strongly colocalized. Regions identified as Golgi, Intermediate, nucleus and tips are shown. (B) Single color and merged images for γ-adaptin (FITC-anti-mouse) and PAM-1 (C-terminus of PAM; Cy3-anti-rabbit) in PAM-1 AtT-20 cells. Scale bar, 10 μm. Linescan (white arrow on merged image) showing relative fluorescence intensity. Both γ-adaptin and PAM-1 concentrated at the Golgi region; PAM-1 was also seen at the tips of the cells. Regions identified as Golgi, Intermediate and Tips are shown. (C) Quantification of images stained for γ-adaptin (FITC-anti-mouse) and POMC/ACTH (Cy3-anti-rabbit) in PAM-1 AtT-20 cells (Figure 2.1A). Ratio of Tip to Golgi signals and Intermediate to Golgi signals are shown; when compared to Golgi staining, γ-adaptin staining was not as concentrated at the tips as POMC/ACTH staining. (n =10 cells; $p < 0.0001$).

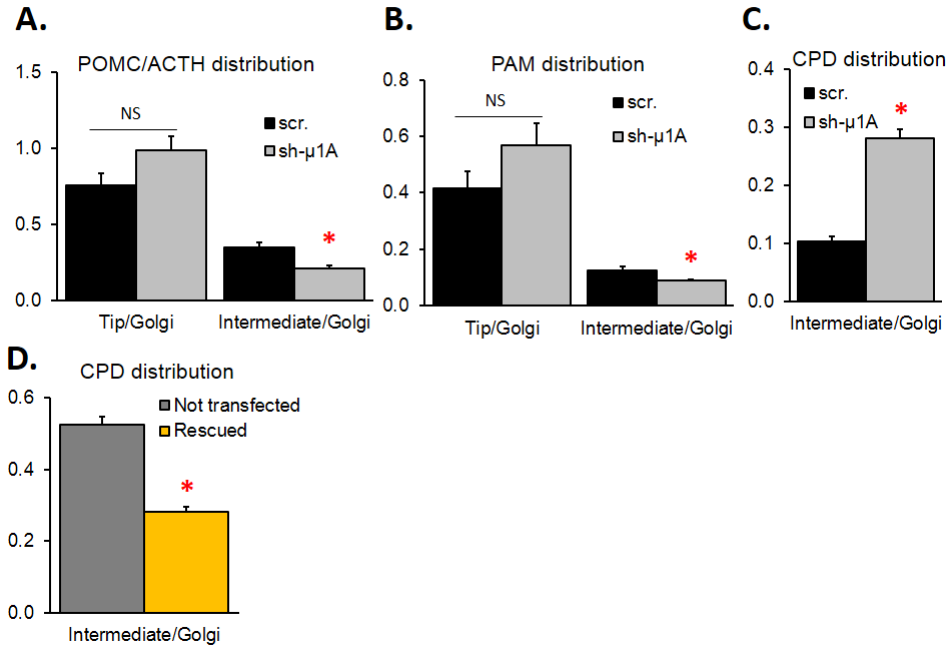

Figure 2.12: Steady state localization of POMC/ACTH, CPD and PAM-1 is altered in sh-μ1A PAM-1 cells. Images from scramble and sh-μ1A PAM-1 cells were quantified as described in Materials and Methods. (A) Images from cells stained for GM130 (FITC-anti-mouse) and POMC/ACTH (Cy3-anti-rabbit) (Figure 2.2A). The Tip/Golgi ratios did not differ (NS) but the Intermediate/Golgi ratio was lower in sh-μ1A PAM-1 cells (n = 14-15 cells; $p < 0.001$). (B) Images from cells stained for GM130 (FITC-anti-mouse) and PAM (Cy3-anti-rabbit) (Figure 2.3A). As for POMC/ACTH, the Tip/Golgi ratios did not differ, but the Intermediate/Golgi ratio was lower in sh-μ1A PAM-1 cells (n = 19-37 cells; $p < 0.005$) (C) Images from cells stained for GM130 (FITC-anti-mouse) and CPD (Cy3-anti-rabbit) (Figure 2.3B). The Intermediate/ Golgi ratio was significantly increased in sh-μ1A PAM-1 cells (n = 12-18 cells; $p < 0.0001$). (D) Images from sh-μ1A PAM-1 cells transiently transfected with a plasmid encoding mCherry-μ1A* were stained for CPD (FITC-anti-mouse). The Intermediate/Golgi ratio was significantly decreased in transfected sh-μ1A PAM-1 cells (n = 24-28 cells; $p < 0.0001$).

Chapter 3

The role of AP-1A in endocytic trafficking in a professional secretory cell

Mathilde L. Bonnemaison, Nils Bäck, Kristiina Kanerva, Elina Ikonen, Richard E. Mains and Betty A. Eipper.

Manuscript in preparation for Experimental Cell Research.

Drafting of the manuscript

Mathilde L. Bonnemaison, Richard E. Mains and Betty A. Eipper.

Acquisition of data

Nils Bäck did the electron microscopy study; Kristiina Kanerva and Elina Ikonen did the bodipy-CHOL experiment; Mathilde L. Bonnemaison did the remaining experiments under

the guidance and supervision of Richard E. Mains and Betty A. Eipper.

3.1 Abstract

The endocytic pathway is essential for the uptake of nutrients into cells. Endocytosed material first enters early endosomes, where it can be routed to the plasma membrane, *trans*-Golgi network (TGN) or lysosomes. Material to be recycled to the plasma membrane can travel directly or indirectly, via recycling endosomes. The bulk of early endosomes then undergoes a maturation process to become late endosomes and their cargo can either be recycled to the TGN or degraded in lysosomes. Professional secretory cells produce peptides, which serve as messengers to communicate between cells. Synthesized as inactive precursors, peptides must undergo post-translational modifications in order to gain bioactivity. One of the peptide modifications is catalyzed by peptidylglycine α-amidating monooxygenase 1 (PAM-1), a membrane protein which generates an α-amide moiety at the C-terminus of peptides. Once at the plasma membrane after exocytosis of peptides, PAM-1 is internalized in endosomes from which it can be recycled to the TGN or degraded in lysosomes. The adaptor protein 1 complex (AP-1) is a cytosolic complex involved in the transport of cargo between the TGN and endosomes and, in professional secretory cells, AP-1 mediates secretory granule biogenesis and maturation. Because exocytosis is balanced with endocytosis, we explored the function of AP-1 in the endocytic pathway of AtT-20 cells, a corticotrope tumor cell line. AtT-20 cells stably expressing PAM-1 were infected with a lentivirus expressing a non-target shRNA (scramble) or an shRNA against the medium subunit of AP-1A, μ1A (sh-μ1A) to abrogate AP-1 function. Early and recycling endosomes concentrated above the Golgi apparatus in sh-μ1A PAM-1 cells instead of being more widely distributed. Late endosomes

were smaller in sh-μ1A PAM-1 cells compared with scramble PAM-1 cells, suggesting that AP-1 controls endosome maturation. Cholesterol, transferrin and PAM-1 trafficking were altered in sh-μ1A PAM-1 cells. Overall, AP-1 is not only a key player in the formation of secretory granules, it plays a critical role in the endocytic pathway as well.

3.2 Introduction

The endocytic pathway performs a vital process in the uptake of nutrients, solute and lipids and is used by viruses and bacteria to invade cells. Internalized material first enters early endosomes (also named sorting endosomes), which are evenly distributed throughout the cell and move toward the perinuclear region during maturation in most cells [230]. The early endosomes consist of a tubular domain containing material to be recycled and a vacuolar domain composed of proteins destined for endosomal maturation, recycling to the TGN and eventually protein degradation in lysosomes. Recycling of cargo to the plasma membrane can occur directly from early endosomes (regulated by Rab4 and Rab35) or indirectly, via recycling endosomes (regulated by Rab11) [230]. Early endosomes undergo a maturation process to become late endosomes, also known as multivesicular bodies, which can either send material back to the TGN for recycling or fuse with lysosomes, the final step of the endocytic pathway for digestion of macromolecules. Key maturation steps involve a drop in pH, from pH 6.4 in early and recycling endosomes to pH 4.9 in lysosomes, along with a switch in the associated small Rab GTPase (from Rab5 for early endosomes to Rab7 for late endosomes). Endosomal maturation is a complex process involving the formation of intraluminal vesicles along with a change in size, morphology, protein content and lipids (Figure 3.1) [230].

Endosomes move along microtubules, powered by a dynein or a kinesin motor. Dynein brings cargo to the minus end of microtubules (from the cell periphery to the cell center) while most kinesins bring cargo to the plus end of microtubules (from the cell center to the cell periphery). The kinesin superfamily can be divided into 15 families containing between one and eight members, referred to as KIFs [231]. Endosomes are connected to microtubules by multiple cytosolic proteins including adaptor protein 1 (AP-1), which interacts with microtubule associated protein 1a and KIF13A, a member of the kinesin 3 family [232, 233]. AP-1 belongs to the adaptor protein family, which is composed of five heterotetrameric complexes, each of which drives a specific cellular transport step. AP-1 carries cargo between the Golgi and endosomes and in secretory cells, AP-1 mediates secretory granule biogenesis and maturation [234, 56, 196, 57, 235, 55]. AP-1 is composed of two large subunits (γ and β1), a medium subunit (μ1) and a small subunit (σ1). Structural and knockout animal models indicate that lack of any one subunit of the AP-1 complex affects the stability and function of the remaining complex [117, 178, 183]. Work done on mouse embryonic fibroblasts isolated from μ1A knockout mice and on HeLa cells transfected with siRNA targeting an AP-1 subunit revealed that AP-1 plays a central role in protein sorting and early and recycling endosome dynamics and distribution [178, 236]. In HeLa cells, Rab4b recruits AP-1 to the tubules of early endosomal membranes [236] and KIF13A, which interacts with Rab11 along with AP-1, is required to generate and transport tubules from early endosomes to recycling endosomes [237]. KIF13A colocalizes with several markers identified on recycling endosomes and the tubular structures of early endosomes, and does not colocalize with EEA1, a Rab5 effector of the vacuolar domain of early endosomes (Figure 3.1) [237].

Peptides are first synthesized as inactive precursors which undergo a maturation process

driven by a set of enzymes in order to become bioactive. Neuroendocrine cells store peptides in secretory granules until a stimulus triggers their secretion. Secretion of the stored peptides results in the fusion of secretory granule membranes with the plasma membrane; retrieval of the granule membrane proteins is accomplished through the endocytic pathway. Although fibroblasts, HeLa cells and neurons have served as a good model to study the function of AP-1 in the endocytic pathway, our knowledge of AP-1 function in the endocytic pathway in neuroendocrine cells, which must retrieve granule membrane proteins for re-use in secretory granules, is limited. Neuroendocrine cells produce several essential secretory granule membrane proteins, one of which is the peptide amidating monooxygenase (PAM). PAM, which acts late in the peptide biosynthetic pathway, is essential for life [238]. PAM-1, a major splice variant, spans the membranes of secretory granules and endosomes (Figure 3.2). When PAM-1 enters secretory granules, prohormone convertase 1/3 can cleave it, producing soluble PHM (45 kDa) and PAL membrane (70 kDa, PALm) [12]. Although less frequent, cleavage between PAL and the transmembrane domain produces soluble PAL (48 kDa) and intermediate 1 (25 kDa), which includes the transmembrane and cytosolic domains of PAM [214]. PAM-1 retrieved from the cell surface can traverse the endocytic pathway, return to secretory granules and generate soluble PHM [195]. On the cell surface or within the endocytic pathway, α-secretase-mediated cleavage closer to the transmembrane domain generates soluble PAM (PAMs) and intermediate 2 (~20 kDa) [214]. Lastly, γ-secretase cleaves intermediates 1 and 2 within the transmembrane domain to generate a soluble fragment of the cytosolic domain (sf-CD) that can enter the nucleus and alter gene expression [223, 214].

To investigate AP-1 function in the endocytic pathway and the trafficking of membrane secretory granule proteins, the AtT-20 corticotrope tumor cell line stably expressing PAM-1

was stably infected, using a lentivirus expressing shRNA against the μ1A subunit of AP-1. The global effects of reduced AP-1 function on the endocytic pathway were investigated first and the endocytic trafficking of PAM-1 was evaluated next.

3.3 Results

3.3.1 Down-regulation of the medium subunit of AP-1 alters the localization of early and recycling endosomes in AtT-20 cells stably expressing PAM-1

AtT-20 cells stably expressing PAM-1 (PAM-1 cells) and infected with a virus encoding an shRNA against the medium subunit of AP-1 (μ1A) (sh-μ1A cells) or encoding a non-target shRNA as a control (scramble cells) were described previously [234]. Since AP-1 plays key functions in early stages of the endocytic pathway, the location of early and recycling endosomes was investigated. Members of the Rab family of small GTPases have served as useful markers to distinguish between early and recycling endosomes. Each Rab exists in a GDP-bound, cytosolic, inactive form plus a GTP-bound, membrane-associated, active form [239].

Rab5 is recruited to early endosome membranes upon activation by Rabex-5, its GDP/GTP exchange factor [240]. In order to visualize early endosomes, sh-μ1A and scramble PAM-1 cells were transiently transfected with a plasmid encoding fluorescently tagged Rab5 (mRFP-Rab5). In scramble PAM-1 cells, mRFP-Rab5 formed a cluster near the nucleus along with puncta evenly distributed throughout the cell (Figure 3.3A). In contrast, in sh-μ1A PAM-1 cells, vesicles formed a cluster near the nucleus with few peripheral puncta. Staining

for EEA1, another early endosomal marker, in embryonic fibroblasts prepared from μ1A knockout mice also revealed an accumulation of EEA1 positive puncta near the nucleus [178]. The formation of a cluster of Rab5 near the nucleus in scramble cells could be due to the overexpression of this protein because it stimulates the association and motility of early endosomes to the minus end of microtubules *in vitro* [241]. Altogether, our data suggest that early endosome location in AtT-20 cells may be driven by a similar AP-1 dependent process in AtT-20 cells and mouse embryonic fibroblasts.

Rab11 has been a useful marker for recycling endosomes [242]. Staining of scramble and sh-μ1A PAM-1 cells with an antibody against endogenous Rab11 revealed puncta and tubular structures along with diffuse staining (Figure 3.3B). The puncta and tubular structures correspond to Rab11 bound to membranes whereas the diffuse staining derives from cytosolic Rab11. While scramble PAM-1 cells contained Rab11-positive structures near the nucleus along with a significant population of Rab11-positive vesicles distributed throughout the cell, sh-μ1A PAM-1 cells contained a more pronounced cluster of Rab11-positive vesicles near the nucleus. A similar phenomenon was also seen in the human melanoma cell line, MNT-1, after the medium subunit of AP-1 had been knocked-down [186].

3.3.2 Cholesterol distribution is altered in sh-μ1A PAM-1 cells

Lack of μ1A in mouse embryonic fibroblasts alters cholesterol trafficking in the endocytic pathway [243]. Two proteins involved in cholesterol trafficking in endosomes are Niemann-Pick type C 1 (NPC1) and NPC2. NPC1, a lysosomal membrane protein, interacts with AP-1 in order to be trafficked to lysosomes. NPC2, a soluble protein, traffics to lysosomes via binding to the mannose-6-phosphate receptor, which requires AP-1 for proper transport.

Cholesterol uptake is first characterized by entry into the endocytic pathway and exit from lysosomes to go to the endoplasmic reticulum. In neuroendocrine cells, cholesterol is an important component of secretory granule membranes and is required for their biogenesis [244, 75]. Use of the dye BODIPY-CHOL allowed the visualization of cholesterol in live cells in non-infected and sh-μ1A PAM-1 cells (Figure 3.3C). In non-infected PAM-1 cells, cholesterol accumulated at the Golgi region, in vesicles surrounding the Golgi and at the tips, where mature secretory granules accumulate. In sh-μ1A PAM-1 cells, cholesterol staining was only concentrated in the Golgi area, with very few positively stained vesicles around the Golgi. No cholesterol staining was seen at the tips of processes in sh-μ1A PAM cells. These data suggested that AP-1 is also required for cholesterol transport in AtT-20 cells.

3.3.3 Trafficking of transferrin is perturbed in sh-μ1A PAM-1 cells

Transferrin, which brings iron into cells, has been widely used to probe endocytic trafficking [245, 246]. Apo-transferrin binds more weakly to the transferrin receptor than Fe^{3+}-loaded transferrin. Once the complex is formed, it is rapidly internalized into early endosomes, where the acidic pH is sufficient to dissociate Fe^{3+} from transferrin but not transferrin binding to its receptor. Transferrin and its receptor are either targeted back to the plasma membrane directly or via recycling endosomes. The neutral pH of the extracellular compartment promotes apo-transferrin dissociation from its receptor to collect more iron (Figure 3.1). Fluorescently-tagged transferrin is thus a good marker for both early and recycling endosomes.

Scramble and sh-μ1A PAM-1 cells were incubated with 25 μg/mL Alexa fluor 546 transferrin for 10 minutes before fixation (Figure 3.4). In scramble PAM-1 cells, puncta of Alexa fluor 546 transferrin were seen distributed throughout the cell, with some accumulation

in the perinuclear region, which could correspond to recycling endosomes. On the other hand, in sh-μ1A PAM-1 cells, puncta of Alexa fluor 546 transferrin were clearly accumulated near the nucleus. These data, along with the staining of Rab5 and Rab11, suggested that early and recycling endosomes form clusters near the nucleus and that endocytic protein trafficking is perturbed in sh-μ1A PAM-1 cells. Knock-down of AP-1 function in HeLa and MNT-1 cells resulted in a similar accumulation of internalized transferrin near the nucleus [186, 236].

3.3.4 Early endosome transport on microtubules is altered in sh-μ1A PAM-1 cells

During maturation, endosomes are transported along microtubules. Since AP-1 interacts directly and indirectly with the kinesins involved in early and recycling endosome function, we hypothesized that the change in early and recycling endosomal location was due to changes in plus-end directed microtubule transport [232, 247]. In order to test this hypothesis, we treated scramble and sh-μ1A PAM-1 cells for a short time with a low dose of nocodazole, a microtubule destabilizing agent; this approach has been shown previously to prevent the accumulation of early and recycling endosomes near the nucleus [39]. Uptake of Alexa fluor 546 transferrin was used to monitor the effect of nocodazole (Figure 3.4). As expected, treatment of scramble PAM-1 cells with nocodazole resulted in the dispersion of Alexa fluor 546 transferrin puncta. However, the effect of nocodazole on sh-μ1A PAM-1 cells was much more dramatic. Alexa fluor 546 transferrin puncta no longer accumulated in the perinuclear region; instead, puncta were broadly distributed throughout the cell. These data clearly demonstrated that early and recycling endosome location in AtT-20 cells is both microtubule and AP-1 dependent; our data suggest that sh-μ1A PAM-1 cells exhibit a deficit

in kinesin-mediated endosomal transport.

3.3.5 The endocytic trafficking of PAM-1 is altered in sh-μ1A PAM-1 cells

Internalized transferrin revealed an AP-1 dependent change in distribution (Figure 3.4), suggesting that the trafficking of additional proteins might be altered. The key function of neuroendocrine cells is to provide sufficient amounts of bioactive peptides when needed. After fusion at the plasma membrane, secretory granule membrane proteins are rapidly internalized into the endocytic pathway, where they can either be degraded or recycled to the secretory granules via the TGN. The amidating enzyme, PAM-1, is a type I transmembrane protein spanning the membranes of secretory granules and endosomes [195]. PAM-1 trafficking in the regulated secretory pathway requires AP-1, but it remains unknown whether AP-1 also controls PAM-1 routing within the endocytic pathway [234]. To investigate PAM-1 trafficking in the endocytic pathway, PAM-1 antibody and Alexa fluor 546 transferrin were added to the medium and cells were fixed after a 10 minute pulse. Internalized PAM-1 was distributed in vesicles throughout the cells and commenced to accumulate in the perinuclear region in scramble PAM-1 cells (Figure 3.5). According to the Bäck et al. study, PAM-1 starts to accumulate in late endosomes after 10 minutes, suggesting that the perinuclear concentration of PAM-1 in scramble cells could correspond to late endosomes. In sh-μ1A PAM-1 cells, PAM-1 accumulated in the perinuclear region (Figure 3.5). Internalized PAM-1 strongly overlapped with Alexa fluor 546 transferrin in both cell lines, suggesting that most internalized PAM-1 is in early endosomes and possibly in recycling endosomes too. These data suggested that changes in PAM-1 and transferrin trafficking were similar. Using electron microscopy, after a 20 minute incubation of AtT-20/PAM-1 cells in gold-labeled

PAM antibody, internalized PAM antibody accumulated in late endosomes in both cell lines (Figure 3.6). However, internalized PAM antibody was also visualized in small vesicles near the Golgi apparatus in sh-μ1A PAM-1 cells; this was not observed in scramble PAM-1 cells (Figure 3.6B). The exact nature of these vesicles is unknown, but could correspond to vesicles targeted toward the TGN for recycling.

3.3.6 Down-regulation of the medium subunit of AP-1A in PAM-1 cells alters endosome maturation

Because the location of early endosomal compartments and the trafficking of transferrin in the endocytic pathway were perturbed when AP-1 function was reduced, we hypothesized that endosome maturation might also be altered. Late endosomes, or multivesicular bodies, are characterized by intraluminal vesicles contained in spherical organelles with sizes ranging from 250 to 1000 nm. In previous studies, the endocytic trafficking of PAM-1 in AtT-20 cells was characterized using transmission electron microscopy to follow the uptake of gold-tagged PAM-1/antibody complexes [195]. The same approach was used to compare the endocytic trafficking of PAM-1 in scramble and sh-μ1A PAM-1 cells. Late endosomes appeared small and irregular in shape in sh-μ1A PAM-1 cells, suggesting that reduced AP-1 function altered endosome maturation (Figure 3.6, red arrows). Late endosomes fuse with lysosomes to form endolysosomes and allow protein degradation. Lysosomes are irregular in shape, with electron dense material on the edges in scramble PAM-1 cells, while they appeared smaller and more rounded in sh-μ1A PAM-1 (Figure 3.6).

3.3.7 The cytosolic domain of PAM-1 is no longer phosphorylated at Ser^{949} in sh-μ1A PAM-1 cells.

The cytosolic domain of PAM-1 controls its trafficking within the biosynthetic and endocytic pathways. Casein kinase II and P-CIP2/KIS/Uhmk1 phosphorylate Ser^{949}, generating a small acidic cluster near the C-terminus of PAM-1 [38, 39]. Phosphorylation at Ser^{949} promotes entry into secretory granules from the TGN but slows down PAM-1 recycling from endosomes to TGN [195, 39]. In order to measure the levels and distribution of PAM-1 phosphorylated at Ser^{949} in scramble and sh-μ1A PAM-1 cells, an antibody that specifically recognizes phosphorylated Ser^{949} was used. As a positive control, we used AtT-20 cells stably expressing PAM-1, where T^{946}S^{949} have been mutated into D^{946}D^{949} (PAM-1 TS/DD) to mimic phosphorylation. Previous work established that the PAM-1 TS/DD mutant protein was seemingly stuck in endosomes and was detected by the phosphospecific antibody; dephosphorylation of these sites in PAM-1 seemed essential to the completion of endocytic trafficking [39]. Scramble and sh-μ1A PAM-1 cells were co-stained with the rabbit antibody that recognizes pSer^{949} and a mouse monoclonal antibody that targets the C-terminus of PAM-1 representing total PAM-1 (Figure 3.7A). In scramble PAM-1 cells, the pSer^{949} distribution was perinuclear and colocalized with the other PAM-1 antibody. Surprisingly, sh-μ1A PAM-1 cells were devoid of signal when visualized using the pSer^{949} antibody, suggesting that phosphorylation of Ser^{949} was reduced in sh-μ1A PAM-1 cells or that PAM-1 phosphorylated at Ser^{949} was more dispersed in the cells. To find out if the reduced PAM-1 pSer^{949} signal were due to a reduction in the level of PAM-1 phosphorylated at this site, cell extracts from AtT-20 cells stably expressing PAM-1 TS/DD, scramble and sh-μ1A PAM-1 cells were collected and analyzed by Western blot (Figure 3.7B). The signal from the antibody that

recognizes the C-terminus of PAM-1 independent of PAM-1 phosphorylation status indicated that scramble and sh-μ1A PAM-1 cells had a similar amount of PAM-1, while the levels of PAM-1 phosphorylated at Ser^{949} in sh-μ1A PAM-1 cells were significantly lower than in scramble PAM-1 cells.

PAM-1 is subject to endoproteolytic cleavage in both secretory granules and in the endocytic pathway; the cleavage products produced in secretory granules and endosomes differ. We demonstrated previously that the levels of PAM-1 secretory granule products (PALm and soluble PHM) were lower in sh-μ1A PAM-1 cells compared with scramble PAM-1 cells (Figure 3.7B), confirming previous results [234]. Production of sPAM and Intermediate 2 is largely limited to the endocytic pathway. Levels of intermediate 2, a PAM-1 processed product generated upon cleavage by α-secretase in endosomes, were lower in sh-μ1A PAM-1 cells than in scramble PAM-1 cells (data not shown). These data along with the PAM-1 antibody uptake experiment demonstrate that PAM-1 endocytic trafficking has changed in sh-μ1A PAM-1 cells.

3.3.8 Recycling of PAM-1 from the endocytic pathway to secretory granules is enhanced in sh-μ1A PAM-1 cells

A study done on AtT-20 cells stably expressing PAM-1 TS/DD showed that PAM-1 recycling from endosomes to secretory granules was reduced [195]. Because PAM-1 is less phosphorylated at Ser^{949} in sh-μ1A PAM-1 cells than in scramble PAM-1 cells, this suggested that PAM-1 might be more efficiently recycled to the biosynthetic pathway. Biotinylation, an irreversible means of tagging proteins on the cell surface, makes it possible to measure the fate of a given protein that has reached the plasma membrane. Scramble and sh-μ1A PAM-1

cells were biotinylated for 10 min at 37°C and chased for 1 hour or for 4 hours. At the end of each time point, cell extracts and media were collected, and biotinylated PAM-1 protein levels were evaluated by western blot (Figure 3.8, top graph). In both scramble and sh-μ1A PAM-1 cells, PAM-1 was degraded at a similar rate. Treatment of scramble and sh-μ1A PAM-1 cells with cycloheximide, which prevents protein synthesis, did not show any difference in the degradation rate of PAM-1, confirming the conclusions drawn with biotin (data not shown).

PHM is only generated from PAM-1 by endoproteases that are in secretory granules (Figure 3.2), meaning that biotinylated PAM-1 that is recycled from endosomes to secretory granules is characterized by the formation of soluble biotinylated PHM. Biotinylated PHM levels were measured in the cell extracts and the medium after a 1 hour and a 4 hour chase. sh-μ1A PAM-1 cells generated more biotinylated PHM than scramble PAM-1 cells, suggesting that, in sh-μ1A PAM-1 cells PAM-1 was more recycled to secretory granules than in scramble PAM-1 cells (Figure 3.8, middle graph). In addition, soluble PHM was more evident in the medium of sh-μ1A PAM-1 cells than of scramble PAM-1 cells after 4 hours of chase (Figure 3.8, bottom graph), confirming previous results where PHM basal secretion was increased [234].

3.4 Discussion

Internalized transferrin trafficking and distribution of early and recycling endosomes is similarly affected between HeLa, fibroblasts and AtT-20 cells where AP-1 function has been reduced, suggesting that the endocytic machinery is similar between different cell types. Surprisingly, the secretory granule membrane protein PAM-1 is recycled to the TGN faster in sh-μ1A PAM-1 cells. Because neuroendocrine function is to produce, store and then release

bioactive peptides upon addition of secretagogues, the endocytic trafficking of secretory granule membrane proteins may be very specialized to prevent trapping of essential secretory granule membrane proteins in the endocytic pathway.

3.4.1 The cellular location of early endosomes in AtT-20 cells is dependent on AP-1

Reducing the function of AP-1 in AtT-20 cells resulted in the formation of a cluster of early endosomes. This is similar to the study in mouse embryonic fibroblasts lacking μ1A expression and in HeLa cells transfected with an siRNA against γ-adaptin, a subunit of AP-1 [178, 236]. The connection between AP-1 and early endosomes is cell type specific, however, because MNT-1 cells lack colocalization between AP-1 and EEA1, and reducing AP-1 function in these cells does not perturb the distribution of early endosomes [186]. Treatment of AtT-20 cells with nocodazole prevented the formation of the perinuclear cluster in sh-μ1A PAM-1 cells, suggesting that the transport of early endosomes on microtubules is prevented when μ1A levels are reduced. Although *in vitro* studies have shown that kinesin 1 (KIF5A, KIF5B, KIF5C) and kinesin 2 (KIF3A, KIF3B, KIF3C and KIF17) families interact with early endosomes, studies done in the fungus Ustilago maytis (KIF1A-like), HeLa cells (KIF16B) and *Drosophila* S2 cells (KIF1A-like) pointed to a role for the kinesin 3 family (KIF1A, KIF1B, KIF1C, KIF13A, KIF13B, KIF14, KIF16A and KIF16B) [248, 249, 250, 251]. Endosomes are connected to microtubules by an interaction between AP-1 and the kinesin 3, KIF13A [237, 232]. Overexpression of KIF13A redistributed mannose-6-phosphate receptor and AP-1 to the periphery, instead of localizing near the nucleus in MDCK cells [232]. In line with this observation, reducing KIF13A levels in MNT-1 cells, a human melanoma cell line

where AP-1 distribution is normally evenly spread in vesicles throughout the cells, resulted in accumulation of AP-1 near the nucleus [186]. It was recently proposed that KIF13A is necessary to generate tubular structures from early endosomes which will be targeted to the recycling endosomes in HeLa cells [237]. It would be interesting to find out whether AP-1 connects early endosomes to KIF13A in AtT-20 cells.

3.4.2 The cellular location of recycling endosomes in AtT-20 cells is dependent on AP-1

Loss of AP-1 function also resulted in accumulation of recycling endosomes near the nucleus in MNT-1, HeLa and AtT-20 cells [186]. In HeLa cells, AP-1 interacts with the S-palmitoylated protein, Gadkin (γ-adaptin and kinesin interactor), which then binds the kinesin 1 KIF5C to transport TGN-derived endosomal recycling vesicles to the cell periphery [247]. Overexpression of Gadkin in HeLa cells resulted in accumulation of Gadkin, AP-1 and several markers of recycling endosomes (transferrin, transferrin receptor, Rab11 and mannose-6-phosphate receptor) to the cell periphery, but did not alter the distribution of EEA1 positive vesicles [247]. Depletion of AP-1 or kinesin 1 prevented endosomal vesicles containing transferrin from locating to plus-end of microtubule tracks in HeLa cells [247]. This is consistent with our results in AtT-20 cells where reducing AP-1 function resulted in perinuclear accumulation of Rab11 positive organelles.

3.4.3 Endosome maturation requires AP-1 to sort proteins out

Sh-μ1A PAM-1 cells had smaller and irregularly shaped late endosomes and lysosomes compared with scramble PAM-1 cells. KIF13A was proposed to form the tubular domains

of early endosomes to sort out proteins in recycling endosomes. When KIF13A levels are diminished, transferrin is found in late endosomes of HeLa cells, suggesting a problem in protein sorting and an alteration of endosome maturation [237]. In addition, Rab4b was shown to interact with the γ-subunit of AP-1 to promote transferrin sorting from early endosomes to recycling endosomes [236]. Down-regulation of AP-1 levels inhibited the slow recycling pathway to the advantage of the fast recycling pathway in HeLa cells [236, 247]. It remains unknown if transferrin fast recycling is more prominent in sh-μ1A PAM-1 cells than in scramble PAM-1 cells.

3.4.4 AP-1 is required for protein sorting in the endosomes of AtT-20 cells

One of the first indications that AP-1 was essential for protein sorting in endosomes came from studies of both types of mannose-6-phosphate receptors, which were trapped together in the endocytic pathway; these proteins bind mannose-6-phosphate groups that are located on the surface of lysosomal proteins, allowing receptor mediated sorting and transport to lysosomes [178]. Cathepsin D, a soluble protease driven to lysosomes by mannose-6-phosphate receptor, is re-routed to the secretory pathway in the absence of AP-1 [178]. Similarly, cholesterol transport and the distribution of Niemann Pick type C protein 2, an important protein for cholesterol transport in lysosomes that interacts with mannose-6-phophate receptor, are altered in μ1A knockout fibroblasts [243]. The tips of AtT-20 cells accumulate secretory granules whose membrane is enriched in cholesterol. Live cell imaging of cholesterol showed accumulation at the tips of non-infected PAM-1 cells but not in sh-μ1A PAM-1 cells, indicating a change in how cholesterol is handled and agreeing with the study on μ1A knockout fibroblasts.

Although both PAM-1 and mannose-6-phosphate receptors interact with AP-1 [234, 252, 90], PAM-1 transport from endosomes to the TGN was increased in sh-μ1A PAM-1 cells. PAM-1 trafficking is driven by both its luminal domain and by the phosphorylation status of its cytosolic tail. Using PAM-1 phosphomimetic mutants, it was observed that PAM-1 TS/DD ($Thr^{946}Ser^{949}$ -> $Asp^{946}Asp^{949}$) does not enter intraluminal vesicles of late endosomes and is not recycled to the TGN as efficiently as PAM-1 TS/AA ($Thr^{946}Ser^{949}$ -> $Ala^{946}Ala^{949}$), where phosphorylation events are prevented [195]. Using an antibody that recognizes phosphorylated Ser^{949}, sh-μ1A PAM-1 cells are quite deficient in phosphorylation at this site compared with scramble PAM-1 cells, agreeing with the increased recycling event from endosomes to secretory granules seen in sh-μ1A PAM-1 cells. Why Ser^{949} is less phosphorylated when μ1A levels are reduced remains to be explored. Ser^{949} can be phosphorylated by casein kinase II or Uhmk1. Phosphofurin Acidic Cluster Sorting protein 1 (PACS-1) interacts with casein kinase II, acidic clusters found on the cytosolic domain of cargo proteins and AP-1. PACS-1 recruitment to membranes is enhanced once the cargo has been phosphorylated by casein kinase II. PAM-1 contains an acidic cluster at its C-terminus which could interact with PACS-1, and then recruit casein kinase II. In the case of furin, it is known that furin, PACS-1 and AP-1 work in concert to drive the trafficking of furin. The complex of casein kinase II/PACS-1 might be misplaced in sh-μ1A PAM-1 cells, resulting in a decrease of PAM phosphorylation.

In conclusion, AP-1 is a key cytosolic complex involved in protein sorting, as well as early and recycling endosomal localization and function. Because exocytosis is coupled with endocytosis, this study had the goal to investigate the effects of AP-1 on the endocytic pathway and compare the consequences of reduced AP-1 function with other cell lines.

Overall, most of AP-1 functions described in the literature comes from studies done with fibroblasts and other cell types that are not specialized for regulated secretion. AP-1 functions identified in AtT-20 cells were similar, suggesting a conserved mechanism. It would be important to find out if the transport of secretory granule membrane proteins is cell-type and protein specific.

3.5 Materials and methods

3.5.1 Tissue culture and generation of scramble and sh-μ1A PAM-1 cells

AtT-20 cells were grown at 37°C with 5% CO_2 in Dulbecco's modified Eagle's medium/F-12 (DMEM/F-12) containing 25 mM HEPES, 100 units/ml penicillin, 100 μg/ml streptomycin, 10% fetal bovine serum, 10% NuSerum. AtT-20 cells stably expressing PAM-1 were described previously [188]. Generation of sh-μ1A and scramble PAM-1 AtT-20 cells using lentivirus targeted to μ1A (Sigma; clone ID TRCN0000111549) and a non-target shRNA (Sigma # SHC002V), respectively, was described previously [234].

3.5.2 Transfection with mRFP-Rab5

Scramble and sh-μ1A PAM-1 cells were plated in 4-well dishes on 12-mm round coverslip (0.16 to 0.19 mm thick, Fisher Scientific) coated with 0.1 mg/ml poly-L-lysine for 5 minutes followed by a rinse in NuSerum and two rinses in AtT-20 growth medium. Two days later, cells were incubated in serum free medium for 30 minutes before being transfected (0.25 μg DNA/well); the Lipofectamine 2000 ® and pmRFP-Rab5 (Addgene, plasmid 14437) were mixed in Optimem (Optimem:DNA:Lipofectamine 2000 ® = 200 μl:1 μg: 2.5 μl) and allowed to sit for 25 minutes. After application of the mixture, cells were incubated at 37°C

for 6 hours. Transfection medium was then replaced with growth medium and the cells were allowed to recover overnight. Cells were fixed the following day in 4% formaldehyde in PBS and immunostained as described above.

3.5.3 Immunofluorescent staining

Cells were plated on coverslips coated as described above. Cells were fixed in 4% formaldehyde in PBS (50 mM NaH2PO4, 150 mM NaCl, pH 7.4) for 20 minutes at room temperature. After rinsing in PBS, cells were permeabilized in 0.075% Triton X-100, 2 mg/ml BSA in PBS for 20 minutes at room temperature and then incubated in block (2 mg/ml BSA in PBS) for 20 minutes at room temperature. Primary antibodies diluted in block were incubated with the cells overnight at 4°C. After three rinses in PBS, cells were incubated for one hour at room temperature in block containing either fluorescein isothiocyanate (FITC, 1:500 dilution) or Cy3 (1:2000 dilution) conjugated donkey antibody to mouse or rabbit immunoglobulin (Jackson ImmunoResearch). After three rinses in PBS, cells were incubated with Hoechst (1:1000 dilution in PBS) for 10 minutes at room temperature. After three rinses in PBS, cells were mounted using ProLong® Gold (Invitrogen).

3.5.4 Cell treatment

Cells were incubated in DMEM/F-12 air medium containing 25 mM HEPES, pH 7.4, 1 mg/ml BSA for 30 minutes at 37°C without CO_2. For transferrin uptake experiments, cells were then incubated in DMEM/F-12 air medium containing 25 mM HEPES, pH 7.4, 1 mg/ml BSA, 25 μg/mL Alexa fluor 546 transferrin (Life Technologies) for 10 minutes at 37°C without CO_2. Cells were fixed using 4% formaldehyde in PBS for 20 minutes at room temperature.

For nocodazole treatment experiments, cells were treated as described above and treated with DMEM/F-12 air medium containing 10 μM nocodazole (Sigma) or the equivalent volume of DMSO for 20 minutes at 37°C without CO_2. For the PAM antibody uptake experiment, PAL antibody was diluted at 1:50 in medium and added onto the cells for 10 minutes at 37°C before fixation.

3.5.5 Cholesterol uptake

BODIPY-cholesterol uptake was done as described previously [253]. Briefly, one day after plating, non-infected and sh-μ1A PAM-1 cells were incubated in lipid depleted medium containing 1 μM of BODIPY-cholesterol overnight, then live cells were photographed with a Leica TCS CARS SP8 confocal microscope equipped with a 37°C chamber.

3.5.6 Electron microscopy

PAM antibody uptake at the electron microscope level was done as described previously [195]. Briefly, for colloidal gold labelling, cells were incubated with exon 16 antibody (JH629, 1:250) in DMEM-Hepes-2 mg/ml BSA for 1 h at 4°C, rinsed with DMEM-Hepes-BSA at 4°C, incubated in DMEM-Hepes with protein A-15 nm colloidal gold (University of Utrecht, Utrecht, Netherlands) at the concentration suggested for immunolabeling by the provider (1:60-75) for 1 h at 4°C, rinsed in DMEM-Hepes at 4°C and then chased in culture medium at 37°C for 20 minutes. Control cells were incubated with protein A-colloidal gold only. After the chase, cells were fixed with 2.5% glutaraldehyde and 2% sucrose in 0.1 M sodium cacodylate buffer, post-fixed with 1% osmium tetroxide and 1.5% potassium ferrocyanide, dehydrated and embedded in Epon. Sections were poststained with uranyl acetate and lead

citrate.

3.5.7 Biotinylation stabilization paradigm

AtT-20 cells plated in a 12-well plate were first incubated for 30 minutes in DMEM/F-12 air medium containing ITS, 25 mM HEPES, pH 7.4, 100 μg/ml BSA. Cells were equilibrated in air medium during two consecutive 30 minute incubations at 37°C without CO_2. Cells were then rinsed with warm HSG buffer (15 mM HEPES, 120 mM NaCl, 2 mM CaCl2, 4 mM KCl, 25 mM glucose, pH 7.4). A solution containing 1.25 mM sulfo-NHS-LC-biotin (Thermo Scientific) in HSG buffer was made fresh and added to the cells for 10 minutes at 37°C. After removing the biotin solution, cells were rinsed twice for 5 minutes with CSFM-air containing 2 mg/ml BSA at 37°C. Cells were either collected directly using TMT (20 mM Na N-Tris[hydroxymethyl]methyl-2-aminoethanesulfonic acid (TES), 10 mM mannitol, 1% Triton X-100, pH 7.4) containing a cocktail of protease inhibitors (final concentrations 0.34 mg/ml phenylmethylsulfonyl fluoride, 50 μg/ml lima bean trypsin inhibitor, 2 μg/ml leupeptin, 16 μg/ml benzamidine, and 2 μg/ml pepstatin) or were incubated at 37°C with air medium for 1 hour or 4 hours before extraction. Cells were solubilized in TMT for 30 minutes at 4°C. Cell extracts were collected into microfuge tubes and centrifuged at 22,000 g for 15 minutes at 4°C. Solubilized cell extracts were then incubated with Streptavidin-agarose beads for 1 hour at 4°C. Beads were rinsed twice with TMT and once with TM (no Triton X-100). The bound fraction was eluted into Laemmli sample buffer by heating the samples for 5 minutes at 95°C.

3.6 Tables

Antigen	Working dilution	Identity, source
C-STOP, PAM-1(965-976)	1:1000	C-stop [223]
Exon 16, PAM-1(409-497)	1:1000	JH629 [224]
C-terminus, PAM-1 (898-976)	1:10	6E6 [189]
PAL, PAM-1(498-604)	1:50 (uptake)	JH877 [77]
$pSer^{949}$, PAM-1 (942-953)	1:500	JH2541 [39]
Rab11	1:250	Millipore

Table 3.1: List of antibodies.

3.7 Figures

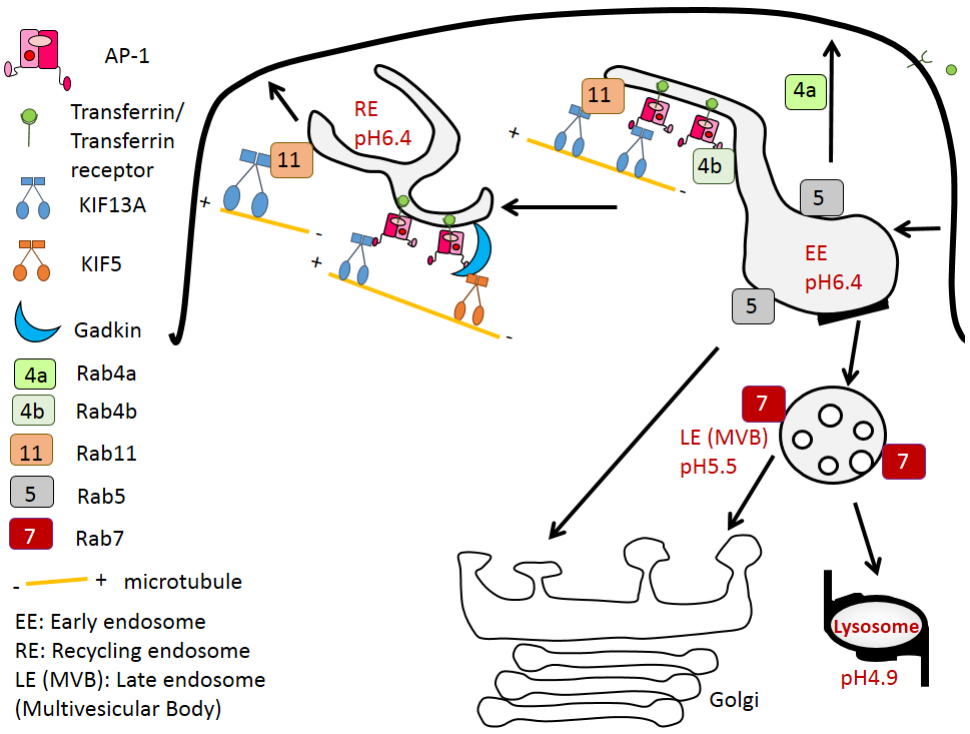

Figure 3.1: Diagram of the endocytic pathway. Internalized material first reaches early endosomes (EE), which sort proteins that can be recycled either directly to the plasma membrane (mediated by Rab4a) or indirectly via recycling endosomes (RE). The bulk of early endosomes not recycled undergo a maturation process characterized by the formation of late endosomes (or multivesicular bodies, MVB). Proteins can be degraded in lysosomes or recycled back to the Golgi. According to the literature, AP-1 is present on early and recycling endosomes, where it connects multiple proteins to microtubules and endosomes.

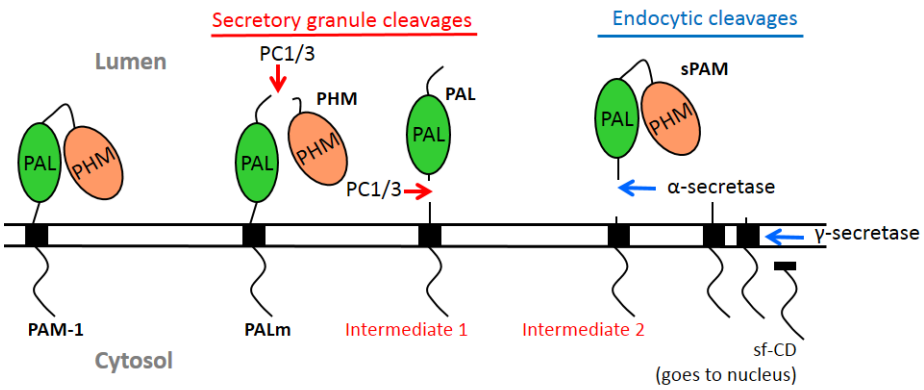

Figure 3.2: PAM processing in the regulated secretory pathway vs. the endocytic pathway. In secretory granules, PAM-1 can be cleaved between the two catalytic core domains, PHM and PAL by prohormone convertase 1/3 (PC1/3) to produce soluble PHM and PAL membrane (PALm). Although less frequent, a second cleavage occurs between PAL and the transmembrane domain generating soluble PAL and intermediate 1. Soluble PAM-1 formation involves α-secretase mediated cleavage between PAL and the transmembrane domain; the other product from this cleavage is intermediate 2. Intermediates 1 and 2 are then cleaved by γ-secretase to generate the soluble fragment of the cytosolic domain (sf-CD).

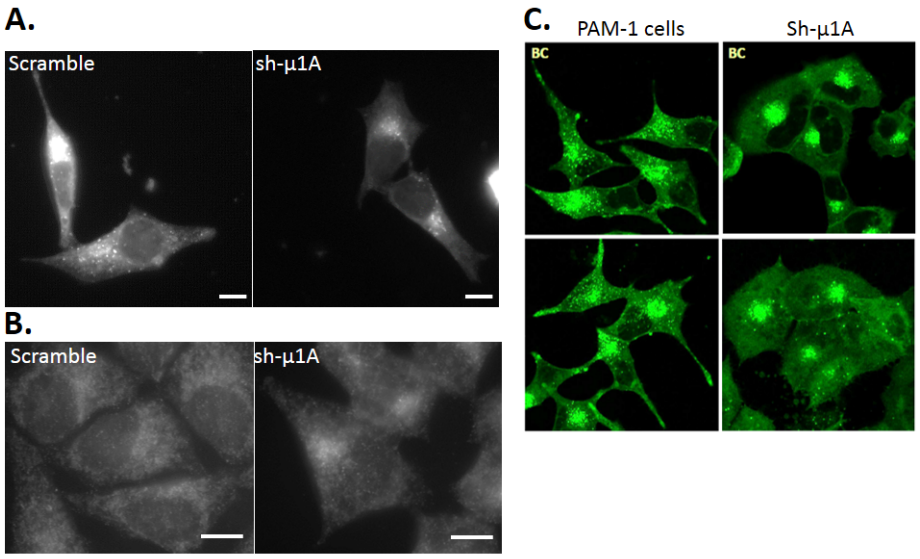

Figure 3.3: The endocytic pathway of sh-μ1A PAM-1 cells is altered. (A) Scramble and sh-μ1A PAM-1 cells were transiently transfected with mRFP-Rab5 in order to visualize early endosomes (see Figure 3.1). Scramble PAM-1 cells contained Rab5 positive vesicles distributed throughout the cells along with a concentrated group near the nucleus while sh-μ1A PAM-1 cells only contained vesicles clustered near the nucleus. (B) Scramble and sh-μ1A PAM-1 cells were immunostained for Rab11 (Cy3 anti-rabbit), a marker of recycling endosomes (see Figure 3.1). Rab11 was more concentrated near the nucleus in sh-μ1A PAM-1 cells than in scramble PAM-1 cells. (C) BODIPY-cholesterol, a dye allowing the visualization of cholesterol in live cells, was applied onto non-infected PAM-1 cells and sh-μ1A PAM-1 cells. BODIPY-CHOL accumulated in vesicles near the Golgi and at the tips of scramble PAM-1 cells while sh-μ1A PAM-1 cells were devoid of signal at the tips and BODIPY-cholesterol formed less dispersed clusters near the nucleus. Scale bar, 10 μm.

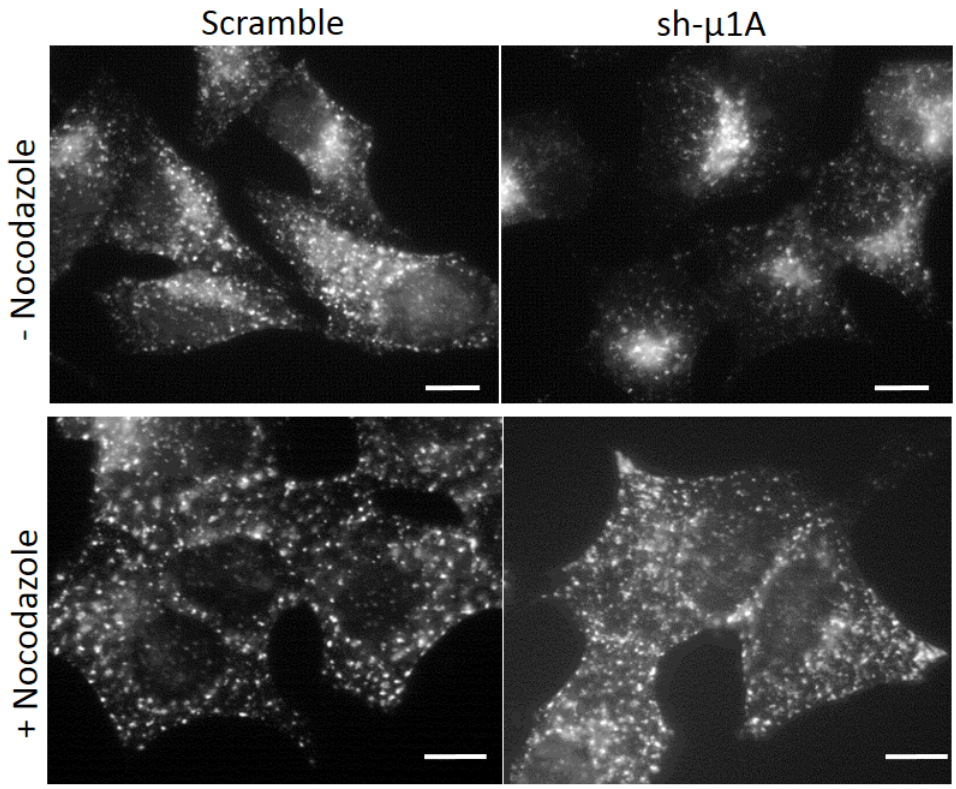

Figure 3.4: Trafficking of internalized transferrin is altered in sh-μ1A PAM-1 cells. Top, scramble and sh-μ1A PAM-1 cells were incubated with 25 μg/mL Alexa fluor 546 transferrin for 10 minutes at 37°C before fixation. Internalized transferrin formed a cluster of vesicles near the nucleus in sh-μ1A PAM-1 cells while transferrin positive vesicles were evenly distributed throughout scramble PAM-1 cells. Bottom, treatment with nocodazole prior to transferrin uptake dispersed transferrin positive vesicles in both cell lines, indicating that transferrin trafficking on microtubules was altered in sh-μ1A PAM-1 cells. Scale bar, 10 μm.

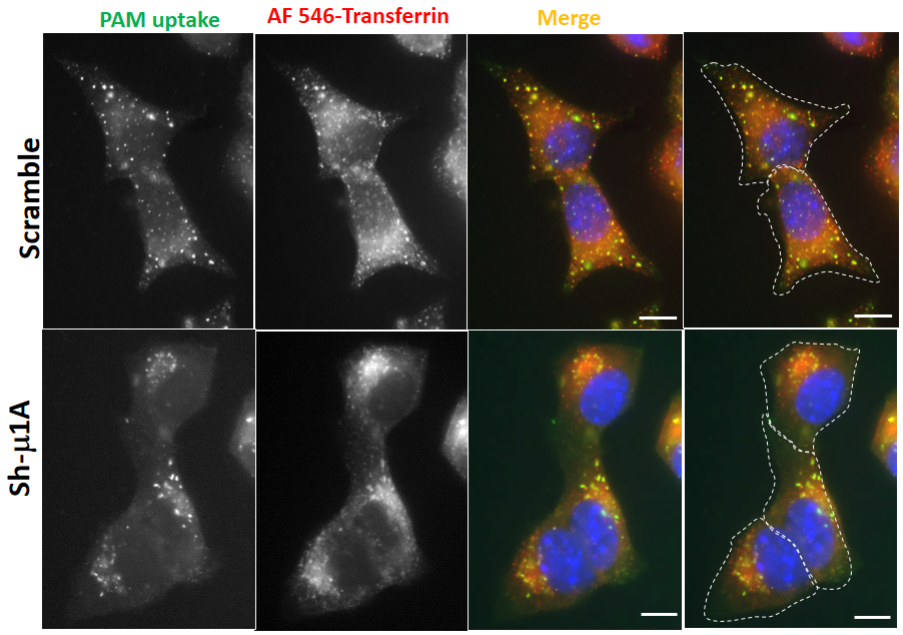

Figure 3.5: Internalization of PAM-1 is altered in sh-μ1A PAM-1 cells. Scramble and sh-μ1A PAM-1 cells were incubated with PAL antibody (1:50 dilution) and 25 μg/mL Alexa fluor transferrin 546 for 10 minutes at 37°C before fixation. Cells were permeabilized and secondary antibody (FITC anti-rabbit) was added to examine the distribution of internalized PAM that was bound to PAL antibody. Strong colocalization between PAM/Antibody complex and transferrin was seen in both cell lines. PAM distribution resembled that of transferrin in each cell line. Scale bar, 10 μm.

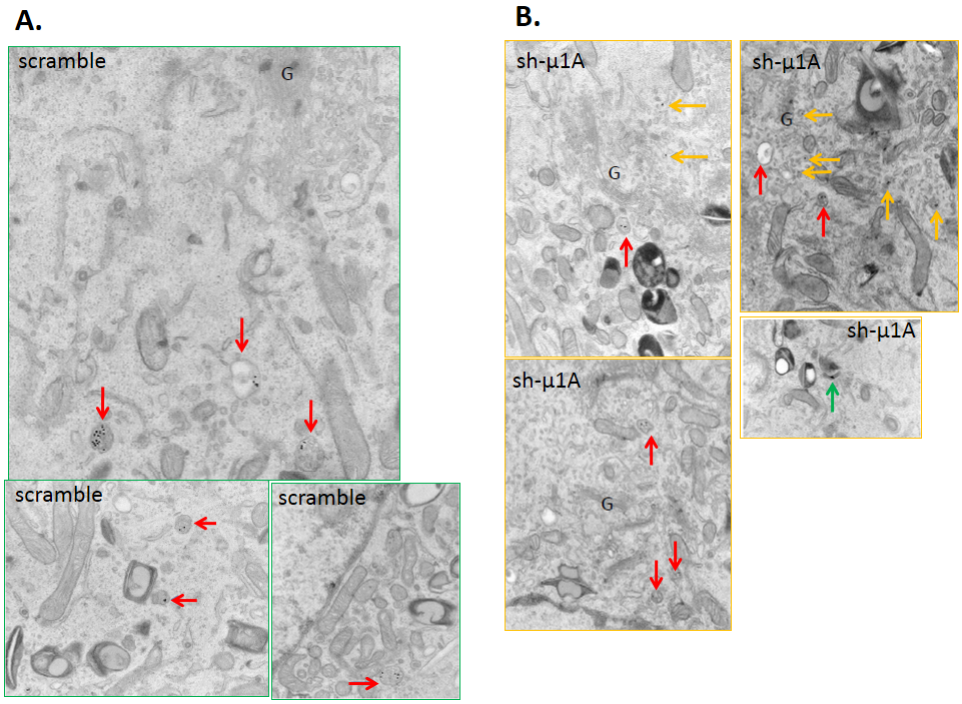

Figure 3.6: Internalized PAM is located in multivesicular bodies and in small vesicles near the Golgi in sh-μ1A PAM-1 cells. Scramble (A) and sh-μ1A (B) PAM-1 cells were incubated with Exon 16 antibody linked to gold particles for 20 minutes at 37°C before fixation and visualization under TEM. Gold particles were identified in multivesicular bodies (red arrows) in both cell lines. Sh-μ1A PAM-1 cells contained a lot of gold particles in small vesicles near the Golgi complex (yellow arrows). Gold particles were also seen in lysosomes of sh-μ1A PAM-1 cells (green arrow). Multivesicular bodies appeared smaller and lysosomes were more rounded in sh-μ1A PAM-1 cells than in scramble PAM-1 cells.

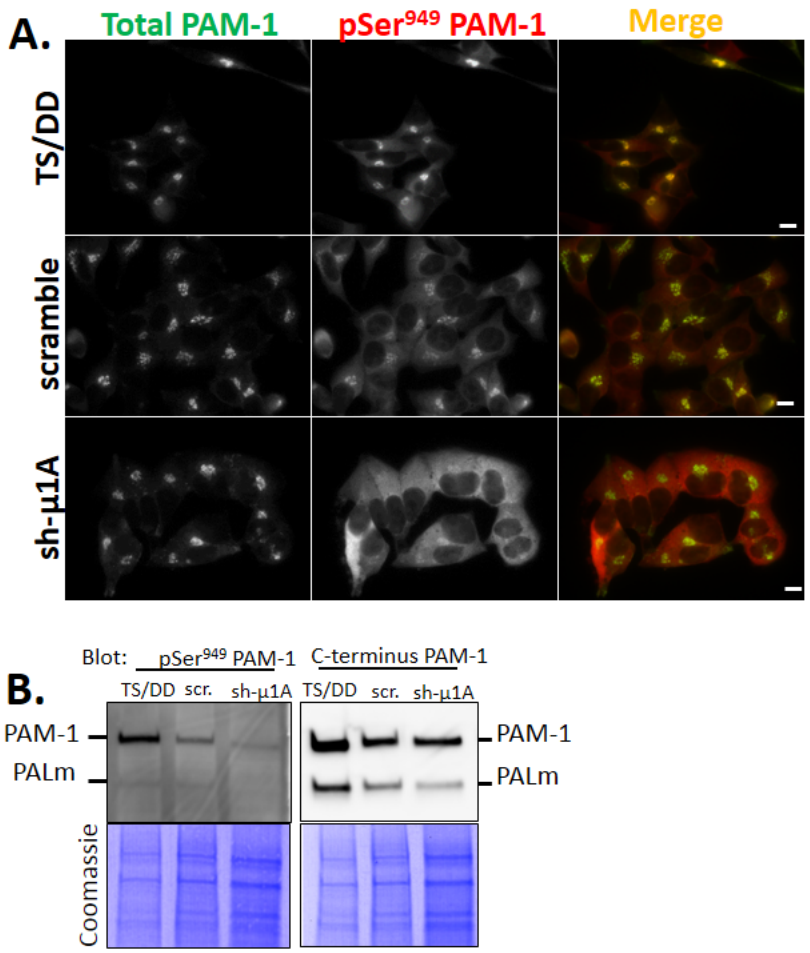

Figure 3.7: Ser^{949} of PAM-1 cytosolic domain is less phosphorylated in sh-μ1A PAM-1 cells. (A) Indirect immunostaining of AtT-20 cells stably expressing PAM-1 TS/DD (TS/DD), scramble and sh-μ1A PAM-1 cells using a PAM antibody which targets the cytosolic tail (FITC-anti-mouse) and a PAM antibody which recognizes PAM cytosolic tail only when Ser^{949} is phosphorylated (Cy3-anti-rabbit). TS/DD served as a positive control. PAM-1 phosphorylated at Ser^{949} concentrated at the Golgi of scramble PAM-1 cells. Although sh-μ1A PAM-1 cells express PAM-1, pSer^{949} antibody failed to reveal a signal at the Golgi; the image shown for sh-μ1A was exposed for a longer time than the images shown for scramble cells. Scale bar, 10 μm. (B) Western Blot analysis looking at phosphorylated Ser^{949} levels (left) or an antibody which targets the C-terminus of PAM-1 independent of phosphorylation (right) in TS/DD, scramble and sh-μ1A PAM-1 cells. The same volume of cell homogenates was loaded for both blots. Levels of pSer^{949} in sh-μ1A PAM-1 cells were considerably lower than in scramble PAM-1 cells.

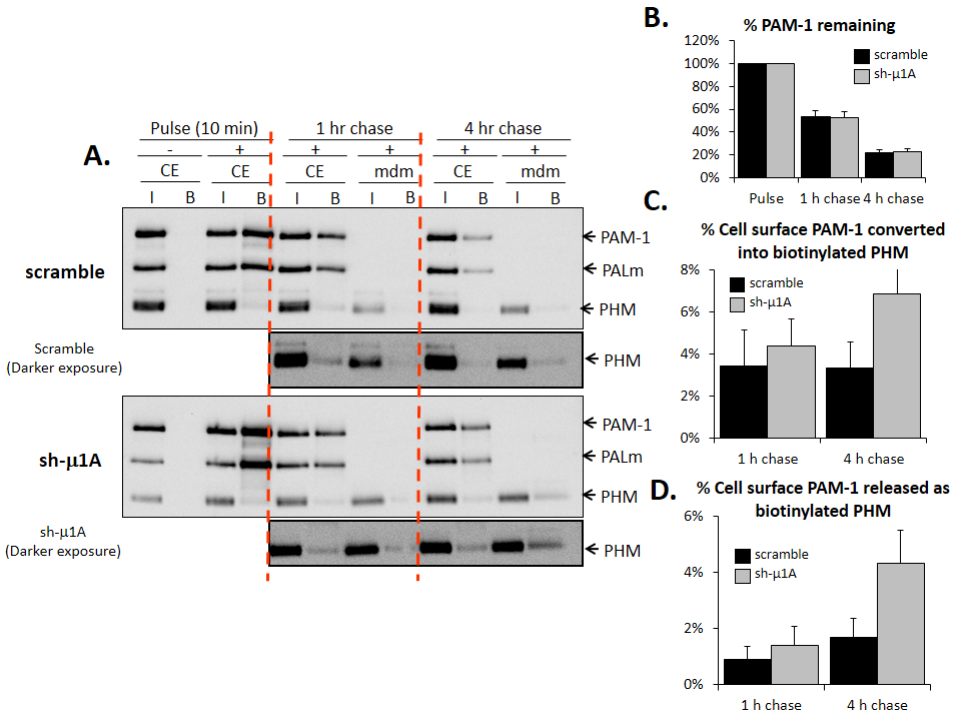

Figure 3.8: Biotinylated PAM-1 is more recycled to secretory granules in sh-μ1A PAM-1 cells than in scramble PAM-1 cells. (A) Scramble and sh-μ1A PAM-1 cells were treated with cell-impermeant activated biotin for 10 minutes at 37°C and then harvested immediately or chased for 1 or 4 hours. Media were collected after the 1 and 4 hour chase incubations. Biotinylated PAM proteins recovered from cells and media were analyzed by Western blot. (B) Quantification of PAM-1 levels over time indicated that the PAM-1 degradation rate was similar between scramble and sh-μ1A PAM-1 cells. (C) Quantification of biotinylated PHM obtained after cleavage of biotinylated PAM-1 in secretory granules was quantified. At 4 hour chase, more biotinylated PHM was generated in sh-μ1A PAM-1 cells than scramble cells. (D) Bbiotinylated PHM obtained after cleavage of biotinylated PAM-1 in secretory granules and secreted in the medium was quantified. At 4 hour chase, secreted biotinylated PHM was more prevalent in sh-μ1A PAM-1 cells than in scramble PAM-1 cells.

Chapter 4

AP-1 plays an essential role in cuproenzyme function in neuroendocrine cells

Mathilde L. Bonnemaison, Richard E. Mains, Megan E. Duffy, Martina Ralle and Betty A. Eipper.

Manuscript in preparation for Journal of Biological Chemistry.

Drafting of the manuscript

Mathilde L. Bonnemaison, Richard E. Mains and Betty A. Eipper.

Acquisition of data

Richard E. Mains did the ELISA; Martina Ralle and Megan Duffy did the ICP-MS; Betty A. Eipper and Darlene D'Amato did the joining peptide amidation study; Mathilde L. Bon-

nemaison did the remaining experiments under the guidance and supervision of Richard E. Mains and Betty A. Eipper.

4.1 Abstract

The adaptor protein 1 complex (AP-1), which transports cargo between the *trans*-Golgi network and endosomes, is known to play a role in the trafficking of Atp7a, a copper-transporting P-type ATPase, and peptidylglycine α-amidating monooxygenase (PAM), a copper-dependent secretory granule membrane enzyme. Lack of any of the four AP-1 subunits is sufficient to impair function and patients with MEDNIK syndrome, a rare genetic disorder caused by lack of expression of the σ1A subunit, exhibit clinical and biochemical signs of impaired copper homeostasis. To explore the role of AP-1 in copper homeostasis in neuroendocrine cells, we used corticotrope tumor cells in which AP-1 function was diminished by reducing expression of its μ1A subunit. Cellular levels of copper and Atp7a were unchanged when AP-1 function was impaired. When AP-1 function was reduced, more internalized transferrin accumulated in the Golgi region, where much of the endogenous Atp7a localized. Nocodazole treatment dispersed the internalized transferrin, revealing that reducing AP-1 function increased the amount of endogenous Atp7a that co-localized with the internalized transferrin. Impaired AP-1 function also led to a significant increase in the ability of bathocuproine disulfonate, a cell impermeant Cu(I) chelator, to inhibit PAM function. Atp7a localization continued to respond to increased copper levels when AP-1 function was impaired; unlike fibroblasts and HeLa cells, little Atp7a appeared on the surface of pituitary cells, even when copper levels were elevated. Co-immunoprecipitation of PAM with Atp7a suggested direct transfer of copper from Atp7a to PAM.

4.2 Introduction

Copper is required in several essential biological processes, including mitochondrial respiration, skin pigmentation, iron transport, connective tissue and blood vessel formation, antioxidant defense, catecholamine synthesis and peptide amidation [254]. It is transported into cells via copper transporter 1 (CTR1), transferred to a cytosolic chaperone and delivered to its final destinations. The chaperone ATOX1 transfers copper to ATP7A and ATP7B, P-type ATPases that transport the metal from the cytosol into the lumen of the secretory pathway for incorporation into luminal cuproproteins. Luminal copper chaperones have not been identified [255], and it has been proposed that a His/Met-rich luminal loop in ATP7A plays an essential role in the delivery process [256, 215].

ATP7A, which is ubiquitously expressed, mediates copper uptake from the gut and delivery in the brain, while ATP7B is expressed primarily in the liver and exports copper into bile. Mutations in ATP7A result in Menkes disease, which is characterized by lack of copper in most tissues, while mutations in ATP7B lead to Wilson disease, which is associated with copper overload. MEDNIK (Mental retardation, Enteropathy, Deafness, peripheral Neuropathy, Ichtyosis, Keratodermia) syndrome is a rare autosomal recessive disorder characterized by symptoms of both Menkes and Wilson disease [254]. MEDNIK syndrome is caused by mutations in the AP1S1A gene, which encodes σ1A, the small subunit of the adaptor protein 1 complex (AP-1) [217]. This cytosolic complex is composed of four subunits: two large subunits (γ and β1), a medium subunit (μ1) and a small subunit (σ1). AP-1 drives the transport of proteins between the *trans*-Golgi network (TGN) and endosomes; in neuroendocrine cells, it mediates secretory granule formation and maturation [234, 168, 257].

Ceruloplasmin, a copper-dependent secreted ferroxidase and the major carrier of copper in serum, incorporates copper during its biosynthesis; lacking copper, apoceruloplasmin is rapidly degraded in plasma [258]. In sera from MEDNIK patients, ceruloplasmin and total copper levels are low while free copper levels are elevated, suggesting that copper delivery to ceruloplasmin is impaired [254, 219]. Consistent with this, in fibroblasts from MEDNIK patients, ATP7A is localized near the cell periphery instead of the Golgi region [219]. Lack of any one AP-1 subunit impairs AP-1 function. Indeed, down-regulation of a different AP-1 subunit, μ1A, in HeLa cells also resulted in accumulation of ATP7A at the cell periphery and the inability of ATP7A to concentrate in the Golgi region when copper levels were diminished [220].

In neuroendocrine cells, ATP7A provides copper to peptidylglycine α-amidating monooxygenase (PAM), an essential enzyme that requires copper to catalyze peptide amidation, one of the final steps in the conversion of inactive peptide precursors into their bioactive peptide products [259]. Although ATP7A trafficking in neuroendocrine cells has not been extensively explored [260, 261], AP-1 was recently shown to play an essential role in secretory granule biogenesis and PAM trafficking in AtT-20 mouse corticotrope tumor cells [234, 220, 219].

In this study, AP-1 function was diminished using an shRNA that reduced expression of the medium subunit of AP-1 (μ1A) to half in AtT-20 cells stably expressing PAM-1. We used cells sh-μ1A PAM-1 cell and cells expressing a control shRNA (scramble PAM-1 cells) to determine whether this modest reduction in AP-1 levels altered Atp7a trafficking and copper delivery to PAM. Impaired production of amidated peptides as a result of diminished delivery of copper to the secretory pathway in MEDNIK patients could contribute to many of the deficits observed.

4.3 Results

4.3.1 Decreased expression of μ1A does not alter levels of Atp7a or intracellular copper

AtT-20 cells stably expressing PAM-1 (PAM-1 cells) infected with a lentivirus expressing shRNA directed against μ1A (sh-μ1A) or a non-target shRNA (scramble) were described previously [234]. In this study, the *trans*-Golgi network region of sh-μ1A PAM-1 cells was vacuolated and non-condensing secretory granules accumulated at the expense of immature secretory granules [234]. In addition, the ability of sh-μ1A PAM-1 cells to secrete secretory granule proteins in response to secretagogue was diminished.

Western blot analysis demonstrated the expected 50% reduction in levels of μ1A in sh-μ1A PAM-1 cells compared to non-infected (N.I.) and scramble PAM-1 cells (Figure 4.1A). As expected, in scramble PAM-1 cells, γ-adaptin, an AP-1 subunit, and TGN38 were largely co-localized in the perinuclear region (Figure 4.1B). In HeLa cells and $\mu1A^{-/-}$ mouse embryonic fibroblasts, lack of the μ1A subunit resulted in a more diffuse distribution of the remaining complex [220, 178]. Consistent with these observations, μ1A was more diffusely distributed in sh-μ1A PAM-1 cells, than in scramble PAM-1 cells (Figure 4.1B).

Since copper homeostasis was altered in MEDNIK patients, intracellular copper levels in scramble and sh-μ1A PAM-1 cells were compared. In order to determine whether copper levels differed in scramble and sh-μ1A PAM-1 cells, trypsinized cells were suspended in isotonic buffer lacking copper and used for cell counting, protein determination and measurement of copper levels by atomic absorption (see Materials and Methods). No difference in intracellular copper levels, whether normalized to cell number or to cell protein,

was seen between scramble and sh-μ1A PAM-1 cells (Figure 4.1C).

We turned to Western blot analysis to compare steady state levels of Atp7a in non-infected, scramble and sh-μ1A PAM-1 cells (Figure 4.1E); no changes in the steady state levels of this pump were observed. Atp7a delivers copper to the lumen of the secretory pathway, where cuproenzymes like PAM must bind it in order to function. When PAM-1 enters secretory granules, it can be cleaved between its two catalytic core domains, PHM (peptidylglycine α-hydroxylating monooxygenase) and PAL (peptidyl-α-hydroxyglycine α-amidating lyase), generating a soluble protein (PHM, ~45 kDa) and a membrane fragment (PALm, ~70 kDa). Using an antibody that recognizes PHM, we observed intact PAM-1 (~120 kDa) and soluble PHM (Figure 4.1D). As seen previously, the diminished steady state levels of PHM in sh-μ1A PAM-1 cells compared with non-infected and scramble PAM-1 cells reflect an increase in basal secretion of PHM when AP-1 function is diminished (Figure 4.1E) [234].

Since AtT-20 cells express amyloid precursor protein (APP), which is known to bind copper with very high affinity [216], we assessed levels of APP in non-infected, scramble and sh-μ1A PAM-1 cells (Figure 4.1E). The levels of APP did not differ in the three cell lines.

4.3.2 Atp7a concentrates at the Golgi region of AtT-20 cells and primary pituitary cells

Because the localization of ATP7A in fibroblasts from MEDNIK patients lacking σ1A and HeLa cells expressing reduced levels of μ1A was altered, we assessed the localization of endogenous Atp7a in AtT-20 cells. Unlike fibroblasts and HeLa cells, AtT-20 cells are professional secretory cells and store the products of prohormone processing in secretory granules for release in response to secretagogue. AtT-20 cells must deliver copper to the secretory

pathway to support the synthesis of amidated peptides. Atp7a concentrates in the perinuclear region, where its distribution overlaps that of the *cis*-Golgi marker, GM130 and γ-adaptin (Figure 4.2A). Co-staining for Atp7a and PAM revealed a strong colocalization in the Golgi region and partial colocalization in vesicles. The tips of AtT-20 cells, where mature secretory granules containing ACTH and the other final products of proopiomelanocortin (POMC) processing accumulate, lack Atp7a (Figure 4.2A, arrows). Internalization of fluorescently tagged transferrin has served as a good marker for early and recycling endosomes [262]. Cells were incubated with Alexa fluor 546 transferrin for 10 minutes at 37°C before fixation; very little overlap between the internalized transferrin and Atp7a was observed.

In order to determine whether the Atp7a distribution in AtT-20 cells was representative of anterior pituitary endocrine cells *in vivo*, dissociated rat primary pituitary cells were maintained in culture for several days and then stained for Atp7a along with several organelle markers (Figure 4.2B). As in AtT-20 cells, Atp7a localized to the Golgi region, where its distribution overlapped that of GM130 and γ-adaptin. PAM expression varies in the different cell types found in the anterior pituitary [263]. In cells expressing high levels of PAM, it either colocalized with secretory granules or was found in secretory granule and in the Golgi region, where it colocalized with Atp7a (Figure 4.2B). In corticotropes, ACTH positive secretory granules were evenly distributed throughout the cell; although ACTH positive secretory granules occupied most of the cellular space, Atp7a staining rarely overlapped staining for ACTH (Figure 4.2B).

4.3.3 Atp7a distribution is altered in sh-μ1A PAM-1 cells

In HeLa cells, reducing levels of μ1A, impaired Atp7a retrograde trafficking from endosomes to the Golgi [220]. In order to find out whether Atp7a localization depended on AP-1 function in AtT-20 cells, scramble and sh-μ1A PAM-1 cells were stained for Atp7a and the *cis*-Golgi marker, GM130. In both neuroendocrine cell lines, Atp7a was concentrated in the Golgi area, largely overlapping with GM130 (Figure 4.3A). Outside of the Golgi area and nucleus, Atp7a appeared evenly dispersed in both cell lines. No difference in the steady state localization of Atp7a was apparent in scramble and sh-μ1A PAM-1.

The Golgi region of AtT-20 cells contains immature secretory granules as well as a complex mixture of endocytic compartments containing secretory granule membrane proteins targeted to the secretory pathway [195, 9]. Early and recycling endosomes are more concentrated toward the cell center when AP-1 function is reduced in HeLa cells or mouse embryonic fibroblasts [178, 236]. In order to disperse early and recycling endosomes to the cell periphery and try to reveal a difference between scramble and sh-μ1A PAM-1 cells, cells were treated with 10 μM nocodazole for 20 minutes [39]. Early and recycling endosome distribution was monitored by internalization of Alexa fluor 546 transferrin for 10 minutes (with or without nocodazole, Figure 4.3B). In scramble PAM-1 cells treated with DMSO as a control, internalized transferrin was found in puncta evenly spread out in the cells, with an accumulation near the nucleus, where recycling endosomes concentrate. In contrast, in sh-μ1A PAM-1 cells, more of the internalized transferrin was concentrated near the nucleus, with less found in peripheral vesicles. After treatment with nocodazole, internalized transferrin was diffusely distributed in both cell lines (Figure 4.3B).

We next examined the localization of Atp7a in scramble and sh-μ1A PAM-1 cells after

treatment with DMSO or nocodazole. Atp7a seemed to colocalize more with internalized transferrin in sh-μ1A PAM-1 cells than in scramble PAM-1 cells. In order to measure the degree of colocalization between the Atp7a and internalized transferrin, scramble and sh-μ1A PAM-1 cells treated with nocodazole were imaged using confocal microscopy (Figure 4.3C). Quantification of images revealed that Atp7a colocalized 1.6 times more with internalized transferrin in sh-μ1A PAM-1 cells than in scramble PAM-1 cells. In AtT-20 cells, as reported in HeLa cells, a decrease in AP-1 function resulted in the accumulation of Atp7a in an endosomal compartment [220].

4.3.4 Establishing an assay for PAM function in intact cells

The decreased ceruloplasmin and increased free copper levels observed in MEDNIK patients suggested a deficit in copper delivery to ceruloplasmin and perhaps to other luminal cuproenzymes [219]. Failure to load copper into ceruloplasmin and its integral membrane homolog, hephaestin, as they are synthesized leads to their degradation [264, 265]. We carried out Western blot analysis to see whether copper chelation affected steady state levels of PAM-1 in scramble or sh-μ1A PAM-1 cells (Figure 4.4A). Overnight incubation with bathocuproine disulfonate (BCS), a membrane impermeant Cu(I) chelator, was used to reduce intracellular copper levels [266, 267]. Unlike ceruloplasmin and hephaestin, which must acquire copper as they are synthesized, the two copper atoms bound to PHM are readily exchangeable. Both newly synthesized PAM-1 and PAM-1 retrieved from the endocytic pathway participate in secretory granule function. Entry of PAM-1 into secretory granules allows its prohormone convertase 1/3 mediated cleavage, producing soluble PHM (45 kDa) and PAL membrane (70 kDa) (Figure 4.1D). Although less frequent, cleavage between PAL

and the transmembrane/cytosolic domain can occur, producing soluble PAL (50 kDa) and a 25 kDa transmembrane/cytosolic domain fragment. In the endocytic pathway, PAM-1 can be cleaved at a site closer to the transmembrane domain, generating soluble PAM-1 (100 kDa) and a 20 kDa transmembrane/cytosolic domain fragment. Using an antibody that recognizes the linker region between PHM and PAL, no change in the levels of intact PAM-1 or its processed products was observed when PAM-1 cells were treated with 50 μM BCS overnight (Figure 4.4A).

In order to evaluate PAM function in scramble vs. sh-μ1A PAM-1 cells, we took advantage of the fact that proopiomelanocortin (POMC) synthesized in AtT-20 cells is cleaved to produce amidated products along with adrenocorticotropic hormone (ACTH) and β-lipotropin (βLPH) [260, 261] (Figure 4.4B). Following cleavage at the C-terminus of ACTH, cleavage at its N-terminus reveals a potential amidation site (-Glu-Gly-Lys-Arg) at the C-terminus of the 18 kDa fragment; PAM cannot act on this substrate until carboxypeptidase E has removed the C-terminal basic amino acids, revealing a C-terminal glycine residue. An additional prohormone convertase-mediated cleavage can generate amidated joining peptide (JP) and 16 kDa fragment (Figure 4.4B). Amidated POMC products can first be detected in the *trans*-Golgi network [192], but pulse/chase studies indicate that amidation occurs largely in secretory granules [268]. An amide-specific antibody was generated by immunizing rabbits with synthetic D-Tyr-Pro-Glu-Pro-Ser-Pro-Arg-Glu-NH_2; affinity-purification yielded an antibody specific for the amidated C-terminus shared by 18 kDa fragment and JP (Figure 4.4B). Based on an ELISA, the affinity-purified JP-NH_2-specific antibody cross-reacted less than 10,000 times as well with synthetic Pro-Glu-Pro-Ser-Pro-Arg-Glu-Gly (Figure 4.4C) [269].

Lysates prepared from wild-type AtT-20 cells depleted of copper by overnight incubation in medium containing 50 μM BCS were used to test the JP-NH_2-specific antibody (Figure 4.4D). An affinity-purified γ_3MSH antibody (Figure 4.4B) was used to monitor levels of POMC, ABI, 18 kDa fragment and 16 kDa fragment [226]. The JP-NH_2-antibody detected a single 18 kDa band in cell lysates while the γ_3MSH-antibody detected 18 kDa fragment along with much larger amounts of 16 kDa fragment, POMC and ABI. JP-NH_2, which has only 18 amino acids, does not bind to PVDF or nitrocellulose membranes and cannot be assessed by Western blot analysis. BCS treatment eliminated the amidated 18 kDa band without affecting levels of POMC, ABI or 16 kDa fragment. As expected, PAM function was inhibited when AtT-20 cells were treated with 50 μM BCS for 16 hours.

4.3.5 PAM function is more sensitive to copper chelation in sh-μ1A PAM-1 cells

We reasoned that a significant alteration in copper homeostasis or protein trafficking caused by decreasing μ1A levels in PAM-1 AtT-20 cells, might alter their sensitivity to BCS. This cell impermeant Cu(I) chelator is generally applied to cells at a level of 50 to 200 μM for 4 to 48 hours [266, 267, 220, 270]. In addition to depleting cellular copper levels by removing Cu(I) from the medium, BCS would be expected to remove copper from enzymes like PAM-1, which reach the plasma membrane after exocytosis, enter the endocytic pathway and can be returned to secretory granules or degraded [195].

We therefore asked whether the amidation of 18 kDa fragment in scramble and sh-μ1A PAM-1 cells exhibited differential sensitivity to BCS (Figure 4.5A). Basal media and cell extracts from both cell lines were examined for POMC processing using the γ_3MSH antibody

and for amidation using the JP-NH_2 antibody; β-III tubulin served as a loading control for cell lysates (Figure 4.5A). Neither the endoproteolytic cleavage of POMC nor secretion of its major cleaved products was altered by BCS treatment in scramble or sh-μ1A PAM-1 cells. In both scramble and sh-μ1A PAM-1 cells, BCS treatment produced a dose-dependent decrease in the amount of 18 kDa fragment detected using the JP-NH_2 antibody. Peptide amidation in scramble PAM-1 cells was decreased to about 50% of control when cells were treated with 20 μM BCS while sh-μ1A PAM-1 cells saw their peptide amidation decrease to about 50% when cells were treated with only 2 μM BCS (Figure 4.5A, graphs). Amidation of 18kDa fragment secreted into the medium throughout the entire time of exposure to BCS showed a similar difference between scramble and sh-μ1A cells. Using an antibody that recognizes the exon 16 region between PHM and PAL, we observed that overnight treatment of both cell lines with 50 μM BCS did not alter the level or processing of PAM-1 (Figure 4.5B). Taken together, the AP-1 complex plays an important role in the ability of AtT-20 cells to provide copper to PAM-1.

With no apparent change in cellular copper levels or in Atp7a levels, we explored the possibility that altered PAM-1 trafficking contributed to its increased sensitivity to BCS in sh-μ1A PAM-1 cells.

4.3.6 Levels of PAM-1 on the cell surface are increased in sh-μ1A PAM-1 cells

Since BCS is a cell-impermeant copper chelator, we hypothesized that PAM-1 reaches the plasma membrane more frequently in sh-μ1A PAM-1 cells than in scramble PAM-1 cells, exposing it to BCS and resulting in increased copper loss and inactivation. To quantify cell surface levels of PAM-1 in scramble and sh-μ1A PAM-1 cells, surface biotinylation

experiments were carried out [195]. Membrane trafficking was blocked by chilling the cells on ice. Cell surface proteins were then biotinylated at 4°C using the cell impermeable sulfo-NHS-LC-biotin; biotinylated proteins were isolated by binding to streptavidin beads. PAM-1 proteins in total cell lysates (inputs) and biotinylated PAM-1 in eluates were compared by Western blot analysis (Figure 4.6). A 75% increase in PAM-1 cell surface levels was observed in sh-μ1A PAM-1 cells vs. scramble PAM-1 cells; the amount of PALm on the cell surface was doubled in sh-μ1A PAM-1 cells. This increase in PAM-1 on the cell surface in sh-μ1A PAM-1 cells would result in increased exposure to BCS, allowing faster removal of bound Cu(I) and inactivation of the enzyme.

4.3.7 Atp7a trafficking differs in neuroendocrine cells and HeLa cells

When fibroblasts or HeLa cells are treated with elevated levels of copper, Atp7a shifts from the Golgi region to the cell periphery; when these cells are treated with a copper chelator, such as BCS, Atp7a exit from the Golgi is prevented [271, 219]. AtT-20 cells were treated with 20 μM or 200 μM of $CuCl_2$ for 2 hours or with 50 μM of BCS overnight and endogenous Atp7a was then localized by immunofluorescent staining (Figure 4.7A). Even after exposure to high levels of $CuCl_2$, Atp7a was largely localized in the Golgi area in AtT-20 cells; the effects of 20 μM and 200 μM $CuCl_2$ were similar. Although a major shift of Atp7a towards the plasma membrane was not observed, exposure to elevated levels of copper did affect the localization of Atp7a. The ratio of average fluorescent intensity for Atp7a in the cytosol (any part of the cell excluding the Golgi and nucleus) to average intensity in the Golgi area increased by about 45% upon treatment with $CuCl_2$; this ratio was not altered by BCS treatment (Figure 4.7A). Treatment with 200 μM $CuCl_2$ resulted in a milder shift of Atp7a to the cell periphery

than treatment with 20 μM $CuCl_2$. This difference might be due to the toxicity of copper at 200 μM. Most Atp7a was still contained in the perinuclear region and colocalized with the *cis*-Golgi marker, GM130.

Since Atp7a trafficking differed in AtT-20 cells and HeLa cells, we next turned to rat primary anterior pituitary cultures to ask whether this difference in Atp7a trafficking was specific to peptide-producing cells. Primary pituitary cells were cultured in vitro for 4 days before being treated with either 50 μM BCS overnight, 20 μM $CuCl_2$ for 2 hours or untreated as a control. Treatment of primary pituitary cells with elevated levels of copper did not produce a change in the localization of Atp7a (Figure 4.7B).

4.3.8 Copper-dependent Atp7a trafficking is not altered in sh-μ1A PAM-1 cells

Since Atp7a distribution shifted to peripheral regions of the cells under elevated copper treatment in AtT-20 cells, we next asked whether this shift still occurred in sh-μ1A PAM-1 cells. Immunofluorescent staining was used to evaluate the effect of copper treatment on Atp7a distribution in scramble and sh-μ1A PAM-1 cells. Both cell lines showed a very similar distribution, with Atp7a accumulated in the perinuclear region, where it colocalized with GM130 (*cis*-Golgi marker), and in vesicles distributed throughout the cells (Figure 4.8A). Scramble and sh-μ1A PAM-1 cells treated with 20 μM $CuCl_2$ for 2 hours showed a similar slight, but reproducible, shift of Atp7a toward the cell periphery (Figure 4.8A, graph).

In order to confirm the immunofluorescent data, Western blot and surface biotinylation were used to quantify the levels of Atp7a in the cell and at the cell surface after cells had been treated with 20 μM $CuCl_2$ for 2 hours (Figure 4.8B). SNAP25, an intracellular protein,

was used as a negative control to ensure that copper treatment did not damage the cells. The total cell lysate (input) shows increased Atp7a levels upon copper treatment. A 2 to 3 fold increase in Atp7a levels was seen in both scramble and sh-μ1A PAM-1 cells in response to elevated copper levels (Figure 4.8C). Only 0.1% of total Atp7a resides on the cell surface at steady state. Atp7a cell surface levels increased 3-fold when cells were incubated with high levels of copper in both scramble and sh-μ1A PAM-1 cells (Figure 4.8D). Taken together, the copper-dependent trafficking of Atp7a was not altered in sh-μ1A PAM-1 cells.

4.3.9 Atp7a and PAM interact in AtT-20 cells

Unlike Cu/Zn superoxide dismutatase (SOD1) and cytochrome c oxidase, which receive copper by interacting with their own specific cytosolic chaperones [216, 272], copper delivery to PAM is not thought to involve a chaperone; Atox1 delivers copper to Atp7a for transport into the lumen of the secretory pathway, but little is known about the status of copper in the luminal compartment [255]. Biophysical studies indicated that copper could be transferred to PHM from a scaffold that incorporated the His/Met-rich luminal loop connecting transmembrane domains 1 and 2 of Atp7a [215]. We decided to use immunoprecipitation to see whether an interaction between Atp7a and PAM could be detected in cells and whether this interaction would be copper dependent. PAM-1 cells were treated with 50 μM BCS overnight or with 20 μM copper for 2 hours before extraction and solubilization for immunoprecipitation using an Atp7a antibody and rabbit IgG as a negative control. In both, the BCS and copper treated samples, Atp7a was successfully immunoprecipitated, with essentially no background. Co-immunoprecipitation of PAM was evaluated using antibody to exon 16; a small percentage of the total PAM-1 and PALm in the lysate was recovered in the Atp7a precipitate (Figure

4.9). Both PAM-1 and PALm were detected at levels above background. Atp7a successfully co-immunoprecipitated PAM-1 under BCS and copper overload conditions, indicating that Atp7a and PAM-1 interact independent of copper levels.

4.4 Discussion

4.4.1 Copper handling is cell type specific

Neuroendocrine cells synthesize and store bioactive neuropeptides; many of these peptides must be amidated before they are fully active [273]. Amidation cannot occur until after a prohormone convertase has cleaved the precursor and carboxypeptidase E has removed any basic amino acids from the C-terminus of the biosynthetic intermediates, revealing a C-terminal glycine. As a result, amidation occurs late in the peptide biosynthetic pathway. Based on pulse/chase metabolic labeling experiments, amidation generally occurs in secretory granules. Quite strikingly, very little Atp7a is found in mature secretory granules. In contrast, mature secretory granules contain both intact PAM-1, which can be recovered from the cell surface after granule exocytosis, and soluble PHM.

Both PAM and Atp7a localize to the Golgi region in pituitary cells. Immature secretory granules, which form from the *trans*-Golgi network, contain PAM-1 along with condensing granule content proteins [234]. Much of the PAM-1 is recovered from the immature granules in a process that involves AP-1 [88, 86, 82, 190]; it is not yet clear whether Atp7a also enters immature secretory granules. If Atp7a delivers copper directly to PAM, the transfer is likely to occur in the *trans*-Golgi network, immature secretory granules or an endocytic compartment. If PAM-1 retrieved from the plasma membrane loses one or both of its copper

ions, copper could again be provided as the protein is returned to secretory granules [195]. If the transfer of copper to PHM is not direct, luminal copper levels would determine where metallation of PAM occurs.

When treated with high amounts of copper, ATP7A was redistributed to the periphery in HeLa cells [271, 220]. Excess of extracellular copper did not dramatically alter the Golgi distribution of Atp7a in AtT-20 cells and primary pituitary cells presumably to ensure that cuproproteins like PAM-1 acquire copper effectively. Upon exposure to high levels of copper, Atp7a protein levels increased. Since Atp7a regulates the exit of copper from the cells, this indicated that neuroendocrine cells respond to increasing levels of copper by augmenting the protein expression level of Atp7a rather than moving Atp7a from the Golgi to the cell periphery. In melanocytes, tyrosinase, a cuproenzyme required for melanin synthesis, receives copper from ATP7A in melanosomes [274]. Lack of Biogenesis of Lysosome-related Organelle Complex 1 resulted in accumulation of ATP7A in early endosomes instead of melanosomes in the human melanoma cell line, MNT-1, indicating that ATP7A trafficking is cell type specific [274].

Increased extracellular copper may also affect other cuproproteins differently in neuroendocrine cells. Ctr1 transports copper across the plasma membrane into the cytosol, where it is rapidly transferred to chaperones [216]. In the small intestine and heart of mice fed a copper-deficient diet, total and cell surface levels of Ctr1 were increased compared with mice fed a normal diet, presumably due to increased stability [270]. Atox1, a copper chaperone, delivers copper to Atp7a. Fibroblasts lacking Atox1 contained increased intracellular levels of copper and had impaired Atp7a translocation to the cell periphery in response to high copper levels [267]. Additional studies looking at Ctr1 and Atox1 expression and trafficking

will help to shed light on how copper is handled in neuroendocrine cells.

4.4.2 Atp7a endocytic trafficking is altered in neuroendocrine cells with reduced AP-1 function

In HeLa cells, internalized transferrin concentrated in a perinuclear Golgi region when expression of one AP-1 subunit was decreased [236]. A similar response was observed in fibroblasts isolated from μ1A knockout mice, where early endosomes tend to group near the nucleus [178]). Atp7a trafficking is strongly dependent on AP-1 in HeLa cells and fibroblasts [220, 219]. Because the peri-nuclear Golgi region contains a complex mixture of biosynthetic and endocytic organelles in AtT-20 cells, scramble and sh-μ1A PAM-1 cells were treated with nocodazole to disperse endosomes. This allowed us to observe an increase in the colocalization of Atp7a and internalized transferrin in sh-μ1A PAM-1 cells compared to scramble PAM-1 cells. Retrieval of Atp7a from the endocytic pathway to the Golgi requires AP-1.

Although cell surface levels of Atp7a were very low in AtT-20 cells (0.1%), surface biotinylation did not show an increase in the amount of Atp7a on the cell surface at steady state in sh-μ1A PAM-1 cells. In addition, treatment of sh-μ1A PAM-1 cells with elevated levels of copper revealed that Atp7a trafficking in response to copper was not prevented. These data indicated that Atp7a requires AP-1 for retrograde trafficking but that AP-1 was not necessary for anterograde and copper-dependent trafficking.

4.4.3 PAM-1 function is sensitive to copper levels and AP-1

Peptide amidation is an essential post-translational modification; neither flies nor mice lacking this activity can complete development [260, 275]. Although PAM requires copper for activity, the PHM/CuA dissociation constant is ~60 nM; in contrast, it is around 6 fM in SOD1, indicating that copper bound to PAM-1 is easily exchangeable [276, 277]. In AtT-20 cells, reduced AP-1 function impairs the formation of immature secretory granules [234]; both PAM and ACTH accumulate in the non-condensing secretory granules that appear in sh-μ1A PAM-1 cells. Basal secretion of PHM is elevated in sh-μ1A PAM-1 cells, suggesting that the trafficking of PAM-1 along the regulated secretory pathway is perturbed when AP-1 function is reduced [234]. In this study, we observed an increase of PAM-1 cell surface levels in sh-μ1A PAM-1 cells. Since PAM-1 does not bind copper very tightly, its increased presence on the cell surface in sh-μ1A PAM-1 cells suggests that PHM loses its copper more readily in the presence of BCS, resulting in reduction ability of these cells to produce amidated product.

Reduced peptide amidation could also be due to changes in PAM-1 endocytic trafficking. The phosphorylation status of the PAM-1 cytosolic domain has been shown to drive PAM-1 within the endocytic pathway [195]. A phosphomimetic mutant of PAM-1, PAM-1 TS/DD, where Thr^{946} and Ser^{949} were mutated into Asp, showed that phosphorylation at these sites prevented entry into intraluminal vesicles of multivesicular bodies and recycling from the endocytic pathway. Levels of PAM-1 phosphorylated at Ser^{949} were reduced and biotinylation experiments indicated that PAM-1 exhibited more recycling from the endocytic pathway to the regulated secretory pathway in sh-μ1A PAM-1 cells (Bonnemaison M.L. et al. manuscript in preparation). This is in contrast with Atp7a, which was trapped in endocytic compartments

in shμ1A PAM-1 cells.

AtT-20 cells thus presented a similar phenotype of altered Atp7a trafficking to that observed in fibroblasts and HeLa cells when AP-1 function was reduced. Patients with MEDNIK lack the expression of σ1A, an AP-1 subunit, and had altered skin pigmentation and organization. Because Atp7a trafficking is different in pituitary cells from HeLa cells, it would be interesting to find out how the lack of AP-1 function can alter other cell types.

4.5 Materials and Methods

4.5.1 Antibodies

The antibodies used in this study are summarized in Table 4.1.

4.5.2 Cell culture and generation of scramble and sh-μ1A PAM-1 cells

AtT-20 cells were grown at 37°C with 5% CO_2 in Dulbecco's modified Eagle's medium/F-12 (DMEM/F-12) containing 25 mM HEPES, 100 units/ml penicillin, 100 μg/ml streptomycin, 10% fetal bovine serum, 10% NuSerum. AtT-20 cells stably expressing PAM-1 were described previously [188]. Generation of sh-μ1A and scramble PAM-1 AtT-20 cells using lentivirus targeted to μ1A (Sigma; clone ID TRCN0000111549) and a non-target shRNA (Sigma # SHC002V), respectively, was described previously [234].

4.5.3 Immunofluorescent staining

Cells were plated onto 0.16 to 0.19 mm thick, glass, 12-mm round coverslips (Fisher Scientific) or 4-chamber glass slides. Both supports were coated with 0.1 mg/ml poly-L-lysine for 5 minutes followed by a rinse in NuSerum and two rinses in growth medium. Cells were fixed

in 4% formaldehyde in PBS (50 mM NaH_2PO_4, 150 mM NaCl, pH 7.4) for 20 minutes at room temperature. After rinsing in PBS, cells were permeabilized in 0.075% Triton X-100, 2 mg/ml BSA in PBS for 20 minutes at room temperature and then incubated in block (2 mg/ml BSA in PBS) for 20 minutes at room temperature. Primary antibodies diluted in block were incubated with the cells overnight at 4°C. After three rinses in PBS, cells were incubated for one hour at room temperature in block containing either fluorescein isothiocyanate (FITC, 1:500 dilution) or Cy3 (1:2000 dilution) conjugated donkey antibody to mouse or rabbit immunoglobulin (Jackson ImmunoResearch). After three rinses in PBS, cells were incubated with Hoechst (1:1000 dilution in PBS) for 10 minutes at room temperature. After three rinses in PBS, cells were mounted using ProLong® Gold (Invitrogen).

4.5.4 Quantification of images

Cells were visualized using a Nikon TE300 epifluorescence microscope with an oil immersion 63X Plan Apochromat objective (NA 1.4). Quantification of fluorescence images was done using NIS Elements Software. Background values were determined by measuring the average intensity in parts of the picture without cells for both green and red images. Background was then subtracted for both green and red images using the average intensity measured as a constant value for the entire image. Three regions were identified in each cell analyzed: Golgi (based on staining for GM130), nucleus and cytosol (region distinct from nucleus and Golgi). For each cell, two identical boxes were drawn: one box was placed over the Golgi while the other box was placed over the cytosol. The average fluorescence signal intensity in each region was measured for 8 to 41 cells. Cytosol/Golgi fluorescence intensity ratios are shown. Statistical analyses were made using paired t-tests on the ratios calculated.

For confocal analyses, cells were visualized using a Zeiss LSM 510-Meta with an oil immersion 63X Plan Apochromat objective (NA 1.4). Colocalization of markers was assessed using Metamorph. For each image, colors were first separated and the background was subtracted as described above. For each color, the image was thresholded using an inclusive threshold at least three times background. Colocalization of markers was measured based on area. Statistical analyses were made using paired t-tests on the ratios calculated.

4.5.5 Inductively coupled plasma mass spectrometry (ICP-MS)

Tubes used for ICP-MS were incubated in 1% HNO_3 (trace metal grade, Fisher Scientific) for at least 24 hours. Scramble and sh-μ1A PAM-1 cells were plated onto a 6 well dish. When confluent, cells were trypsinized and resuspended in HSG buffer (15 mM HEPES, 120 mM NaCl, 2 mM $CaCl_2$, 4 mM KCl, 25 mM glucose, pH 7.4). Resuspended cells were split into three equal aliquots, which were used for cell counting, measurement of protein concentration and ICP-MS. Cells for ICP-MS were spun and the supernatant was discarded. Samples were digested with 200 μL 50% HNO_3 (trace metal grade, Fisher Scientific) in Eppendorf tubes at room temperature overnight. The digested samples were brought to a total volume of 1 mL with 1% HNO_3, mixed by vortexing, and spun at 3500 rcf for 3 minutes to remove debris. ICP-MS analysis was carried out in the Elemental Analysis Core at Oregon Health and Science University using an Agilent 7700x equipped with an ASX 250 autosampler. The system was operated at a radio frequency power of 1550 W, an argon plasma gas flow rate of 15 L/min, and Ar carrier gas flow rate of 1.08 L/min. Elements were measured in kinetic energy discrimination (KED) mode using He gas (4.2 mL/min). For measurement, samples were transferred to acid-treated 15-mL conical tubes. Data were quantified using a 9-point

calibration curve (0, 0.5, 1, 2, 5, 10, 50, 100, 1000 ppb (ng/g)) for Ca, Mn, Fe, Cu, and Zn using an external standard (Common Elements Mix 2 Multi-Element Aqueous Standard, VHG Labs) in 1% HNO_3. For each sample, data were acquired in triplicate and averaged. A Ge-72 internal standard (Internal Standard Multi-Element Mix 3, VHG Labs) introduced with the sample was used to correct for plasma instabilities, and frequent measurements of a 10 ppb all-analyte solution as well as a blank (containing 1% HNO_3 only) were used as quality control and to determine the coefficient of variance. To access recovery rates of elements and probe background contamination from containers a certified NIST standard reference material (Trace Elements in Water, 1643e) was digested and analyzed by the same method as the samples. HSG buffer was also analyzed to determine background contributions.

4.5.6 Primary anterior pituitary cell culture

Rat anterior pituitary cells were plated on 0.16 to 0.19 mm thick glass, 12-mm round coverslips (Fisher Scientific) coated with 0.1 mg/ml poly-L-lysine for 5 minutes followed by a rinse in NuSerum and two rinses in AtT-20 growth medium as described previously [278]. Briefly, rat anterior pituitary was rinsed in CSFM-air medium (DMEM/F-12 air, 25 mM HEPES, 100 units/ml penicillin, 100 μg/ml streptomycin, 1-2 mg/mL BSA, ITS, 50 μM ascorbate) and diced. Pituitary pieces were incubated in 0.75 mL collagenase solution (4 mg/mL crude collagenase, 1 mg/mL hyaluronidase, 0.1 U/mL benzonase, 10 mg/mL BSA) for 20 minutes at 37°C without CO_2 under agitation. Pituitary fragments were diluted with 14 mL of CSFM-air and spun down at room temperature for 5 minutes. Supernatant was removed and cells were incubated with 0.75 mL of 3 mg/mL trypsin I-300 dissolved in CSFM-air for 5 minutes at 37°C without CO_2 under agitation. Trypsin was blocked by adding

0.75 mL of 0.2 mg/mL LBTI (Lima Bean Trypsin Inhibitor) dissolved in AtT-20 medium. The dissociated cells were then filtered through a 70 μm filter. After centrifugation of the flow through, the cell pellet was resuspended in 5 mL of 160 mM NH_4Cl to lyse red blood cells and then spun again for 5 minutes at room temperature. The cell pellet was resuspended in 5 mL of AtT-20 growth medium. 1/25th of a rat anterior pituitary was plated per well of a 24-well dish. Cells remained in AtT-20 growth medium for 2 days and were then switched to DMEM/F-12, 25 mM HEPES, 100 units/ml penicillin, 100 μg/ml streptomycin, 1-2 mg/mL BSA, Insulin-Transferrin-Selenium (ITS), 50 μM ascorbate. Cells were used on days 3 and 4.

4.5.7 Manipulation of cells

Cells were incubated in DMEM/F-12 air medium containing 25 mM HEPES, pH 7.4, 1 mg/ml BSA for 30 minutes at 37°C without CO_2. For transferrin uptake experiments, cells were then incubated in DMEM/F-12 air medium containing 25 mM HEPES, pH 7.4, 1 mg/ml BSA, 25 μg/mL Alexa fluor 546 transferrin (Life Technologies) for 10 minutes at 37°C without CO_2. Cells were fixed using 4% formaldehyde in PBS for 20 minutes at room temperature. For nocodazole treatment experiments, cells were treated as described above and treated with DMEM/F-12 air medium containing 10 μM nocodazole (Sigma) or the equivalent volume of DMSO for 20 minutes at 37°C without CO_2.

4.5.8 BCS and copper treatment of AtT-20 cells

Cells were first incubated for 30 minutes in DMEM/F-12 medium or DMEM/F-12 air medium containing ITS, 25 mM HEPES, pH 7.4, 1 mg/ml BSA. Cells were equilibrated in air medium during two consecutive 30 minute incubations at 37°C with or without CO_2. Cells were then

treated with medium containing 50 μM bathocuproinedisulfonic acid (BCS, Sigma) overnight or $CuCl_2$ (20 μM or 200 μM, Sigma) for 2 hours or medium only as a control. Cells were either fixed for immunostaining, lysed in detergent for biochemical analysis or chilled for cell surface biotinylation.

4.5.9 Detection of joining peptide (JP) amidation

Antibody specific to the amidated C-terminus of JP was generated by linking D-Tyr-Pro-Glu-Pro-Ser-Pro-Arg-Glu-NH_2 [D-Tyr JP(12-18)NH_2]] to BSA as described [269]. The addition of a Gly residue to the C-terminus of this peptide [JP(12-19)] reduced its cross-reactivity with this antiserum by 10,000-fold [269]. For Western blot analysis, a fraction enriched in immunoglobulin by precipitation with ammonium sulfate (45% saturation) was dialyzed into 100 mM NaPhosphate, pH7.4 and incubated with JP(12-19) bound to Affi-Gel15 (4mg peptide/2ml resin) for 1h at 4°C to remove any antibodies capable of recognizing this peptide. The unbound fraction was applied to a column of JP(12-18)NH_2 linked to AffiGel10 (5mg peptide/2ml resin); bound antibodies were eluted with 0.2 M Glycine HCl, 0.1M NaCl, 0.1 % TX-100, pH 2.3; the eluate was rapidly neutralized with 3M Tris HCl, pH 8.0 and BSA (final concentration in eluate = 0.2 mg/ml) was added before dialysis against 100 mM NaPhosphate, pH7.4. Preparation of an antibody specific for γ_3MSH [226] was described previously. Affinity purification was carried out as described above using bovine γ_3MSH linked to Affi-Gel10.

4.5.10 ELISA

Protein A Coated Plates (Pierce) were rinsed three times with 200 μl Tween-Tris-Buffered-Saline (TTBS, 0.5% Tween 20, 50 mM Tris, 150 mM NaCl, pH 7.5). Affinity-purified JP-NH_2 antibody (1:500,000 dilution), standard peptide (rat joining peptide; Phoenix Pharmaceuticals) and sample diluted into TTBS was allowed to bind to the strips for two hours. Biotinylated JP-NH_2 (labeled using Pierce EZ-Link NHS-PEG4-Biotinylation Kit, per manufacturer's instructions; nominally 20 pg=11 fmol per well) was added for 1 h. After 4 rinses (200 μl TTBS), wells were incubated in 100 μl 1:5000 Pierce High sensitivity Streptavidin-HRP for 1 h, followed by TTBS rinses. Color was developed using 100 μl TMB (Pierce 1-Step Ultra TMB-ELISA, diluted 1:3 in 100 mM Na-acetate pH 5.0) for 5-10 min and stopped with 110 μl 2 M H_2SO_4; OD was determined at 450 nm.

4.5.11 Biotinylation

AtT-20 cells plated in a 12-well plate were first incubated for 30 minutes in DMEM/F-12 air medium containing ITS, 25 mM HEPES, pH 7.4, 100 μg/ml BSA. Cells were equilibrated in air medium during two consecutive 30 minute incubations at 37°C without CO_2. Cells were then treated with air medium containing 20 μM $CuCl_2$ or air medium only as a control. Dishes were placed on ice and incubated 10 minutes at 4°C. Cells were rinsed with ice cold HSG buffer (15 mM HEPES, 120 mM NaCl, 2 mM $CaCl_2$, 4 mM KCl, 25 mM glucose, pH 7.4). A solution containing 1.25 mM sulfo-NHS-LC-biotin (Thermo Scientific) in HSG buffer was made fresh and added to the cells for 10 minutes at 4°C. After removing the biotin solution, cells were rinsed twice for 5 minutes with CSFM-air containing 2 mg/ml BSA. Cell extracts were collected using TMT [20 mM Na N-Tris[hydroxymethyl]methyl-2-aminoethanesulfonic

acid (TES), 10 mM mannitol, 1% Triton X-100, pH 7.4] containing a cocktail of protease inhibitors (final concentrations 0.34 mg/ml phenylmethylsulfonyl fluoride, 50 μg/ml lima bean trypsin inhibitor, 2 μg/ml leupeptin, 16 μg/ml benzamidine, and 2 μg/ml pepstatin). Cells were solubilized in TMT for 30 minutes at 4°C. Cell extracts were collected into microfuge tubes and centrifuged at 22,000 x g for 15 minutes at 4°C. Solubilized cell extracts were then incubated with Streptavidin-agarose beads for 1 hour at 4°C. Beads were rinsed twice with TMT and once with TM (no Triton X-100). The bound fraction was eluted into Laemmli sample buffer by heating the samples for 5 minutes at 95°C (PAM-1) or 55°C (Atp7a).

4.5.12 Co-immunoprecipitation

A confluent well of a 6-well dish of AtT-20 cells expressing PAM-1 was lysed in 500 μl TMT, 1 mM EDTA and a cocktail of protease inhibitors (final concentrations 0.34 mg/ml phenylmethylsulfonyl fluoride, 50 μg/ml lima bean trypsin inhibitor, 2 μg/ml leupeptin, 16 μg/ml benzamidine, and 2 μg/ml pepstatin) was added. After incubation at 4°C for 30 min, cell extracts were centrifuged at 22,000 x g for 15 minutes at 4°C. Supernatants (220 μl) were pre-cleared by incubation with 10 μl packed protein A (Repligen BioProcessing) for 30 minutes at 4°C. After centrifugation at 1,000 x g for 5 minutes, 10 μl of supernatant was collected as the input for the Western blot and the rest of supernatant was transferred into a new tube containing 1 μg antibody (affinity-purified rabbit antibody to Atp7a or rabbit IgG as control). Samples were tumbled overnight at 4°C and then centrifuged at 22,000 x g for 15 minutes at 4°C to remove insoluble material. The supernatants were added to protein A beads (10 μl packed resin) and tumbled for 1 hour at 4°C. Beads were washed twice in pH

7.4 TMT containing 1 mM EDTA and protease inhibitors, and once in pH 7.4 TM containing 1 mM EDTA and protease inhibitors. The bound fraction was eluted by incubation for 30 minutes at 55°C in Laemmli sample buffer, fractionated by SDS-PAGE on 4-15% gradient gels (Bio-Rad) and subjected to Western blot analysis.

4.6 Tables

Antigen	Working dilution	Identity, source
Atp7a	1:1000	CT77 [261]
APP (rabbit)	1:1000	ZEMED laboratories
rat PAM:		
C-STOP, PAM-1(965-976)	1:1000	C-stop [223]
Exon 16, PAM-1(409-497)	1:1000	JH629 [224]
Secretory granule proteins:		
POMC (γ_3-MSH)	1:1000	JH189 [226]
JP-NH_2	1:1000	[269]
ACTH	1:1000	ABCAM (clone # 56)
AP-1 components:		
μ1A	1:500	ProteinTech Group
γ-adaptin	1:1000	BD Biosciences
Golgi markers:		
GM130	1:1000	BD Biosciences
TGN38 (155-249)	1:1000	[189]

Table 4.1: Antibody list.

4.7 Figures

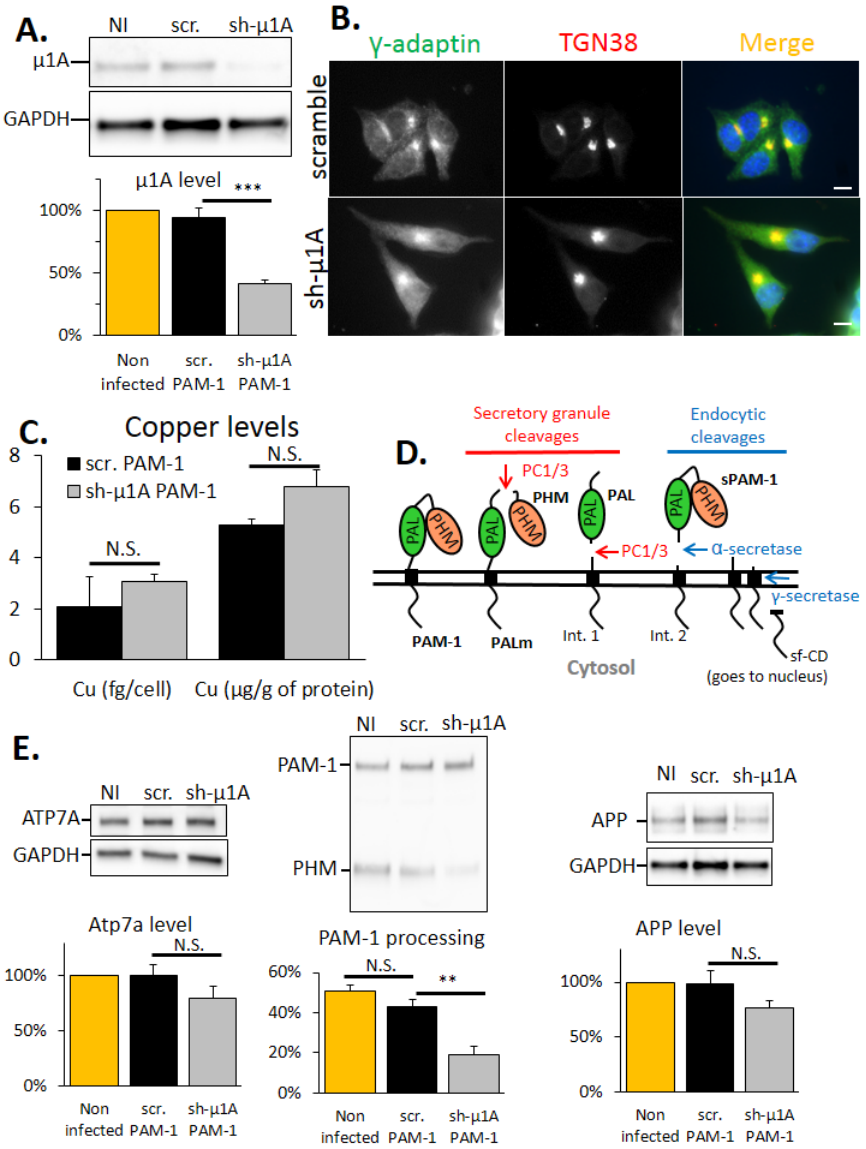

Figure 4.1: Reduced μ1A levels in AtT-20 cells stably expressing PAM-1 do not alter cuproprotein levels.

Figure 4.1: (A) Western blot showing μ1A levels in non-infected (N.I.) PAM-1 cells (N.I.), PAM-1 cells infected with a non-target shRNA expressing lentivirus (scramble, scr.) and PAM-1 cells infected with the #549 lentivirus (sh-μ1A). GAPDH was used as a loading control. The graph below indicates μ1A levels normalized to GAPDH compared between N.I., scramble and sh-μ1A PAM-1 cells (***, p<0.001, n=5). (B) Indirect immunofluorescent staining of γ-adaptin (FITC anti-mouse) and TGN38 (Cy3 anti-rabbit) in scramble and sh-μ1A PAM-1 cells. Nuclei were stained with Hoechst (scale bar, 10 μm). (C) Copper levels in scramble and sh-μ1A PAM-1 cells normalized to number of cells or amount of protein (N.S., not significant; n=3; error bars represent SEM). (D) PAM-1 processing in secretory granules and endosomes is shown. PC1/3 mediated cleavage produces PHM, PALm, PAL and intermediate 1 (Int. 1). In endosomes, α-secretase cleaves PAM-1 generating soluble PAM-1 (sPAM-1) and intermediate 2 (Int. 2). Intermediates 1 and 2 undergo another cleavage catalyzed by γ-secretase to provide a soluble fragment of the cytosolic domain (sf-CD), which goes to the nucleus [223]. (E) Western blots showing Atp7a, PAM-1 and APP in N.I., scramble and sh-μ1A PAM-1 cells. GAPDH was used as a loading control for Atp7a and APP. Graphs indicate normalized levels of Atp7a and APP over GAPDH and PAM-1 processing (PHM/(PAM-1+PHM)) compared between N.I., scramble and sh-μ1A PAM-1 cells (**, p<0.01, n=5).

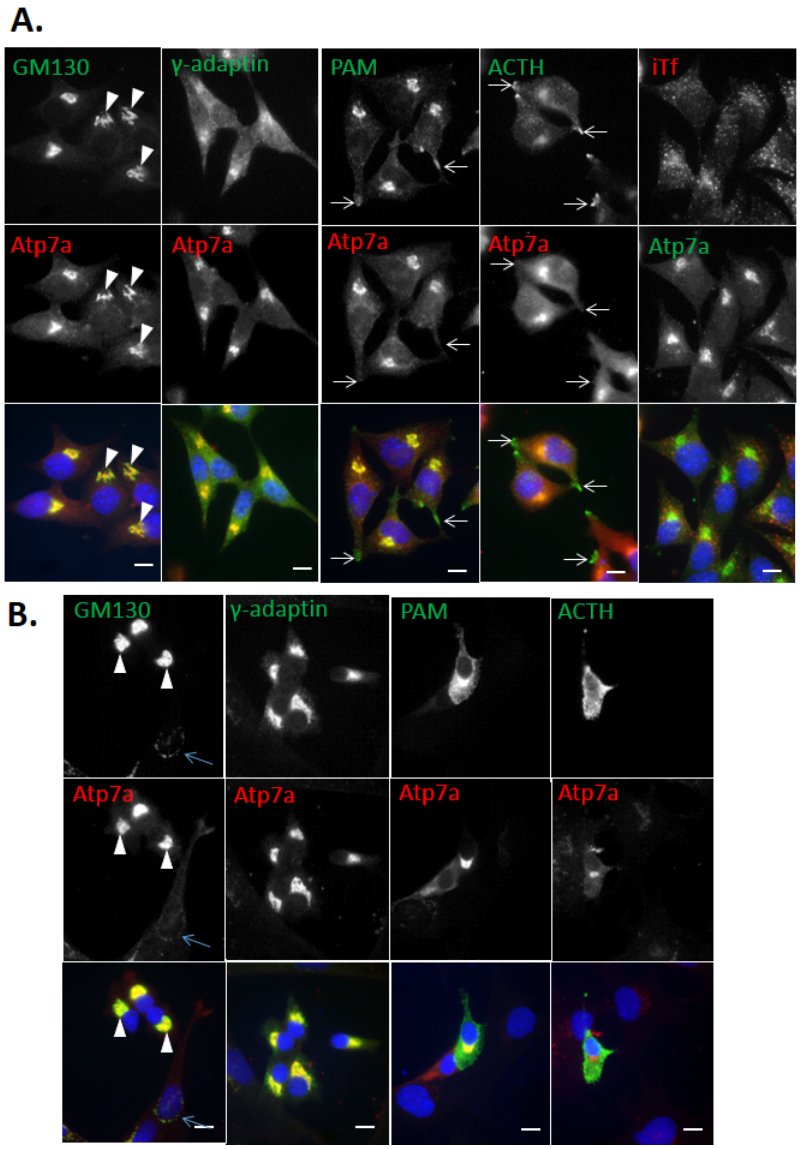

Figure 4.2: Atp7a concentrates in the Golgi region in pituitary cells. Indirect immunofluorescent staining of Atp7a (Cy3 anti-rabbit) and GM130 (*cis*-Golgi; FITC anti-mouse), γ-adaptin (FITC anti-mouse), PAM (C-terminus, FITC anti-mouse) or ACTH (secretory granule; FITC anti-mouse) in non-infected PAM-1 cells (A) and rat anterior pituitary cells (B). Nuclei were stained with Hoechst. Non-infected PAM-1 cells also show Atp7a (FITC anti-rabbit) co-stained with internalized Alexa fluor 546 transferrin (early and recycling endosomes, iTf; white arrowheads point to the Golgi; white arrows point to the tips, where secretory granules accumulate; blue arrow points to a fibroblast; scale bar, 10 μm).

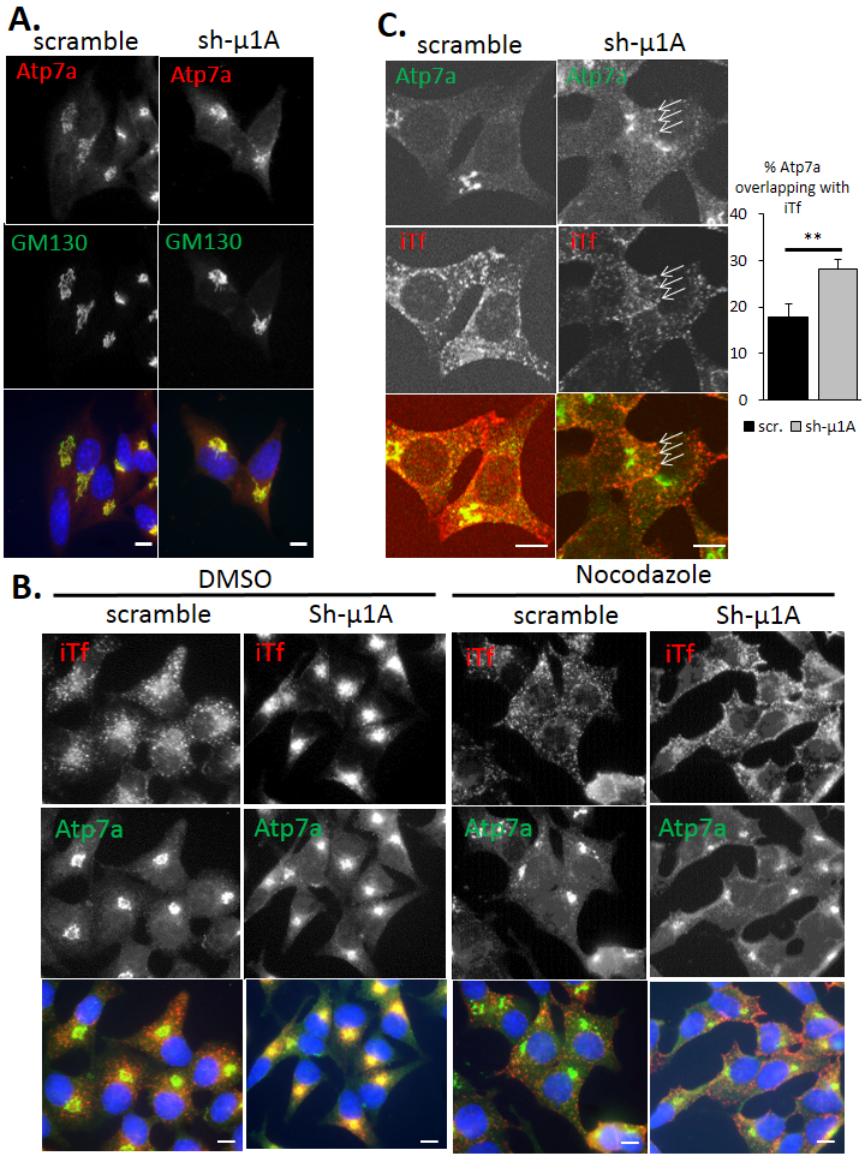

Figure 4.3: Atp7a is shifted to endosomes in sh-μ1A PAM-1 cells. (A) Indirect immunofluorescent staining of Atp7a (Cy3 anti-rabbit) and GM130 (*cis*-Golgi; FITC anti-mouse) in scramble and sh-μ1A PAM-1 cells. (B) Indirect immunofluorescent staining of Atp7a (FITC anti-rabbit) and internalized Alexa fluor 546 transferrin (iTf) in scramble and sh-μ1A PAM-1 cells after treatment with DMSO or nocodazole. (C) Confocal images of cells treated with nocodazole as described in B. Nuclei were stained with Hoechst; white arrows indicate colocalization of internalized transferrin and Atp7a; scale bar, 10 μm). Graph: % Atp7a area overlapping with internalized transferrin was increased in sh-μ1A vs. scramble PAM-1 cells.

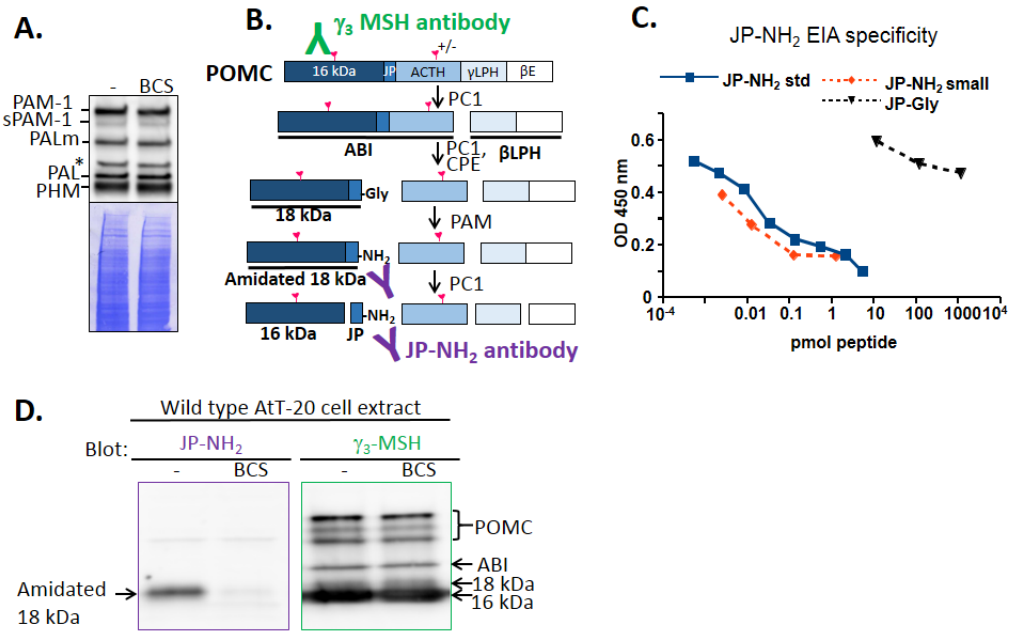

Figure 4.4: Cell based assay for peptide amidation. (A) Western blot showing PAM-1 products in control and BCS-treated non-infected PAM-1 cells. The antibody used targets exon 16, the region between PHM and PAL. Coomassie staining revealed similar amounts of protein loaded in both lanes (*, non-specific band). (B) Diagram of POMC processing in AtT-20 cells showing sites cleaved by prohormone convertase 1/3 (PC1/3) and amidated by PAM. The first cleavage generates ACTH biosynthetic intermediate (ABI) and β-lipotropin (βLPH). ABI is further cleaved to produce ACTH and 18 kDa fragment, which can be amidated by PAM only after CPE removes any C-terminal basic amino acids. Amidated 18 kDa fragment is cleaved to generate 16 kDa fragment and amidated joining peptide (JP-NH_2). Further cleavage of βLPH produces γ-lipotropin (γLPH) and β-endorphin (βE). The epitopes recognized by the γ_3MSH and JP-NH_2 antibodies are shown. (C) ELISA showing the specificity of the JP-NH_2 antibody for the amidated JP. JP-NH_2 Std, AEEETAGGDGRPEPSPRE-NH_2; JP-NH_2 small, PEPSPRE-NH_2; JP-Gly, PEPSPREG. (D) Western blot of AtT-20 cells treated or not with 50 μM BCS overnight. Antibodies against JP-NH_2 and γ_3MSH were used. Amidated 18 kDa fragment levels were strongly reduced after treatment with BCS (blot with JP-NH_2); POMC products detected with the γ_3MSH antibody were not affected by BCS.

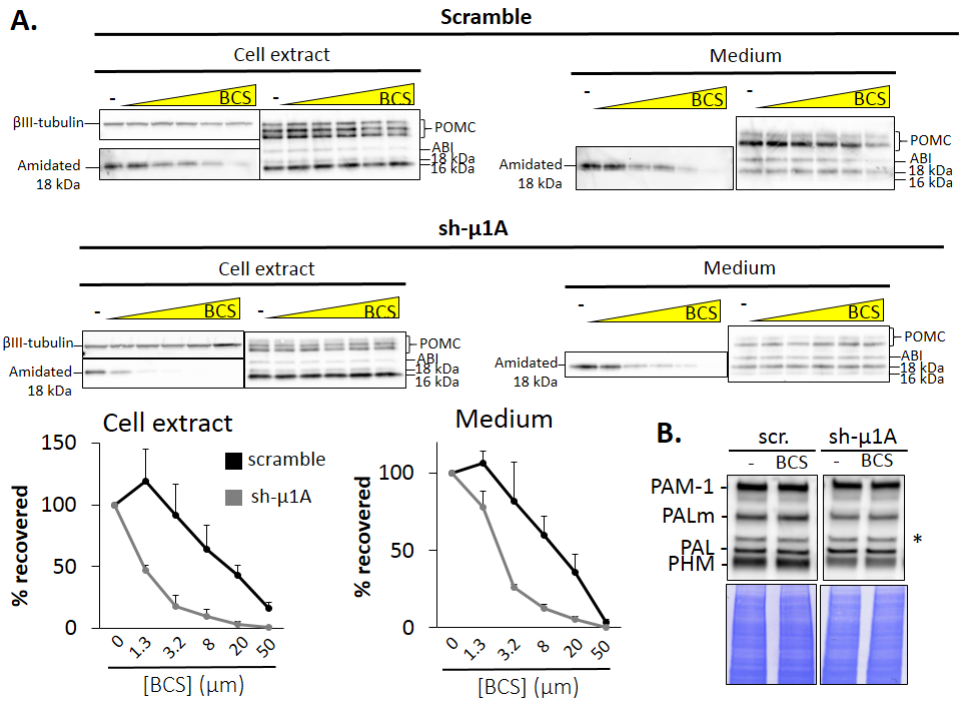

Figure 4.5: Amidation is more sensitive to BCS in sh-μ1A PAM-1 cells than in scramble PAM-1 cells. (A) Scramble and sh-μ1A PAM-1 cells were treated with increasing amounts of BCS overnight. Media and cell extracts were collected and analyzed using JP-NH_2 and γ_3MSH antibodies. βIII-tubulin was used as a loading control for cell extracts. Amidated 18 kDa fragment levels decreased as the concentration of BCS increased. Graphs: duplicate wells from three separate experiments were analyzed; levels of amidated 18 kDa fragment were expressed as a percentage of the levels observed in control samples. POMC cleavage and secretion were not altered by BCS treatment. (B) Western blot showing PAM-1 processing of scramble and sh-μ1A PAM-1 cells untreated or treated with 50 μM BCS overnight. The antibody used targets exon 16, the region between PHM and PAL. Coomassie staining revealed similar amounts of proteins loaded in all lanes (*, non-specific band).

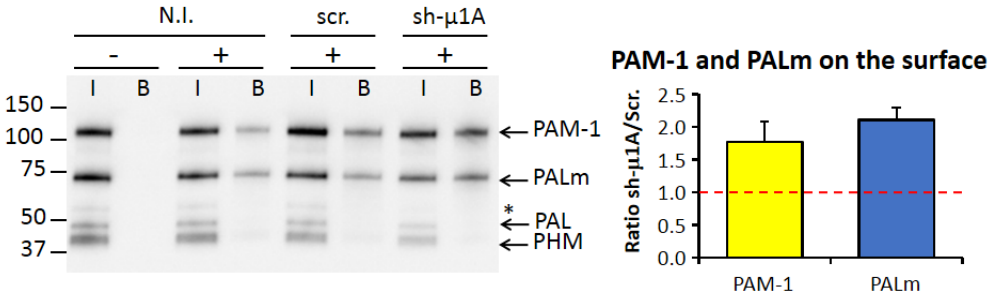

Figure 4.6: Cell surface levels of PAM are higher in sh-μ1A than in scramble PAM-1 cells. Western blot of cell surface biotinylation experiment carried out on cells chilled to 4C. Streptavidin bound samples (B) represent 125-times more material than Input (I) samples. The antibody used recognizes the region between PHM and PAL. The graph shows the ratio of PAM-1 and PALm cell surface levels in sh-μ1A PAM-1 cells over scramble PAM-1 cells (n = 3). (+, with biotin; -, without biotin; *, non-specific band).

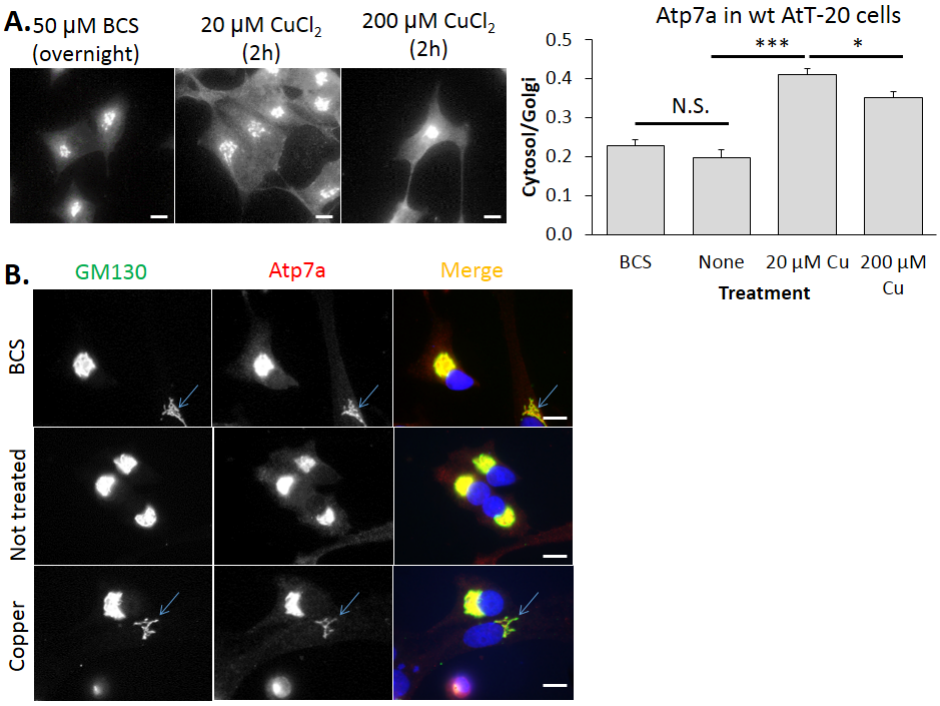

Figure 4.7: Atp7a trafficking in pituitary cells is different from HeLa cells. (A) Wild-type AtT-20 cells treated with 50 μM BCS overnight or with 20 or 200 μM $CuCl_2$ for 2 hours were fixed and stained for Atp7a (Cy3 anti-Rabbit). Graph shows the ratio for mean Atp7a fluorescence intensity in the cytosol (any part of the cell excluding nucleus and Golgi) and the Golgi region. A 50% increase in the ratio was observed when cells were treated with copper. Treatment with BCS did not alter the ratio (n = 8-25; ***, $p<0.001$; *, $p<0.05$). (B) Rat primary pituitary cells treated with 50 μM BCS overnight, with 20 μM $CuCl_2$ for 2 hours or untreated were fixed and stained for Atp7a (Cy3 anti-Rabbit) and GM130 (*cis*-Golgi, FITC anti-mouse). Atp7a distribution was not altered by BCS or copper treatment (Blue arrows point to fibroblasts; scale bar, 10 μm).

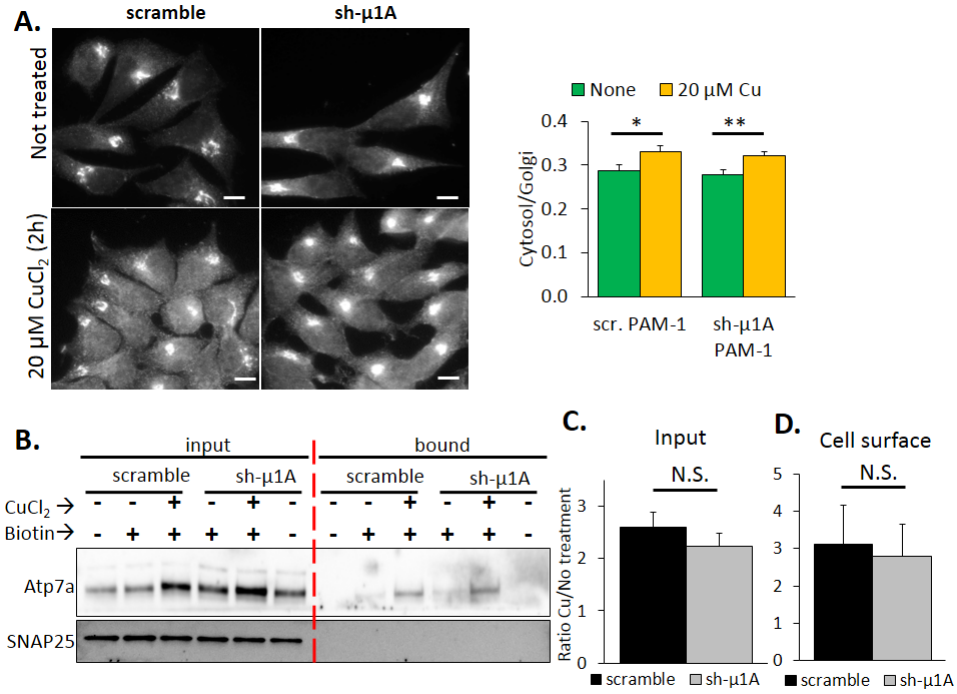

Figure 4.8: Copper-dependent trafficking of Atp7a in sh-μ1A PAM-1 cells. (A) Scramble and sh-μ1A PAM-1 cells treated with 20 μM $CuCl_2$ for 2 hours or untreated were fixed and stained for Atp7a (Cy3 anti-Rabbit). Graph shows the ratio for mean Atp7a fluorescence intensity in the cytosol over the Golgi region. A 20% increase in the ratio was observed when either cell type was treated with copper (n = 35-44; *, $p<0.05$; **, $p<0.01$). (B) Cell surface biotinylation after treatment of scramble and sh-μ1A PAM-1 cells with 20 μM $CuCl_2$ for 2 hours. Streptavidin bound samples (B) represent 100-times more material than Input samples (I); Atp7a was visualized on the upper part of the blot and SNAP25, an intracellular protein used as a negative control, on the bottom part. (C) A two-to-three fold increase in total Atp7a levels was observed in both scramble and sh-μ1A PAM-1 cells. (D) No difference between scramble and sh-μ1A PAM-1 cells was seen (+ $CuCl_2$, with 20 μM $CuCl_2$ for 2 hours; -$CuCl_2$, no treatment; + biotin, with biotin; - biotin, without biotin).

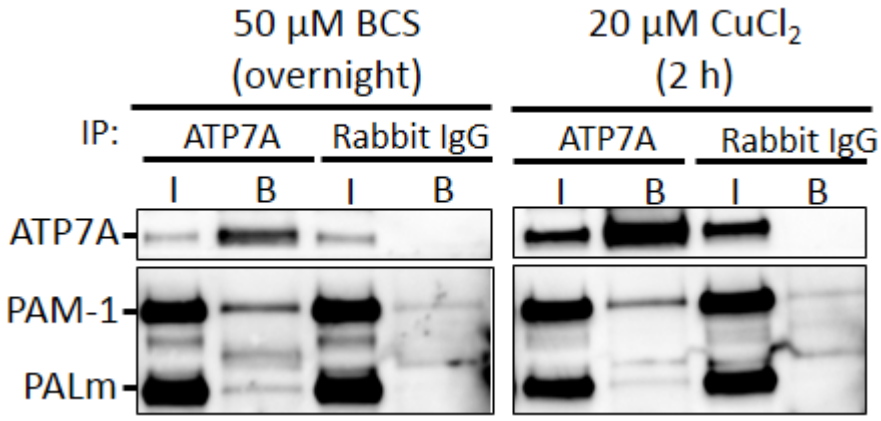

Figure 4.9: Atp7a and PAM interact in AtT-20 cells. PAM-1 cells treated with 50 μM BCS overnight or 20 μM $CuCl_2$ for 2 hours were extracted for immunoprecipitation with antibody to Atp7a; rabbit IgG was used as control for background. (I, Input; B, Bound; I/B: 1/20).

Chapter 5

Copper: a metal present in secretory granules of the anterior pituitary gland

Mathilde L. Bonnemaison, Megan E. Duffy, Martina Ralle, Richard E. Mains and Betty A. Eipper.

Manuscript in preparation for Metallomics.

Drafting of the manuscript

Mathilde L. Bonnemaison, Richard E. Mains and Betty A. Eipper.

Acquisition of data

Martina Ralle and Megan Duffy did the ICP-MS and XFM; Richard E. Mains, Betty A. Eipper and Mathilde L. Bonnemaison prepared the samples; Maya Yankova did the electron

microscopy study; Betty A. Eipper and Darlene D'Amato did the purification of PAM 820s and evaluated the amount of PAM in fractions enriched in secretory granules; Mathilde L. Bonnemaison did the remaining experiments under the guidance and supervision of Richard E. Mains and Betty A. Eipper.

5.1 Abstract

Copper is required for several biological processes such as peptide biogenesis. Because the anterior pituitary gland produces large amounts of peptides, the distribution of copper in this tissue was investigated. Subcellular fractionation of mouse and rat pituitary glands points to an accumulation of copper in fractions enriched in secretory granules. These granules store peptides along with processing enzymes, and secrete their content upon demand. The lumen of the secretory pathway contains several cuproenzymes that receive copper from Atp7a, the P-type ATPase that transports copper from the cytosol into the lumen. Lack of ATP7A function results in Menkes disease, an X-linked, infantile onset, lethal condition characterized by the inability to take up and utilize dietary copper. Peptidylglycine α-amidating monooxygenase (PAM), a cuproenzyme that amidates many peptides to render them bioactive, functions in the lumen of the secretory pathway. PAM receives copper from Atp7a, and loss of ATP7A function results in impaired peptide amidation. Quantification of copper and PAM levels in secretory granule enriched fractions indicated that copper levels exceeded PAM levels by about 70-fold on a molar basis. This study provides the first quantitative description of copper localization in the anterior pituitary gland.

5.2 Introduction

Copper is an essential metal in human physiology as it is involved in a wide variety of cellular processes, such as mitochondrial respiration, blood vessel formation and iron transport [279]. Formation of reactive oxygen species caused by copper is limited by the fact that copper is bound to a variety of cuproproteins. A study done in yeast reported that less than one atom of copper was free per yeast cell [277]. Copper enters the cell via copper transporter 1, Ctr1, and is then rapidly transferred to specific chaperones that deliver the metal to mitochondria, the secretory pathway or cytosolic proteins. Transport of copper from the cytosol into the lumen of the secretory pathway is governed by two P-type ATPases, ATP7A and ATP7B. Lack of ATP7A or ATP7B results in Menkes and Wilson disease, respectively. Menkes disease is characterized by an overall lack of copper in most tissues resulting in neurodegeneration, coarse hair, decreased bone density, and patients rarely survive past age 3 [279]. On the other hand, the first signs of Wilson disease appear during the teenage years and are accompanied by an overload of copper in most tissues, in particular the liver and the brain [280].

Copper is vital for neuropeptide and peptide hormone biogenesis, key chemical messengers for cell communication. These peptides are first synthesized as larger, inactive precursors, which undergo a sequence of post-translational modifications in order to gain bioactivity [180]. The peptide precursors, biosynthetic intermediates and processing enzymes exit the *trans*-Golgi network (TGN) in immature secretory granules. The luminal environment in the TGN promotes aggregation of many secretory granule proteins, a process thought to promote the sorting of granule proteins from cargo that is not stored in granules [180]. One of the last steps in the sequence of post-translational modifications is amidation of glycine-extended peptide intermediates, which is catalyzed by peptidylglycine α-amidating monooxygenase

(PAM). This enzyme is composed of two catalytic core domains, PHM and PAL, which work in sequence to complete the amidation reaction [238]. PAM is a demanding enzyme as PHM requires copper, oxygen and ascorbate to catalyze the first reaction and PAL needs zinc and calcium for structure and catalysis [276, 281, 282, 283]. Lack of PAM is embryonic lethal in mice and *Drosophila* lacking *PHM* do not survive the larval stage, indicating that PAM is required for development and that PAM is the sole protein to provide this function [260, 275].

In rodents, only the atrium of the heart expresses higher levels of PAM than the anterior pituitary [284, 285]. This gland is composed of five major peptide-producing cell types, somatotropes (50%), lactotropes (20%), corticotropes (15%), gonadotropes (10%) and thyrotropes (5%) [286]. Although none of the main anterior pituitary hormones is modified by PAM, these same cells produce much lower levels of several amidated peptides (substance P, neuropeptide Y, vasoactive intestinal peptide, galanin, GnRH, TRH, and pyroglutamylglutamylprolineamide); these amidated peptides are thought to function more as autocrine and paracrine agents [263].

The roles of copper in the brain and liver have been extensively explored to understand Menkes and Wilson diseases. Although PAM is an essential cuproenzyme heavily expressed in the pituitary gland, the distribution of copper in the pituitary has not been explored. Rat and mouse pituitary glands were used to evaluate the concentration of copper and its distribution using subcellular fractionation, X-ray fluorescence microscopy, and ICP-MS (Inductively Coupled Plasma - Mass Spectometry).

5.3 Results

5.3.1 The rat pituitary contains 40-50 μM copper

A rat pituitary was collected and frozen in cryoprotectant; 10 μm thick sections were cut and the sections were stained with hematoxylin and eosin (Figure 5.1A). The anterior lobe can be easily distinguished from the neural lobe in the center. The anterior pituitary is composed primarily of peptide producing cells (chromophils; purple), while the neural lobe is composed of the axons and terminals of neurosecretory neurons situated in the hypothalamus (light pink).

X-ray fluorescence microscopy was used to determine the concentration of several elements, including copper. This technique can also generate a diffraction phase image as shown in Figure 5.1A. Overall, sulfur, chloride, potassium, calcium, manganese and iron were more concentrated in the neural lobe than in the anterior lobe, while phosphorus and copper were present at similar concentrations in both regions (Figure 5.1B). Zinc is the only element examined that was shown to be more concentrated in the anterior lobe. Somatotropes and lactotropes, which represent about 70% of the anterior pituitary, produce growth hormone and prolactin, respectively; the aggregation and storage of both hormones in secretory granules is facilitated by the presence of zinc [287, 288]. Phosphorus, a key component of nucleic acids, is the prevalent element with an average concentration of 75-80 mM (Figure 5.1C), followed by sulfur and potassium with concentrations of 44 mM and 26 mM in the anterior lobe and 78 mM and 32 mM in the neural lobe. The concentrations of chloride, calcium, iron and zinc in both the anterior and neural lobes were in the low mM range. The least prevalent metals were manganese and copper, with both present at about 40 μM in the neural lobe and 30-45

μM in the anterior lobe (Figure 5.1C). By comparison, brain copper levels were estimated to be 100-250 μM at the synapse and up to 400 μM in senile plaques with Alzheimer's disease [216].

5.4 Copper is in secretory granule enriched pellets

Copper is required in the regulated secretory pathway, where the peptide amidating enzyme functions, in mitochondria for cytochrome c oxidase and in the cytosol, where the Cu/Zn-dependent enzyme superoxide dismutase 1 and MEK reside. In order to evaluate the distribution of copper in the pituitary gland, pituitaries were collected, homogenized and subjected to differential centrifugation (Figure 5.2A). ICP-MS analysis of the resuspended pellets and the cytosolic fraction (S4) indicated that S4 contained the largest amount of iron, copper and zinc (Figure 5.2B). The P2 pellet, obtained after centrifuging samples at 4,000 g for 17 minutes, contained more iron, copper and zinc than the other pellets combined (Figure 5.2B). Based on previous studies, we expected the P2 and P3 pellets to contain secretory granules [289]. The peptide amidating enzyme, PAM, which spans the membrane of secretory granules, endosomes and Golgi, has been identified in multiple subcellular fractions. Within secretory granules, the isoform PAM-1 can be cleaved between PHM and PAL, generating soluble PHM and PAL membrane (PALm). Soluble PHM has served as a useful marker for secretory granules. Western blot analysis using an antibody specific for PAM exon 16, the linker region between PHM and PAL, was used to characterize the subcellular fractions. P2 contained more PHM than the other fractions, indicating that it was enriched in secretory granules (Figure 5.2C). Soluble PAL was also prevalent in P2, consistent with its presence in secretory granules; PALm, which is retrieved through the endocytic pathway, was also found

in P3 and P4, which contain endosomes and microsomes.

5.5 Copper is present in secretory granules

Because P2 contained most of the copper and protein and was enriched in secretory granules, we next asked whether copper was present in secretory granules. The P2 pellet was gently resuspended and loaded onto the top of a non-linear sucrose gradient to separate organelles based on their density. Fractions of the sucrose gradient were collected from the top (low sucrose) to bottom (high sucrose), fractionated by SDS-PAGE and western blotted for the exon 16 region of PAM-1 (Figure 5.3A). Fractions 10-13 contained the highest amounts of PHM and were thus identified as the secretory granule enriched fractions. Fractions 3-5 contained intact PAM-1 along with a significant amount of PALm, consistent with their identification as an endosomal compartment. The small amount of PHM at the top of the gradient represents secretory granules that were lysed during fractionation.

To determine the copper concentration in each sucrose fraction, ICP-MS was performed. A peak of copper was observed between fractions 10-13, matching the secretory granule enriched fractions (Figure 5.3B). The sucrose-containing buffer contained a significant amount of copper (open symbols); the copper background contributed by the buffer was subtracted to determine the level associated with the secretory granules. No peak of copper was associated with the endosomal fractions containing PALm, but a substantial amount of copper was recovered from the densest fraction, which would be expected to contain mitochondria.

Fractions 12 and 13 were combined and further analyzed by transmission electron microscopy after negative staining in order to verify the presence of secretory granules and to assess purity. Secretory granules were identified as round structures filled with electron dense

material (Figure 5.3C). On average, the secretory granules had a diameter of 283 +/- 34 nm.

Unlike other cuproenzymes, the PHM domain of PAM does not bind copper with extremely high affinity. We therefore wanted to compare the concentrations of copper and PAM in the secretory granule enriched fractions. Using recombinant purified PAM 820s protein as a standard, the total amount of PAM protein (intact + processed) in fractions #12 and #13 was determined (Figure 5.3D). The concentration of copper in the same fractions was determined using ICP-MS (Figure 5.3B). The ratio of the molar concentration of copper to the molar concentration of PAM protein was about 70 for both fractions. Similar results were obtained when whole mouse pituitaries were used; a copper to PAM ratio of 60 was observed (data not shown). If most of the copper and most of the PAM protein in these fractions is contained in secretory granules, copper is present in a significant molar excess. Assumptions about the number and volume of the secretory granules must be made in order to use the concentrations measured in fractions #12 and #13 to calculate the molarity of copper and PAM in the secretory granule lumen.

5.6 Discussion

Copper is essential for the generation of many bioactive peptides, notably because PAM is a cuproenzyme that catalyzes the α-amidation of most peptide hormones. The anterior pituitary contains five major cell types producing peptide hormones, and copper is present in secretory granules of the anterior pituitary. Each peptide producing cell can be distinguished from the other types by their morphology and the size of their secretory granules, ranging from 100 nm diameter in thyrotropes to 900 nm diameter in lactotropes [290]. The amount and concentration of copper in anterior pituitary secretory granules may be cell type specific.

In addition, heterogeneity in secretory granule content protein from the same cell has been observed in corticotrope and somatotrope tumor cell lines, suggesting that copper amounts within secretory granules of the same cell may also vary [187].

In an earlier study, metabolic labeling was used to estimate secretory granule content of peptide hormone vs. processing enzyme; the conclusion reached was that each secretory granule contained only about one PAM molecule [291]. Our data demonstrated the presence of a substantially higher concentration of copper than PAM in fractions enriched in secretory granules. The dissociation constant for copper binding to the CuH site of PHM is about 0.06 μM and copper must be bound to both the CuH and CuM site for the enzyme to function [276]. With one PAM protein per 300 nm diameter secretory granule, the concentration of PAM would be about 0.12 μM, making the concentration of copper in the secretory granule lumen about 8 μM. Our data suggest that copper levels in secretory granules are high enough to prevent PAM from becoming inactive in secretory granules due to a lack of copper. Interestingly, no luminal copper chaperone has been identified, leaving it unclear how secretory granules remain protected from copper toxicity [255]. Our data indicate that secretory granule copper concentrations are not higher than the average copper concentration in the pituitary. With no copper chaperones in the lumen of the secretory pathway, delivering the correct amount of copper to the granule lumen may be the key step. Cytosolic copper binding proteins would serve as a reservoir of copper that could be delivered by Atp7a when needed.

Defining and understanding the distribution of metals such as copper is becoming important for comprehending and possibly treating multiple diseases. Menkes and Wilson disease are the most well described pathologies linked with impaired copper homeostasis. Other

pathologies have been associated with mutations in ATP7A. Occipital horn syndrome is caused by a change in splicing events and a reduction of functional ATP7A [292]. A more recently described form of ATP7A mutation has been associated with distal motor neuropathy; in these cases, ATP7A is functional, but its trafficking is altered [293, 294]. MEDNIK (Mental Retardation Enteropathy Deafness Peripheral Neuropathy Ichtyosis Keratodermia) is a disorder caused by lack of the small subunit of adaptor protein 1, a cytosolic protein complex involved in post-Golgi trafficking [217]. This syndrome combines characteristics of both Menkes and Wilson disease, presumably because ATP7A trafficking has been shown to be perturbed in cells with reduced AP-1 function [220, 219]. Alzheimer's disease, the most common form of dementia, may involve an interaction of copper with amyloid β peptides, promoting their aggregation and generating a cytotoxic environment that triggers neuronal cell death [216]. On the contrary, when copper binds islet amyloid polypeptide, it prevents this 37-residue peptide from forming amyloid fibrils and thus protects β-cells from apoptosis [295]. Since aggregation of amyloid polypeptide has been observed in about 95% of patients with type 2 diabetes, mild dietary copper augmentation might help prevent the development of this disorder.

5.7 Material and Methods

5.7.1 X-ray fluorescence microscopy

Rat pituitaries were collected and frozen in cryoprotectant and stored at -80°C until sectioning. 10 μm thick sections were obtained and imaged using X-ray fluorescence microscopy as described previously [296]. In parallel, a section was cut and stained with hematoxylin and

eosin to compare regions of interest.

5.7.2 Inductively coupled plasma mass spectrometry (ICP-MS)

Tubes used for ICP-MS were incubated in 1% HNO_3 (trace metal grade, Fisher Scientific) for at least 24 hours. Samples were digested with 50% HNO_3 (trace metal grade, Fisher Scientific) in Eppendorf tubes at room temperature overnight. The digested samples were brought to a total volume of 1 mL with 1% HNO_3, mixed by vortexing, and centrifuged at 3500 rcf for 3 minutes to remove debris. ICP-MS analysis was carried out as described previously [297]. Homogenization buffer and sucrose solutions were also analyzed to determine background contributions.

5.7.3 Differential centrifugation and subcellular fractionation

Anterior pituitaries from adult male Sprague-Dawley rats or mouse pituitaries were homogenized at 4°C in 10 volumes (w/v) of homogenization buffer: 0.32 M sucrose in 10 mM Tris-HCl, pH 7.4, containing 34 mg/ml phenylmethylsulfonyl fluoride, 16 mg/ml benzamidine, 2 mg/ml leupeptin, and 10 mg/ml lima bean trypsin inhibitor (inhibitor mix) using six strokes of a motor-driven glass Potter-Elvehjem homogenizer with a Teflon pestle. The homogenate was subjected to differential centrifugation at 4°C. The homogenate was first centrifuged for 5 minutes at 800 g yielding a pellet (P1) containing nuclei and cell debris. The supernatant (S1) was centrifuged at 4,000 g for 17 minutes to obtain a pellet (P2) and a supernatant (S2), which was then centrifuged at 10,000 g for 15 minutes generating a pellet (P3), and a supernatant (S3). Lastly, S3 was centrifuged at 350,000 g for 15 minutes and provided another pellet (P4) and a cytosolic fraction (S4). Each pellet was resuspended in

225 μL of homogenization buffer and either kept at -80°C for further analysis or loaded on top of a non-linear sucrose gradient. Sucrose solutions were always made fresh in 10 mM Tris-HCl, pH 7.4, containing inhibitor mix. P2 was resuspended in homogenization buffer and loaded onto a discontinuous sucrose density gradient composed (bottom to top) of: 200 μL 2M sucrose, 350 μL of 1.6M sucrose, 350 μL 1.4M sucrose, 350 μL 1.2M sucrose, 200 μL 1M sucrose, 200 μL 0.8M sucrose, 200 μL 0.4M sucrose, all in homogenization buffer. After centrifugation at 120,000 x g in a TLS-55 rotor for two hours at 4°C, aliquots of 150 μL were collected from top to bottom and kept at -80°C for further analysis.

5.7.4 Negative staining and transmission electron microscopy

Fractions 12 and 13 (100 μL) from the subcellular fractionation were combined and 200 μL of 10 mM HEPES, pH 7.4 containing protease inhibitors. The sample was centrifuged at 10,000 g for 15 minutes at 4°C. The supernatant was discarded and 200 μL of 2.5% glutaraldehyde in 10 mM HEPES, pH 7.4 was added on top of the pellet. The sample was then centrifuged at 10,000 g for 10 minutes at 4°C. The pellet was resuspended in 100 μL of 10 mM HEPES, pH 7.4 and used for negative staining. 4-5 μL of sample were added on top of a copper mesh grid. After waiting for 1 minute for the sample to diffuse across the grid, excess sample was removed using a filter paper. Uranyl acetate solution (4-5 μL of 1% to 3% uranyl acetate dissolved in water) was added on top. After allowing the uranyl acetate to diffuse for 1 minute, excess salt was removed with filter paper. The sample was then imaged using a Hitachi H-7650 Transmission Electron Microscope.

5.7.5 Purification of PAM 820s

A CHO-DG44 cell line stably expressing pCIS-PAM3-ΔPro-ΔGly 820s was grown in serum-free medium in CellMax artificial capillary cartridges (Spectrum laboratories, CA, USA; Cartridge #400-023) [298]. Spent medium was collected (three times per week or daily, depending on density) and stored frozen after addition of PMSF. Secreted proteins were concentrated by addition of solid $(NH_4)_2SO_4$. PAM 820s was purified on a DEAE-Sepharose FF column (20 mm x 150 mm) equilibrated with 20 mM NaTES (pH 7.0) and eluted with a 150 ml gradient to 0.5M NaCl in the same buffer followed by gel filtration on a Superose 6 10/300GL column (25 x 350 mm) equilibrated with 20 mM NaTES, 150 mM NaCl (pH 7.0). The purity and homogeneity of the protein was evaluated by SDS-PAGE (Bio-Rad Criterion TGX gels, 4-15% gradient) followed by staining with Coomassie Brilliant Blue R250.

5.8 Acknowledgments

Support was provided by NIH DK-32949. We thank Darlene D'Amato and Yanping Wang for technical support, Maya Yankova for electron microscopy, and the neuropeptide lab for their comments.

5.9 Figures

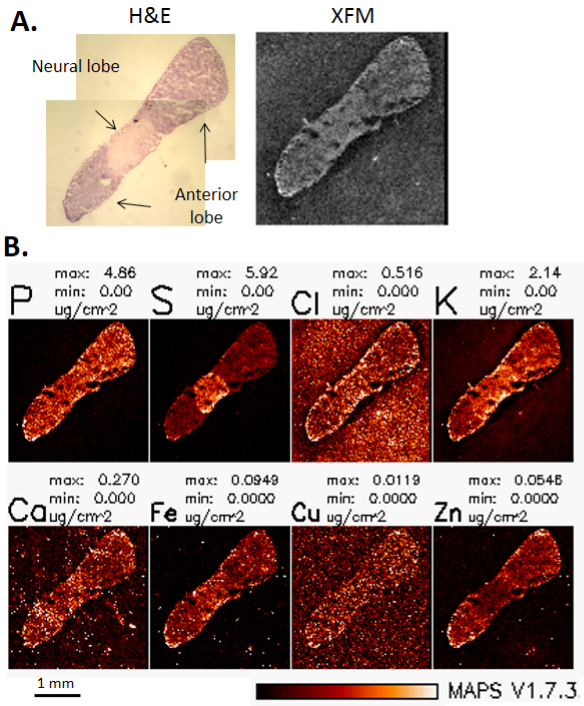

C.

	Concentration (μM)	
Metal	Anterior	Neural
P	80,725	75,211
S	43,810	77,985
Cl	2,627	3,196
K	25,898	32,081
Ca	2,319	3,028
Mn	29	40
Fe	553	731
Cu	45	43
Zn	271	220

Figure 5.1: The pituitary gland contains 40-50 μM copper. (A) Left, Hematoxylin and eosin staining (H&E) showing the anterior and neural lobes of a 10 μm thick of a transverse section. Right, Phase image of another 10 μm thick transverse section observed by X-ray fluorescence microscopy. (B) X-ray fluorescence microscopy scans of a rat pituitary showing the distribution of P, S, Cl, K, Ca, Fe, Cu and Zn. The max and min values for each metal are indicated in μg/cm^2. (C) Two boxes were drawn either in the anterior or neural lobe to determine the concentration of each element measured. The concentration is expressed in micromolar. Samples were 10 μm thick and the density used was 1.025 g/cm^3.

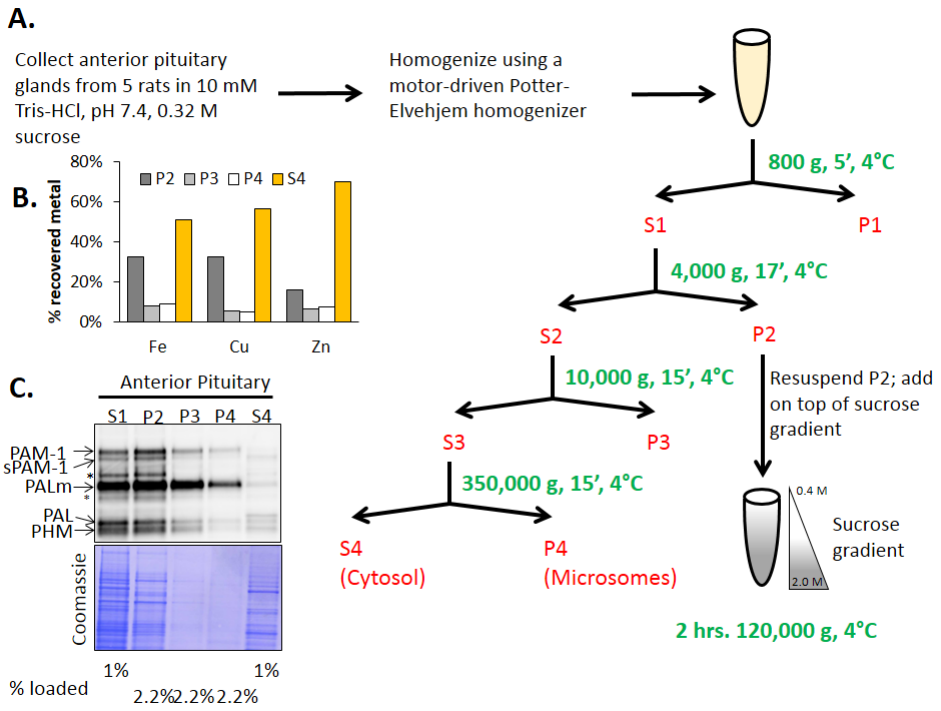

Figure 5.2: Copper is enriched in P2. (A) Differential centrifugation followed by subcellular fractionation protocol. After separation on a sucrose gradient, 150 μL fractions were collected from top (#1) to bottom (#15). (B) Percentage of iron, copper and zinc in P2, P3 and P4 pellets from the differential centrifugation after measurement by atomic absorption. P2 contains all 3 metals. (C) Western blots show the distribution of PAM-1 and its processed products after differential centrifugation. P2 is enriched in PHM, a PAM-1 processed product generated in secretory granules [12].

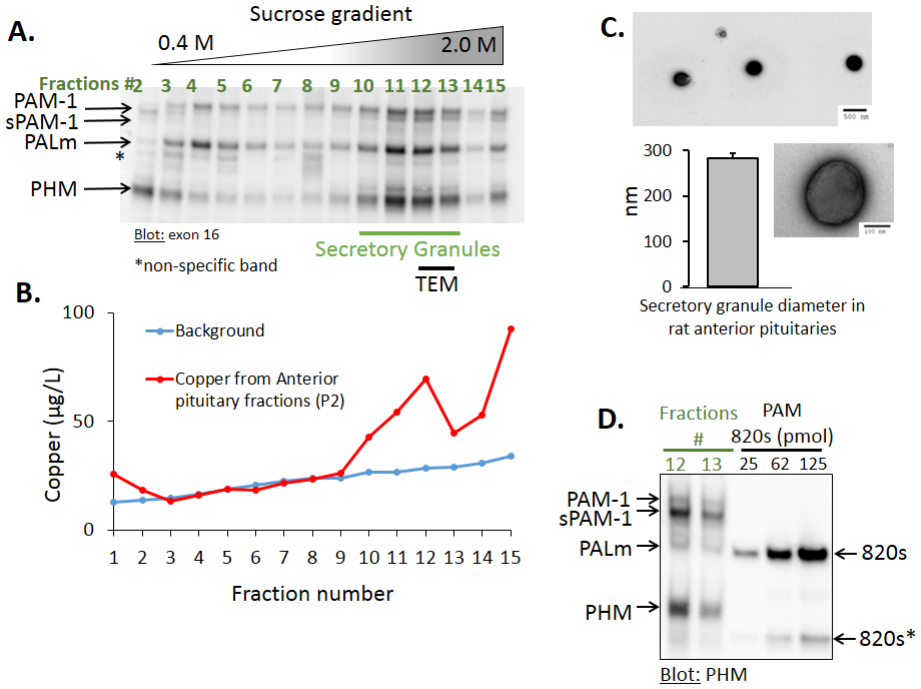

Figure 5.3: Copper is in secretory granules. (A) Western Blot of fractions #2 to #15 collected after separation of P2 on sucrose gradient. Fraction #15 corresponds to the bottom of the gradient. PHM, the marker for secretory granules, accumulates in fractions #10 to #13. Fractions #12 and #13 were collected for analysis by transmission electron microscopy. (B) Copper concentration was measured for the fractions of the sucrose gradient by atomic absorption. A peak of copper was seen in fractions #10 to #13. Sucrose solutions were used to define the background signal shown in blue. This experiment was repeated with mouse pituitaries with a similar result. (C) Two representative images of secretory granules taken at different magnifications are shown. Secretory granules are round and darker than the background. The average diameter of 13 secretory granules measured using negative staining was 283 nm. (D) Western Blot of fractions #12 and #13 along with known amounts of purified PAM 820s, which is truncated at residue 820, is shown. 820s* corresponds to degraded PAM 820s and was included in the quantification.

Chapter 6

The peptide amidating enzyme is developmentally regulated in the cortex and hippocampus

Mathilde L. Bonnemaison, Yan Yan, Richard E. Mains and Betty A. Eipper.

Drafting of the chapter

Mathilde L. Bonnemaison, Richard E. Mains and Betty A. Eipper.

Acquisition of data

Yan Yan and Richard E. Mains prepared the samples; Richard E. Mains and Mathilde L. Bonnemaison designed the primers; Mathilde L. Bonnemaison did the remaining experiments under the supervision and guidance of Richard E. Mains and Betty A. Eipper.

6.1 Abstract

Neuropeptides, which are expressed along with a classical neurotransmitter by most neurons, play an essential role in physiological responses such as satiety and pain perception. For one third of the neuropeptides, the presence of an α-amidated amino acid at the C-terminus is essential for bioactivity. This post-translational modification requires a bifunctional integral membrane enzyme, peptidylglycine α-amidating monooxygenase (PAM). PAM is composed of two catalytic core domains, peptidylglycine α-hydroxylating monooxygenase (PHM) and peptidyl-α-hydroxyglycine α-amidating lyase (PAL), which work in sequence to convert a peptidylglycine substrate into an amidated product plus glyoxylate. Deletion of the gene encoding PAM results in larval lethality in *Drosophila melanogaster* and embryonic lethality in the mouse, demonstrating its importance. The expression of PAM protein was followed during postnatal development (P0, 7, 14, 21, 28 and adult) in the rat hippocampus and cortex. The PAM protein is subject to endoproteolytic cleavage, creating soluble, catalytically active fragments that can be secreted along with their amidated peptide products. Western blot analyses revealed a substantial increase in the expression of PAM-1, a major PAM splice variant, from birth until a peak at P21 in both brain regions. At P0, intact PAM-1 was a major product; soluble 45 kDa PHM accumulated in both tissues as development progressed. The subcellular distribution of PAM-1 was determined by immunofluorescent staining of cultured E18.5 rat hippocampal neurons maintained *in vitro* for 7, 10 or 14 days: PAM was concentrated in perinuclear tubuloreticular structures in the cell soma and in vesicular structures distributed throughout both dendrites and axons. Neuropeptide Y (NPY), one of the most prevalent amidated neuropeptides, is concentrated in secretory granules located in dendrites and axons of hippocampal neurons. Co-staining for PAM-1 indicated that NPY and

PAM-1 partially colocalized in vesicles distributed in processes.

6.2 Introduction

Most neurons produce both small molecule neurotransmitters and neuropeptides to communicate with other cells. Conventional or small molecule neurotransmitters accumulate in small synaptic vesicles at presynaptic terminals whose release is regulated by action potentials that depolarize the membrane at the presynaptic terminal. Released neurotransmitters bind to their receptors on the postsynaptic side to generate an action potential or alter signaling and are either degraded or recaptured in the presynaptic neuron [299]. Neuropeptides act as neurotransmitters, autocrine or paracrine agents, or as hormones acting over long distances [300]. After transiting through the endoplasmic reticulum and the Golgi, newly synthesized neuropeptides are targeted into secretory granules located in the cell soma, dendrites and axons [299, 300]. In contrast with small molecule neurotransmitters, which are secreted at presynaptic terminals, neuropeptide exocytosis was observed from the perikaryon, along the dendrites and axons near synapses [299]. Once secreted, neuropeptides are degraded and not recaptured.

Neuropeptides are synthesized as inactive precursors that must undergo several modification steps in order to become bioactive [187]. Many peptides contain an α-amide moiety at their C-terminus that is required for binding to their receptor [273]. This modification is catalyzed by peptidylglycine α-amidating monooxygenase (PAM), composed of two catalytic core domains, peptidylglycine α-hydroxylating monooxygenase (PHM) and peptidyl-α-hydroxyglycine-α-amidating lyase (PAL), which work in sequence in the amidation reaction [238]. Although only one gene encodes PAM, at least seven splice variants have been identi-

fied in rodents (Figure 6.1) [301]. PAM-1, PAM-2 and PAM-3 are the three major isoforms expressed with PAM-3, the only major isoform that is not a membrane protein. PAM-1 and PAM-4 are the only isoforms containing exon 16, which can be endoproteolytically cleaved in secretory granules. PAM-4 does not encode PAL and PAM-5 encodes a truncated version of PHM that is inactive. Because peptide amidation is a two-step reaction catalyzed by PHM and then PAL, PAM-4 cannot catalyze the full reaction rendering its function unclear. After transiting though the endoplasmic reticulum and the Golgi en route to the regulated secretory pathway, PAM exits the Golgi in secretory granules with neuropeptides [12]. The environment of secretory granules is ideal for PAM activity. Upon exocytosis, soluble PAM isoforms are secreted along with the neuropeptides, while the membrane isoforms of PAM that reach the plasma membrane are subsequently internalized into the endocytic pathway [12]. Studies done on pituitary cells indicated that membrane PAM isoforms found in the endocytic compartments can be degraded in lysosomes or recycled to the Golgi for re-entry into secretory granules [195, 189].

High levels of PAM mRNA were identified in the heart atrium, anterior and neurointermediate lobes of the pituitary gland, sublingual and submandibular salivary glands and specific regions of the central nervous system in rodents [302, 303, 304]. PAM is an enzyme essential for development in mice and flies [260, 275]. A previous study indicated that PAM mRNA levels and PAM activity in rat heart atrium and ventricle are developmentally regulated [305]. Since PAM is highly expressed in the central nervous system, we investigated PAM mRNA and protein levels in the rat cortex and hippocampus during postnatal development. In addition, cultures of E18.5 rat hippocampal neurons were maintained for 7 to 14 days *in vitro* to allow determination of the distribution of PAM.

6.3 Results

6.3.1 PAM-1 mRNA is the major isoform expressed in cortex and hippocampus during development

PAM mRNA expression in adult rat brain was detected in every brain region except the cerebellum. The hippocampus, the supraoptic nucleus and the anterior olfactory nucleus were the brain regions where PAM mRNA was the most prevalent [304]. Investigation of which PAM mRNA isoforms are predominantly expressed during cortical and hippocampal development was done using PCR. A set of primers were first designed to distinguish between membrane and soluble PAM isoforms (membrane primers) (Figure 6.2A). Using the membrane primers, the membrane isoforms of PAM were prevalent at P2, P16 and P30 in both tissues suggesting that PAM-1, PAM-2 or PAM-3b were the most expressed isoforms (Figures 6.1 and 6.2B). One difference between the three membrane isoforms of PAM is the presence of exon 16 in PAM-1 only. To find out if PAM-1 is the major isoform expressed in cortex and hippocampus of rats during postnatal development, a second set of primers was generated to differentiate PAM-1 from PAM isoforms lacking exon 16 (Figure 6.2A). In the cortex and hippocampus, PAM-1 mRNA levels increased during development while mRNA from PAM isoforms lacking exon 16 did not (Figure 6.2C). In the cortex at P2, PAM-1 mRNA levels were similar to PAM isoforms lacking exon 16 suggesting the presence of PAM-2 while PAM-1 mRNA is already the main isoform in the hippocampus. PAM-1 mRNA at P16 in the cortex migrated faster compared with the other samples. This sample was analyzed a second time using less material and no difference with the other samples was seen, suggesting that this difference was due to the high amount of material and not a change in mRNA processing

of PAM (data not shown).

6.3.2 PAM-1 is developmentally regulated in rat cortex and hippocampus

The protein levels of PAM-1 during development in the hippocampus and the cortex were investigated. Cortices and hippocampi from rats were collected at P0, P7, P14, P21, P28 and during adulthood, and Western blots using an antibody targeting the exon 16 region of PAM-1 was performed (Figure 6.3A). Based on PCR data, we expected PAM-1 protein levels to increase during development in the cortex while it would be constant in the hippocampus. In the cortex, intact PAM-1 protein levels increase after the first week of birth until P21, where PAM-1 levels were about 7 times higher than at birth. Intact PAM-1 protein levels then reach the PAM-1 levels seen in adults, corresponding to about 3 times the amount observed at birth. Interestingly, intact PAM-1 levels only slightly increase during development in the hippocampus and were about 60% lower in adults than at birth. Based on studies in AtT-20 cells, when PAM-1 reaches secretory granules, it is endoproteolytically cleaved between the two catalytic core domains producing membrane associated PAL (PALm) and soluble PHM [12]. PHM and PALm expression profiles were similar in both tissues. In the cortex, PALm and PHM expression levels resemble PAM-1 profile during development, while hippocampal PHM and PALm levels were very low at birth, augmented very strongly until P21-P28 and declining toward adult levels. Although PHM levels in the cortex were about 20 times higher at P21 than at birth, hippocampal PHM levels were more than 70 times higher at P21 than at birth.

The expression profile of PAM-1 was compared with another marker of secretory granules, prohormone convertase 2 (PC2) (Figure 6.3B). PC2 is first synthesized as an inactive precursor

that undergoes an endoproteolytic cleavage in secretory granules to generate the mature active form [199]. In both tissues, PC2 precursor levels increased until P7 and then remained stable throughout development. The expression profile of the mature form of PC2 matched that of PHM and PALm in both tissues.

6.3.3 PAM-1 is localized in soma and processes of hippocampal neurons

In order to find out where PAM is localized in neurons, E18.5 rat hippocampal neurons were maintained *in vitro* for 7, 8, 10 or 14 days (Figure 6.4). Immunofluorescent staining of PAM-1 was performed using an antibody recognizing exon 16. Co-staining with βIII tubulin, a marker that identifies the cell soma and all processes of neurons, showed that PAM-1 was in the cell soma, where it concentrated in a perinuclear region and in puncta observed in processes (Figure 6.4A). A strong colocalization between PAM-1 and γ-adaptin, a Golgi region marker, was observed at the perinuclear region where PAM-1 accumulates, indicating that PAM-1 concentrates at the Golgi of the perikaryon (Figure 6.4B). Transferrin and transferrin receptor were reported to be excluded from the axon in hippocampal neurons [185]. DIV8 hippocampal neurons were thus incubated with Alexa fluor 546 transferrin for 10 minutes, fixed and stained for PAM-1. Alexa fluor 546 transferrin puncta were easily identified in processes and near the nucleus in the cell soma. One process lacking internalized transferrin but containing PAM-1 suggested that PAM-1 goes to the dendrites and axons of hippocampal neurons (Figure 6.4C). Co-labeling of neurons for PAM-1 and ankyrin G, a marker of the axon initial segment, in DIV10 hippocampal neurons, indicated the presence of PAM-1 in axons (Figure 6.4D). Lastly, PAM-1 staining of DIV14 hippocampal neurons with MAP2 (Microtubule Associated Protein 2), a dendritic marker, revealed the presence of one

process per cell that contained PAM-1 but was devoid of MAP2 (Figure 6.4E). Altogether, these data indicated that PAM-1 concentrates in the Golgi region of the cell soma, in dendrites and axons of hippocampal neurons at different days *in vitro*.

6.3.4 PAM-1 and neuropeptide Y colocalize in hippocampal neurons

Neuropeptide Y is an amidated peptide expressed in a subset of hippocampal neurons. Studies on mice and human hippocampi indicated that neuropeptide Y acts as an essential anti-epileptic agent [306, 307, 308]. Before PAM catalyzes the final modification of neuropeptide Y, this peptide undergoes an endoproteolytic cleavage, catalyzed by prohormone convertase 2, followed by trimming of basic residues at the C-terminus by carboxypeptidase E (Figure 6.5A). Prohormone convertase 2, carboxypeptidase E and PAM-1 are more active at acidic pH found in secretory granules. Although peptide amidation was observed at the *trans*-Golgi network (TGN), this modification occurs mainly in secretory granules suggesting that neuropeptide Y and PAM must leave the (TGN) to go to secretory granules together. In order to compare neuropeptide Y distribution with that of PAM-1, hippocampal neurons maintained *in vitro* for 10 days were stained with an antibody that recognizes all forms of neuropeptide Y and an antibody that targets the exon 16 region of PAM-1. Both markers strongly colocalized at the perinuclear region and in vesicles located in processes (Figure 6.5B). PAM-1 is a membrane protein known to span the membrane of secretory granules and endosomes. PAM-1 positive vesicles lacking neuropeptide Y are likely to represent endosomes. Interestingly, the ratio of neuroepeptide Y over PAM-1 in vesicles was not the same within the same neuron suggesting that secretory granules are not all identical as previously observed in a corticotrope and a somatotrope tumor cell lines [187].

6.4 Discussion

Small molecule neurotransmitters from the synaptic cleft can be re-captured at the presynaptic terminal and re-used. This is in contrast with neuropeptides which are degraded or diffuse away once secreted in the extracellular compartment. After secretion of peptides, neurons have to synthesize neuropeptides and processing enzymes to replenish their pool of secretory granules. Because neurons can extend over long distances and the perikaryon is the only place to generate secretory granules, it is not entirely clear how the cell soma senses the status of the secretory granule pool in processes. PAM amidates many neuropeptides, rendering them bioactive, and is essential during development [260, 275]. The membrane isoform, PAM-1, is subject to regulated intramembrane proteolysis generating a soluble fragment of the cytosolic domain capable of entering nuclei and altering gene expression in neuroendocrine cells and neurons [223].

This study provides an overview of the PAM expression profile in the cortex and hippocampus. The cortex is involved in perception and movement while the hippocampus controls learning and memory. Although seven PAM isoforms were detected in rodents, PAM-1 was the major PAM isoform expressed in the developing cortex and hippocampus. In the cortex, glia develop the most after birth while the number of neurons is mostly defined before birth. This is in contrast with the hippocampus, where the dentate gyrus can generate new neurons postnatally [309]. Although the PAM-1 protein and PC2 detected could come from neurons and glia, the level of these secretory granule markers increased during postnatal development until P21 and then reached adult levels. Even though peptides can be secreted from the cell soma, along the processes and at synapse, P21 marks the peak of synaptogenesis in rodents. This suggested that secretory granules and synapses form at a similar moment in

the cortex and hippocampus. Interestingly, the expression pattern of proopiomelanocortin and the formation of its cleavage products (β-endorphin and adrenocorticotropin) in the pituitary gland resembles that of PAM-1 [310].

The adaptor protein 1 complex (AP-1) is a heterotetrameric complex involved in the transport of cargo between the *trans*-Golgi network and endosomes and mediates the biogenesis and maturation of secretory granules. A previous study in hippocampal neurons indicated that AP-1 interacts with transferrin receptor to prevent its entry into the axon [185]. Mutation of the AP-1 binding site on the cytosolic domain of the transferrin receptor resulted in equal distribution of the membrane protein between axons and dendrites [185]. Interestingly, the cytosolic domain of PAM was shown to interact with AP-1 in neuroendocrine cells and in a yeast two-hybrid screen [234]. Cultured hippocampal neurons indicated that PAM-1 concentrated at the Golgi region and was distributed in both axons and dendrites. This suggested that AP-1 function in PAM trafficking is different from AP-1 function in transferrin receptor trafficking. Since AP-1 is required for retrograde trafficking, it would be interesting to find out whether AP-1 is required for PAM-1 retrograde trafficking into the Golgi in neurons [220, 178].

Regulated secretion prevails in neurons and diseases like autism are associated with diminished neuronal connectivity [311]. During development, neurons secrete peptides to promote neuron survival, growth, differentiation and synapse formation. Impairment in providing the right peptide during a specific time window and at a defined location can thus alter brain development severely. Understanding PAM trafficking in neurons will thus provide insight in the roles of peptide synthesis in brain development.

6.5 Material and methods

6.5.1 Polymerase Chain Reaction (PCR)

For time course studies, cortices and hippocampi were collected in TRIzol and homogenized using a Polytron. Each sample received 0.2 ml of chloroform per ml of TRIzol, and was shaken by hand for 15 seconds. After sitting for 2-3 minutes, samples were spun at 10,000 g for 15 minutes at 4°C. The aqueous phase was collected, received 0.65 ml of isopropyl alcohol per ml of TRIzol reagent used and kept at -20°C overnight. After centrifuging at 10,000 g for 10 minutes at 4°C, the supernatant was discarded and the RNA pellet was washed using 75% ethanol twice. 20 μL of DEPC treated water was added to the dried pellet. The cDNA samples were prepared from 1 μg RNA using Superscript II (Invitrogen) and iScript (BioRad) with random primers. Samples were kept at 65°C for 5 minutes before chilling and adding the iScript reverse transcriptase. Samples were then incubated at room temperature for 5 minutes followed by an incubation at 42°C for 45 minutes and 65°C incubation for 5 minutes. Samples were kept at -80°C until analysis. PCR was performed using a BioRad MJ Mini Personal Thermal Cycler (#PTC-1148) and Sybr-Green (BioRad), with the following parameters: 95°C 3 min; 95°C 30 sec, 58°C 1 min, 72°C 1 min; repeat 40x. The last parameter was hold at 72°C for 5 minutes. The primers used are shown in Table 6.1.

6.5.2 Western Blot Analysis

For time course studies, cortices and hippocampi collected from rats of different ages were sonicated into the SDS lysis buffer used for half-life studies, heated for 5 min at 95 °C, and centrifuged to remove insoluble debris as described [312]. 20 μg of total protein was loaded

onto each lane for analysis of PAM and PC2.

6.5.3 Cell culture

Cultures of rat hippocampal neurons were described previously [312]. Briefly, hippocampi from embryonic day 18 Sprague-Dawley rats were collected and digested using 0.28% trypsin for 15 min at 37°C with gentle shaking. Cells were dissociated with a fire-polished glass pipette and plated at about 2-4 x 10^4 cells/mL onto 12 mm coverslips coated with poly-L-lysine (1 mg/mL). At plating, cells were incubated in Dulbecco's Modified Eagle Medium/F-12 (DMEM/F-12) containing 10% fetal calf serum, 5% heat-inactivated horse serum, 0.5 mM glutamine, 50 U/mL of penicillin, and 50 μg/mL of streptomycin and maintained at 37°C in a 5% CO_2 atmosphere (all reagents were from Life Technologies). Twenty-four hours later, plating medium was replaced with Neurobasal medium containing 3% horse serum, 0.5 mM glutamine, 50 U/mL of penicillin, and 50 μg/mL of streptomycin. Thereafter, 50% of the culture medium was exchanged with Neurobasal medium containing 2% B27 supplement, 0.5 mM glutamine, 50 U/mL of penicillin, and 50 μg/mL of streptomycin twice a week. For transferrin uptake, neurons were directly incubated in neurobasal medium containing 25 μg/mL of Alexa fluor 546 transferrin for 10 minutes and then fixed using 4% formaldehyde in PBS for 20 minutes at room temperature.

6.5.4 Immunofluorescent staining

Hippocampal neurons were fixed at DIV7, DIV8, DIV10 and DIV14 using 4% formaldehyde in phosphate buffer saline (PBS, 50 mM NaH_2PO_4, 150 mM NaCl, pH 7.4). After rinsing in PBS once, cells were permeabilized in 0.2% Triton X-100, 2 mg/ml BSA in PBS for 20

minutes at room temperature and then incubated in block (2 mg/ml BSA in PBS) for an hour at room temperature. Primary antibodies diluted in block buffer were incubated with the cells overnight at 4°C. After three rinses in PBS, cells were incubated for one hour at room temperature in block containing either fluorescein isothiocyanate (FITC, 1:500 dilution) or Cy3 (1:2000 dilution) conjugated donkey antibody to mouse or rabbit immunoglobulin (Jackson ImmunoResearch). After three rinses in PBS, cells were incubated with Hoechst (1:1000 dilution in PBS) for 10 minutes at room temperature. After three rinses in PBS, cells were mounted using ProLong® Gold (Invitrogen). Neurons were visualized using either a Nikon TE300 epifluorescence microscope or a Zeiss LSM 510-Meta with an oil immersion 63X Plan Apochromat objective (NA 1.4).

6.6 Tables

Name	Sequence	Tm (°C)
Membrane For	CACCGTGTGGAAGTTCACCCTGAC	62
Membrane Rev	GAAATTTCCCAGATTTAAGCCGCCGC	61
Exon 16 For	GCACGGGCATCACAAAGAAGCAGAAAAC	62.5
Exon 16 Rev	CAGGCCAGTCCAGTTCTTCTTCCA	61.5

Table 6.1: List of primers used for PCR.

Antigen	Working dilution	Identity, source
Exon-16, PAM-1(409-497)	1:500	JH629 [224]
βIII tubulin	1:1000	Covance (Tuj1)
γ-adaptin	1:1000	BD Biosciences
Ankyrin G	1:500	NeuroMAb (Clone N106/36)
MAP2	1:500	Sigma (Clone AP-20)
PC2 (626-638)	1:500	JH1159 [199]
Neuropeptide Y	1:500	Abnova (Clone 2C10)

Table 6.2: List of antibodies used.

6.7 Figures

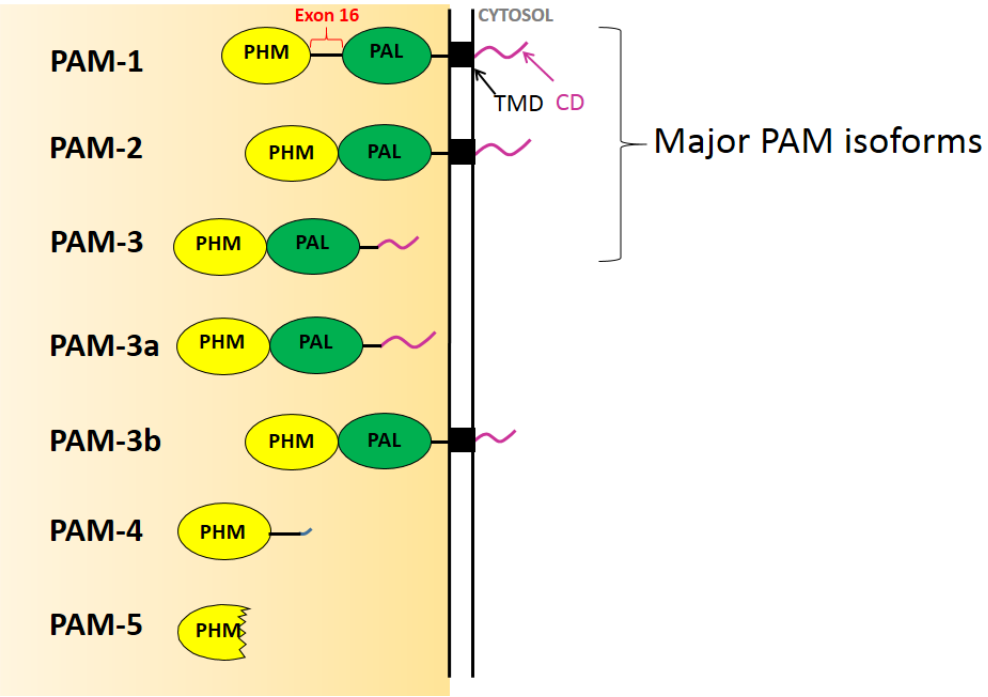

Figure 6.1: PAM isoforms produced by alternative splicing. In all tissues studied so far, PAM-1, PAM-2 and PAM-3b are the membrane isoforms while PAM-3, PAM-3a, PAM-4 and PAM-5 are the soluble isoforms. PAM-1, PAM-2 and PAM-3 are the three major PAM isoforms. PAM-1 is the only major isoform containing exon 16 while PAM-3 is the only major isoform lacking a transmembrane domain. TMD, transmembrane domain; CD, cytosolic domain.

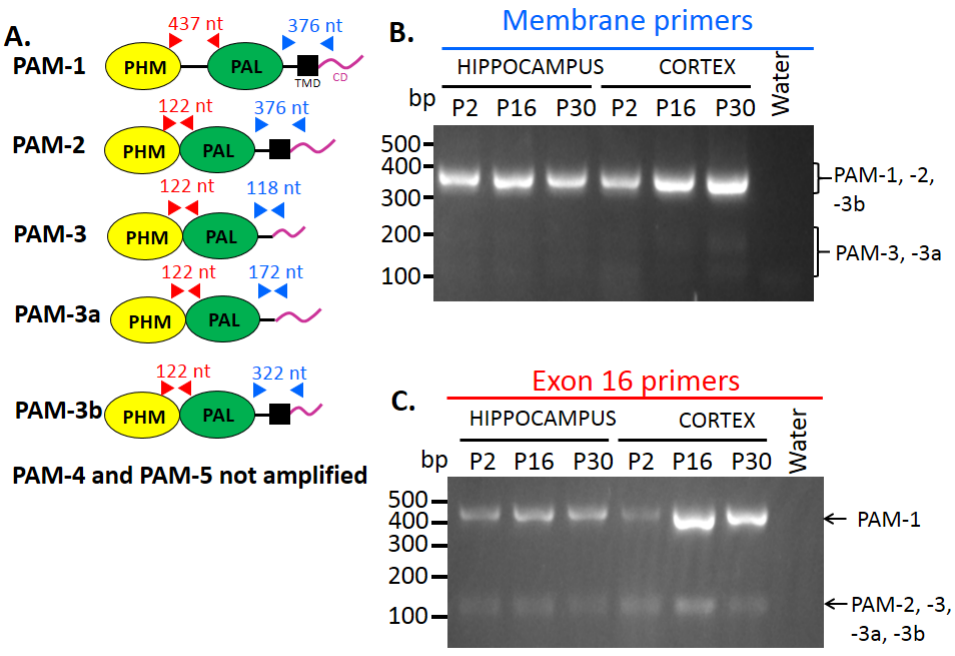

Figure 6.2: PAM-1 mRNA predominates during development of cortex and hippocampus. (A) Two sets of primers were used: membrane primers (blue) and exon 16 primers (red). The membrane primers were designed to amplify exons 24-27 encoding the transmembrane domain. Expected band size after amplification for each primer pair is noted on top of each PAM isoform. (B) PCR results after using the membrane primers (blue). Membrane forms of PAM (PAM-1, PAM-2 and PAM-3b) predominate throughout development in both cortex and hippocampus. (C) PCR results after using exon 16 primers (red). Similar amounts of PAM mRNA with and without exon 16 are detected at P2 in cortex suggesting presence of PAM-2. At P30, PAM-1 mRNA is the predominant isoform in both the cortex and the hippocampus. TMD, transmembrane domain; CD, cytosolic domain.

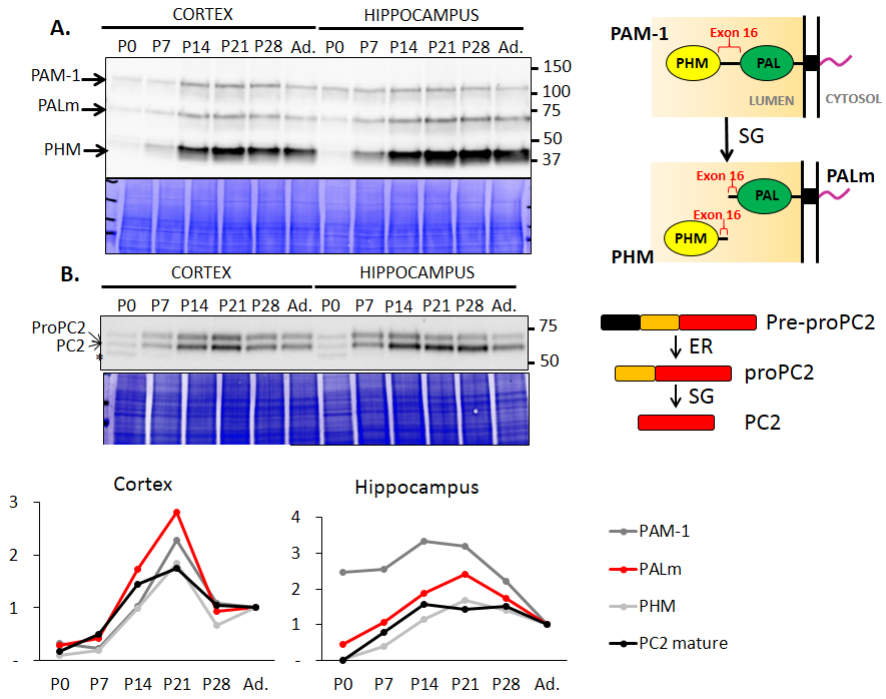

Figure 6.3: PAM and PC2 are developmentally regulated. Western blot using an antibody specific for Exon 16 identifies intact PAM-1 at all ages (A) and an antibody specific for PC2 (B). On the right of each blot is shown the endoproteolytic cleavage of PAM-1 and PC2. The cleavage generating PHM occurs primarily in secretory granules (SG). PC2 is first synthesized as pre-proPC2. The signal sequence (shown in black) is cleaved in the endoplasmic reticulum (ER) while the pro-sequence (shown in yellow) is cleaved in secretory granule (SG) to generate the mature form of PC2 (shown in red). In both cortex and hippocampus, the most dramatic change during development is an increase in the amount of soluble PHM and the mature form of PC2, markers of secretory granule. In B, Coomassie staining reveals equal amounts of protein per lane. Graphs show the levels of PAM-1, PALm, PHM and PC2 in the cortex and hippocampus normalized to the levels in adulthood.

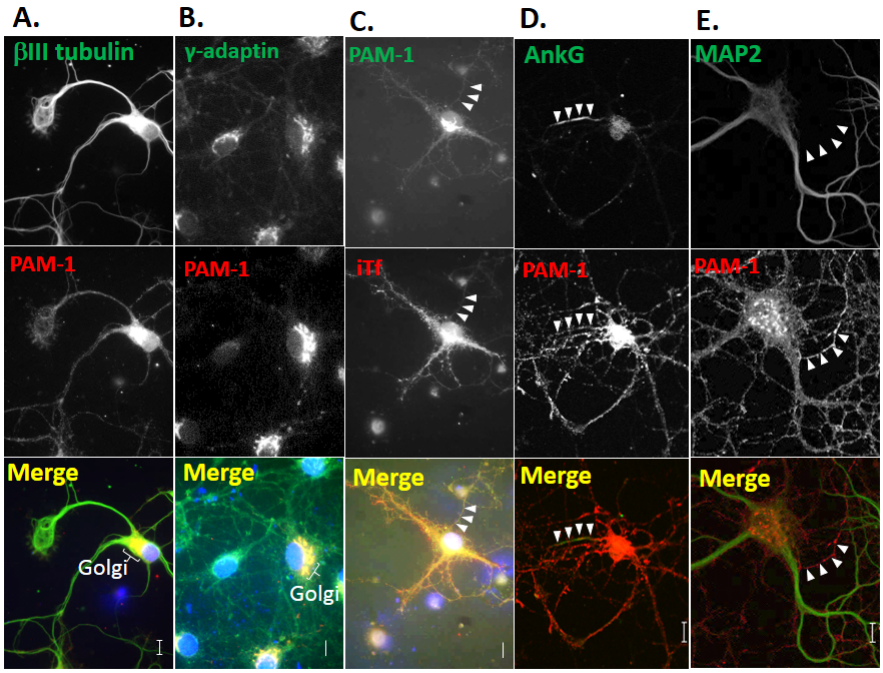

Figure 6.4: PAM-1 is located in the cell soma, dendrites and axons of hippocampal neurons. Immunofluorescent staining of cultured E18.5 rat hippocampal neurons maintained *in vitro* for 7 days (A), 8 days (B), 10 days (C and D),14 days (E) revealed PAM-1 in the cell soma, dendrites and axon. Immunostaining for PAM-1 used an antibody specific for exon 16 (Cy3 anti-rabbit in A, C and D and FITC anti-rabbit in B). (A) PAM-1 accumulates in the perinuclear region of the cell soma corresponding to the region occupied by the Golgi complex and is evenly distributed in processes. βIII tubulin (FITC anti-mouse) reveals the cell soma and all processes. (B) Alexa fluor 546 transferrin was incubated with DIV8 hippocampal neurons for 10 minutes. Transferrin is not taken up by the axon [185]. (C) PAM (Cy3 anti-rabbit) and an antibody that recognizes γ-adaptin, a subunit of AP-1. Both markers strongly colocalized in the perinuclear region which corresponds to the Golgi region. (D) Ankyrin G (FITC anti-mouse) shows the axon initial segment [312]. (E) MAP2 stains the dendrites and cell soma. White arrowheads delineate the axon, where PAM is present. In (A), (B) and (C), the nuclei were stained with Hoechst. Scale bar, 10 μm.

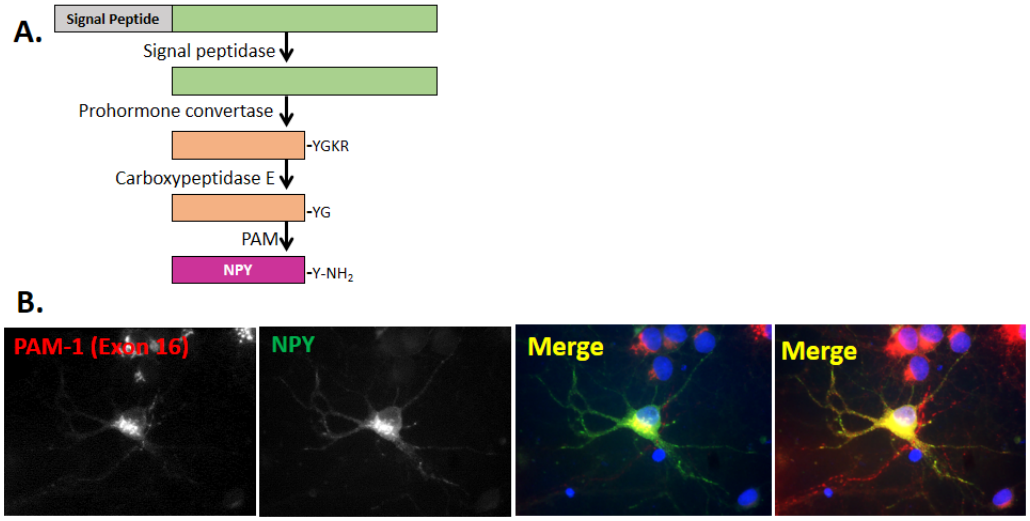

Figure 6.5: Neuropeptide Y and PAM share a similar distribution. (A) Neuropeptide Y processing is characterized by four modifications. The last step is catalyzed by PAM, generating the bioactive peptide. (B) Immunostaining of DIV10 hippocampal neurons used an antibody that recognizes exon 16 of PAM (Cy3 anti-rabbit) and an antibody that recognizes all forms of neuropeptide Y (NPY, FITC anti-mouse). Strong colocalization in the cell soma and processes was observed. On the right, the same image is shown but the signal was greatly enhanced to observe the processes. Surrounding neurons express PAM at a different level but they do not express NPY. Nuclei were stained with Hoechst in blue. Scale bar, 10 μm.

Chapter 7

Conclusions and future directions

Mathilde L. Bonnemaison.

Acquisition of data

Yan Yan and Richard E. Mains prepared the neurons; Mathilde L. Bonnemaison did the remaining experiments under the supervision and guidance of Ann E. Cowan, Richard E. Mains and Betty A. Eipper.

7.1 Introduction

The adaptor protein 1 complex (AP-1), a cytosolic complex composed of two large subunits (γ and β1), a medium subunit (μ1) and a small subunit (σ1), plays a central role in both the regulated secretory pathway and endocytic pathway. Reduced AP-1 function in AtT-20 cells had profound effects on the architecture of the *trans*-Golgi network (Chapter 2), the formation of secretory granules (Chapter 2), the regulated secretion of peptides (Chapter 2), the maturation of endosomes (Chapter 3), the trafficking of vital proteins and cholesterol

(Chapters 2-4) and copper homeostasis (Chapter 4).

AP-1 is part of a family of adaptor protein complexes where each member has a similar structural organization. Lack of any one AP subunit is sufficient to alter the stability and the function of the remaining complex. Although yeast that lack expression of AP-1 subunits do not show any phenotype, mice lacking the expression of γ or μ1A die during the prenidation period and at embryonic day E13.5, respectively, indicating that AP-1 is essential for development of multicellular organisms [92, 178, 183]. In humans, MEDNIK (Mental retardation, Enteropathy, Deafness, peripheral Neuropathy, Ichthyosis, Keratodermia) syndrome and a type of X-linked mental retardation have been associated with mutations in σ1A and σ1B respectively, [254, 217, 218]. Both subunits are ubiquitously expressed isoforms of the small subunit of AP-1 [92]. Both pathologies identified as mutations of an AP-1 subunit are associated with mental retardation. Patients with X-linked mental retardation also have hypotonia early in life, delay in walking and basal ganglia calcification, underlining that AP-1 containing σ1B is important for motor neuron function [313, 218]. MEDNIK patients have hypotonia, growth and psychomotor delay, alternating diarrhea and constipation episodes, and red patches on the skin [219].

7.2 Which AP-1 subunit is expressed in the brain?

Several subunit isoforms of AP-1 have been observed: AP-1 has two γ subunits (γ1, γ2), two medium subunits (μ1A, μ1B) and three small subunits (σ1A, σ1B, σ1C). Although most AP subunit isoforms are ubiquitously expressed, μ1B is expressed only in polarized epithelial cells [92]. It is currently not known which AP-1 subunit isoforms form the AP-1 complex in the various brain regions and, more specifically, in neurons and glia. Establishing a map

of the AP-1 subunits expressed per brain region or cell type would be very informative and helpful to decipher symptoms of MEDNIK and X-linked mental retardation. An overview of AP-1 subunits mRNA was determined via *in situ* hybridization and is available on the Allen Brain Atlas (http://mouse.brain-map.org). Focusing on the mRNA distribution of the three small subunit isoforms (σ1A, gene ID: 11769; σ1B, gene ID: 108012; σ1C, gene ID: 252903) in the cortex and hippocampus, no striking difference was observed. The subunit composition of AP-1 complex in the brain can be investigated by Western blot and immunofluorescence in brain slices or cultured neurons.

7.3 How does AP-1 regulate the release of neurotransmitters and neuropeptides in neurons?

Since the regulated secretory pathway is necessary for the brain to function properly, studying the role of AP-1 in regulated secretion in neurons will help understand the phenotypes observed in patients with MEDNIK and X-linked mental retardation. Since AP-1 is required for secretory granule biogenesis in neuroendocrine cells (Chapter 2), and in the formation of other types of secretory granules, such as glue granules in *Drosophila*, rhoptries in *Toxoplasma gondii*, and Weibel Palade bodies in endothelial cells, we hypothesized that AP-1 is necessary for generating secretory granules in neurons. In addition, AP-1 interacts with synaptophysin, a synaptic vesicle protein important for neurotransmitter release, suggesting that AP-1 function may also be required in synaptic vesicle biogenesis and function [314]. One approach would be to use mouse embryonic fibroblasts from μ1A deficient mice, reprogram the cells into neurons and investigate AP-1 function in secretory granule biogenesis and neurotransmitter

release.

7.4 Is PAM-1 trafficking altered in neurons from MEDNIK and X-linked mental retardation?

Neuroendocrine cells and neurons produce large amounts of peptides many of which require the presence of an α-amide group at the C-terminus to be functional. This modification is catalyzed by peptidylglycine α-amidating monooxygenase (PAM), a bifunctional enzyme composed of peptidylglycine α-hydroxylating monooxygenase (PHM) and peptidyl-α-hydroxyglycine-α-amidating lyase (PAL) catalytic core domains working sequentially. Although PAM-1 is the main isoform expressed in developing hippocampus and cortex, very little is known about PAM-1 trafficking in neurons (Chapter 6). In hippocampal neurons, PAM-1 is concentrated at the Golgi and scattered in vesicles of dendrites and axons (Chapter 6). Investigating PAM-1 distribution in hippocampal neurons after reduction of AP-1 function would provide information on the efficiency of PAM activity and insights into understanding MEDNIK and X-linked mental retardation. In addition, transfection of a plasmid encoding PAM-1 or PAM-2 linked to GFP into hippocampal neurons was performed, suggesting that investigating PAM trafficking in live neurons is also possible (Figure 7.1). Since endogenous PAM is PAM-1 (containing Exon 16), this creates the opportunity to examine whether endogenous PAM-1 (stained with JH629) is trafficked differentially from PAM-2-GFP. Previous work focused only on soluble PHM-GFP transfected into sensory neurons and indicated what the dynamics of secretory granules containing PHM-GFP were under basal and stimulated conditions [300].

7.5 What are the dynamics of PAM-1 trafficking in neuroendocrine cells?

Although biochemical studies of PAM-1 trafficking have provided extensive amounts of information on this protein in neuroendocrine cells, the dynamics of PAM-1 movement in live cells is lacking (Figure 7.2). According to previous studies done in AtT-20 cells, about 5% of PAM-1 is in the endoplasmic reticulum and Golgi, 30% at the TGN, 5% in immature secretory granules, about a third in mature secretory granules, less than 5% at the cell surface and 25% in endosomes. Exit of PAM-1 from the TGN into secretory granules was evidenced by the formation of PHM after PAM-1 endoproteolytic cleavage. Because holding the temperature at 20°C blocks the exit of proteins from the TGN, it was possible to control the trafficking of newly synthesized PAM-1 at this stage. Calculating PHM formation after release of temperature blockade, Milgram and Mains were able to estimate that about 15%/hour PAM-1 exited the TGN to go into immature secretory granules [12]. The constitutive-like secretory pathway is well developed in cancer cell lines, such as AtT-20 cells. The secreted material from this type of secretory pathway consists of proteins that were removed from immature secretory granules. It was proposed that material that is retrieved from immature secretory granules is transported to endosomes before being released constitutively as shown in figure 7.2. Measuring the rate of secretion of newly synthesized PHM under basal condition was synonym of measuring constitutive-like secretion rate of PAM-1. About 2/3 of PAM-1 that exited the TGN for immature secretory granules, exited immature secretory granules for constitutive like secretion. Work done by De et al. and Bäck et al. demonstrated that a lot of PAM-1 cycled between plasma membrane and endosomes and only 2-3% of PAM-1

was present on the cell surface at steady state [195, 266]. We generated a plasmid encoding PAM-1 linked to photoactivatable GFP (PAGFP) at its C-terminus 3.1A). PAGFP contains a few crucial point mutations when compared with wild-type GFP, making it behave like a GFP only after UV excitation. Thus, only the PAGFP which has been irradiated at the proper wavelength will be seen under a fluorescence microscope 3.1B). Photoactivation at a perinuclear region corresponding to the Golgi revealed that PAM vesicular transport across the cell is mediated by microtubules (Figure 7.3C). This technique would also enable visualization of PAM trafficking from the tips, where mature secretory granules accumulate. A complete study on PAM-1 trafficking in AtT-20 cells can then be compared with the information obtained using biochemical studies (Figure 7.3C).

7.6 What is the distribution of copper in pituitary cells?

Even though very few proteins require copper for activity, copper is an essential metal. Copper in the brain and liver has been investigated in detail, but data remain limited on how copper is handled in other tissues. PAM-1 requires copper to amidate neuropeptides and the pituitary gland expresses high levels of PAM, suggesting that copper must be handled appropriately in order to synthesize bioactive peptides. X-ray fluorescence microscopy (XFM) allowed the visualization of copper content in the pituitary gland (Chapter 5). In addition, determination of cellular distribution and concentration of metals is now possible [315]. Using XFM, it is possible to identify copper distribution in pituitary cells, to see whether a difference is observed between pituitary cell types and to compare with other cell types. A clear identification of copper distribution is needed to understand copper associated diseases.

AP-1 is at the heart of post-Golgi trafficking. This work provided a view of AP-1 function

in neuroendocrine cells and how its function impacted directly or indirectly the trafficking of many proteins, as seen for PAM, POMC, carboxypeptidase D, Atp7a and transferrin. During HIV infection, AP-1 is sequestered from its biological function to interact with the viral protein Nef. Together, they promote the down-regulation of the Major Histocompatibility Complex (MHC) class I [316]. Insight into AP-1 trafficking in different cell types would help prevent the re-routing of MHC class I and possibly increase resistance to viral infection.

7.7 Figures

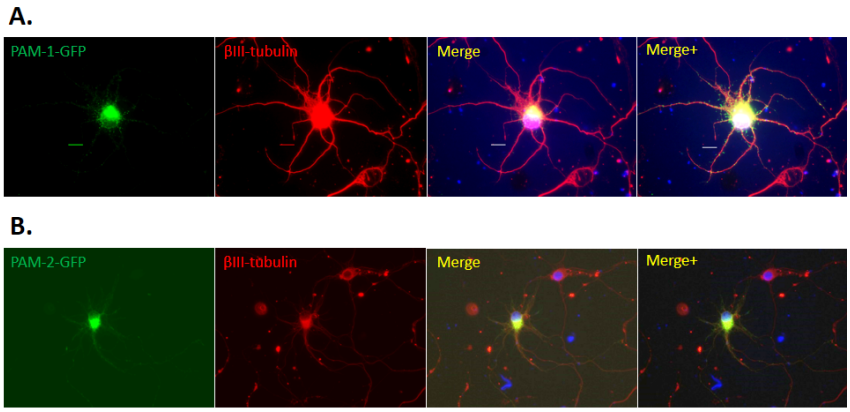

Figure 7.1: PAM-1 and PAM-2 GFP expression in hippocampal neurons. Hippocampal neurons were maintained for 7 days *in vitro* before being transfected with pCI-neo PAM-1 GFP (A) or pEGFP Kr PAM-2 (B) using lipofectamine (0.5 μg DNA/well of a 4 well dish; see Chapters 2 or 3 for methods about lipofectamine). A day after transfection, neurons were fixed and immunostained for βIII-tubulin (Tuj1, Covance, 1:1000 dilution, Cy3 anti-mouse) to visualize processes. To enhance PAM signal, neurons transfected with PAM-1 GFP were immunostained with Exon 16 antibody (JH629, 1:1000 dilution, FITC anti-rabbit) and neurons transfected with PAM-2 GFP were co-stained with a PHM antibody (JH1761, 1:1000, dilution, FITC anti-rabbit) [224, 225]. Merge+ images show the same neuron for which FITC/GFP signal was greatly enhanced in order to visualize processes. Scale bar, 10 μm.

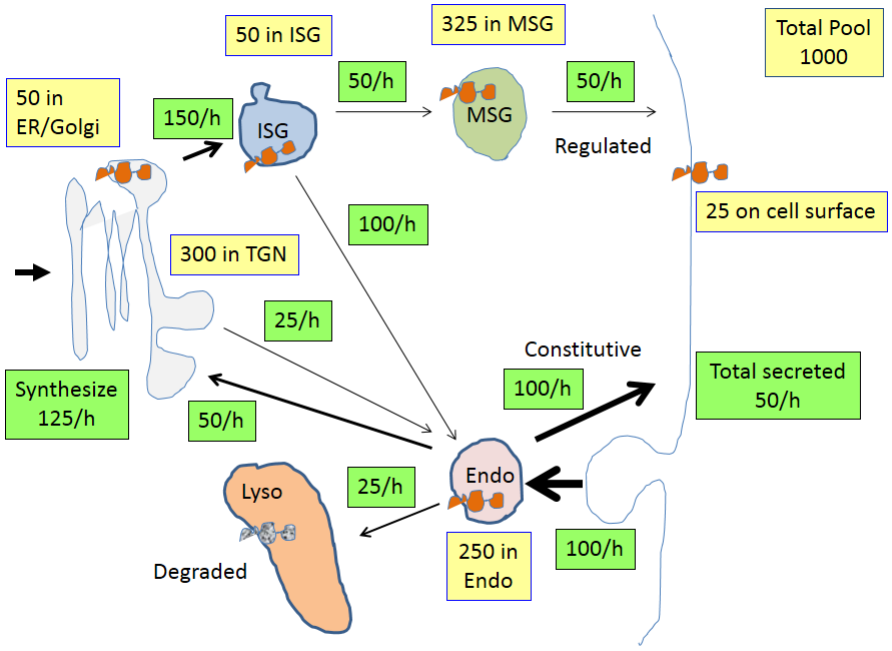

Figure 7.2: Summary of PAM trafficking in AtT-20 cells. Cell diagram representing the number of PAM proteins in a pool of 1000 PAM molecules (yellow boxes) and the rate at which PAM navigates from an organelle to another (green boxes). These numbers were based on previous studies looking at PAM trafficking using biochemical techniques [317, 318, 195, 190, 188, 189, 12, 37, 176]. ISG, Immature Secretory Granule; MSG, Mature Secretory Granule; TGN, *trans*-Golgi network; Endo, endosome; Lyso, lysosome; ER, endoplasmic reticulum.

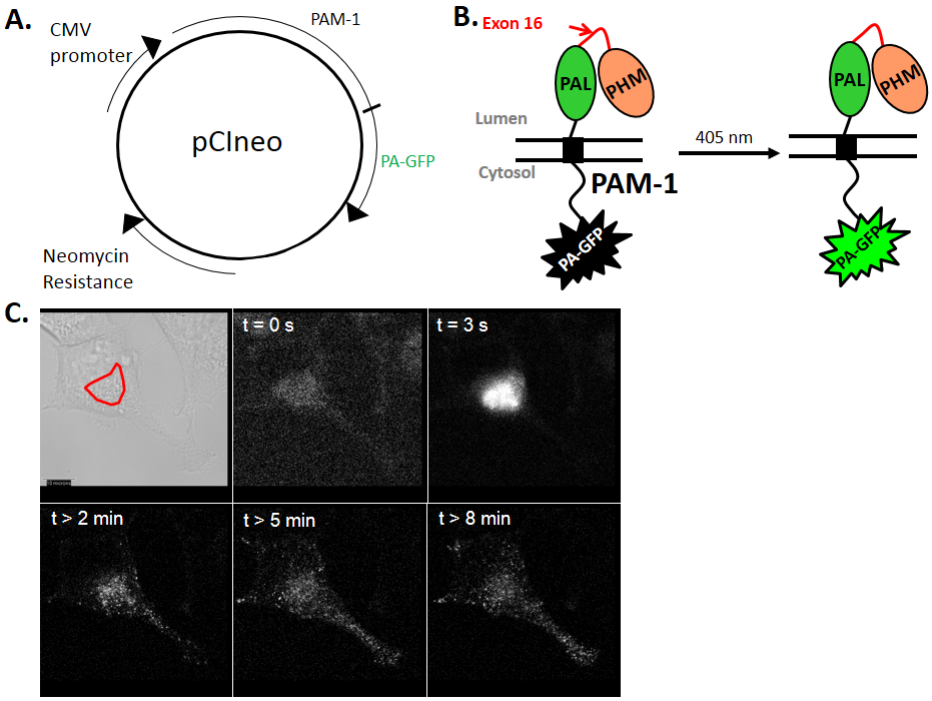

Figure 7.3: PAM PAGFP in an AtT-20 cell. (A) Diagram of PAGFP vector. (B) Principle of photoactivatable GFP (PA-GFP); once PAM-1 PA-GFP has been synthesized, it is not fluorescent. Only after imaging the protein at 405 nm, a conformational change in PA-GFP occurs rendering it fluorescent with similar properties of GFP. (C) AtT-20 cells were transfected with pCI-neo PAM-1 PAGFP using nucleofection. A few weeks after transfection, cells were imaged to examine the dynamics of PAM-PAGFP. Panels representing an AtT-20 cells transfected with PAM-PAGFP. The region that was photoactivated is delineated in red on the brightfield image. Several images taken after photoactivation are shown.

Bibliography

[1] G. E. Palade, "Intracellular aspects of the process of protein secretion," *Science*, vol. 189, no. 4206, p. 867, 1975.

[2] F. Schuit, P. In't Veld, and D. Pipeleers, "Glucose stimulates proinsulin biosynthesis by a dose-dependent recruitment of pancreatic beta cells," *Proceedings of the National Academy of Sciences*, vol. 85, no. 11, pp. 3865–3869, 1988.

[3] B. Alberts, A. Johnson, J. Lewis, M. Raff, K. Roberts, P. Walter, *et al.*, "Intracellular compartments and protein sorting," 2008.

[4] S. M. Colgan, A. A. Al-Hashimi, and R. C. Austin, "Endoplasmic reticulum stress and lipid dysregulation," *Expert reviews in molecular medicine*, vol. 13, p. e4, 2011.

[5] R. E. Mains, E. I. Cullen, V. May, and B. A. Eipper, "The Role of Secretory Granules in Peptide Biosynthesisa," *Annals of the New York Academy of Sciences*, vol. 493, no. 1, pp. 278–291, 1987.

[6] O. Hori, M. Miyazaki, T. Tamatani, K. Ozawa, K. Takano, M. Okabe, M. Ikawa, E. Hartmann, P. Mai, D. M. Stern, *et al.*, "Deletion of SERP1/RAMP4, a component

of the endoplasmic reticulum (ER) translocation sites, leads to ER stress," *Molecular and cellular biology*, vol. 26, no. 11, pp. 4257–4267, 2006.

[7] B. Alberts, A. Johnson, J. Lewis, M. Raff, K. Roberts, P. Walter, *et al.*, "Intracellular vesicular traffic," 2008.

[8] L. Orci, M. Ravazzola, M. Amherdt, D. Louvard, and A. Perrelet, "Clathrin-immunoreactive sites in the Golgi apparatus are concentrated at the trans pole in polypeptide hormone-secreting cells," *Proceedings of the National Academy of Sciences*, vol. 82, no. 16, pp. 5385–5389, 1985.

[9] J. Tooze and S. A. Tooze, "Clathrin-coated vesicular transport of secretory proteins during the formation of ACTH-containing secretory granules in AtT20 cells.," *The Journal of cell biology*, vol. 103, no. 3, pp. 839–850, 1986.

[10] J. Morvan and S. A. Tooze, "Discovery and progress in our understanding of the regulated secretory pathway in neuroendocrine cells," *Histochemistry and cell biology*, vol. 129, no. 3, pp. 243–252, 2008.

[11] S. Urbé, L. J. Page, and S. A. Tooze, "Homotypic fusion of immature secretory granules during maturation in a cell-free assay," *The Journal of cell biology*, vol. 143, no. 7, pp. 1831–1844, 1998.

[12] S. L. Milgram and R. E. Mains, "Differential effects of temperature blockade on the proteolytic processing of three secretory granule-associated proteins," *Journal of cell science*, vol. 107, no. 3, pp. 737–745, 1994.

[13] L. Orci, M. Ravazzola, M. Amherdt, O. Madsen, J.-D. Vassalli, and A. Perrelet, "Direct identification of prohormone conversion site in insulin-secreting cells," *Cell*, vol. 42, no. 2, pp. 671–681, 1985.

[14] P. Arvan and D. Castle, "Protein sorting and secretion granule formation in regulated secretory cells," *Trends in cell biology*, vol. 2, no. 11, pp. 327–331, 1992.

[15] T. L. Burgess and R. B. Kelly, "Constitutive and regulated secretion of proteins," *Annual review of cell biology*, vol. 3, no. 1, pp. 243–293, 1987.

[16] S. A. Tooze, T. Flatmark, J. Tooze, and W. B. Huttner, "Characterization of the immature secretory granule, an intermediate in granule biogenesis.," *The Journal of cell biology*, vol. 115, no. 6, pp. 1491–1503, 1991.

[17] G. Noel and R. E. Mains, "The ordered secretion of bioactive peptides: oldest or newest first?," *Molecular Endocrinology*, vol. 5, no. 6, pp. 787–794, 1991.

[18] J. Suckale and M. Solimena, "The insulin secretory granule as a signaling hub," *Trends in Endocrinology & Metabolism*, vol. 21, no. 10, pp. 599–609, 2010.

[19] G. A. De Toledo, R. Fernandez-Chacon, and J. Fernandez, "Release of secretory products during transient vesicle fusion," *Nature*, vol. 363, no. 6429, pp. 554–558, 1993.

[20] A. Surprenant, "Correlation between electrical activity and ACTH/beta-endorphin secretion in mouse pituitary tumor cells.," *The Journal of cell biology*, vol. 95, no. 2, pp. 559–566, 1982.

[21] P. ARVAN and D. CASTLE, "Sorting and storage during secretory granule biogenesis: looking backward and looking forward," *Biochem. J*, vol. 332, pp. 593–610, 1998.

[22] S. A. Tooze and W. B. Huttner, "Cell-free protein sorting to the regulated and constitutive secretory pathways," *Cell*, vol. 60, no. 5, pp. 837–847, 1990.

[23] E. Chanat and W. B. Huttner, "Milieu-induced, selective aggregation of regulated secretory proteins in the trans-Golgi network.," *The Journal of cell biology*, vol. 115, no. 6, pp. 1505–1519, 1991.

[24] V. Colomer, G. A. Kicska, and M. J. Rindler, "Secretory granule content proteins and the luminal domains of granule membrane proteins aggregate in vitro at mildly acidic pH," *Journal of Biological Chemistry*, vol. 271, no. 1, pp. 48–55, 1996.

[25] H.-H. Gerdes, P. Rosa, E. Phillips, P. Baeuerle, R. Frank, P. Argos, and W. Huttner, "The primary structure of human secretogranin II, a widespread tyrosine-sulfated secretory granule protein that exhibits low pH-and calcium-induced aggregation.," *Journal of Biological Chemistry*, vol. 264, no. 20, pp. 12009–12015, 1989.

[26] M. Blazquez, C. Thiele, W. Huttner, K. Docherty, and K. Shennan, "Involvement of the membrane lipid bilayer in sorting prohormone convertase 2 into the regulated secretory pathway," *Biochem. J*, vol. 349, pp. 843–852, 2000.

[27] J. D. Dikeakos, P. Di Lello, M.-J. Lacombe, R. Ghirlando, P. Legault, T. L. Reudelhuber, and J. G. Omichinski, "Functional and structural characterization of a dense core secretory granule sorting domain from the PC1/3 protease," *Proceedings of the National Academy of Sciences*, vol. 106, no. 18, pp. 7408–7413, 2009.

[28] M. Hosaka, M. Suda, Y. Sakai, T. Izumi, T. Watanabe, and T. Takeuchi, "Secretogranin III binds to cholesterol in the secretory granule membrane as an adapter for chromogranin A," *Journal of Biological Chemistry*, vol. 279, no. 5, pp. 3627–3634, 2004.

[29] M. Hosaka and T. Watanabe, "Secretogranin III: a bridge between core hormone aggregates and the secretory granule membrane.," *Endocrine journal*, vol. 57, no. 4, pp. 275–286, 2009.

[30] M. Hosaka, T. Watanabe, Y. Sakai, Y. Uchiyama, and T. Takeuchi, "Identification of a chromogranin A domain that mediates binding to secretogranin III and targeting to secretory granules in pituitary cells and pancreatic β-cells," *Molecular biology of the cell*, vol. 13, no. 10, pp. 3388–3399, 2002.

[31] D. R. Cool, E. Normant, F.-s. Shen, H.-C. Chen, L. Pannell, Y. Zhang, and Y. P. Loh, "Carboxypeptidase E Is a Regulated Secretory Pathway Sorting Receptor: Genetic Obliteration Leads to Endocrine Disorders in *Cpefat* Mice," *Cell*, vol. 88, no. 1, pp. 73–83, 1997.

[32] J.-C. Irminger, C. B. Verchere, K. Meyer, and P. A. Halban, "Proinsulin Targeting to the Regulated Pathway Is Not Impaired in Carboxypeptidase E-deficientCpe fat/Cpe fat Mice," *Journal of Biological Chemistry*, vol. 272, no. 44, pp. 27532–27534, 1997.

[33] S. Srinivasan, D. O. Bunch, Y. Feng, R. M. Rodriguiz, M. Li, R. L. Ravenell, G. X. Luo, A. Arimura, L. D. Fricker, E. M. Eddy, *et al.*, "Deficits in reproduction and pro-gonadotropin-releasing hormone processing in male Cpe fat mice," *Endocrinology*, vol. 145, no. 4, pp. 2023–2034, 2004.

[34] N. Saito, T. Takeuchi, A. Kawano, M. Hosaka, N. Hou, and S. Torii, "Luminal interaction of phogrin with carboxypeptidase E for effective targeting to secretory granules," *Traffic*, vol. 12, no. 4, pp. 499–506, 2011.

[35] S. Torii, N. Saito, A. Kawano, S. Zhao, T. Izumi, and T. Takeuchi, "Cytoplasmic transport signal is involved in phogrin targeting and localization to secretory granules," *Traffic*, vol. 6, no. 12, pp. 1213–1224, 2005.

[36] C. Wasmeier, P. V. Burgos, T. Trudeau, H. W. Davidson, and J. C. Hutton, "An Extended Tyrosine-Targeting Motif for Endocytosis and Recycling of the Dense-Core Vesicle Membrane Protein Phogrin," *Traffic*, vol. 6, no. 6, pp. 474–487, 2005.

[37] S. L. Milgram, R. E. Mains, and B. A. Eipper, "COOH-terminal signals mediate the trafficking of a peptide processing enzyme in endocrine cells.," *The Journal of cell biology*, vol. 121, no. 1, pp. 23–36, 1993.

[38] C. Rajagopal, K. L. Stone, V. P. Francone, R. E. Mains, and B. A. Eipper, "Secretory Granule to the Nucleus ROLE OF A MULTIPLY PHOSPHORYLATED INTRINSICALLY UNSTRUCTURED DOMAIN," *Journal of Biological Chemistry*, vol. 284, no. 38, pp. 25723–25734, 2009.

[39] T. C. Steveson, G. C. Zhao, H. T. Keutmann, R. E. Mains, and B. A. Eipper, "Access of a membrane protein to secretory granules is facilitated by phosphorylation," *Journal of Biological Chemistry*, vol. 276, no. 43, pp. 40326–40337, 2001.

[40] D. E. Krantz, C. Waites, V. Oorschot, Y. Liu, R. I. Wilson, P. K. Tan, J. Klumperman, and R. H. Edwards, "A phosphorylation site regulates sorting of the vesicular acetyl-

choline transporter to dense core vesicles," *The Journal of cell biology*, vol. 149, no. 2, pp. 379–396, 2000.

[41] F. A. Barr and W. B. Huttner, "A role for ADP-ribosylation factor 1, but not COP I, in secretory vesicle biogenesis from the trans-Golgi network," *FEBS letters*, vol. 384, no. 1, pp. 65–70, 1996.

[42] Y.-G. Chen and D. Shields, "ADP-ribosylation factor-1 stimulates formation of nascent secretory vesicles from the trans-Golgi network of endocrine cells," *Journal of Biological Chemistry*, vol. 271, no. 10, pp. 5297–5300, 1996.

[43] R. A. Kahn and A. G. Gilman, "The protein cofactor necessary for ADP-ribosylation of Gs by cholera toxin is itself a GTP binding protein.," *Journal of Biological Chemistry*, vol. 261, no. 17, pp. 7906–7911, 1986.

[44] A. K. Gillingham and S. Munro, "The small G proteins of the Arf family and their regulators," *Annu. Rev. Cell Dev. Biol.*, vol. 23, pp. 579–611, 2007.

[45] R. A. Kahn, "Toward a model for Arf GTPases as regulators of traffic at the Golgi," *FEBS letters*, vol. 583, no. 23, pp. 3872–3879, 2009.

[46] J. Goldberg, "Structural basis for activation of ARF GTPase: mechanisms of guanine nucleotide exchange and GTP–myristoyl switching," *Cell*, vol. 95, no. 2, pp. 237–248, 1998.

[47] D. U. Gommel, A. R. Memon, A. Heiss, F. Lottspeich, J. Pfannstiel, J. Lechner, C. Reinhard, J. B. Helms, W. Nickel, and F. T. Wieland, "Recruitment to Golgi

membranes of ADP-ribosylation factor 1 is mediated by the cytoplasmic domain of p23," *The EMBO journal*, vol. 20, no. 23, pp. 6751–6760, 2001.

[48] J. Lowery, T. Szul, M. Styers, Z. Holloway, V. Oorschot, J. Klumperman, and E. Sztul, "The Sec7 guanine nucleotide exchange factor GBF1 regulates membrane recruitment of BIG1 and BIG2 guanine nucleotide exchange factors to the trans-Golgi network (TGN)," *Journal of Biological Chemistry*, vol. 288, no. 16, pp. 11532–11545, 2013.

[49] C. J. Fernandez, M. Haugwitz, B. Eaton, and H.-P. H. Moore, "Distinct molecular events during secretory granule biogenesis revealed by sensitivities to brefeldin A," *Molecular biology of the cell*, vol. 8, no. 11, pp. 2171–2185, 1997.

[50] L. C. Hendricks, S. L. McClanahan, G. E. Palade, and M. G. Farquhar, "Brefeldin A affects early events but does not affect late events along the exocytic pathway in pancreatic acinar cells," *Proceedings of the National Academy of Sciences*, vol. 89, no. 15, pp. 7242–7246, 1992.

[51] R. Puertollano, P. A. Randazzo, J. F. Presley, L. M. Hartnell, and J. S. Bonifacino, "The GGAs promote ARF-dependent recruitment of clathrin to the TGN," *Cell*, vol. 105, no. 1, pp. 93–102, 2001.

[52] C. Austin, I. Hinners, and S. A. Tooze, "Direct and GTP-dependent interaction of ADP-ribosylation factor 1 with clathrin adaptor protein AP-1 on immature secretory granules," *Journal of Biological Chemistry*, vol. 275, no. 29, pp. 21862–21869, 2000.

[53] A. S. Dittié, N. Hajibagheri, and S. A. Tooze, "The AP-1 adaptor complex binds to immature secretory granules from PC12 cells, and is regulated by ADP-ribosylation factor.," *The Journal of cell biology*, vol. 132, no. 4, pp. 523–536, 1996.

[54] H. Weintraub, A. Abramovici, D. Amichai, T. Eldar, L. Ben-Dor, P. Pentchev, and I. Hammel, "Morphometric studies of pancreatic acinar granule formation in NCTR-Balb/c mice," *Journal of cell science*, vol. 102, no. 1, pp. 141–147, 1992.

[55] H. M. Ngô, M. Yang, K. Paprotka, M. Pypaert, H. Hoppe, and K. A. Joiner, "AP-1 in Toxoplasma gondii mediates biogenesis of the rhoptry secretory organelle from a post-Golgi compartment," *Journal of Biological Chemistry*, vol. 278, no. 7, pp. 5343–5352, 2003.

[56] J. Burgess, M. Jauregui, J. Tan, J. Rollins, S. Lallet, P. A. Leventis, G. L. Boulianne, H. C. Chang, R. Le Borgne, H. Krämer, *et al.*, "AP-1 and clathrin are essential for secretory granule biogenesis in Drosophila," *Molecular biology of the cell*, vol. 22, no. 12, pp. 2094–2105, 2011.

[57] W. W. Lui-Roberts, L. M. Collinson, L. J. Hewlett, G. Michaux, and D. F. Cutler, "An AP-1/clathrin coat plays a novel and essential role in forming the Weibel-Palade bodies of endothelial cells," *The Journal of cell biology*, vol. 170, no. 4, pp. 627–636, 2005.

[58] Y. J. Wang, J. Wang, H. Q. Sun, M. Martinez, Y. X. Sun, E. Macia, T. Kirchhausen, J. P. Albanesi, M. G. Roth, and H. L. Yin, "Phosphatidylinositol 4 phosphate regulates targeting of clathrin adaptor AP-1 complexes to the Golgi," *Cell*, vol. 114, no. 3, pp. 299–310, 2003.

[59] A. Godi, A. Di Campli, A. Konstantakopoulos, G. Di Tullio, D. R. Alessi, G. S. Kular, T. Daniele, P. Marra, J. M. Lucocq, and M. A. De Matteis, "FAPPs control Golgi-to-cell-surface membrane traffic by binding to ARF and PtdIns (4) P," *Nature cell biology*, vol. 6, no. 5, pp. 393–404, 2004.

[60] A. Balla, G. Tuymetova, M. Barshishat, M. Geiszt, and T. Balla, "Characterization of type II phosphatidylinositol 4-kinase isoforms reveals association of the enzymes with endosomal vesicular compartments," *Journal of Biological Chemistry*, vol. 277, no. 22, pp. 20041–20050, 2002.

[61] B. Barylko, Y. S. Mao, P. Wlodarski, G. Jung, D. D. Binns, H.-Q. Sun, H. L. Yin, and J. P. Albanesi, "Palmitoylation controls the catalytic activity and subcellular distribution of phosphatidylinositol 4-kinase IIα," *Journal of Biological Chemistry*, vol. 284, no. 15, pp. 9994–10003, 2009.

[62] S. Minogue, K. E. Chu, E. J. Westover, D. F. Covey, J. J. Hsuan, and M. G. Waugh, "Relationship between phosphatidylinositol 4-phosphate synthesis, membrane organization, and lateral diffusion of PI4KIIα at the trans-Golgi network," *Journal of lipid research*, vol. 51, no. 8, pp. 2314–2324, 2010.

[63] M. Waugh, S. Minogue, D. Blumenkrantz, J. ANDERSON, and J. HSUAN, "Identification and characterization of differentially active pools of type IIα phosphatidylinositol 4-kinase activity in unstimulated A431 cells," *Biochem. J*, vol. 376, pp. 497–503, 2003.

[64] B. Barylko, S. H. Gerber, D. D. Binns, N. Grichine, M. Khvotchev, T. C. Südhof, and J. P. Albanesi, "A novel family of phosphatidylinositol 4-kinases conserved from yeast to humans," *Journal of Biological Chemistry*, vol. 276, no. 11, pp. 7705–7708, 2001.

[65] S. Gasman, S. Chasserot-Golaz, P. Hubert, D. Aunis, and M.-F. Bader, "Identification of a Potential Effector Pathway for the Trimeric Go Protein Associated with Secretory Granules. Go Stimulates a Granule-Bond Phosphatidylinositol 4-kinase by Activat-

ing RhoA in Chromaffin Cells," *Journal of Biological Chemistry*, vol. 273, no. 27, pp. 16913–16920, 1998.

[66] C. Wiedemann, T. Schäfer, and M. M. Burger, "Chromaffin granule-associated phosphatidylinositol 4-kinase activity is required for stimulated secretion.," *The EMBO journal*, vol. 15, no. 9, p. 2094, 1996.

[67] Z. Xu, G. Huang, and K. V. Kandror, "Phosphatidylinositol 4-kinase type IIα is targeted specifically to cellugyrin-positive glucose transporter 4 vesicles," *Molecular Endocrinology*, vol. 20, no. 11, pp. 2890–2897, 2006.

[68] J. Burgess, L. M. Del Bel, C.-I. J. Ma, B. Barylko, G. Polevoy, J. Rollins, J. P. Albanesi, H. Krämer, and J. A. Brill, "Type II phosphatidylinositol 4-kinase regulates trafficking of secretory granule proteins in Drosophila," *Development*, vol. 139, no. 16, pp. 3040–3050, 2012.

[69] J. Guo, M. R. Wenk, L. Pellegrini, F. Onofri, F. Benfenati, and P. De Camilli, "Phosphatidylinositol 4-kinase type IIα is responsible for the phosphatidylinositol 4-kinase activity associated with synaptic vesicles," *Proceedings of the National Academy of Sciences*, vol. 100, no. 7, pp. 3995–4000, 2003.

[70] C. Panaretou and S. TOOZE, "Regulation and recruitment of phosphatidylinositol 4-kinase on immature secretory granules is independent of ADP-ribosylation factor 1," *Biochem. J*, vol. 363, pp. 289–295, 2002.

[71] T. R. Graham and C. G. Burd, "Coordination of Golgi functions by phosphatidylinositol 4-kinases," *Trends in cell biology*, vol. 21, no. 2, pp. 113–121, 2011.

[72] M. G. Waugh, S. Minogue, D. Chotai, F. Berditchevski, and J. J. Hsuan, "Lipid and peptide control of phosphatidylinositol 4-kinase IIα activity on Golgi-endosomal rafts," *Journal of Biological Chemistry*, vol. 281, no. 7, pp. 3757–3763, 2006.

[73] S. Dhanvantari and Y. P. Loh, "Lipid raft association of carboxypeptidase E is necessary for its function as a regulated secretory pathway sorting receptor," *Journal of Biological Chemistry*, vol. 275, no. 38, pp. 29887–29893, 2000.

[74] R. Wang, M. Hosaka, L. Han, H. Yokota-Hashimoto, M. Suda, D. Mitsushima, S. Torii, and T. Takeuchi, "Molecular probes for sensing the cholesterol composition of subcellular organelle membranes," *Biochimica et Biophysica Acta (BBA)-Molecular and Cell Biology of Lipids*, vol. 1761, no. 10, pp. 1169–1181, 2006.

[75] Y. Wang, C. Thiele, and W. B. Huttner, "Cholesterol is required for the formation of regulated and constitutive secretory vesicles from the trans-Golgi network," *Traffic*, vol. 1, no. 12, pp. 952–962, 2000.

[76] S. Urbe, A. Dittié, and S. Tooze, "pH-dependent processing of secretogranin II by the endopeptidase PC2 in isolated immature secretory granules," *Biochem. J*, vol. 321, pp. 65–74, 1997.

[77] E. J. Husten and B. A. Eipper, "Purification and characterization of PAM-1, an integral membrane protein involved in peptide processing," *Archives of biochemistry and biophysics*, vol. 312, no. 2, pp. 487–492, 1994.

[78] M. G. Farquhar, J. J. Reid, and L. W. Daniell, "Intracellular Transport and Packaging of Prolactin: A Quantitative Electron Microscope Autoradiographic Study of

Mammotrophs Dissociated from Rat Pituitaries*," *Endocrinology*, vol. 102, no. 1, pp. 296–311, 1978.

[79] M. Ahras, G. P. Otto, and S. A. Tooze, "Synaptotagmin IV is necessary for the maturation of secretory granules in PC12 cells," *The Journal of cell biology*, vol. 173, no. 2, pp. 241–251, 2006.

[80] F. Wendler, L. Page, S. Urbé, and S. A. Tooze, "Homotypic fusion of immature secretory granules during maturation requires syntaxin 6," *Molecular biology of the cell*, vol. 12, no. 6, pp. 1699–1709, 2001.

[81] J. Bock, J. Klumperman, S. Davanger, and R. Scheller, "Syntaxin 6 functions in trans-Golgi network vesicle trafficking.," *Molecular biology of the cell*, vol. 8, no. 7, pp. 1261–1271, 1997.

[82] J. Klumperman, R. Kuliawat, J. M. Griffith, H. J. Geuze, and P. Arvan, "Mannose 6–phosphate receptors are sorted from immature secretory granules via adaptor protein AP-1, clathrin, and syntaxin 6–positive vesicles," *The Journal of cell biology*, vol. 141, no. 2, pp. 359–371, 1998.

[83] B. A. Eaton, M. Haugwitz, D. Lau, and H.-P. H. Moore, "Biogenesis of regulated exocytotic carriers in neuroendocrine cells," *The Journal of Neuroscience*, vol. 20, no. 19, pp. 7334–7344, 2000.

[84] K. Ibata, M. Fukuda, T. Hamada, H. Kabayama, and K. Mikoshiba, "Synaptotagmin IV is present at the Golgi and distal parts of neurites," *Journal of neurochemistry*, vol. 74, no. 2, pp. 518–526, 2000.

[85] J. A. Pickett and J. M. Edwardson, "Compound exocytosis: mechanisms and functional significance," *Traffic*, vol. 7, no. 2, pp. 109–116, 2006.

[86] I. Hinners, F. Wendler, H. Fei, L. Thomas, G. Thomas, and S. A. Tooze, "AP-1 recruitment to VAMP4 is modulated by phosphorylation-dependent binding of PACS-1," *EMBO reports*, vol. 4, no. 12, pp. 1182–1189, 2003.

[87] A. A. Peden, G. Y. Park, and R. H. Scheller, "The Di-leucine motif of vesicle-associated membrane protein 4 is required for its localization and AP-1 binding," *Journal of Biological Chemistry*, vol. 276, no. 52, pp. 49183–49187, 2001.

[88] A. S. Dittié, L. Thomas, G. Thomas, and S. A. Tooze, "Interaction of furin in immature secretory granules from neuroendocrine cells with the AP-1 adaptor complex is modulated by casein kinase II phosphorylation," *The EMBO journal*, vol. 16, no. 16, pp. 4859–4870, 1997.

[89] A. S. Dittié, J. Klumperman, and S. A. Tooze, "Differential distribution of mannose-6-phosphate receptors and furin in immature secretory granules," *Journal of cell science*, vol. 112, no. 22, pp. 3955–3966, 1999.

[90] F. Mauxion, R. Le Borgne, H. Munier-Lehmann, and B. Hoflack, "A casein kinase II phosphorylation site in the cytoplasmic domain of the cation-dependent mannose 6-phosphate receptor determines the high affinity interaction of the AP-1 Golgi assembly proteins with membranes," *Journal of Biological Chemistry*, vol. 271, no. 4, pp. 2171–2178, 1996.

[91] L. L. Tortorella, F. B. Schapiro, and F. R. Maxfield, "Role of an Acidic Cluster/Dileucine Motif in Cation-Independent Mannose 6-Phosphate Receptor Traffic," *Traffic*, vol. 8, no. 4, pp. 402–413, 2007.

[92] M. Boehm and J. S. Bonifacino, "Genetic analyses of adaptin function from yeast to mammals," *Gene*, vol. 286, no. 2, pp. 175–186, 2002.

[93] J. Hirst, L. D. Barlow, G. C. Francisco, D. A. Sahlender, M. N. Seaman, J. B. Dacks, and M. S. Robinson, "The fifth adaptor protein complex," *PLoS biology*, vol. 9, no. 10, p. e1001170, 2011.

[94] M. S. Robinson, "Adaptable adaptors for coated vesicles," *Trends in cell biology*, vol. 14, no. 4, pp. 167–174, 2004.

[95] M. S. Robinson and J. S. Bonifacino, "Adaptor-related proteins," *Current opinion in cell biology*, vol. 13, no. 4, pp. 444–453, 2001.

[96] E. C. Dell'Angelica, H. Ohno, C. E. Ooi, E. Rabinovich, K. W. Roche, and J. S. Bonifacino, "AP-3: an adaptor-like protein complex with ubiquitous expression," *The EMBO journal*, vol. 16, no. 5, pp. 917–928, 1997.

[97] L. S. Newman, M. O. McKeever, H. J. Okano, and R. B. Darnell, "β-NAP, a cerebellar degeneration antigen, is a neuron-specific vesicle coat protein," *Cell*, vol. 82, no. 5, pp. 773–783, 1995.

[98] H. Ohno, J. Stewart, M.-C. Fournier, H. Bosshart, I. Rhee, S. Miyatake, T. Saito, A. Gallusser, T. Kirchhausen, and J. S. Bonifacino, "Interaction of tyrosine-based

sorting signals with clathrin-associated proteins," *Science*, vol. 269, no. 5232, pp. 1872–1875, 1995.

[99] J. Pevsner, W. Volknandt, B. R. Wong, and R. H. Scheller, "Two rat homologs of clathrin-associated adaptor proteins," *Gene*, vol. 146, no. 2, pp. 279–283, 1994.

[100] F. Simpson, A. A. Peden, L. Christopoulou, and M. S. Robinson, "Characterization of the adaptor-related protein complex, AP-3," *The Journal of cell biology*, vol. 137, no. 4, pp. 835–845, 1997.

[101] H. Ohno, T. Tomemori, F. Nakatsu, Y. Okazaki, R. C. Aguilar, H. Foelsch, I. Mellman, T. Saito, T. Shirasawa, and J. S. Bonifacino, "μ1B, a novel adaptor medium chain expressed in polarized epithelial cells," *FEBS letters*, vol. 449, no. 2, pp. 215–220, 1999.

[102] R. C. Aguilar, M. Boehm, I. Gorshkova, R. J. Crouch, K. Tomita, T. Saito, H. Ohno, and J. S. Bonifacino, "Signal-binding specificity of the μ4 subunit of the adaptor protein complex AP-4," *Journal of Biological Chemistry*, vol. 276, no. 16, pp. 13145–13152, 2001.

[103] J. Hirst, N. A. Bright, B. Rous, and M. S. Robinson, "Characterization of a fourth adaptor-related protein complex," *Molecular biology of the cell*, vol. 10, no. 8, pp. 2787–2802, 1999.

[104] H. Ohno, R. C. Aguilar, D. Yeh, D. Taura, T. Saito, and J. S. Bonifacino, "The medium subunits of adaptor complexes recognize distinct but overlapping sets of tyrosine-based sorting signals," *Journal of Biological Chemistry*, vol. 273, no. 40, pp. 25915–25921, 1998.

[105] B. Doray, I. Lee, J. Knisely, G. Bu, and S. Kornfeld, "The $\gamma/\sigma1$ and $\alpha/\sigma2$ hemicomplexes of clathrin adaptors AP-1 and AP-2 harbor the dileucine recognition site," *Molecular biology of the cell*, vol. 18, no. 5, pp. 1887–1896, 2007.

[106] K. Janvier, Y. Kato, M. Boehm, J. R. Rose, J. A. Martina, B.-Y. Kim, S. Venkatesan, and J. S. Bonifacino, "Recognition of dileucine-based sorting signals from HIV-1 Nef and LIMP-II by the AP-1 γ–$\sigma1$ and AP-3 δ–$\sigma3$ hemicomplexes," *The Journal of cell biology*, vol. 163, no. 6, pp. 1281–1290, 2003.

[107] B. Doray, P. Ghosh, J. Griffith, H. J. Geuze, and S. Kornfeld, "Cooperation of GGAs and AP-1 in packaging MPRs at the trans-Golgi network," *Science*, vol. 297, no. 5587, pp. 1700–1703, 2002.

[108] J. Hirst, W. W. Lui, N. A. Bright, N. Totty, M. N. Seaman, and M. S. Robinson, "A family of proteins with γ-adaptin and VHS domains that facilitate trafficking between the trans-Golgi network and the vacuole/lysosome," *The Journal of cell biology*, vol. 149, no. 1, pp. 67–80, 2000.

[109] L. J. Page, P. J. Sowerby, W. W. Lui, and M. S. Robinson, "γ-Synergin An Eh Domain–Containing Protein That Interacts with γ-Adaptin," *The Journal of cell biology*, vol. 146, no. 5, pp. 993–1004, 1999.

[110] S. Wasiak, V. Legendre-Guillemin, R. Puertollano, F. Blondeau, M. Girard, E. de Heuvel, D. Boismenu, A. W. Bell, J. S. Bonifacino, and P. S. McPherson, "Enthoprotin a novel clathrin-associated protein identified through subcellular proteomics," *The Journal of cell biology*, vol. 158, no. 5, pp. 855–862, 2002.

[111] E. C. Dell'Angelica, J. Klumperman, W. Stoorvogel, and J. S. Bonifacino, "Association of the AP-3 adaptor complex with clathrin," *Science*, vol. 280, no. 5362, pp. 431–434, 1998.

[112] A. Gallusser and T. Kirchhausen, "The beta 1 and beta 2 subunits of the AP complexes are the clathrin coat assembly components.," *The EMBO journal*, vol. 12, no. 13, p. 5237, 1993.

[113] D. Owen, Y. Vallis, B. Pearse, H. McMahon, and P. Evans, "The structure and function of the β2-adaptin appendage domain," *The EMBO journal*, vol. 19, no. 16, pp. 4216–4227, 2000.

[114] E. C. DellâĂŹAngelica, C. E. Ooi, and J. S. Bonifacino, "β3A-adaptin, a subunit of the adaptor-like complex AP-3," *Journal of Biological Chemistry*, vol. 272, no. 24, pp. 15078–15084, 1997.

[115] B. Doray and S. Kornfeld, "γ subunit of the AP-1 adaptor complex binds clathrin: implications for cooperative binding in coated vesicle assembly," *Molecular biology of the cell*, vol. 12, no. 7, pp. 1925–1935, 2001.

[116] O. B. Goodman and J. H. Keen, "The chain of the AP-2 adaptor is a clathrin binding subunit," *Journal of Biological Chemistry*, vol. 270, no. 40, pp. 23768–23773, 1995.

[117] E. E. Heldwein, E. Macia, J. Wang, H. L. Yin, T. Kirchhausen, and S. C. Harrison, "Crystal structure of the clathrin adaptor protein 1 core," *Proceedings of the National Academy of Sciences of the United States of America*, vol. 101, no. 39, pp. 14108–14113, 2004.

[118] M. S. Robinson and T. E. Kreis, "Recruitment of coat proteins onto Golgi membranes in intact and permeabilized cells: effects of brefeldin A and G protein activators," *Cell*, vol. 69, no. 1, pp. 129–138, 1992.

[119] X. Ren, G. G. Farías, B. J. Canagarajah, J. S. Bonifacino, and J. H. Hurley, "Structural basis for recruitment and activation of the AP-1 clathrin adaptor complex by Arf1," *Cell*, vol. 152, no. 4, pp. 755–767, 2013.

[120] M. A. Stamnes and J. E. Rothman, "The binding of AP-1 clathrin adaptor particles to Golgi membranes requires ADP-ribosylation factor, a small GTP-binding protein," *Cell*, vol. 73, no. 5, pp. 999–1005, 1993.

[121] L. M. Traub, J. A. Ostrom, and S. Kornfeld, "Biochemical dissection of AP-1 recruitment onto Golgi membranes.," *The Journal of cell biology*, vol. 123, no. 3, pp. 561–573, 1993.

[122] P. Ghosh and S. Kornfeld, "AP-1 binding to sorting signals and release from clathrin-coated vesicles is regulated by phosphorylation," *The Journal of cell biology*, vol. 160, no. 5, pp. 699–708, 2003.

[123] B. M. Collins, A. J. McCoy, H. M. Kent, P. R. Evans, and D. J. Owen, "Molecular architecture and functional model of the endocytic AP2 complex," *Cell*, vol. 109, no. 4, pp. 523–535, 2002.

[124] S. Molloy, L. Thomas, J. VanSlyke, P. Stenberg, and G. Thomas, "Intracellular trafficking and activation of the furin proprotein convertase: localization to the TGN and recycling from the cell surface.," *The EMBO journal*, vol. 13, no. 1, p. 18, 1994.

[125] J. S. Bonifacino and L. M. Traub, "Signals for Sorting of Transmembrane Proteins to Endosomes and Lysosomes*," *Annual review of biochemistry*, vol. 72, no. 1, pp. 395–447, 2003.

[126] L. Wan, S. S. Molloy, L. Thomas, G. Liu, Y. Xiang, S. L. Rybak, and G. Thomas, "PACS-1 Defines a Novel Gene Family of Cytosolic Sorting Proteins Required for *trans*-Golgi Network Localization," *Cell*, vol. 94, no. 2, pp. 205–216, 1998.

[127] B. Jones, L. Thomas, S. Molloy, C. Thulin, M. Fry, K. Walsh, and G. Thomas, "Intracellular trafficking of furin is modulated by the phosphorylation state of a casein kinase ii site in its cytoplasmic tail.," *The EMBO journal*, vol. 14, no. 23, p. 5869, 1995.

[128] C. M. Crump, Y. Xiang, L. Thomas, F. Gu, C. Austin, S. A. Tooze, and G. Thomas, "PACS-1 binding to adaptors is required for acidic cluster motif-mediated protein traffic," *The EMBO journal*, vol. 20, no. 9, pp. 2191–2201, 2001.

[129] G. K. Scott, H. Fei, L. Thomas, G. R. Medigeshi, and G. Thomas, "A PACS-1, GGA3 and CK2 complex regulates CI-MPR trafficking," *The EMBO journal*, vol. 25, no. 19, pp. 4423–4435, 2006.

[130] G. K. Scott, F. Gu, C. M. Crump, L. Thomas, L. Wan, Y. Xiang, and G. Thomas, "The phosphorylation state of an autoregulatory domain controls PACS-1-directed protein traffic," *The EMBO journal*, vol. 22, no. 23, pp. 6234–6244, 2003.

[131] A. L. Boman, C.-j. Zhang, X. Zhu, and R. A. Kahn, "A family of ADP-ribosylation factor effectors that can alter membrane transport through the trans-Golgi," *Molecular biology of the cell*, vol. 11, no. 4, pp. 1241–1255, 2000.

[132] E. C. Dell'Angelica, R. Puertollano, C. Mullins, R. C. Aguilar, J. D. Vargas, L. M. Hartnell, and J. S. Bonifacino, "Ggas A Family of Adp Ribosylation Factor-Binding Proteins Related to Adaptors and Associated with the Golgi Complex," *The Journal of cell biology*, vol. 149, no. 1, pp. 81–94, 2000.

[133] J. S. Bonifacino, "The GGA proteins: adaptors on the move," *Nature reviews Molecular cell biology*, vol. 5, no. 1, pp. 23–32, 2004.

[134] A. Poussu, O. Lohi, and V.-P. Lehto, "Vear, a novel Golgi-associated protein with VHS and γ-adaptin âĂIJearâĂİ domains," *Journal of Biological Chemistry*, vol. 275, no. 10, pp. 7176–7183, 2000.

[135] J. McCullough, P. E. Row, Ó. Lorenzo, M. Doherty, R. Beynon, M. J. Clague, and S. Urbé, "Activation of the endosome-associated ubiquitin isopeptidase AMSH by STAM, a component of the multivesicular body-sorting machinery," *Current Biology*, vol. 16, no. 2, pp. 160–165, 2006.

[136] R. Puertollano, R. C. Aguilar, I. Gorshkova, R. J. Crouch, and J. S. Bonifacino, "Sorting of mannose 6-phosphate receptors mediated by the GGAs," *Science*, vol. 292, no. 5522, pp. 1712–1716, 2001.

[137] P. S. Bilodeau, S. C. Winistorfer, M. M. Allaman, K. Surendhran, W. R. Kearney, A. D. Robertson, and R. C. Piper, "The GAT domains of clathrin-associated GGA proteins have two ubiquitin binding motifs," *Journal of Biological Chemistry*, vol. 279, no. 52, pp. 54808–54816, 2004.

[138] R. Puertollano and J. S. Bonifacino, "Interactions of GGA3 with the ubiquitin sorting machinery," *Nature cell biology*, vol. 6, no. 3, pp. 244–251, 2004.

[139] Y. Shiba, Y. Katoh, T. Shiba, K. Yoshino, H. Takatsu, H. Kobayashi, H.-W. Shin, S. Wakatsuki, and K. Nakayama, "GAT (GGA and Tom1) domain responsible for ubiquitin binding and ubiquitination," *Journal of Biological Chemistry*, vol. 279, no. 8, pp. 7105–7111, 2004.

[140] J. Wang, H.-Q. Sun, E. Macia, T. Kirchhausen, H. Watson, J. S. Bonifacino, and H. L. Yin, "PI4P promotes the recruitment of the GGA adaptor proteins to the trans-Golgi network and regulates their recognition of the ubiquitin sorting signal," *Molecular biology of the cell*, vol. 18, no. 7, pp. 2646–2655, 2007.

[141] Y. Kim, Y. Deng, and C. C. Philpott, "GGA2-and ubiquitin-dependent trafficking of Arn1, the ferrichrome transporter of Saccharomyces cerevisiae," *Molecular biology of the cell*, vol. 18, no. 5, pp. 1790–1802, 2007.

[142] P. M. Scott, P. S. Bilodeau, O. Zhdankina, S. C. Winistorfer, M. J. Hauglund, M. M. Allaman, W. R. Kearney, A. D. Robertson, A. L. Boman, and R. C. Piper, "GGA proteins bind ubiquitin to facilitate sorting at the trans-Golgi network," *Nature cell biology*, vol. 6, no. 3, pp. 252–259, 2004.

[143] H. Bai, B. Doray, and S. Kornfeld, "GGA1 interacts with the adaptor protein AP-1 through a WNSF sequence in its hinge region," *Journal of Biological Chemistry*, vol. 279, no. 17, pp. 17411–17417, 2004.

[144] B. Doray, K. Bruns, P. Ghosh, and S. A. Kornfeld, "Autoinhibition of the ligand-binding site of GGA1/3 VHS domains by an internal acidic cluster-dileucine motif," *Proceedings of the National Academy of Sciences*, vol. 99, no. 12, pp. 8072–8077, 2002.

[145] P. Ghosh and S. Kornfeld, "Phosphorylation-induced conformational changes regulate GGAs 1 and 3 function at the trans-Golgi network," *Journal of Biological Chemistry*, vol. 278, no. 16, pp. 14543–14549, 2003.

[146] J. F. Cramer, C. Gustafsen, M. A. Behrens, C. L. Oliveira, J. S. Pedersen, P. Madsen, C. M. Petersen, and S. S. Thirup, "GGA autoinhibition revisited," *Traffic*, vol. 11, no. 2, pp. 259–273, 2010.

[147] H. Takatsu, K. Yoshino, and K. Nakayama, "Adaptor γ ear homology domain conserved in γ-adaptin and GGA proteins that interact with γ-synergin," *Biochemical and biophysical research communications*, vol. 271, no. 3, pp. 719–725, 2000.

[148] R. Mattera, C. N. Arighi, R. Lodge, M. Zerial, and J. S. Bonifacino, "Divalent interaction of the GGAs with the Rabaptin-5–Rabex-5 complex," *The EMBO journal*, vol. 22, no. 1, pp. 78–88, 2003.

[149] Y. Zhu, B. Doray, A. Poussu, V.-P. Lehto, and S. Kornfeld, "Binding of GGA2 to the lysosomal enzyme sorting motif of the mannose 6-phosphate receptor," *Science*, vol. 292, no. 5522, pp. 1716–1718, 2001.

[150] O. Kakhlon, P. Sakya, B. Larijani, R. Watson, and S. A. Tooze, "GGA function is required for maturation of neuroendocrine secretory granules," *The EMBO journal*, vol. 25, no. 8, pp. 1590–1602, 2006.

[151] J. Hirst, G. H. Borner, R. Antrobus, A. A. Peden, N. A. Hodson, D. A. Sahlender, and M. S. Robinson, "Distinct and overlapping roles for AP-1 and GGAs revealed by the âĂIJknocksidewaysâĂİ system," *Current Biology*, vol. 22, no. 18, pp. 1711–1716, 2012.

[152] L. Daboussi, G. Costaguta, and G. S. Payne, "Phosphoinositide-mediated clathrin adaptor progression at the trans-Golgi network," *Nature Cell Biology*, vol. 14, no. 3, pp. 239–248, 2012.

[153] M. Steegmaier, J. Klumperman, D. L. Foletti, J.-S. Yoo, and R. H. Scheller, "Vesicle-associated Membrane Protein 4 is Implicated inTrans-Golgi Network Vesicle Trafficking," *Molecular biology of the cell*, vol. 10, no. 6, pp. 1957–1972, 1999.

[154] T. Braulke and J. S. Bonifacino, "Sorting of lysosomal proteins," *Biochimica et Biophysica Acta (BBA)-Molecular Cell Research*, vol. 1793, no. 4, pp. 605–614, 2009.

[155] J. Glickman, E. Conibear, and B. Pearse, "Specificity of binding of clathrin adaptors to signals on the mannose-6-phosphate/insulin-like growth factor II receptor.," *The EMBO journal*, vol. 8, no. 4, p. 1041, 1989.

[156] K. F. Johnson, W. Chan, and S. Kornfeld, "Cation-dependent mannose 6-phosphate receptor contains two internalization signals in its cytoplasmic domain," *Proceedings of the National Academy of Sciences*, vol. 87, no. 24, pp. 10010–10014, 1990.

[157] S. Meresse, T. Ludwig, R. Frank, and B. Hoflack, "Phosphorylation of the cytoplasmic domain of the bovine cation-independent mannose 6-phosphate receptor. Serines 2421 and 2492 are the targets of a casein kinase II associated to the Golgi-derived HAI adaptor complex.," *Journal of Biological Chemistry*, vol. 265, no. 31, pp. 18833–18842, 1990.

[158] J. Stöckli, S. Höning, and J. Rohrer, "The acidic cluster of the CK2 site of the cation-dependent mannose 6-phosphate receptor (CD-MPR) but not its phosphorylation is

required for GGA1 and AP-1 binding," *Journal of Biological Chemistry*, vol. 279, no. 22, pp. 23542–23549, 2004.

[159] O. Varlamov and L. D. Fricker, "Intracellular trafficking of metallocarboxypeptidase D in AtT-20 cells: localization to the trans-Golgi network and recycling from the cell surface," *Journal of cell science*, vol. 111, no. 7, pp. 877–885, 1998.

[160] O. Varlamov, F. J. Eng, E. G. Novikova, and L. D. Fricker, "Localization of Metallocarboxypeptidase D in AtT-20 Cells POTENTIAL ROLE IN PROHORMONE PROCESSING," *Journal of Biological Chemistry*, vol. 274, no. 21, pp. 14759–14767, 1999.

[161] E. Kalinina, O. Varlamov, and L. D. Fricker, "Analysis of the carboxypeptidase D cytoplasmic domain: Implications in intracellular trafficking," *Journal of cellular biochemistry*, vol. 85, no. 1, pp. 101–111, 2002.

[162] C. L. Waites, A. Mehta, P. K. Tan, G. Thomas, R. H. Edwards, and D. E. Krantz, "An acidic motif retains vesicular monoamine transporter 2 on large dense core vesicles," *The Journal of cell biology*, vol. 152, no. 6, pp. 1159–1168, 2001.

[163] L. A. Caromile, A. Oganesian, S. A. Coats, R. A. Seifert, and D. F. Bowen-Pope, "The neurosecretory vesicle protein phogrin functions as a phosphatidylinositol phosphatase to regulate insulin secretion," *Journal of Biological Chemistry*, vol. 285, no. 14, pp. 10487–10496, 2010.

[164] A. Nykjaer and T. E. Willnow, "Sortilin: a receptor to regulate neuronal viability and function," *Trends in neurosciences*, vol. 35, no. 4, pp. 261–270, 2012.

[165] Z.-Y. Chen, A. Ieraci, H. Teng, H. Dall, C.-X. Meng, D. G. Herrera, A. Nykjaer, B. L. Hempstead, and F. S. Lee, "Sortilin controls intracellular sorting of brain-derived neurotrophic factor to the regulated secretory pathway," *The Journal of neuroscience*, vol. 25, no. 26, pp. 6156–6166, 2005.

[166] M. Yang, Y. Lim, X. Li, J.-H. Zhong, and X.-F. Zhou, "Precursor of brain-derived neurotrophic factor (proBDNF) forms a complex with Huntingtin-associated protein-1 (HAP1) and sortilin that modulates proBDNF trafficking, degradation, and processing," *Journal of Biological Chemistry*, vol. 286, no. 18, pp. 16272–16284, 2011.

[167] M. S. Nielsen, P. Madsen, E. I. Christensen, A. Nykjær, J. Gliemann, D. Kasper, R. Pohlmann, and C. M. Petersen, "The sortilin cytoplasmic tail conveys Golgi–endosome transport and binds the VHS domain of the GGA2 sorting protein," *The EMBO journal*, vol. 20, no. 9, pp. 2180–2190, 2001.

[168] M. Canuel, S. Lefrancois, J. Zeng, and C. R. Morales, "AP-1 and retromer play opposite roles in the trafficking of sortilin between the Golgi apparatus and the lysosomes," *Biochemical and biophysical research communications*, vol. 366, no. 3, pp. 724–730, 2008.

[169] C. S. Asensio, D. W. Sirkis, and R. H. Edwards, "RNAi screen identifies a role for adaptor protein AP-3 in sorting to the regulated secretory pathway," *The Journal of cell biology*, vol. 191, no. 6, pp. 1173–1187, 2010.

[170] D. J. Gauthier, J. A. Sobota, F. Ferraro, R. E. Mains, and C. Lazure, "Flow cytometry-assisted purification and proteomic analysis of the corticotropes dense-core secretory granules," *Proteomics*, vol. 8, no. 18, pp. 3848–3861, 2008.

[171] J. L. Wegrzyn, S. J. Bark, L. Funkelstein, C. Mosier, A. Yap, P. Kazemi-Esfarjani, A. R. La Spada, C. Sigurdson, D. T. OâĂŹConnor, and V. Hook, "Proteomics of Dense Core Secretory Vesicles Reveal Distinct Protein Categories for Secretion of Neuroeffectors for Cell- Cell Communication," *Journal of proteome research*, vol. 9, no. 10, pp. 5002–5024, 2010.

[172] O. Katsumata, J. Fujita-Yoshigaki, M. Hara-Yokoyama, M. Yanagishita, S. Furuyama, and H. Sugiya, "Syntaxin6 separates from GM1a-rich membrane microdomain during granule maturation," *Biochemical and biophysical research communications*, vol. 357, no. 4, pp. 1071–1077, 2007.

[173] R. Youker, U. Shinde, R. Day, and G. Thomas, "At the crossroads of homoeostasis and disease: roles of the PACS proteins in membrane traffic and apoptosis," *Biochem. J*, vol. 421, pp. 1–15, 2009.

[174] H. Stettler, N. Beuret, C. Prescianotto-Baschong, B. Fayard, L. Taupenot, and M. Spiess, "Determinants for chromogranin A sorting into the regulated secretory pathway are also sufficient to generate granule-like structures in non-endocrine cells," *Biochem. J*, vol. 418, pp. 81–91, 2009.

[175] F. J. Eng, O. Varlamov, and L. D. Fricker, "Sequences within the cytoplasmic domain of gp180/carboxypeptidase D mediate localization to the trans-Golgi network," *Molecular biology of the cell*, vol. 10, no. 1, pp. 35–46, 1999.

[176] S. L. Milgram, R. E. Mains, and B. A. Eipper, "Identification of routing determinants in the cytosolic domain of a secretory granule-associated integral membrane protein," *Journal of Biological Chemistry*, vol. 271, no. 29, pp. 17526–17535, 1996.

[177] M. G. Farquhar and G. E. Palade, "The Golgi apparatus (complex)-(1954-1981)-from artifact to center stage.," *The Journal of cell biology*, vol. 91, no. 3, pp. 77s–103s, 1981.

[178] C. Meyer, D. Zizioli, S. Lausmann, E.-L. Eskelinen, J. Hamann, P. Saftig, K. von Figura, and P. Schu, "μ1A-adaptin-deficient mice: lethality, loss of AP-1 binding and rerouting of mannose 6-phosphate receptors," *The EMBO journal*, vol. 19, no. 10, pp. 2193–2203, 2000.

[179] W. Shih, A. Gallusser, and T. Kirchhausen, "A clathrin-binding site in the hinge of the 2 chain of mammalian AP-2 complexes," *Journal of Biological Chemistry*, vol. 270, no. 52, pp. 31083–31090, 1995.

[180] M. L. Bonnemaison, B. A. Eipper, and R. E. Mains, "Role of adaptor proteins in secretory granule biogenesis and maturation," *Frontiers in endocrinology*, vol. 4, 2013.

[181] P. Arvan, R. Kuliawat, D. Prabakaran, A. Zavacki, D. Elahi, S. Wang, and D. Pilkey, "Protein discharge from immature secretory granules displays both regulated and constitutive characteristics.," *Journal of Biological Chemistry*, vol. 266, no. 22, pp. 14171–14174, 1991.

[182] K. Rousseau, S. Kauser, L. E. Pritchard, A. Warhurst, R. L. Oliver, A. Slominski, E. T. Wei, A. J. Thody, D. J. Tobin, and A. White, "Proopiomelanocortin (POMC), the ACTH/melanocortin precursor, is secreted by human epidermal keratinocytes and melanocytes and stimulates melanogenesis," *The FASEB Journal*, vol. 21, no. 8, pp. 1844–1856, 2007.

[183] D. Zizioli, C. Meyer, G. Guhde, P. Saftig, K. von Figura, and P. Schu, "Early embryonic death of mice deficient in γ-adaptin," *Journal of Biological Chemistry*, vol. 274, no. 9, pp. 5385–5390, 1999.

[184] K. Radhakrishnan, J. Baltes, J. W. Creemers, and P. Schu, "Trans-Golgi network morphology and sorting is regulated by prolyl-oligopeptidase-like protein PREPL and the AP-1 complex subunit μ1A," *Journal of cell science*, vol. 126, no. 5, pp. 1155–1163, 2013.

[185] G. G. Farías, L. Cuitino, X. Guo, X. Ren, M. Jarnik, R. Mattera, and J. S. Bonifacino, "Signal-mediated, AP-1/clathrin-dependent sorting of transmembrane receptors to the somatodendritic domain of hippocampal neurons," *Neuron*, vol. 75, no. 5, pp. 810–823, 2012.

[186] C. Delevoye, I. Hurbain, D. Tenza, J.-B. Sibarita, S. Uzan-Gafsou, H. Ohno, W. J. Geerts, A. J. Verkleij, J. Salamero, M. S. Marks, *et al.*, "AP-1 and KIF13A coordinate endosomal sorting and positioning during melanosome biogenesis," *The Journal of cell biology*, vol. 187, no. 2, pp. 247–264, 2009.

[187] J. A. Sobota, F. Ferraro, N. Bäck, B. A. Eipper, and R. E. Mains, "Not all secretory granules are created equal: Partitioning of soluble content proteins," *Molecular biology of the cell*, vol. 17, no. 12, pp. 5038–5052, 2006.

[188] S. L. Milgram, R. C. Johnson, and R. E. Mains, "Expression of individual forms of peptidylglycine alpha-amidating monooxygenase in AtT-20 cells: endoproteolytic processing and routing to secretory granules," *The Journal of cell biology*, vol. 117, no. 4, pp. 717–728, 1992.

[189] S. L. Milgram, S. T. Kho, G. V. Martin, R. E. Mains, and B. A. Eipper, "Localization of integral membrane peptidylglycine alpha-amidating monooxygenase in neuroendocrine cells," *Journal of cell science*, vol. 110, no. 6, pp. 695–706, 1997.

[190] S. L. Milgram, B. A. Eipper, and R. E. Mains, "Differential trafficking of soluble and integral membrane secretory granule-associated proteins," *The Journal of cell biology*, vol. 124, no. 1, pp. 33–41, 1994.

[191] R. E. Mains and B. A. Eipper, "Synthesis and secretion of corticotropins, melanotropins, and endorphins by rat intermediate pituitary cells.," *Journal of Biological Chemistry*, vol. 254, no. 16, pp. 7885–7894, 1979.

[192] E. Schnabel, R. E. Mains, and M. G. Farquhar, "Proteolytic processing of pro-ACTH/endorphin begins in the Golgi complex of pituitary corticotropes and AtT-20 cells," *Molecular Endocrinology*, vol. 3, no. 8, pp. 1223–1235, 1989.

[193] G. D. Ciccotosto, M. R. Schiller, B. A. Eipper, and R. E. Mains, "Induction of integral membrane PAM expression in AtT-20 cells alters the storage and trafficking of POMC and PC1," *The Journal of cell biology*, vol. 144, no. 3, pp. 459–471, 1999.

[194] L. Matsuuchi, K. M. Buckley, A. W. Lowe, and R. B. Kelly, "Targeting of secretory vesicles to cytoplasmic domains in AtT-20 and PC-12 cells," *The Journal of cell biology*, vol. 106, no. 2, pp. 239–251, 1988.

[195] N. Bäck, C. Rajagopal, R. E. Mains, and B. A. Eipper, "Secretory granule membrane protein recycles through multivesicular bodies," *Traffic*, vol. 11, no. 7, pp. 972–986, 2010.

[196] K. Harasaki, N. B. Lubben, M. Harbour, M. J. Taylor, and M. S. Robinson, "Sorting of Major Cargo Glycoproteins into Clathrin-Coated Vesicles," *Traffic*, vol. 6, no. 11, pp. 1014–1026, 2005.

[197] P. Hornby, S. Rosenthal, J. Mathis, O. Vindrola, and I. Lindberg, "Immunocytochemical localization of the neuropeptide-synthesizing enzyme PC1 in AtT-20 cells," *Neuroendocrinology*, vol. 58, no. 5, pp. 555–563, 1993.

[198] H. Stettler, G. Suri, and M. Spiess, "Proprotein convertase PC3 is not a transmembrane protein," *Biochemistry*, vol. 44, no. 14, pp. 5339–5345, 2005.

[199] A. Zhou and R. E. Mains, "Endoproteolytic processing of proopiomelanocortin and prohormone convertases 1 and 2 in neuroendocrine cells overexpressing prohormone convertases 1 or 2.," *Journal of Biological Chemistry*, vol. 269, no. 26, pp. 17440–17447, 1994.

[200] Y. Sharoni, S. Eimerl, and M. Schramm, "Secretion of old versus new exportable protein in rat parotid slics. Control by neurotransmitters.," *The Journal of cell biology*, vol. 71, no. 1, pp. 107–122, 1976.

[201] B. A. Eipper, A. C. Myers, and R. E. Mains, "Peptidyl-Glycine α-Amidation Activity in Tissues and Serum of the Adult Rat*," *Endocrinology*, vol. 116, no. 6, pp. 2497–2504, 1985.

[202] L. Orci, P. Halban, M. Amherdt, M. Ravazzola, J.-D. Vassalli, and A. Perrelet, "Nonconverted, amino acid analog-modified proinsulin stays in a Golgi-derived clathrin-coated membrane compartment.," *The Journal of cell biology*, vol. 99, no. 6, pp. 2187–2192, 1984.

[203] R. E. Smith and M. G. Farquhar, "Lysosome function in the regulation of the secretory process in cells of the anterior pituitary gland," *The Journal of cell biology*, vol. 31, no. 2, pp. 319–347, 1966.

[204] C. J. Rhodes and C. Alarcón, "What β-cell Defect Could Lead to Hyperproinsulinemia in NIDDM?: Some Clues From Recent Advances Made in Understanding the Proinsulin-Processing Mechanism," *Diabetes*, vol. 43, no. 4, pp. 511–517, 1994.

[205] R. Taylor, "Type 2 Diabetes Etiology and reversibility," *Diabetes care*, vol. 36, no. 4, pp. 1047–1055, 2013.

[206] J. Meko, MD and J. Norton, MD, "Management of patients with Zollinger-Ellison syndrome," *Annual review of medicine*, vol. 46, no. 1, pp. 395–411, 1995.

[207] D. N. Orth, "Cushing's syndrome," *New England Journal of Medicine*, vol. 332, no. 12, pp. 791–803, 1995.

[208] M. von Zastrow and J. D. Castle, "Protein sorting among two distinct export pathways occurs from the content of maturing exocrine storage granules.," *The Journal of cell biology*, vol. 105, no. 6, pp. 2675–2684, 1987.

[209] J. D. Castle and A. M. Castle, "Two regulated secretory pathways for newly synthesized parotid salivary proteins are distinguished by doses of secretagogues," *Journal of cell science*, vol. 109, no. 10, pp. 2591–2599, 1996.

[210] R. Kuliawat and P. Arvan, "Protein targeting via the" constitutive-like" secretory pathway in isolated pancreatic islets: passive sorting in the immature granule compartment.," *The Journal of cell biology*, vol. 118, no. 3, pp. 521–529, 1992.

[211] M. D. Turner and P. Arvan, "Protein traffic from the secretory pathway to the endosomal system in pancreatic β-cells," *Journal of Biological Chemistry*, vol. 275, no. 19, pp. 14025–14030, 2000.

[212] B. Ortega, A. K. Mason, and P. A. Welling, "A Tandem Di-hydrophobic Motif Mediates Clathrin-dependent Endocytosis via Direct Binding to the AP-2 $\alpha\sigma$2 Subunits," *Journal of Biological Chemistry*, vol. 287, no. 32, pp. 26867–26875, 2012.

[213] P. V. Burgos, G. A. Mardones, A. L. Rojas, L. L. daSilva, Y. Prabhu, J. H. Hurley, and J. S. Bonifacino, "Sorting of the Alzheimer's disease amyloid precursor protein mediated by the AP-4 complex," *Developmental cell*, vol. 18, no. 3, pp. 425–436, 2010.

[214] C. Rajagopal, K. L. Stone, R. E. Mains, and B. A. Eipper, "Secretion stimulates intramembrane proteolysis of a secretory granule membrane enzyme," *Journal of Biological Chemistry*, vol. 285, no. 45, pp. 34632–34642, 2010.

[215] A. Otoikhian, A. N. Barry, M. Mayfield, M. Nilges, Y. Huang, S. Lutsenko, and N. J. Blackburn, "Lumenal loop M672-P707 of the Menkes protein (ATP7A) transfers copper to peptidylglycine monooxygenase," *Journal of the American Chemical Society*, vol. 134, no. 25, pp. 10458–10468, 2012.

[216] E. D. Gaier, B. A. Eipper, and R. E. Mains, "Copper signaling in the mammalian nervous system: synaptic effects," *Journal of neuroscience research*, vol. 91, no. 1, pp. 2–19, 2013.

[217] A. Montpetit, S. Côté, E. Brustein, C. A. Drouin, L. Lapointe, M. Boudreau, C. Meloche, R. Drouin, T. J. Hudson, P. Drapeau, *et al.*, "Disruption of AP1S1, causing a

novel neurocutaneous syndrome, perturbs development of the skin and spinal cord," *PLoS genetics*, vol. 4, no. 12, p. e1000296, 2008.

[218] P. S. Tarpey, C. Stevens, J. Teague, S. Edkins, S. OâĂŹMeara, T. Avis, S. Barthorpe, G. Buck, A. Butler, J. Cole, *et al.*, "Mutations in the Gene Encoding the Sigma 2 Subunit of the Adaptor Protein 1 Complex, *AP1S2*, cause x-linked mental retardation," *The American Journal of Human Genetics*, vol. 79, no. 6, pp. 1119–1124, 2006.

[219] D. Martinelli, L. Travaglini, C. A. Drouin, I. Ceballos-Picot, T. Rizza, E. Bertini, R. Carrozzo, S. Petrini, P. de Lonlay, M. El Hachem, *et al.*, "MEDNIK syndrome: a novel defect of copper metabolism treatable by zinc acetate therapy," *Brain*, vol. 136, no. 3, pp. 872–881, 2013.

[220] Z. G. Holloway, A. Velayos-Baeza, G. J. Howell, C. Levecque, S. Ponnambalam, E. Sztul, and A. P. Monaco, "Trafficking of the Menkes copper transporter ATP7A is regulated by clathrin-, AP-2–, AP-1–, and Rab22-dependent steps," *Molecular biology of the cell*, vol. 24, no. 11, pp. 1735–1748, 2013.

[221] E. R. Weibel, G. S. Kistler, and W. F. Scherle, "Practical stereological methods for morphometric cytology," *The Journal of cell biology*, vol. 30, no. 1, pp. 23–38, 1966.

[222] H. Ohno, M.-C. Fournier, G. Poy, and J. S. Bonifacino, "Structural determinants of interaction of tyrosine-based sorting signals with the adaptor medium chains," *Journal of Biological Chemistry*, vol. 271, no. 46, pp. 29009–29015, 1996.

[223] V. P. Francone, M. F. Ifrim, C. Rajagopal, C. J. Leddy, Y. Wang, J. H. Carson, R. E. Mains, and B. A. Eipper, "Signaling from the secretory granule to the nucleus: Uhmk1 and PAM," *Molecular Endocrinology*, vol. 24, no. 8, pp. 1543–1558, 2010.

[224] J. Maltese and B. Eipper, "Developmental expression of peptidylglycine alpha-amidating monooxygenase (PAM) in primary cultures of neonatal rat cardiocytes: a model for studying regulation of PAM expression in the rat heart.," *Molecular Endocrinology*, vol. 6, no. 12, pp. 1998–2008, 1992.

[225] H.-Y. Yun, R. C. Johnson, R. E. Mains, and B. A. Eipper, "Topological switching of the COOH-terminal domain of peptidylglycine α-amidating monooxygenase by alternative RNA splicing," *Archives of biochemistry and biophysics*, vol. 301, no. 1, pp. 77–84, 1993.

[226] E. I. Cullen and R. E. Mains, "Biosynthesis of amidated joining peptide from pro-adrenocorticotropin-endorphin," *Molecular Endocrinology*, vol. 1, no. 9, pp. 583–594, 1987.

[227] L. Song and L. D. Fricker, "Tissue distribution and characterization of soluble and membrane-bound forms of metallocarboxypeptidase D," *Journal of Biological Chemistry*, vol. 271, no. 46, pp. 28884–28889, 1996.

[228] I. M. Dickerson and M. R. E, "Cell-Type Specific Posttranslational Processing of Peptides by Different Pituitary Cell Lines," *Endocrinology*, vol. 127, no. 1, pp. 133–140, 1990.

[229] D. Mahaffey, J. Peeler, F. Brodsky, and R. Anderson, "Clathrin-coated pits contain an integral membrane protein that binds the AP-2 subunit with high affinity.," *Journal of Biological Chemistry*, vol. 265, no. 27, pp. 16514–16520, 1990.

[230] J. Huotari and A. Helenius, "Endosome maturation," *The EMBO journal*, vol. 30, no. 17, pp. 3481–3500, 2011.

[231] N. Hirokawa, Y. Noda, Y. Tanaka, and S. Niwa, "Kinesin superfamily motor proteins and intracellular transport," *Nature reviews Molecular cell biology*, vol. 10, no. 10, pp. 682–696, 2009.

[232] T. Nakagawa, M. Setou, D.-H. Seog, K. Ogasawara, N. Dohmae, K. Takio, and N. Hirokawa, "A novel motor, KIF13A, transports mannose-6-phosphate receptor to plasma membrane through direct interaction with AP-1 complex," *Cell*, vol. 103, no. 4, pp. 569–581, 2000.

[233] E. Orzech, L. Livshits, J. Leyt, H. Okhrimenko, V. Reich, S. Cohen, A. Weiss, N. Melamed-Book, M. Lebendiker, Y. Altschuler, *et al.*, "Interactions between adaptor protein-1 of the clathrin coat and microtubules via type 1a microtubule-associated proteins," *Journal of Biological Chemistry*, vol. 276, no. 33, pp. 31340–31348, 2001.

[234] M. Bonnemaison, N. Bäck, Y. Lin, J. S. Bonifacino, R. Mains, and B. Eipper, "AP-1A Controls Secretory Granule Biogenesis and Trafficking of Membrane Secretory Granule Proteins," *Traffic*, vol. 15, no. 10, pp. 1099–1121, 2014.

[235] C. Meyer, E.-L. Eskelinen, M. R. Guruprasad, K. von Figura, and P. Schu, "μ1A deficiency induces a profound increase in MPR300/IGF-II receptor internalization rate," *Journal of cell science*, vol. 114, no. 24, pp. 4469–4476, 2001.

[236] L. Perrin, S. Lacas-Gervais, J. Gilleron, F. Ceppo, F. Prodon, A. Benmerah, J.-F. Tanti, and M. Cormont, "Rab4b controls an early endosome sorting event by interacting with the γ-subunit of the clathrin adaptor complex 1," *Journal of cell science*, vol. 126, no. 21, pp. 4950–4962, 2013.

[237] C. Delevoye, S. Miserey-Lenkei, G. Montagnac, F. Gilles-Marsens, P. Paul-Gilloteaux, F. Giordano, F. Waharte, M. S. Marks, B. Goud, and G. Raposo, "Recycling endosome tubule morphogenesis from sorting endosomes requires the kinesin motor KIF13A," *Cell reports*, vol. 6, no. 3, pp. 445–454, 2014.

[238] D. Bousquet-Moore, R. E. Mains, and B. A. Eipper, "Peptidylglycine α-amidating monooxygenase and copper: A gene–nutrient interaction critical to nervous system function," *Journal of neuroscience research*, vol. 88, no. 12, pp. 2535–2545, 2010.

[239] H. Stenmark, "Rab GTPases as coordinators of vesicle traffic," *Nature reviews Molecular cell biology*, vol. 10, no. 8, pp. 513–525, 2009.

[240] C. Raiborg, K. O. Schink, and H. Stenmark, "Class III phosphatidylinositol 3–kinase and its catalytic product PtdIns3P in regulation of endocytic membrane traffic," *FEBS Journal*, vol. 280, no. 12, pp. 2730–2742, 2013.

[241] E. Nielsen, F. Severin, J. M. Backer, A. A. Hyman, and M. Zerial, "Rab5 regulates motility of early endosomes on microtubules," *Nature Cell Biology*, vol. 1, no. 6, pp. 376–382, 1999.

[242] A. H. Hutagalung and P. J. Novick, "Role of Rab GTPases in membrane traffic and cell physiology," *Physiological reviews*, vol. 91, no. 1, pp. 119–149, 2011.

[243] S. Poirier, G. Mayer, S. R. Murphy, W. S. Garver, T. Y. Chang, P. Schu, and N. G. Seidah, "The Cytosolic Adaptor AP-1A Is Essential for the Trafficking and Function of Niemann-Pick Type C Proteins," *Traffic*, vol. 14, no. 4, pp. 458–469, 2013.

[244] J. S. Bogan, Y. Xu, and M. Hao, "Cholesterol accumulation increases insulin granule size and impairs membrane trafficking," *Traffic*, vol. 13, no. 11, pp. 1466–1480, 2012.

[245] F. Mallard, C. Antony, D. Tenza, J. Salamero, B. Goud, and L. Johannes, "Direct pathway from early/recycling endosomes to the Golgi apparatus revealed through the study of shiga toxin B-fragment transport," *The Journal of cell biology*, vol. 143, no. 4, pp. 973–990, 1998.

[246] E. M. van Dam, T. ten Broeke, K. Jansen, P. Spijkers, and W. Stoorvogel, "Endocytosed transferrin receptors recycle via distinct dynamin and phosphatidylinositol 3-kinase-dependent pathways," *Journal of Biological Chemistry*, vol. 277, no. 50, pp. 48876–48883, 2002.

[247] M. R. Schmidt, T. Maritzen, V. Kukhtina, V. A. Higman, L. Doglio, N. N. Barak, H. Strauss, H. Oschkinat, C. G. Dotti, and V. Haucke, "Regulation of endosomal membrane traffic by a Gadkin/AP-1/kinesin KIF5 complex," *Proceedings of the National Academy of Sciences*, vol. 106, no. 36, pp. 15344–15349, 2009.

[248] S. Hoepfner, F. Severin, A. Cabezas, B. Habermann, A. Runge, D. Gillooly, H. Stenmark, and M. Zerial, "Modulation of receptor recycling and degradation by the endosomal kinesin KIF16B," *Cell*, vol. 121, no. 3, pp. 437–450, 2005.

[249] T. M. Huckaba, A. Gennerich, J. E. Wilhelm, A. H. Chishti, and R. D. Vale, "Kinesin-73 is a processive motor that localizes to Rab5-containing organelles," *Journal of Biological Chemistry*, vol. 286, no. 9, pp. 7457–7467, 2011.

[250] S. Loubéry, C. Wilhelm, I. Hurbain, S. Neveu, D. Louvard, and E. Coudrier, "Different microtubule motors move early and late endocytic compartments," *Traffic*, vol. 9, no. 4, pp. 492–509, 2008.

[251] G. Steinberg and J. Perez-Martin, "*Ustilago maydis*, a new fungal model system for cell biology," *Trends in cell biology*, vol. 18, no. 2, pp. 61–67, 2008.

[252] R. Le Borgne, A. Schmidt, F. Mauxion, G. Griffiths, and B. Hoflack, "Binding of AP-1 Golgi adaptors to membranes requires phosphorylated cytoplasmic domains of the mannose 6-phosphate/insulin-like growth factor II receptor.," *Journal of Biological Chemistry*, vol. 268, no. 30, pp. 22552–22556, 1993.

[253] M. Hölttä-Vuori, R.-L. Uronen, J. Repakova, E. Salonen, I. Vattulainen, P. Panula, Z. Li, R. Bittman, and E. Ikonen, "BODIPY-Cholesterol: A New Tool to Visualize Sterol Trafficking in Living Cells and Organisms," *Traffic*, vol. 9, no. 11, pp. 1839–1849, 2008.

[254] D. Martinelli and C. Dionisi-Vici, "AP1S1 defect causing MEDNIK syndrome: a new adaptinopathy associated with defective copper metabolism," *Annals of the New York Academy of Sciences*, vol. 1314, no. 1, pp. 55–63, 2014.

[255] R. El Meskini, V. C. Culotta, R. E. Mains, and B. A. Eipper, "Supplying copper to the cuproenzyme peptidylglycine α-amidating monooxygenase," *Journal of Biological Chemistry*, vol. 278, no. 14, pp. 12278–12284, 2003.

[256] A. N. Barry, A. Otoikhian, S. Bhatt, U. Shinde, R. Tsivkovskii, N. J. Blackburn, and S. Lutsenko, "The Lumenal Loop Met672–Pro707 of Copper-transporting ATPase

ATP7A Binds Metals and Facilitates Copper Release from the Intramembrane Sites," *Journal of Biological Chemistry*, vol. 286, no. 30, pp. 26585–26594, 2011.

[257] M. S. Robinson, D. A. Sahlender, and S. D. Foster, "Rapid inactivation of proteins by rapamycin-induced rerouting to mitochondria," *Developmental cell*, vol. 18, no. 2, pp. 324–331, 2010.

[258] N. E. Hellman, S. Kono, G. M. Mancini, A. Hoogeboom, G. De Jong, and J. D. Gitlin, "Mechanisms of copper incorporation into human ceruloplasmin," *Journal of Biological Chemistry*, vol. 277, no. 48, pp. 46632–46638, 2002.

[259] D. Bousquet-Moore, X. Ma, E. Nillni, T. Czyzyk, J. Pintar, B. Eipper, and R. Mains, "Reversal of physiological deficits caused by diminished levels of peptidylglycine α-amidating monooxygenase by dietary copper," *Endocrinology*, vol. 150, no. 4, pp. 1739–1747, 2009.

[260] T. A. Czyzyk, Y. Ning, M.-S. Hsu, B. Peng, R. E. Mains, B. A. Eipper, and J. E. Pintar, "Deletion of peptide amidation enzymatic activity leads to edema and embryonic lethality in the mouse," *Developmental biology*, vol. 287, no. 2, pp. 301–313, 2005.

[261] T. C. Steveson, G. D. Ciccotosto, X.-M. Ma, G. P. Mueller, R. E. Mains, and B. A. Eipper, "Menkes protein contributes to the function of peptidylglycine α-amidating monooxygenase," *Endocrinology*, vol. 144, no. 1, pp. 188–200, 2003.

[262] A. N. Luck and A. B. Mason, "Transferrin-mediated cellular iron delivery.," *Current topics in membranes*, vol. 69, pp. 3–35, 2011.

[263] R. El Meskini, R. E. Mains, and B. A. Eipper, "Cell Type-Specific Metabolism of Peptidylglycineα-Amidating Monooxygenase in Anterior Pituitary 1," *Endocrinology*, vol. 141, no. 8, pp. 3020–3034, 2000.

[264] N. E. Hellman and J. D. Gitlin, "Ceruloplasmin metabolism and function," *Annual review of nutrition*, vol. 22, no. 1, pp. 439–458, 2002.

[265] T. Nittis and J. D. Gitlin, "Role of copper in the proteosome-mediated degradation of the multicopper oxidase hephaestin," *Journal of Biological Chemistry*, vol. 279, no. 24, pp. 25696–25702, 2004.

[266] M. De, G. D. Ciccotosto, R. E. Mains, and B. A. Eipper, "Trafficking of a secretory granule membrane protein is sensitive to copper," *Journal of Biological Chemistry*, vol. 282, no. 32, pp. 23362–23371, 2007.

[267] I. Hamza, J. Prohaska, and J. D. Gitlin, "Essential role for Atox1 in the copper-mediated intracellular trafficking of the Menkes ATPase," *Proceedings of the National Academy of Sciences*, vol. 100, no. 3, pp. 1215–1220, 2003.

[268] S. Tanaka, T. Yora, K. Nakayama, K. Inoue, and K. Kurosumi, "Proteolytic processing of pro-opiomelanocortin occurs in acidifying secretory granules of AtT-20 cells," *Journal of Histochemistry & Cytochemistry*, vol. 45, no. 3, pp. 425–436, 1997.

[269] B. Eipper, L. Park, H. Keutmann, and R. Mains, "Amidation of joining peptide, a major pro-ACTH/endorphin-derived product peptide.," *Journal of Biological Chemistry*, vol. 261, no. 19, pp. 8686–8694, 1986.

[270] Y. Nose, L. K. Wood, B.-E. Kim, J. R. Prohaska, R. S. Fry, J. W. Spears, and D. J. Thiele, "Ctr1 is an apical copper transporter in mammalian intestinal epithelial cells in vivo that is controlled at the level of protein stability," *Journal of Biological Chemistry*, vol. 285, no. 42, pp. 32385–32392, 2010.

[271] C. Cobbold, S. Ponnambalam, M. J. Francis, and A. P. Monaco, "Novel membrane traffic steps regulate the exocytosis of the Menkes disease ATPase," *Human molecular genetics*, vol. 11, no. 23, pp. 2855–2866, 2002.

[272] R. Polishchuk and S. Lutsenko, "Golgi in copper homeostasis: a view from the membrane trafficking field," *Histochemistry and cell biology*, vol. 140, no. 3, pp. 285–295, 2013.

[273] B. A. Eipper, D. A. Stoffers, and R. E. Mains, "The biosynthesis of neuropeptides: peptide alpha-amidation," *Annual review of neuroscience*, vol. 15, no. 1, pp. 57–85, 1992.

[274] S. R. G. Setty, D. Tenza, E. V. Sviderskaya, D. C. Bennett, G. Raposo, and M. S. Marks, "Cell-specific ATP7A transport sustains copper-dependent tyrosinase activity in melanosomes," *Nature*, vol. 454, no. 7208, pp. 1142–1146, 2008.

[275] N. Jiang, A. S. Kolhekar, P. S. Jacobs, R. E. Mains, B. A. Eipper, and P. H. Taghert, "*PHM* Is Required for Normal Developmental Transitions and for Biosynthesis of Secretory Peptides in *Drosophila*," *Developmental biology*, vol. 226, no. 1, pp. 118–136, 2000.

[276] J. Bell, R. El Meskini, D. D'Amato, R. E. Mains, and B. A. Eipper, "Mechanistic investigation of peptidylglycine α-hydroxylating monooxygenase via intrinsic tryptophan fluorescence and mutagenesis," *Biochemistry*, vol. 42, no. 23, pp. 7133–7142, 2003.

[277] T. Rae, P. Schmidt, R. Pufahl, V. Culotta, and T. O'halloran, "Undetectable intracellular free copper: the requirement of a copper chaperone for superoxide dismutase," *Science*, vol. 284, no. 5415, pp. 805–808, 1999.

[278] V. MAY and B. A. EIPPER, "Long Term Culture of Primary Rat Pituitary Adrenocorticotropin/Endorphin-Producing Cells in Serum-Free Medium*," *Endocrinology*, vol. 118, no. 4, pp. 1284–1295, 1986.

[279] S. G. Kaler, "ATP7A-related copper transport diseasesâĂŤemerging concepts and future trends," *Nature reviews Neurology*, vol. 7, no. 1, pp. 15–29, 2011.

[280] D. Huster, "Structural and metabolic changes in Atp7b-/- mouse liver and potential for new interventions in Wilson's disease," *Annals of the New York Academy of Sciences*, vol. 1315, no. 1, pp. 37–44, 2014.

[281] E. E. Chufán, M. De, B. A. Eipper, R. E. Mains, and L. M. Amzel, "Amidation of bioactive peptides: the structure of the lyase domain of the amidating enzyme," *Structure*, vol. 17, no. 7, pp. 965–973, 2009.

[282] S. T. Prigge, B. A. Eipper, R. E. Mains, and L. M. Amzel, "Dioxygen binds end-on to mononuclear copper in a precatalytic enzyme complex," *Science*, vol. 304, no. 5672, pp. 864–867, 2004.

[283] S. T. Prigge, A. S. Kolhekar, B. A. Eipper, R. E. Mains, and L. M. Amzel, "Amidation of bioactive peptides: the structure of peptidylglycine α-hydroxylating monooxygenase," *Science*, vol. 278, no. 5341, pp. 1300–1305, 1997.

[284] B. Eipper, V. May, and K. Braas, "Membrane-associated peptidylglycine alpha-amidating monooxygenase in the heart.," *Journal of Biological Chemistry*, vol. 263, no. 17, pp. 8371–8379, 1988.

[285] V. May, E. I. Cullen, K. M. Braas, and B. A. Eipper, "Membrane-associated forms of peptidylglycine alpha-amidating monooxygenase activity in rat pituitary. Tissue specificity.," *Journal of Biological Chemistry*, vol. 263, no. 16, pp. 7550–7554, 1988.

[286] C.-M. Yeung, C.-B. Chan, P.-S. Leung, and C. H. Cheng, "Cells of the anterior pituitary," *The international journal of biochemistry & cell biology*, vol. 38, no. 9, pp. 1441–1449, 2006.

[287] B. C. Cunningham, M. G. Mulkerrin, and J. A. Wells, "Dimerization of human growth hormone by zinc," *Science*, vol. 253, no. 5019, pp. 545–548, 1991.

[288] B.-J. Sankoorikal, Y. L. Zhu, M. E. Hodsdon, E. Lolis, and P. S. Dannies, "Aggregation of human wild-type and H27A-prolactin in cells and in solution: Roles of Zn2+, Cu2+, and pH," *Endocrinology*, vol. 143, no. 4, pp. 1302–1309, 2002.

[289] A. M. Oyarce and B. A. Eipper, "Identification of subcellular compartments containing peptidylglycine alpha-amidating monooxygenase in rat anterior pituitary," *Journal of cell science*, vol. 108, no. 1, pp. 287–297, 1995.

[290] C. R. Hopkins and M. G. Farquhar, "Hormone secretion by cells dissociated from rat anterior pituitaries," *The Journal of cell biology*, vol. 59, no. 2, pp. 276–303, 1973.

[291] A. M. Oyarce, T. A. Hand, R. E. Mains, and B. A. Eipper, "Dopaminergic Regulation of Secretory Granule-Associated Proteins in Rat Intermediate Pituitary," *Journal of neurochemistry*, vol. 67, no. 1, pp. 229–241, 1996.

[292] S. G. Kaler, L. K. Gallo, V. K. Proud, A. K. Percy, Y. Markl, N. A. Segan, D. S. Goldstein, C. S. Holmes, and W. A. Gahl, "Occipital horn syndrome and a mild Menkes phenotype," *Nature genetics*, vol. 8, pp. 195–202, 1994.

[293] M. L. Kennerson, G. A. Nicholson, S. G. Kaler, B. Kowalski, J. F. Mercer, J. Tang, R. M. Llanos, S. Chu, R. I. Takata, C. E. Speck-Martins, *et al.*, "Missense Mutations in the Copper Transporter Gene *ATP7A* cause x-linked distal hereditary motor neuropathy," *The American Journal of Human Genetics*, vol. 86, no. 3, pp. 343–352, 2010.

[294] L. Yi, A. Donsante, M. L. Kennerson, J. F. Mercer, J. Y. Garbern, and S. G. Kaler, "Altered intracellular localization and valosin-containing protein (p97 VCP) interaction underlie ATP7A-related distal motor neuropathy," *Human molecular genetics*, vol. 21, no. 8, pp. 1794–1807, 2012.

[295] B. Ward, K. Walker, and C. Exley, "Copper (II) inhibits the formation of amylin amyloid in vitro," *Journal of inorganic biochemistry*, vol. 102, no. 2, pp. 371–375, 2008.

[296] H. Öhrvik, Y. Nose, L. K. Wood, B.-E. Kim, S.-C. Gleber, M. Ralle, and D. J. Thiele, "Ctr2 regulates biogenesis of a cleaved form of mammalian Ctr1 metal transporter

lacking the copper-and cisplatin-binding ecto-domain," *Proceedings of the National Academy of Sciences*, vol. 110, no. 46, pp. E4279–E4288, 2013.

[297] E. D. Gaier, M. B. Miller, M. Ralle, D. Aryal, W. C. Wetsel, R. E. Mains, and B. A. Eipper, "Peptidylglycine α-amidating monooxygenase heterozygosity alters brain copper handling with region specificity," *Journal of neurochemistry*, vol. 127, no. 5, pp. 605–619, 2013.

[298] A. S. Kolhekar, A. S. Quon, C. A. Berard, R. E. Mains, and B. A. Eipper, "Post-translational N-glycosylation of a truncated form of a peptide processing enzyme," *Journal of Biological Chemistry*, vol. 273, no. 36, pp. 23012–23018, 1998.

[299] M. Ludwig and G. Leng, "Dendritic peptide release and peptide-dependent behaviours," *Nature Reviews Neuroscience*, vol. 7, no. 2, pp. 126–136, 2006.

[300] J. A. Sobota, W. A. Mohler, A. E. Cowan, B. A. Eipper, and R. E. Mains, "Dynamics of peptidergic secretory granule transport are regulated by neuronal stimulation," *BMC neuroscience*, vol. 11, no. 1, p. 32, 2010.

[301] B. A. Eipper, S. L. Milgram, E. Jean Husten, H.-Y. Yun, and R. E. Mains, "Peptidylglycine α-amidating monooxygenase: A multifunctional protein with catalytic, processing, and routing domains," *Protein Science*, vol. 2, no. 4, pp. 489–497, 1993.

[302] K. M. Braas, S. A. Harakall, L. Ouafik, B. A. Eipper, and V. May, "Expression of peptidylglycine alpha-amidating monooxygenase: an in situ hybridization and immunocytochemical study.," *Endocrinology*, vol. 130, no. 5, pp. 2778–2788, 1992.

[303] K. M. Braas, D. A. Stoffers, B. A. Eipper, and V. May, "Tissue specific expression of rat peptidylglycine α-amidating monooxygenase activity and mRNA," *Molecular endocrinology*, vol. 3, no. 9, pp. 1387–1398, 1989.

[304] M. Schafer, D. Stoffers, B. A. Eipper, and S. J. Watson, "Expression of peptidylglycine alpha-amidating monooxygenase (EC 1.14. 17.3) in the rat central nervous system," *The Journal of neuroscience*, vol. 12, no. 1, pp. 222–234, 1992.

[305] L. Ouafik, V. May, H. Keutmann, and B. A. Eipper, "Developmental regulation of peptidylglycine alpha-amidating monooxygenase (PAM) in rat heart atrium and ventricle. Tissue-specific changes in distribution of PAM activity, mRNA levels, and protein forms.," *Journal of Biological Chemistry*, vol. 264, no. 10, pp. 5839–5845, 1989.

[306] C. Dubé, "Neuropeptide Y: potential role in recurrent developmental seizures," *Peptides*, vol. 28, no. 2, pp. 441–446, 2007.

[307] S. Furtinger, S. Pirker, T. Czech, C. Baumgartner, G. Ransmayr, and G. Sperk, "Plasticity of Y1 and Y2 receptors and neuropeptide Y fibers in patients with temporal lobe epilepsy," *The Journal of Neuroscience*, vol. 21, no. 15, pp. 5804–5812, 2001.

[308] C. Richichi, E.-J. D. Lin, D. Stefanin, D. Colella, T. Ravizza, G. Grignaschi, P. Veglianese, G. Sperk, M. J. During, and A. Vezzani, "Anticonvulsant and antiepileptogenic effects mediated by adeno-associated virus vector neuropeptide Y expression in the rat hippocampus," *The Journal of neuroscience*, vol. 24, no. 12, pp. 3051–3059, 2004.

[309] H. G. Kuhn, H. Dickinson-Anson, and F. H. Gage, "Neurogenesis in the dentate gyrus of the adult rat: age-related decrease of neuronal progenitor proliferation," *The Journal of neuroscience*, vol. 16, no. 6, pp. 2027–2033, 1996.

[310] S. M. Sato and R. E. Mains, "Posttranslational Processing of Proadrenocorticotropin/Endorphin-Derived Peptides during Postnatal Development in the Rat Pituitary*," *Endocrinology*, vol. 117, no. 2, pp. 773–786, 1985.

[311] Y. Shinoda, T. Sadakata, and T. Furuichi, "Animal models of Autism Spectrum Disorder (ASD): A synaptic-level approach to autistic-like behavior in mice," *Experimental Animals*, vol. 62, no. 2, pp. 71–78, 2013.

[312] Y. Yan, B. A. Eipper, and R. E. Mains, "Kalirin-9 and Kalirin-12 Play Essential Roles in Dendritic Outgrowth and Branching," *Cerebral Cortex*, p. bhu182, 2014.

[313] G. Borck, A. Mollà-Herman, N. Boddaert, F. Encha-Razavi, A. Philippe, L. Robel, I. Desguerre, F. Brunelle, A. Benmerah, A. Munnich, *et al.*, "Clinical, cellular, and neuropathological consequences of AP1S2 mutations: further delineation of a recognizable X-linked mental retardation syndrome," *Human mutation*, vol. 29, no. 7, pp. 966–974, 2008.

[314] H. P. Horikawa, M. Kneussel, O. El Far, and H. Betz, "Interaction of synaptophysin with the AP-1 adaptor protein γ-adaptin," *Molecular and Cellular Neuroscience*, vol. 21, no. 3, pp. 454–462, 2002.

[315] S. Vogt and M. Ralle, "Opportunities in multidimensional trace metal imaging: taking copper-associated disease research to the next level," *Analytical and bioanalytical chemistry*, vol. 405, no. 6, pp. 1809–1820, 2013.

[316] N. B. Lubben, D. A. Sahlender, A. M. Motley, P. J. Lehner, P. Benaroch, and M. S. Robinson, "HIV-1 Nef-induced down-regulation of MHC class I requires AP-1 and clathrin but not PACS-1 and is impeded by AP-2," *Molecular biology of the cell*, vol. 18, no. 9, pp. 3351–3365, 2007.

[317] M. R. Alam, B. D. Caldwell, R. C. Johnson, D. N. Darlington, R. E. Mains, and B. A. Eipper, "Novel proteins that interact with the COOH-terminal cytosolic routing determinants of an integral membrane peptide-processing enzyme," *Journal of Biological Chemistry*, vol. 271, no. 45, pp. 28636–28640, 1996.

[318] M. R. Alam, T. C. Steveson, R. C. Johnson, N. Bäck, B. Abraham, R. E. Mains, and B. A. Eipper, "Signaling mediated by the cytosolic domain of peptidylglycine α-amidating monooxygenase," *Molecular biology of the cell*, vol. 12, no. 3, pp. 629–644, 2001.